UNIVERSIDADE DE LISBOA

INSTITUTO SUPERIOR TÉCNICO

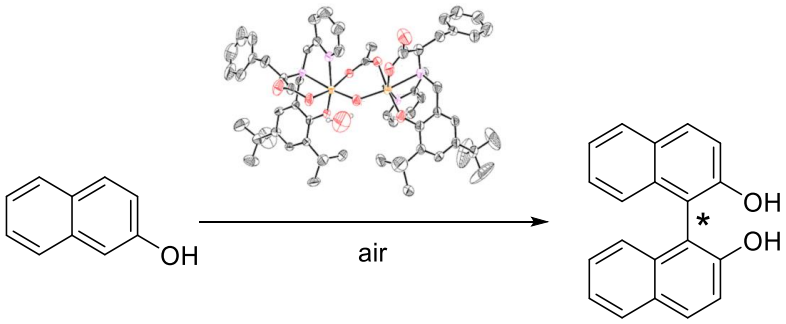

Synthesis and Application of New Amino Acid-derived Iron(III) and Molybdenum(VI) Complexes in Oxidative Catalysis

Carlos Manuel Brandão Teixeira

Supervisor:

Doctor Pedro Miguel Santos Ferreira Adão

Co-Supervisors:

Doctor João Emídio da Silva da Costa Pessoa

Doctor Beatriz Royo Cantabrana

Thesis approved in public session to obtain the PhD Degree in Chemistry

Jury final classification: Pass with Distinction

2019

UNIVERSIDADE DE LISBOA
INSTITUTO SUPERIOR TÉCNICO

Synthesis and Application of New Amino Acid-derived Iron(III) and Molybdenum(VI) Complexes in Oxidative Catalysis

Carlos Manuel Brandão Teixeira

Supervisor:
Doctor Pedro Miguel Santos Ferreira Adão

Co-Supervisors:
Doctor João Emídio da Silva da Costa Pessoa

Doctor Beatriz Royo Cantabrana

Jury

Chairperson: Doctor Maria Matilde Soares Duarte Marques, Instituto Superior Técnico, Universidade de Lisboa

Members of the committee:

Doctor Armando José Latourrette de Oliveira Pombeiro, Instituto Superior Técnico, Universidade de Lisboa;

Doctor Anthony Joseph Burke, Escola de Ciências e Tecnologia, Universidade de Évora;

Doctor Ana Margarida Sousa Dias Martins, Instituto Superior Técnico, Universidade de Lisboa;

Doctor Mário Manuel Quialheiro Simões, Universidade de Aveiro;

Doctor Maria Isabel Rodrigues Correia, Instituto Superior Técnico, Universidade de Lisboa;

Doctor Pedro Miguel Santos Ferreira Adão, MARE-Centro de Ciências do Mar e do Ambiente.

Funding Institutions

Fundação para a Ciência e a Tecnologia through CATSUS Doctoral Programme

2019

The work presented in this thesis was carried out with the financial support of Fundação para a Ciência e a Tecnologia, under the CATSUS FCT PhD Programme and under the PhD Scholarship reference PD/BD/106078/2015.

FCT Fundação para a Ciência e a Tecnologia

MINISTÉRIO DA EDUCAÇÃO E CIÊNCIA

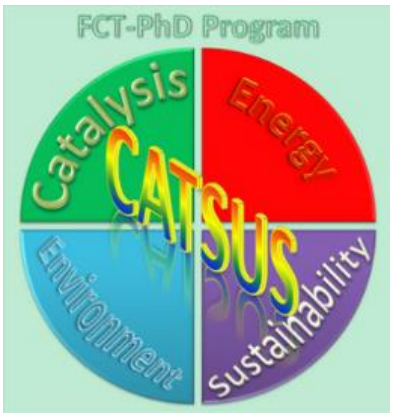

The experimental and theoretical work was executed at Centro de Química Estrutural (CQE) in Instituto Superior Técnico (IST) and at Laboratório de Catálise Homogénea in Instituto de Tecnologia Química e Biológica António Xavier (ITQB).

TÉCNICO LISBOA

CQE Química Estrutural

ITQB UNIVERSIDADE NOVA DE LISBOA

To all the referred institutions, I must address the most sincere acknowledgements for all the support.

Carlos Manuel Brandão Teixeira

To my beloved family and friends

To Marta

Abstract

The work presented in this thesis describes the synthesis, characterization and catalytic application of amino acid-derived iron(III) and molybdenum(VI) complexes in homogeneous oxidative catalysis.

A general introduction to the thesis context and objective is firstly presented. The synthesis and characterization of chiral amino acid-derived ligand precursors is described, followed by the preparation and characterization of the respective iron(III) and molybdenum(VI) complexes. All compounds were prepared using mild and sustainable one-pot synthetic procedures whenever possible.

The obtained iron(III) complexes were applied as pre-catalysts in the asymmetric oxidative coupling of 2-naphthol and 3-bromo-2-naphthol, epoxidation of benzalacetophenones and oxidation of 1-phenylethan-1-ol to acetophenone; the prepared molybdenum(VI) compounds were tested in the epoxidation of benzalacetophenones.

In the oxidative coupling of 2-naphthol, using air as oxidant and organic bases as additives, low to good BINOL yields were obtained (up to 84%). Depending on the iron(III) complex used as pre-catalyst, distinct enantioselectivities in BINOL formation were observed: 39% *ee* for (a*S*)-BINOL with **FeL2** and phenanthroline, 17% *ee* for (a*R*)-BINOL with **FeL14** and collidine. In the oxidative coupling of 3-bromo-2-naphthol were observed good enantioselectivities for the preparation of (a*S*)-BrBINOL with **FeL2** as pre-catalyst and phenanthroline (up to 85% *ee*), but with low yields (up to 15%).

In the epoxidation of benzalacetophenones under Mukaiyama conditions with air and isobutyraldehyde, moderate epoxide yields were obtained with several iron(III) complexes as pre-catalysts (up to 64%) with excellent selectivities towards epoxide formation (up to 96%).

In the oxidation of 1-phenylethan-1-ol with TBHP as oxidant in MeCN, excellent yields of acetophenone were obtained after 4 hours of reaction for several iron(III) complexes as pre-catalysts, especially with **FeL3** (99%).

Resumo

O trabalho apresentado nesta tese pretende descrever a síntese, caracterização e aplicação de complexos de ferro(III) e molibdénio(VI), contendo ligandos derivados de aminoácidos, como catalisadores em catálise oxidativa homogénea.

Uma introdução geral ao contexto e objetivo da tese é apresentada inicialmente. A síntese e caracterização de precursores de ligandos derivado de aminoácidos quirais é apresentada, seguida pela síntese e caracterização dos respectivos complexos de ferro(III) e molibdénio(VI). Todos os compostos foram sintetizados utilizando tanto quanto possível procedimentos sintéticos suaves, sustentáveis e pouco morosos.

Os complexos de ferro(III) obtidos foram aplicados como pré-catalisadores no acoplamento oxidativo assimétrico de 2-naftol e 3-bromo-2-naftol, na epoxidação de benzalacetofenonas e na oxidação de 1-feniletan-1-ol a acetofenona; os compostos de molibdénio(VI) obtidos foram testados como pré-catalisadores na epoxidação de benzalacetofenonas.

No acoplamento oxidativo de 2-naftol, utilizando ar como oxidante e bases orgânicas como aditivos, foram obtidos rendimentos de BINOL baixos a bons (até 84%). Dependendo do complexo de ferro(III) usado como pré-catalisador, foram observadas diferentes enantiosseletividades na formação de BINOL: 39% *ee* para (a*S*)-BINOL com **FeL2** e fenantrolina, 17% *ee* para (a*R*)-BINOL com **FeL14** e colidina. No acoplamento oxidativo de 3-bromo-2-naftol foram observadas boas enantiosseletividades para a preparação de (a*S*)-BrBINOL com **FeL2** como pré-catalisador e fenantrolina (até 85% *ee*), mas com rendimentos baixos (até 15%).

Na epoxidação de benzalacetofenonas, aplicando condições de Mukaiyama com ar e isobutiraldeído, foram obtidos rendimentos moderados dos respectivos epóxidos com vários complexos de ferro(III) como pré-catalisadores (até 64%), tendo sido observadas excelentes selectividades em relação à formação de epóxido (até 96%).

Na oxidação de 1-feniletan-1-ol com TBHP em acetonitrilo, excelentes rendimentos de acetofenona foram obtidos após 4 horas de reação para vários complexos de ferro(III) como pré-catalisadores, especialmente com **FeL3** (99%).

Keywords

One-pot synthesis

Amino acid-derived ligands

Iron complexes

Molybdenum complexes

Homogeneous catalysis

Asymmetric catalysis

Oxidative coupling

Epoxidations

Alcohol oxidations

Palavras-chave

Síntese num passo

Ligandos derivados de aminoácidos

Complexos de ferro

Complexos de molibdénio

Catálise homogénea

Catálise assimétrica

Acoplamento oxidativo

Epoxidações

Oxidação de alcoóis

Acknowledgements

The work presented in this thesis was mainly performed at Centro de Química Estrutural (CQE) in Instituto Superior Técnico (IST) under the supervision of Doctor Pedro Adão, with co-supervision of Professor João Costa Pessoa. The work presented in the oxidation of alcohols was executed at Laboratório de Catálise Homogénea in Instituto de Tecnologia Química e Biológica António Xavier (ITQB), with supervision of Professora Beatriz Royo. I am grateful to both institutions for the use of the facilities.

I am profoundly grateful to Fundação para a Ciência e Tecnologia (FCT) (PD/BD/106078/2015) and to the CATSUS Doctoral Programme for a PhD grant and all the financial support. Without this support it would be very difficult to me to attend this PhD and to execute this work.

I must specially thank my PhD supervisor Pedro Adão for his guidance, support, readiness and patience showed during my PhD. His valuable and inspirational knowledge, know-how and suggestions prove to be very important in order to understand and develop the work presented in this thesis. I have learned enormously from his teachings and advices, and I am profoundly grateful for his dedication in all the stages of the preparation of this work.

I must thank my PhD co-supervisor João Costa Pessoa for his constant availability, patience and guidance during my PhD. The opportunity to be included in his research group and to use CQE facilities was very important, as well as his constant availability whenever doubts came trough in the development of this work. I am also thankfull for his valuable suggestions during the writing of this thesis.

I must thank my PhD co-supervisor Beatriz Royo for her guidance, readiness and support in the work developed in ITQB in the oxidation of 1-phenylethan-1-ol. Her valuable knowledge and advices lead me to enrich this work in the catalytic application of iron complexes, as well as during the writing of this thesis.

I would like to profoundly thank Doctor Fernanda Carvalho for her guidance, readiness, assistance and support in the characterization of iron(III) and molybdenum(VI) complexes by Cyclic Voltammetry. Her wisdom, knowledge and very valuable advices clearly enriched this work in the better understanding of the electrochemical behaviour of the compounds prepared in this work.

I would like to thank Doctor Clara Gomes for her guidance, assistance and support in the characterization of iron complexes by X-Ray diffraction. Her contribution was very relevant in

the enrichment of the information present in this work regarding the structure of the obtained compounds, as well as in the elucidation of the many questions I had.

I would like to thank Doctor Maria da Conceição Oliveira and MsC Ana Dias for their assistance regarding mass spectrometry.

I would like to thank Laboratório de Análises of IST for its assistance regarding Elemental Analysys.

A special thanks to Doctor José Virgílio Prata. Even not participating in this work, his valuable teachings in the field of Organic Chemistry during my academic career, as well as his strict work methodology has always been a source of inspiration. I will always see him as a reference.

I must thank all my friends Pedro Bartilotti, Gonçalo Esteves, Nuno Mattoso, Nuno Correia and Luis Miranda for the truly friendship demonstrations during my lifetime and for all the good moments of relaxation.

A big thanks to all my lab colleagues and all CATSUS colleagues for the good working environment and for all the good moments in general: Isabel Correia, Cristina Matos, Nádia Ribeiro, Patrique Nunes, Tiago Duarte, Nuno Martins, Mara Pinto, Rita Lopes, Gonçalo Tiago, Bruno Rocha, Mohammed Mostafa, Abdallah Gamal, Tiago Cruz, Joana Hipólito and for all those that, by involuntary omission, are not mentioned herein.

A loving thanks to my mother and to all my brothers and sisters who have always shown great pride in me. A “thank you very much” will certainly not be enough to thank the support and unconditional patience that has always been demonstrated and motivated me so much during my life course and in the accomplishment of this work. Last, but definitely not least, I thank my beloved Marta for her love, support, patience and for always believing in me.

Carlos Manuel Brandão Teixeira

Table of Contents

Index of Figures

Index of Schemes

Index of Tables

Symbols and Abreviations

A	– Electrode area
AB	– Two-spin system involving nucleus A and nucleus B
acac	– Acetylacetonate ligand
AcOEt	– Ethyl acetate
AcOH	– Acetic acid
AcOOH	– Peracetic acid
AMX	– Three-spin system involving nucleus A, nucleus M and nucleus X
a*R*	– Absolute configuration *R* in an axis of chirality
a*S*	– Absolute configuration *S* in an axis of chirality
b	– Broad
BINOL	– 1,1'-bi-2-naphthol
bpmen	– *N,N′*-dimethyl-*N,N′*-bis(2-pyridylmethyl)-1,2-diaminoethane ligand
Bn	– Benzyl
BrBINOL	– 3,3'-dibromo-BINOL
C	– Concentration
ca.	– Approximately
CD	– Circular Dichroism
^{13}C-{1H} APT	– Carbon Attached Proton Test
CHP	– Cumene hydroperoxide
^{13}C NMR	– Carbon Nuclear Magnetic Resonance
Coll	– 2,4,6-trimethylpyridine (collidine)
Conv.	– Conversion
CT	– Charge transfer
CV	– Cyclic Voltammetry
D	– Diffusion coefficient
d	– Doublet

dd	– Double doublet
DCIB	– 1,2-dichloro-2-methylpropane
DMF	– *N,N*-dimethylformamide
DMSO	– Dimethyl Sulfoxide
1D NMR	– One-dimensional Nuclear Magnetic Resonance
2D NMR	– Two-dimensional Nuclear Magnetic Resonance
E_p^{red}	– Reduction peak potential
E_p^{ox}	– Oxidation peak potential
$E_{1/2}^{Red}$	– Half wave reduction peak potential
$E_{1/2}^{ox}$	– Half wave oxidation peak potential
EA	– Elemental Analysis
EC	– Electrochemical-Chemical process
ee	– Enantiomeric excess
e.g.	– *Exempli gratia* (from Latin, for example)
eq	– Equivalent
ESI-MS	– Electrospray Ionization Mass Spectrometry
Et_3N	– Triethylamine
Et_2O	– Diethyl ether
EtOH	– Ethanol
FT-IR	– Infrared Spectroscopy
GC	– Gas Chromatography
HC	– (*E*)-1,3-diphenylprop-2-enone
HFIP	– 1,1,1,3,3,3-hexafluoropropan-2-ol
HMBC	– Heteronuclear Multiple Bond Correlation
^1H NMR	– Proton Nuclear Magnetic Resonance
HPLC	– High Performance Liquid Chromatography
H_2Pydic	– Pyridine 2,6-dicarboxylic acid

HSQC – Heteronuclear Single Quantum Coherence

I_p – Current intensity

J – Coupling constant

LMCT – Ligand-to-Metal Charge Transfer

L-Phe – L-phenylalanine

L-Val – L-valine

L-Trp – L-tryptophan

m – Multiplet in NMR / Medium in FT-IR

M – Moleculer weight

m^p – Concentration of solute

M^p – Molecular weight of solute

MeCN – Acetonitrile

MeOC – (*E*)-1-(4-methoxyphenyl)-3-phenylprop-2-enone

MeOH – Methanol

MMO – Methane monooxygenase

n – Number of electrons transferred in the redox process

NADPH – Nicotinamide Adenine Dinucleotide Phosphate

NaOAc – Sodium acetate

Naph – Naphthyl

NMe_2 – Dimethylamino group

NMR – Nuclear Magnetic Resonance

Ph – Phenyl

Phen – Phenanthroline

PhEtOH – 1-phenylethan-1-ol

Pic – Picolinate ligand

Py – Pyridine

q – Quartet

Quin – Quinoline

RDO – Rieske dioxygenases

r.d.s. – Rate-determining step

r.t. – Room temperature

s – Singlet in NMR / Strong in FT-IR

S – Spin quantum number

SCE – Saturated calomel electrode

S_f – Shape factor of the NMR spectrometer

SET – Single electron transfer

t – Triplet

T – Temperature

TBAI – *tert*-butylammonium iodide

TBHP – *tert*-butyl hydroperoxide

TBP – *tert*-butylperoxide

THF – Tetrahydrofuran

THP – Tritylhydroperoxide

tpa – Tris(2-pyridylmethyl)amine ligand

UV – Ultraviolet

UV-Vis – Ultraviolet-visible

v – Scan rate

w – Weak

Symbols

δ – Chemical shift

ν – Stretching mode

λ – Wavelenght

ε – Molar absorptivity

λ_{max} – Maximum absorption wavelenght

$\Delta\varepsilon$	– Molar circular dichroism
χ_M^P	– Magnetic molar susceptibility
δ_v^p	– Shift in frequency for an internal inert reference
ν_o	– Frequency of the NMR spectrometer
χ_M^{dia}	– Diamagnetic constant
μ_{eff}	– Magnetic moment

CHAPTER 1

Introduction

I – Introduction

I.1 – Preamble

In the last decades, the field of synthetic chemistry has been fulfilled with more environmentally-friendly and economical procedures, based on the Green Chemistry principles. Catalysis has played significant roles in these concepts, due to its application in about 80% of industrial processes nowadays, such as active pharmaceutical ingredients, cosmetics and dyes, granting much more sustainable, selective and efficient synthetic routes than the previous non-catalytic techniques.[1] Organometallic compounds, especially those containing late-transition metals from 2nd and 3rd rows of the periodic table, are well established catalysts for a wide spectrum of reactions, but their inherent toxicity and high cost represent serious drawbacks. Hence, the search for more viable alternatives to these transition metal compounds began at the end of the 20th Century and good candidates are, for example, complexes of the 1st and early 2nd row transition metals, where iron and molybdenum compounds stand out due to their biological and environmental relevance and increasing role in catalytic reactions. Iron has a very important biological role and is the most abundant transition-metal in the biosphere, being the fourth most abundant element in the earth's crust. It is cheap, exhibits relatively low toxicity and meets economic and environmental requests that must be present in Green Chemistry procedures.[2] Molybdenum compounds play an important role in industrial catalysis and in chemical and photooxidation processes, being also an essential trace element found in a broad range of enzymes, responsible for the growth and other relevant roles in many organisms.[3]

In this Chapter will be presented an overview of the state-of-the-art of sustainable catalytic procedures regarding arene coupling mediated by iron complexes, especially the work developed in homo and cross-coupling of 2-naphthol and substituted derivatives, and epoxidation of olefins catalysed by iron and molybdenum complexes.

I.2 – Iron-catalyzed carbon-carbon bond forming reactions

Carbon-Carbon bond forming reactions (C-C reactions) represent one of the major group of reactions in Organic Chemistry, playing a central role in the synthesis of many industrial and relevant fine chemicals such as active pharmaceutical ingredients, polymers, natural products, pesticides, fragrances, flavours and dyes. Innovation and study of these reactions comes with huge importance in the improvement of existing synthetic processes, as well as in the synthesis of new compounds of interest in relevant scientific fields of industry, cosmetics, medicine, and others. Among the vast examples of C-C bond forming reactions existing today, metal-

mediated coupling transformations represent an important type of these synthetic procedures. The work developed by Ullmann[4] in the beginning of the 20th century in the copper-promoted cross-coupling of arenes set the starting point for the study of these type of reactions.

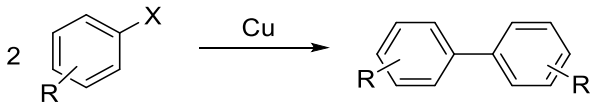

X= I, Br
R= Alkyl, aryl

Scheme I-1: Schematic representation of the Cu-promoted Ullmann coupling.

Copper remained the catalytic reference element for these synthetic procedures until the early 1970´s, when palladium-catalysed reactions emerged as the prime catalytic choice, owing to the pioneering work developed by Heck,[5] Suzuki,[6] Sonogashira[7] and others. Palladium-promoted reactions can generally occur under milder conditions and with a broader range of substrates when compared with reactions catalysed by copper, therefore justifying the choice of this metal as catalyst.[8]

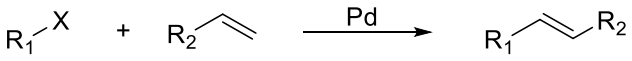

X= I, Br
R_1, R_2= Alkyl, aryl

Scheme I-2: Schematic representation of the Heck cross-coupling reaction between an alkyl halide and a terminal alkene unit.[5]

Notwithstanding the clear dominance and importance of palladium-mediated cross-coupling methodologies nowadays the development of more sustainable and less toxic procedures naturally emerged. Within that purpose, iron-catalysed cross-coupling reactions may be an interesting alternative for the traditional metal-mediated C-C coupling reactions. Iron made one of its first appearances in coupling reactions after Dianin and von Richter[9] reported, in 1873, the synthesis of 1,1'-bi-2-naphthol (BINOL), by oxidative coupling of 2-naphthol, using iron(III) chloride or potassium hexacyanoferrate(III) as catalyst.

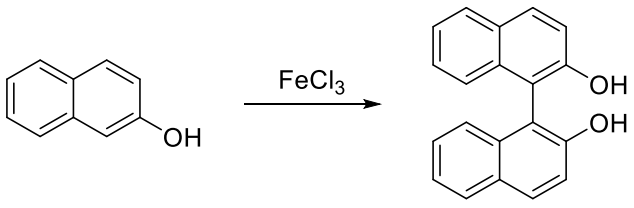

90%

Scheme I-3: Homocoupling reaction of 2-naphthol with iron(III) chloride as catalyst, firstly reported by von Richter[9] in 1873.

Some decades after, Kharasch[10] reported studies in the synthesis of biphenyl by reacting phenylmagnesium bromide and bromobenzene.[11,12] In 1971, Kochi and co-workers developed the first iron-catalysed cross-coupling reactions of alkenyl halides with Grignard reagents, even before the appearance of palladium and nickel methodologies.[13,14] After a gap of approximately 30 years iron-mediated coupling processes seem now back in force, which is possible to note by the growing number of publications issued since the beginning of the millennium. Examples of iron-promoted homo- and cross-coupling reactions (i) between electrophilic (alkyl, alkenyl, alkynil, aryl) substrates and Grignard reagents; (ii) between two previously activated substrates (from previous inclusion of halogen, sulfonate, phosphate, carboxylate and chalcogen moieties); (iii) by C-H activation and (iv) by decarboxylative and decarbonylative coupling have been widely reviewed in literature.[12,15,16,17]

I.2.1 – Coupling reactions of arene units by C-H activation

The regioselective synthesis of biaryls typically make use of transition-metal-catalyzed coupling reactions between an haloarene unit and (i) a stoichiometric amount of an organometallic reagent (**Scheme I-4**, b), with X_2= MgBr) or (ii) a previously functionalized arene unit, as in the example of Suzuki coupling reaction which utilizes aryl boronic acids or aryl boronate esters (**Scheme I-4**, b), X_2= $B(OR)_2$). To assure high regioselectivity and efficiency, the referred methods demand previous functionalization of either one or both coupling substrates by adding functional groups (**Scheme I-4:** a), which often requires purification of reagents and products by means of several synthetic operations and utilization of harsh reaction conditions. These regular necessities are normally time-demanding and tend to increase production costs and generate huge amounts of hazardous waste in these procedures.[18] Thus, it is recognized the need of alternative methods to reduce the environmental impact and associated expenditures with these synthetic methods. Such has prompted great interest in the development of new coupling methods to avoid the undesirable issues of traditional aryl-aryl bond formation methods, and more recent methods for the synthesis of such compounds rely on C-H bond activation of either one or both aromatic coupling reactants (**Scheme I-4**, c and d).[18,19]

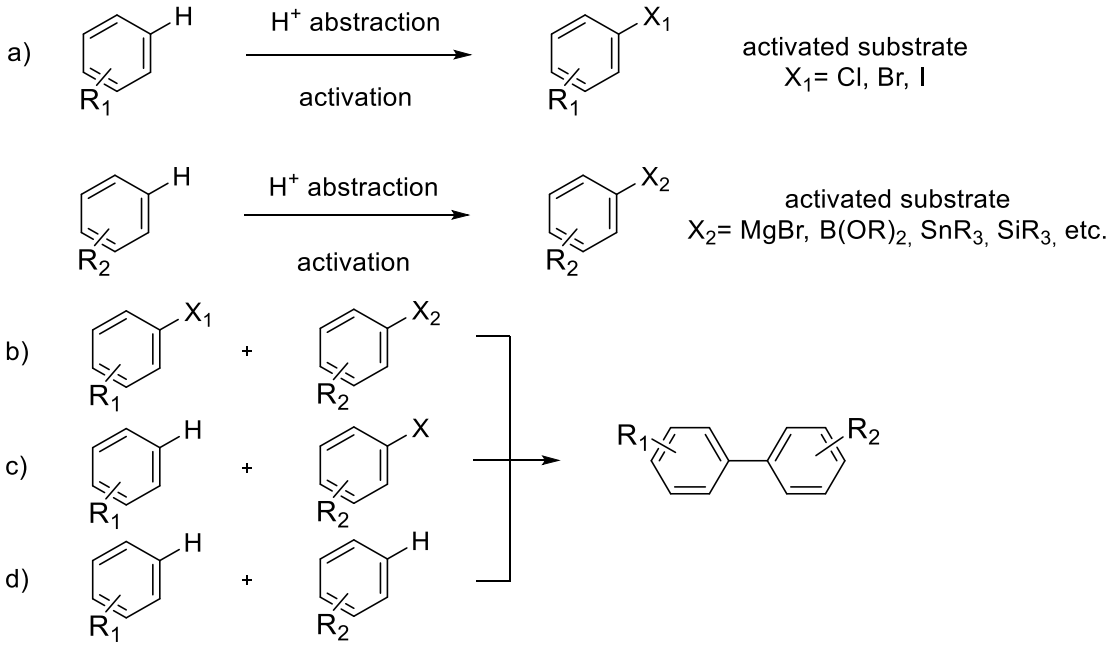

Scheme I-4: General representation of arene cross-coupling methodologies: a) activation of both coupling partners by previous functionalization; b) cross-coupling reaction between two previously functionalized substrates; c) single C-H bond activation coupling reaction; d) double C-H activation coupling reaction.[19]

Two main procedures exist to perform C-C coupling of arenes by C-H activation: (iii) direct arylation with aryl (pseudo)halides (single C-H bond activation), where an activated substrate, either an aryl halide or an organometallic/carbonylative reagent, undergoes a C-C bond formation with an unfunctionalized arene in the presence of a metal catalyst (**Scheme I-4**, c)[18,19,20] ; (iv) dehydrogenative arylation (double C-H activation), consisting on oxidative C-C reaction by activation of two C-H bonds (**Scheme I-4**, d).[18,19,21] Both coupling procedures are capable of high regioselectivity and efficiency, but single C-H activation still demands previous insertion/removal of functional groups in one arene unit and treatment of the corresponding residues. The second approach retains, as main advantage, the significant increase of reaction efficiency without pre-activation of substrates, thus it is a much “greener” and atom economical methodology. Even so, the strength and multiple availability of C-H bonds turn this approach quite demanding thermodynamically and less regioselective.[19] The careful selection of reaction conditions and ligand structures of the metal catalyst can be essential to overcome these issues; reaction conditions need to be controlled to avoid formation of undesired products, ligand steric and electronic nature can be essential to promote regioselectivity.[19,22]

Palladium and other 2nd row metal-promoted coupling reactions of arenes by C-H activation have been extensively revised in the literature,[14,15,22,23] and even acknowledging their

importance nowadays such procedures fall beyond the scope of this work and will not be discussed. Iron-catalysed homo and cross-coupling reactions of arenes by C-H activation are well reviewed in the literature,[11,18,19,23,24,25] counting with significant developments especially since the beginning of the 21st century, and some of the more relevant works regarding these subject will be presented below.

I.2.1.1 – Iron-mediated direct arylation with aryl (pseudo)halides and an unfunctionalized arene unit

Iron-promoted direct arylation is a relatively recent catalytic procedure. The iron source utilized is normally an Fe(III) salt which is mixed into the reaction in catalytic amounts with a *N,N*-donor ligand, forming *in situ* the active catalytic species or its precursor. The unactivated arene unit then reacts with an aryl Grignard reagent, often in the presence of an oxidant which is typically an alkyl dihalide or peroxides.

The first appearance of an iron-mediated oxidative coupling of arenes by direct arylation was reported by Nakamura and co-workers[26] in 2008 (**Scheme I-5**). The authors managed to couple 2-arylpyridines, 2- and 6-arylpyrimidines and 2-phenylpyrazole with arylzinc reagents and an Fe(III) source ($Fe(acac)_3$). The regioselectivity of the C-H bond activation at the *ortho*-position of the aryl group was directed by the nitrogen atom present at the pyridyl moiety of the substrate. Yields up to 99% of the respective products were obtained and, in some cases, di-substituted products were formed. The usage of additives has shown to be crucial for the success of the reaction: 1,2-dichloro-2-methylpropane (DCIB) worked as an oxidant and 1,10-phenanthroline coordinates to iron, contributing to a redox cycle of iron with DCIB, which acts as an electron acceptor.[26]

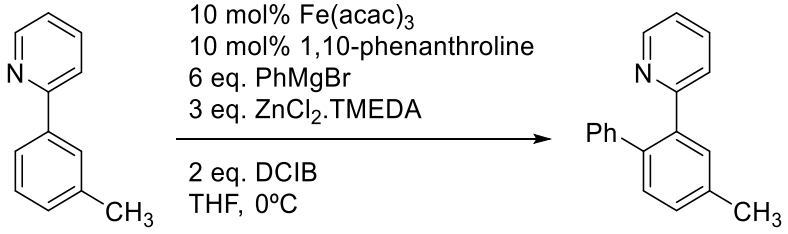

TMEDA= *N,N,N′,N′*-tetramethylethylenediamine 82%

Scheme I-5: Iron-catalyzed arylation of 2-arylpiridines by directed single C-H bond activation.[26]

Later, Yu and co-workers[27] presented the first iron-promoted Suzuki-type coupling of arylboronic acids and unactivated aromatic compounds. Utilizing arylboronic acids and benzene, catalysed in the presence of $Fe_2(SO_4)_3 \cdot 7H_2O$, the authors managed to obtain the corresponding coupling product in 31-83% yield (**Scheme I-6**). To grant such yields the

reaction needed to be carried out in air, with stoichiometric amount of the iron source, high temperatures and additives. Despite the need of a large quantity of iron precursor the requirement of stable and easy to handle reactants is an advantage of this transformation. This work set the starting point for the interest in iron-mediated Suzuki-coupling procedures for a large variety of aromatic substrates, *e.g.* pyrrole and pyridine,[28] quinones,[29,30] pyrazines, quinoxalines and quinolines.[31]

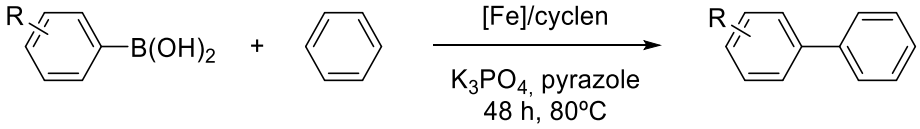

R= Cl, Br, CH_3, OCH_3, $COOCH_3$, COOH, NO_2 31-83%

Scheme I-6: Iron-mediated Suzuki-type coupling reaction between arylboronic acids and benzene.[27]

Several other interesting synthetic procedures were developed in the following years for iron-mediated direct arylation reactions, such as the oxidative coupling of heteroarenes and methyl amines by Itami, Wünsch and collaborators;[32] Nakamura and co-workers continued to contribute in the development of this synthetic procedure by presenting chemoselective *ortho*-arylation of arylimines[33] and arylation between arylpyridines and imines, which uses molecular oxygen as oxidant.[34] Cyanoarene compounds are of substantial interest in the preparation of dyes, herbicides, pharmaceuticals and other fine chemicals. Chen and collaborators[35] presented the first example of iron-mediated aromatic cyanation in 2011, using di- and trimethoxybenzenes as substrates (**Scheme I-7**). The optimized conditions allowed the usage of air or $PhI(OAc)_2$ as oxidants and FeI_2 as catalysts, but the usage of the second oxidant afforded better yields. Indole and 2-arylpyridine derivatives were also used as substrates in cyanation, utilizing similar reaction conditions and allowing the preparation of the corresponding products in moderate to good yields.[35]

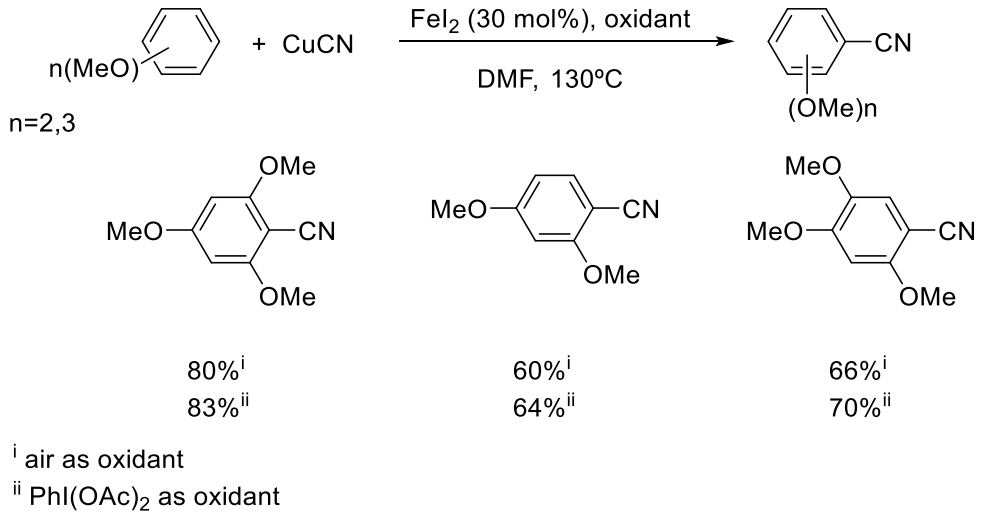

Scheme I-7: Iron-mediated cyanation of di- and trimethoxybenzenes.[35]

I.2.1.2 – Iron-mediated dehydrogenative arylation

As previously mentioned, dehydrogenative arylation is based on the oxidative C-C coupling between two unfuntionalized arenes by activation of two C-H bonds. Iron-promoted dehydrogenative arylation is an older synthetic procedure in comparison to direct arylation, with examples described in the literature since the 19th Century.[9] The vast majority of these reaction procedures rely in the usage of soft synthetic conditions such as moderate temperatures, oxygen from air, peroxides or peracids as oxidants and Fe(III) salts as coupling agent, typically iron(III) chloride, which is environmentally-friendly and inexpensive. This procedure revealed to be very useful in racemic dehydrogenative arylations and count with an extensive number of Fe(III)-promoted reactions revised in the literature between phenols, catechols, anilines, azarenes, furans and thiophenes.[16]

Asymmetric dehydrogenative arylation of phenols allows the preparation of axially chiral biaryls and a relevant example is the asymmetric coupling of 2-naphthol which yields BINOL, an important biaryl compound whose enantiomeric atropisomers have become, since the fall of 20th Century, among the most widely used ligands for both stoichiometric and catalytic asymmetric reactions, by exploiting their application as chiral inducers in asymmetric reactions.[36] The preparation of chiral coupling products of 2-naphthol and derivatives count with examples reviewed in the literature utilizing copper(II),[37] vanadium(V)[38] or iron(III)[39] catalysts. In the present work the focus will be on iron(III)-mediated processes and the most relevant examples will be presented below.

In 2009, Katsuki and collaborators[40] presented the first example of Fe(III)-promoted asymmetric coupling of 2-naphthol, catalysed by (di-μ-hydroxido)iron-salan complexes using air as oxidant at 60ºC, in the absence of any kind of additives (**Scheme I-8**). The authors also tested similar homocoupling reactions with C3-, C6- or C7-substituted 2-naphthol derivatives, and some conclusions were obtained: (i) complex **1** in **Scheme I-8** presented the best enantioselectivities and moderate to good yields in homocoupling reactions of C6- and C7-substituted substrates, irrespectively of the electronic effects preconized by the substituents; (ii) complex **2** in **Scheme I-8** depicted moderate to excellent yields and enantioselectivities for C3-substituted substrates, especially those containing bulkier substituents. This proved to be an excellent result since 3,3'-dissubstituted BINOLs are very valuable chiral inducers and very hard to synthesize.[40]

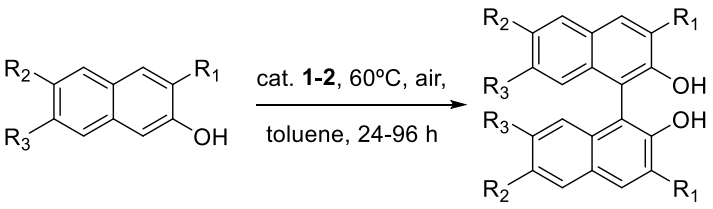

R_1= H, R_2= H, R_3= H; yield= 87% with **1**, 72h, (ee= 64% (*R*))
R_1= H, R_2= Br, R_3= H; yield= 93% with **1**, 72h, (ee= 47% (*R*))
R_1= H, R_2= MeO, R_3= H; yield= 79% with **1**, 24h, (ee= 56% (*R*))
R_1= H, R_2= H, R_3= MeO; yield= 86% with **1**, 48h, (ee= 74% (*R*))
R_1= Ph, R_2= H, R_3= H; yield= 93% with **2**, 24h, (ee= 93% (*R*))
R_1= Me, R_2= H, R_3= H; yield= 89% with **2**, 72h, (ee= 77% (*R*))

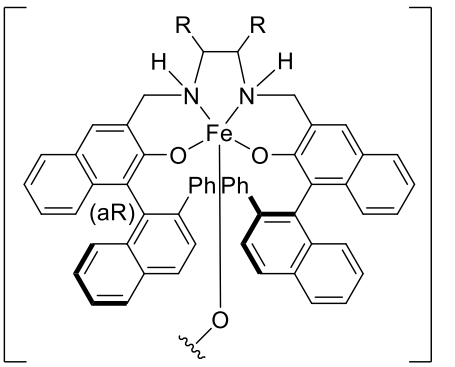

1: (a*R*, *S*), R= -$(CH_2)_4$-

Scheme I-8: Homocoupling reactions of C3-, C6- and C7-substituted 2-naphthol reported by Katsuki and Egami.[40]

Katsuki and collaborators[41] extended their studies with this system in cross-coupling procedures, obtaining C_1-symmetric BINOLs. Such compounds are normally hard to synthesize and there was a scarcity of literature reports regarding the use of iron complexes in these reactions. Asymmetric oxidative cross-coupling of substituted 2-naphthols normally yields two homocoupling and one cross-coupling compounds (**Scheme I-9**).

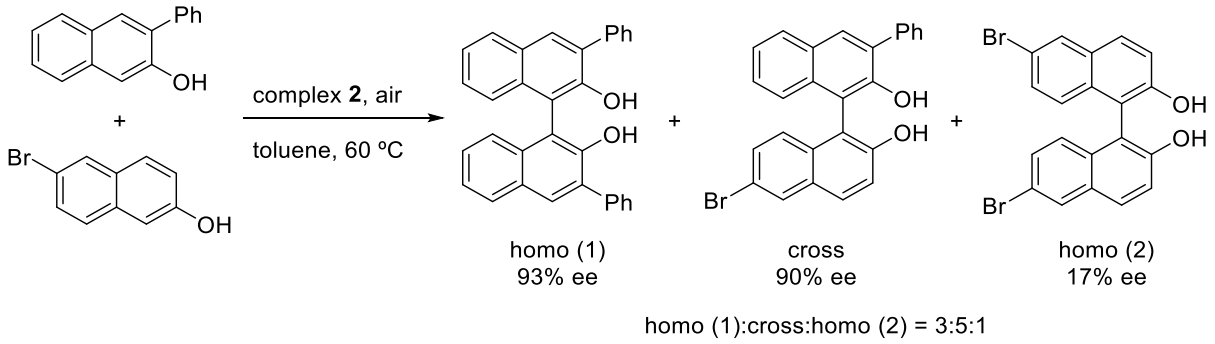

Scheme I-9: Example of asymmetric aerobic oxidative coupling of two 2-naphthols carried out by Katsuki and co-workers.[41]

The authors further concluded that (i) cross-coupling preferentially occurs. Homocoupling products were obtained in a greater extent to 2-naphthols containing electron donating substituents in C3 or C6 positions, but cross-coupling products still show higher yields; (ii) higher differences in the electron-richness of the cross-coupling partners granted higher cross-coupling yields; (iii) the presence of a C3-substituent revealed to be crucial for moderate to excellent enatioselectivities; the combination of a C3-substituted 2-naphthol and a less electron-rich 2-naphthol, either with or without a C3 substituent, would yield higher enantioselectivities.

After these observations some kinetic studies were executed, indicating that the coupling of 2-naphthols is first order dependent on 2-naphthol and dioxygen concentrations and no coupling reaction occurred in inert atmosphere. Also, the relationship between the enantiomeric excess of both Fe(III) complex and cross-coupling products was linear, indicating that possibly the dimeric (di-μ-hydroxido)iron-salan complex dissociate in solution and form a monomeric species. Mixing complex **2** with 3-bromo-2-naphthol confirmed this hypothesis since a monomeric Fe(III)-salan species containing a coordinated naphthoxido ligand was identified and isolated.

The referred observations and kinetic studies allowed the authors to propose a radical-anion coupling mechanism, presented in **Scheme I-10**. Complex **2** dissociates in solution and is in equilibrium with monomeric species **A** and **A'**, formed after coordination of 2-naphthols with electron-donating and electron-withdrawing groups, respectively. Due to its more electron-rich nature, monomeric species **A** is oxidised faster than **A'** to give **B**, and a more electron-deficient 2-naphthol preferentially binds to **B** after dissociation affording **C**, in which a phenolic proton shifts between the two phenolic oxygen atoms, preferentially. Intermediate **C** can be converted to **A** via proton and hydrogen atom abstraction and subsequent ligand exchange. Based on

the kinetic studies and in the fact that species **A** is isolable, the rate-determining step (r.d.s.) of this oxidation was attributed to the step from **A** to **B**. Conformation of **B** seems to play a crucial role in the determination of the stereochemistry of this coupling.

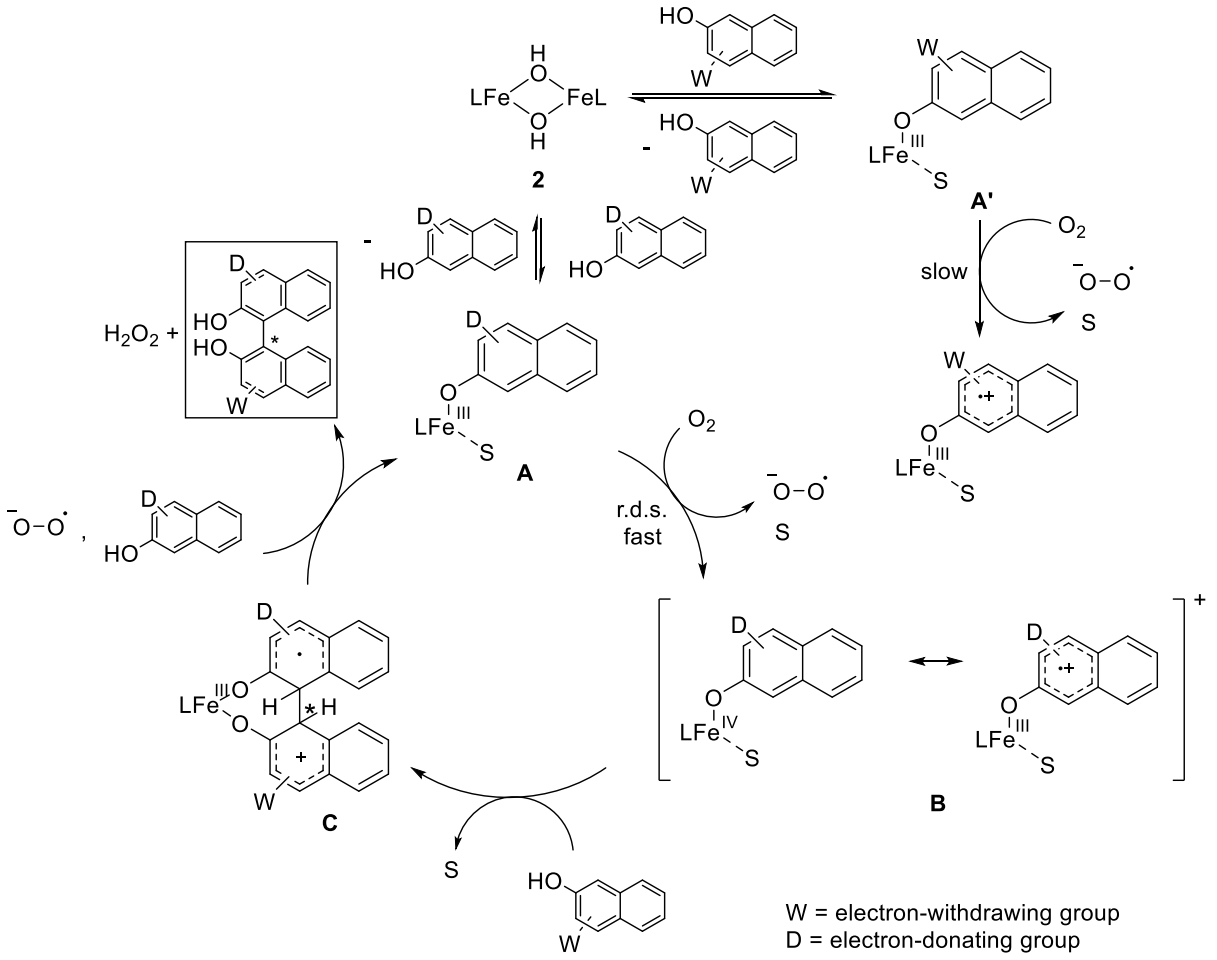

Scheme I-10: Proposed catalytic cycle by Katsuki and co-workers[41] in the aerobic oxidative cross-coupling of substituted 2-naphthols, catalysed by (di-μ-hydroxido)iron-salan complexes.

In 2016, Pappo and co-workers[42] prepared novel chiral Fe(III) phosphate complexes as pre-catalysts for the enantioselective oxidative coupling of 2-naphthol and C6- or C7-substituted derivatives with *tert*-butylperoxyde as terminal oxidant. Within the applied catalytic conditions, complex **3** mediated homo- and cross-coupling of these substrates with a high degree of optical purity and moderate chemoselectivity, allowing the preparation of C_1- and C_2-symmetric BINOLs (**Scheme I-11**). Regarding 2-naphthol coupling, this catalytic system proved to be more selective towards the formation of enantiopure BINOL in comparison to the Katsuki (di-μ-hydroxido)iron-salan system.[40]

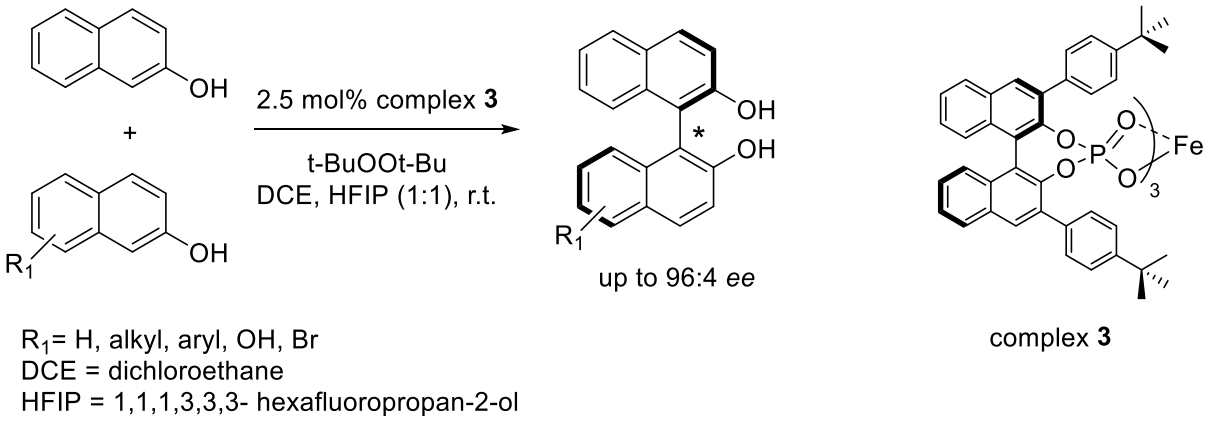

Scheme I-11: Catalytic enantioselective cross-coupling between 2-naphthol and C3- or C6-substituted 2-naphthols reported by Pappo and co-workers.[42]

This reaction was also tested with molecular dioxygen as terminal oxidant and in inert atmosphere, but low conversions and enantiomeric ratios were observed in both cases in comparison to values obtained with *tert*-butylperoxyde as terminal oxidant. A kinetic study of the oxidative coupling of 2-naphthol with catalyst precursor **3** showed a first-order dependence of the reaction rate on the concentration of 2-naphthol and a zero-order dependence on the terminal oxidant, and these results were consistent with the radical-anion coupling mechanism proposed by Katsuki. Therefore, the authors proposed a catalytic cycle, presented in **Scheme I-12**, which starts with coordination of the peroxide to the iron complex **3**, followed by cleavage of the peroxide bond, generating a high-valent intermediate species **D**. Intermediary species **E** is formed after substitution of a phosphate ligand in **D** by a naphtholate unit. Then, a single electron transfer (SET) occurs, forming an electrophilic naphthoxyl radical species **E**' which undergoes radical-anion coupling with a second nucleophilic 2-naphtholate coupling partner, affording intermediate **G**. During the ligand exchange between a phosphate unit and (*R*)-BINOL, an undesired competitive SET process occurs (**G**↔**H**) resulting in reduction of the optical purity of the product.

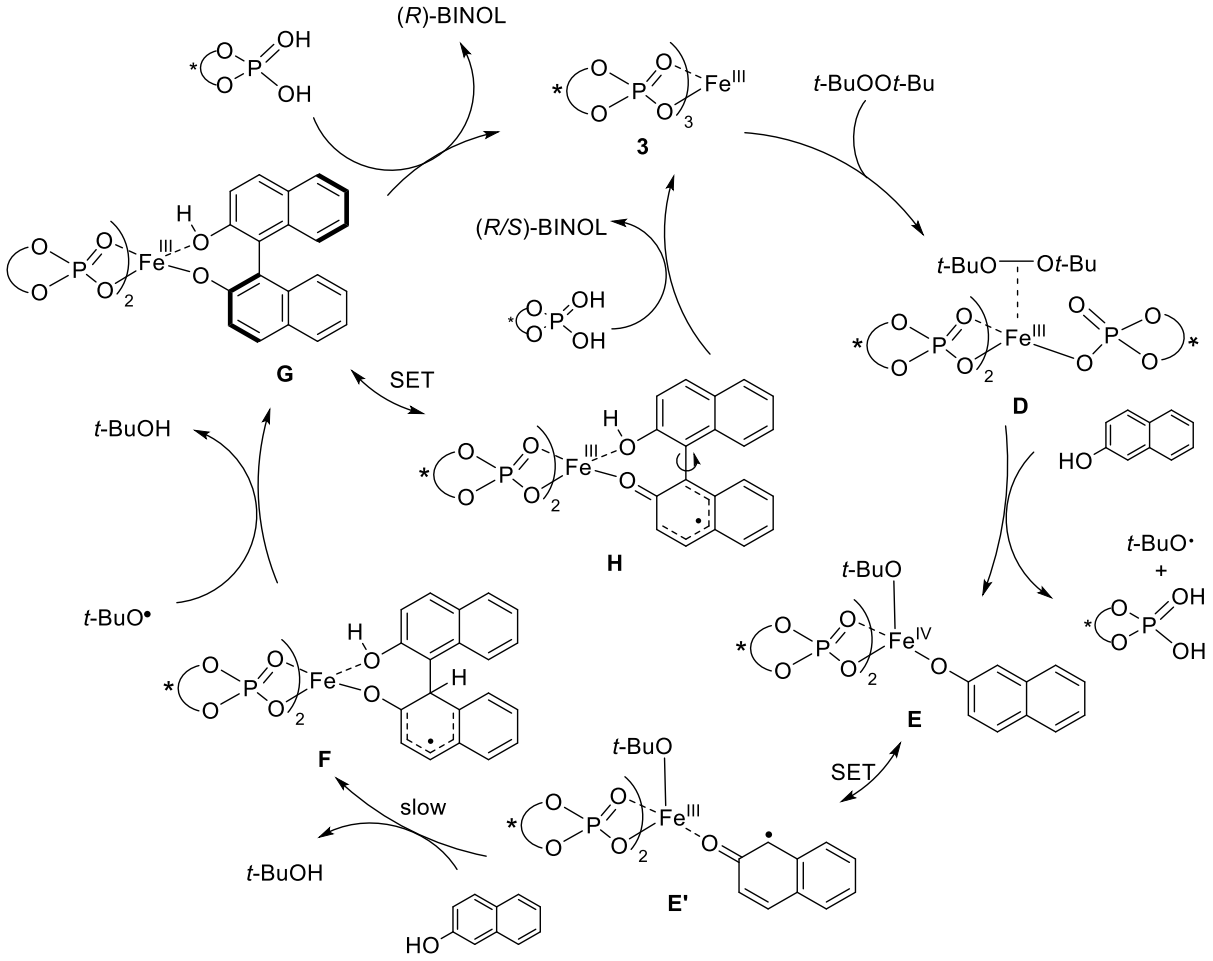

Scheme I-12: Proposed catalytic cycle by Pappo and co-workers in the oxidative coupling of 2-naphthol, catalysed by chiral Fe(III) phosphate complex **3**.[42]

The main advancement of this catalytic process relies in the great selectivity towards the preparation of nearly enantiopure homo- and cross-coupling products. Such results are possible due to the suppression, to a high extent, of an undesired secondary racemization observed by the authors during optimization of the catalytic reaction conditions and previously observed by Kočovski[43] and Brusee,[44] during their early works on oxidative coupling of 2-naphthol by stoichiometric amounts of Cu(II)-chiral amine complexes.

I.3 – Iron and molybdenum-catalyzed epoxidation reactions

Epoxidation of olefins is a type of reaction of high importance in both chemical industry and academic environment. At a laboratorial scale, important examples of epoxidations have appeared since the beginning of the 20th Century, such as the Prileschajew and Weitz-Scheffer epoxidations,[45] whereas catalytic asymmetric epoxidations have gained increasing importance and relevance in the last 40 years. Excellent examples are the Katsuki-Sharpless epoxidation[46] of allylic alcohols and the Jacobsen-Katsuki epoxidation[47,48] of unfunctionalized alkyl- and aryl-

substituted olefins, both catalysed by titanium(IV) and manganese(II) homogeneous catalysts, respectively. Undoubtedly, these two distinct processes represent the greatest breakthrough in homogeneous catalysis in the field of asymmetric epoxidation of olefins.

In this introduction homogeneous asymmetric epoxidation reactions catalysed by iron and molybdenum compounds will be briefly reviewed, and some examples of these procedures will be presented.

I.3.1 – Non-Heme iron-catalysed olefin epoxidations

Iron-catalysed epoxidation procedures are often inspired on natural models (biomimetic), and in the last 30 years synthetic porphyrin-based heme-iron complexes have been widely studied as catalysts for epoxidations, in the attempt to mimic the oxygen transfer reactions of cytochrome P450 family of enzymes, whose active site contain a heme-iron center tethered to the protein via a cysteine-thiolate ligand.[49,50] A simplified representation of the accepted catalytic mechanism of oxygenation by cytochrome P450 is showed in **Scheme I-13**.[50,51,52] Substrate binds to the metal center, inducing an electron transfer from NADPH via cytochrome P450 reductase or another associated reductase. Then, molecular oxygen binds to the resulting ferrous heme center, affording a dioxygen adduct, which suffers a second electron transfer, reducing the Fe-O_2 adduct into a Fe-peroxido species. The peroxido group rapidly protonates twice, releasing one molecule of water and forming a ferryl species (oxido-iron(IV) porphyrin cation radical, Fe(IV)=O), a highly reactive intermediate to which is attributed the role of the reactive oxidative species. The ferryl species then oxidises the substrate molecule, which is released, and the enzyme returns to its original state, completing the catalytic cycle.[51] During the 1970´s was reported that several oxygen donors such as periodate, peroxy acids, peroxides or iodosylarenes were able to complete a short-circuited catalytic cycle for the oxygenation of cytochrome P450, named “shunt”, and successful epoxidation of olefins were demonstrated by this alternative.[50,51] This observation set the starting point in the mimetization of cytochrome P450 models in oxidations of organic substrates in general and in epoxidation of olefins in particular.

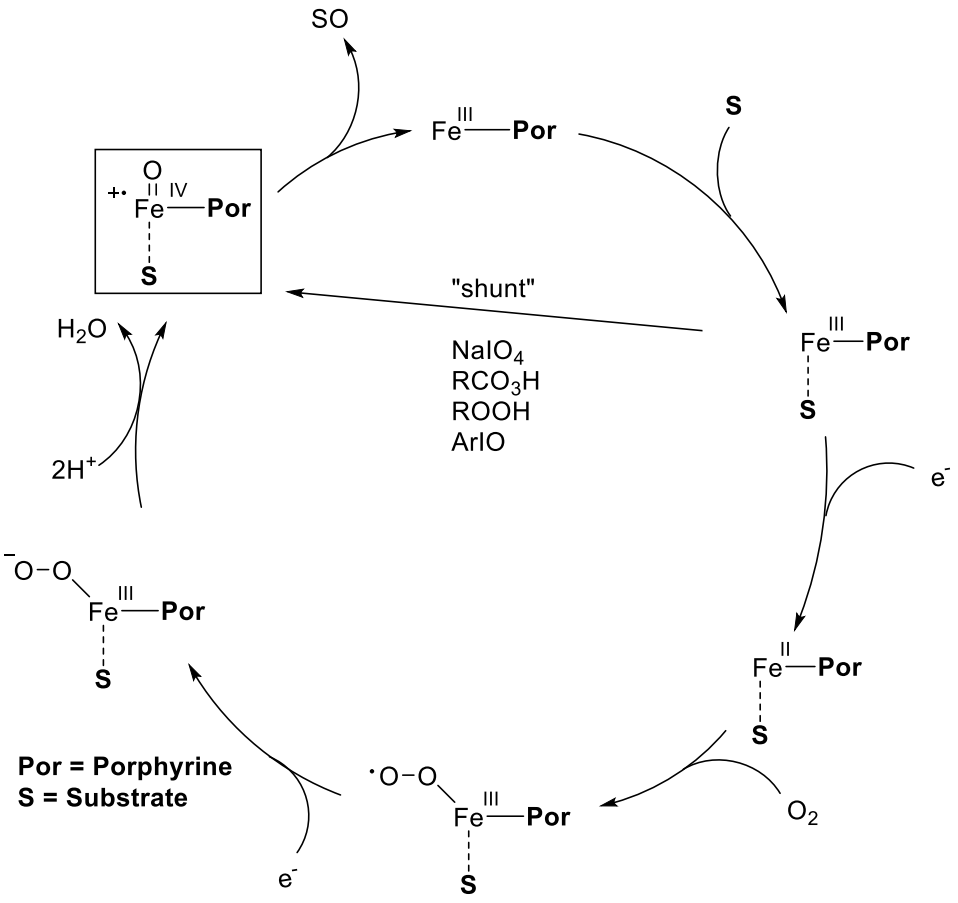

Scheme I-13: Simplified catalytic cycle of oxygenation reactions by cytochrome P450. The short-circuited “shunt” mechanism is also represented.[51]

After the “shunt” mechanism observation, the major class of iron complexes designed to mimic the behaviour of cytochrome P450 enzymes in the epoxidation of olefins were porphyrin-based complexes. Despite the great importance of these compounds, some drawbacks can be pointed on their preparation and catalytic applications, which are common in the metalloporphyrin chemistry: (i) the synthesis of the porphyrin ring system demands extensive purifications; (ii) harsh reaction conditions are normally applied in their synthesis; (iii) porphyrin compounds are typically obtained with very low global yields; (iv) use of toxic reagents in the catalytic reactions, (*e.g.* iodosobenzene as oxidant).[50,53] Some of these concerns may justify the increasing interest on epoxidation procedures using non-heme iron catalysts since early 2000’s, seeking easier structural and electronic fine tuning and more appealing synthetic procedures. In addition, the utilization of non-heme iron catalysts might provide much “greener” solutions to epoxidations, while the development of a universal non-heme iron catalyst for epoxidations remains a challenge, especially in the case of tri-substituted, tetra-substituted electron deficient and terminal olefins.[54,55] It is within the scope of this introduction to present the state-of-the-art of non-heme homogeneous iron catalysts for enantioselective epoxidation

of olefins, which has been widely reviewed in the literature.[53,54,56] Notwithstanding the great influence and importance of heme-based iron catalytic systems, those type of compounds will not be referred in this work.

Iron-mediated epoxidation of olefins typically uses an Fe(II) or Fe(III) catalyst, obtained *in situ* or after isolation, with chiral *N*-donor ligands. Since the 1970's that several reports appeared in the literature regarding iron salts or complexes used as catalysts for iron-mediated epoxidation of olefins with H_2O_2, an environmentally-friendly oxidant.[54,56] Que Jr. and co-workers[54,56,57] presented in 1986 the first example of synthetic binuclear iron complexes capable of racemic olefin epoxidation with H_2O_2, based on a natural non-heme enzymatic model, hemerythrin, which holds O-O bond activation properties. The homologue asymmetric procedures appeared in 1996 with the work of Jin and co-workers,[58] introducing a chiral dinuclear Fe(III) catalyst for enantioselective epoxidations.

The development of epoxidation processes with more environmentally benign and inexpensive oxidising agents like H_2O_2 or aerobic O_2 motivated Jacobsen and co-workers[59] to develop catalytic systems capable of enantioselective epoxidation of olefins in a "greener" way. In attempts to discover new efficient catalytic systems, several polymer-supported metal-ligand combinations were synthesized, with the ligands being prepared from chiral amino-acids containing a variety of donor side chains. A total of 5760 Fe(II)-ligand combinations were screened for epoxidation of *trans*-*β*-methylstyrene, using H_2O_2 as oxidant. Low enantioselectivities and good conversions were obtained, with an example of these systems being depicted in **Scheme I-14**.

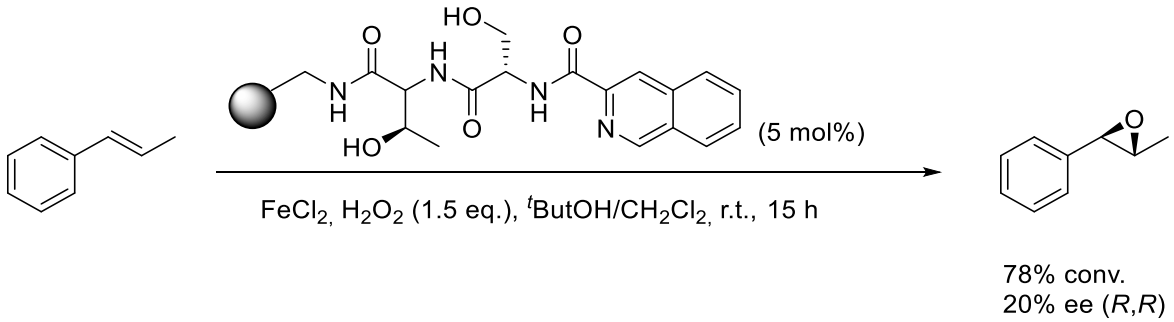

Scheme I-14: Example of an enantioselective epoxidation procedure of *trans*-*β*-methylstyrene made by Jacobsen and co-workers.[59]

In a following study, the same authors prepared a catalytic Fe(II)-system presented in **Figure I-1**, containing the tetradentate *N,N′*-dimethyl-*N,N′*-bis(2-pyridylmethyl)-1,2-diaminoethane ligand (bpmen), based on the attempt to mimic the oxidation behaviour of methane monooxygenase (MMO), a non-heme enzyme with excellent catalytic properties for the selective hydroxylation of small hydrocarbons, also capable to catalyse olefin epoxidation.

During this study it was observed that the addition of a stoichiometric amount of acetic acid in the reaction mixture could drastically reduce reaction times and catalyst loadings, resulting in an increase in both selectivity and activity towards epoxide formation.[60]

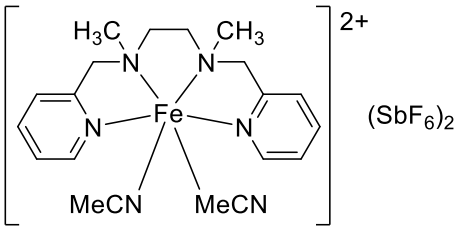

Figure I-1: Fe(II)-bpmen complex sinthesized by Jacobsen and co-workers[60] and applied as catalyst in enantioselective olefin epoxidation, based on the attempt to mimetize the oxidation behaviour of MMO.

These observations motivated further catalytic and mechanistic studies in the attempt to identify the active oxidative species and in understanding the influence of acetic acid in the increase of epoxide selectivity in these reactions.[61,62] In attempts to mimic Rieske dioxygenases (RDO), Que Jr. and co-workers[63] studied olefin oxidations with H_2O_2 catalyzed by a group of non-heme iron(II) complexes such as $[Fe(bpmen)]^{2+}$, $[Fe(tpa)]^{2+}$ and their 6- and 5-methyl-substituted derivatives, presented in **Figure I-2**. Ligand tpa stands for tris(2-pyridylmethyl)amine.

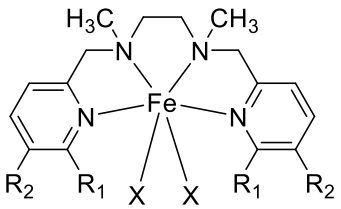

$[Fe(bpmen)(MeCN)_2](ClO_4)_2$

4: $R_1 = R_2 = H$

$[Fe(bpmen)(OTf)_2]$

5: $R_1 = CH_3$, $R_2 = H$
6: $R_1 = H$, $R_2 = CH_3$

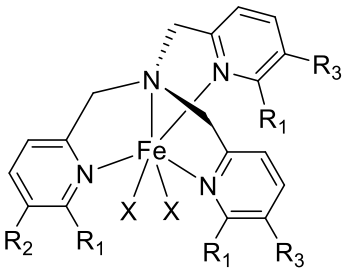

$[Fe(tpa)(MeCN)_2](ClO_4)_2$

7: $R_1 = R_2 = R_3 = H$
8: $R_1 = CH_3$, $R_2 = R_3 = H$
9: $R_1 = R_3 = H$, $R_2 = CH_3$
10: $R_1 = R_2 = H$, $R_3 = CH_3$
11: $R_1 = H$, $R_2 = R_3 = CH_3$

Figure I-2: Fe(II)-bpmen (**4**-**6**) and Fe(II)-tpa (**7**-**11**) compounds synthesized by Que Jr. and co-workers.[63]

The referred study was very important in order to understand the formation of the active oxidising species and the origin of the labelled oxygen atom into the olefin during the oxidation. In the catalytic conditions applied by the authors for the epoxidation of cyclooctene, using H_2O_2 with or without added H_2O and in the absence of acetic acid as co-reagent, both *cis*-dihydroxylations and epoxidations occur and are derived from the reactivity of a common Fe(III) hydroperoxido intermediate, Fe(III)-OOH, responsible for the formation of the active oxizyding

perferryl-oxido species, Fe(V)=O, in these reactions. The mechanism of formation of Fe(III)-OOH suggested by the authors is presented in **Scheme I-15**, where an excess of H_2O_2 proved to be essential for the formation of the Fe(III)-OOH intermediate.

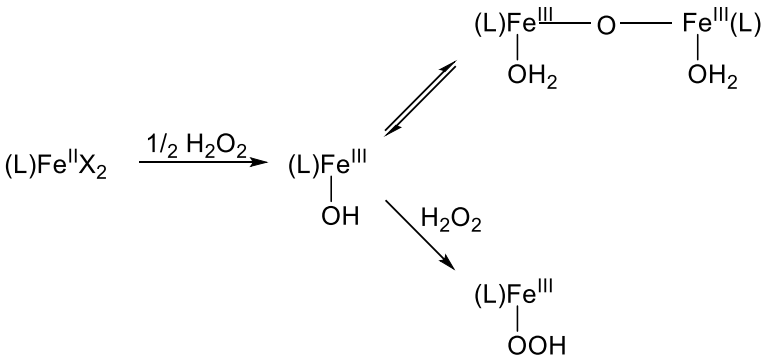

Scheme I-15: Formation of Fe(III) peroxide, Fe(III)-OOH, after addition of H_2O_2 into the catalytic reaction mixture.[63]

The authors also studied the influence of the ligand steric and electronic properties. Highly stereoselective epoxidation is favoured by catalysts with no more than one 6-methyl substituent, affording low-spin Fe(III)-OOH species (category A, compounds **4**, **5**, **7** and **8** in **Figure I-2**). On the other hand, *cis*-dihydroxylation is favoured by catalysts with more than one 6-methyl substituent, granting high-spin Fe(III)-OOH species (category B, compounds **6**, **10** and **11** in **Figure I-2**). By ^{18}O-labeling experiments, it was demonstrated that the incorporated oxygen in the epoxide and *cis*-diol products was derived either from the H_2O_2 or H_2O added into the reaction. A catalytic cycle was proposed by the authors and it is shown in **Scheme I-16**.

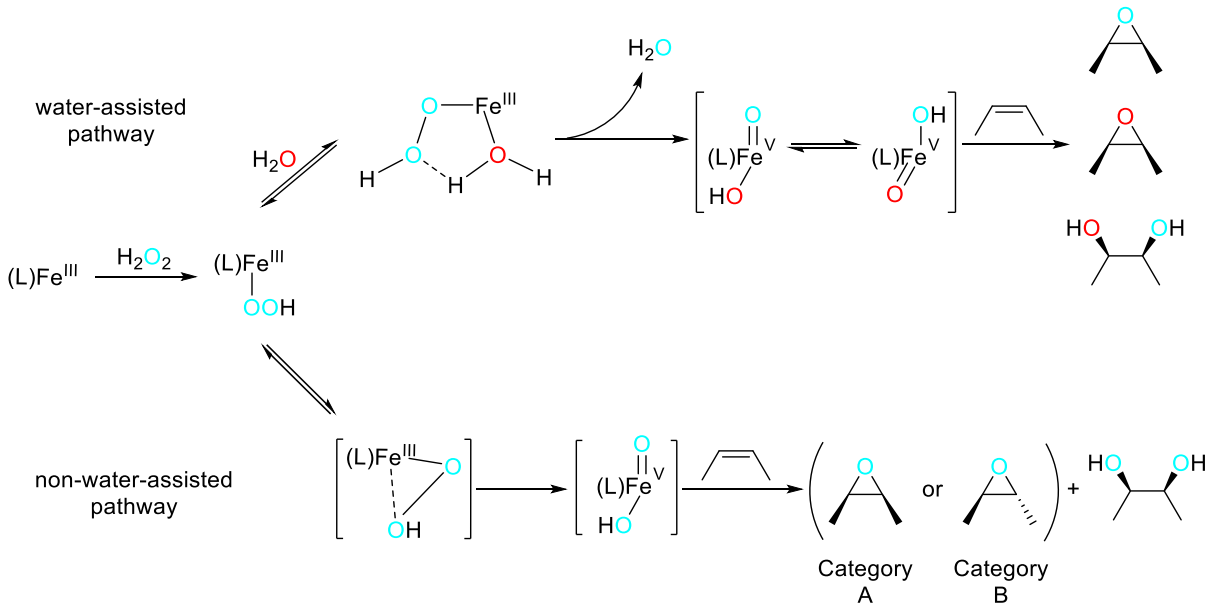

Scheme I-16: Mechanism of catalysis proposed by Que Jr. and co-workers.[63]

The lower branch of the proposed cycle accounts for the non-water-assisted pathway, where the stereoselective epoxide and *cis*-diols products obtained their oxygen atoms exclusively from H_2O_2. Stereoselectivity of the obtained epoxide is determined by the category of the catalyst used and the most effective are those from category A. The upper branch of the proposed cycle corresponds to the water-assisted pathway. Peroxide activation occurs by preequilibrium water binding to the adjacent labile site of Fe(III)-OOH, generating a five membered ring which will promote heterolysis of O-O bond to generate a *cis*-H^{18}O-Fe(V)=O oxidant. Partial labelling of the epoxide product with ^{18}O from $H_2{}^{18}O$ would occur by oxido-hydroxido tautomerism of the *cis*-H^{18}O-Fe(V)=O oxidant species, which would introduce ^{18}O into the terminal Fe(V)=O unit before the epoxide formation; *cis*-dihydroxylation entails the transfer of two oxygens from oxidant to substrate, where one derives from H_2O and other from H_2O_2.

Que Jr. and Fujita[61] studied the addition of AcOH and AcOOH as additives in the oxidation of cyclooctene with H_2O_2 with $[Fe(bpmen)]^{2+}$ and $[Fe(tpa)]^{2+}$ complexes as catalysts, motivated by the results obtained by Jacobsen and co-workers[60] with AcOH as additive and by Stack and co-workers[64] who reported $[\{(phen)_2Fe^{III}(OH_2)\}_2(\mu\text{-}O)]^{4+}$ as a highly efficient catalyst for epoxidation with AcOOH. Que Jr. and Fujita[61] observed, as Jacobsen and co-workers,[60] that addition of acetic acid to the reaction mixture increased both selectivity and activity towards epoxide formation. The authors proposed that the catalytic combination of iron complex/H_2O_2/AcOH may react to form a different oxidant *in situ*, namely peracetic acid, which then reacts with the iron complex forming the oxidising species. Such conclusion derived from the observation that the same products and yields were obtained for olefin oxidations catalyzed by Fe(bpmen) and Fe(tpa) with either AcOOH or H_2O_2 as oxidants in the presence of AcOH. Also, the reaction of $[Fe(tpa)]^{2+}$ complex with AcOOH resulted in stoichiometric conversion to the ferryl $[(tpa)Fe(O)]^{2+}$species, and the hypothesis that this ferryl species could be the oxidising species in the Fe/H_2O_2/AcOH system gained strength.

Que Jr. and co-workers[65] then developed efforts in attempts to elucidate the epoxidation mechanism involved in the iron complex/H_2O_2/AcOH system and in determining the most probable oxidising species. In an extensive and complete study in the epoxidation of cyclooctene with the $[Fe(tpa)]^{2+}$/H_2O_2/AcOH system, the authors concluded that the ferryl $[(tpa)Fe(O)]^{2+}$species was not the oxidising intermediate formed *in situ*, as expected, even observing that this ferryl species was present in the epoxidation reactions. After inducing the preformation of the ferryl species in solution, it was observed that (i) epoxide yield was lower that 10% relative to Fe(IV)=O, far lower than the previous observed results by Que Jr. and Fujita[61] (ii) addition of an excess of AcOH to the Fe(IV)=O solution prior to the addition also

afforded low yields. The authors proposed the following mechanism of the epoxidation of olefins with the Fe/H_2O_2/AcOH system, presented in **Scheme I-17**.

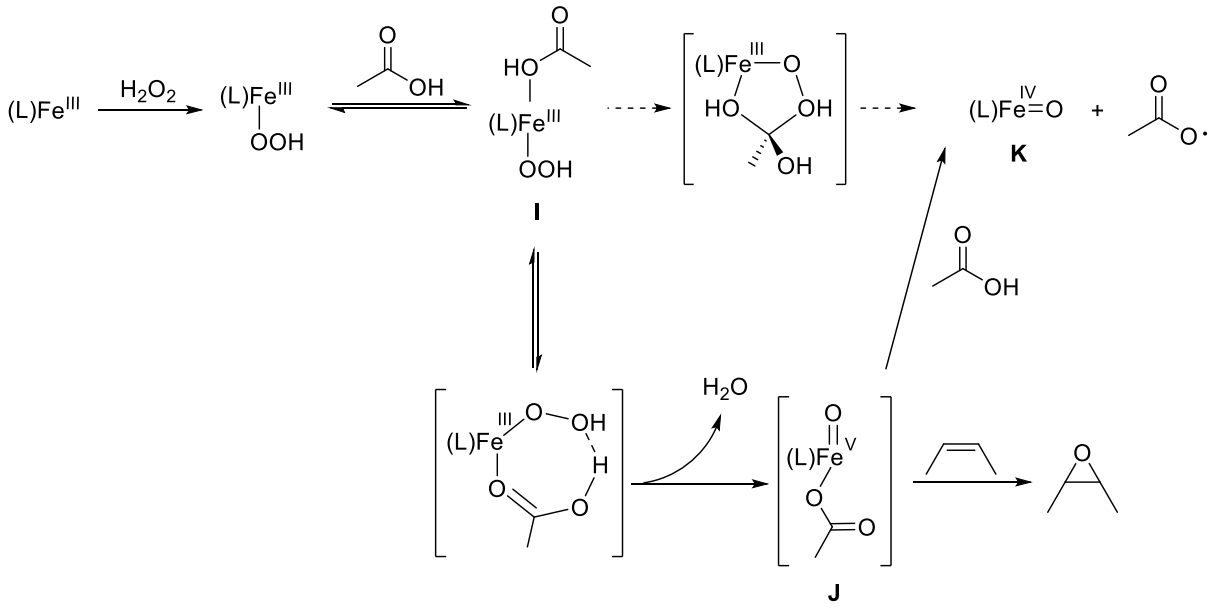

Scheme I-17: Acetic acid-assisted mechanism proposed by Que Jr. and co-workers.[65]

The epoxidising species formed *in situ* is the species **J**, derived from O-O heterolysis of species **I**, promoted by a previously bound acetic acid unit. Once formed, species **J** is a powerful enough oxidant to epoxidise olefins or, in the absence of these substrates, to the oxidation of the coordinated carboxylate, which generates **K** and the corresponding carboxyl radical. Finally, the high selectivity of **J** species for epoxide formation is also justified. Epoxides are obtained after nucleophilic attack of the olefin on the oxido group of the oxidising species, whereas *cis*-dihydroxylation results from attack of the olefin on the hydroxido ligand. By adding AcOH to the reaction mixture, this additive will compete with residual H_2O in the formation of the Fe(V)=O species of the acetic-acid-promoted pathway. Thus, attack of the olefin on the bound acetate may be much less favoured than attack on the oxido group, so epoxidation becomes the dominant reaction in the presence of AcOH.

The work of Que Jr. and co-workers in the understanding of Fe/H_2O_2/AcOH systems for the epoxidation of olefins was a major development. Since then, several work developments were reviewed in the literature,[53,54,56] and some examples will be presented.

In 2007, Beller and co-workers[66] developed the first truly Fe(III) catalytic system for enantioselective epoxidation of styrene derivatives, with H_2O_2 as oxidant. Till then, only low enantioselectivities were reported in similar processes with the same oxidant.[60,66] Driven by this observation, the authors developed the referred catalytic procedure, achieving excellent yields and enantioselectivities (up to 97%) in the case of non-terminal substrates. The chiral

iron catalyst was generated *in-situ* from $FeCl_3 \cdot 6H_2O$ and with ethylenediamine-based ligands. Pyridine 2,6-dicarboxylic acid (H_2Pydic) was found to be an optimal additive affording high enantioselectivities for sterically hindered substrates. Lower *ee* values were observed in the case of terminal alkenes (8-26%, **Scheme I-18**).

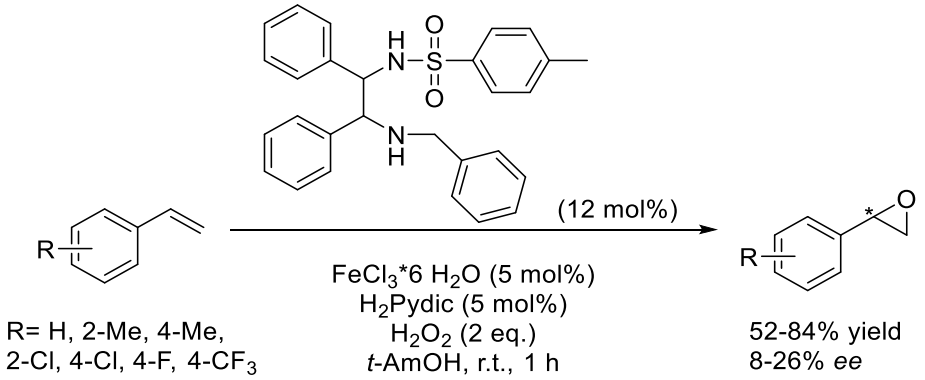

Scheme I-18: Enantioselective epoxidation of styrene and styrene derivatives performed by Beller and co-workers.[66]

Beller's work inspired others to develop enantioselective iron-catalysed olefin epoxidation protocols with H_2O_2 as oxidant. Kwong and co-authors[67] reported the enantioselective epoxidation of α-substituted styrenes with a chiral diiron μ-oxido-sexipyridine complex, resulting in 43% *ee* in the best examples. After the successful epoxidation of β-β-substituted enones done by Yamamoto and co-workers,[68] which represents the first enantioselective iron(II)-based catalytic system reported for these types of substrates, Sun and co-workers[69,70] managed to epoxidise α-substituted-unsaturated ketones (chalcones), employing H_2O_2 as oxidant, AcOH as additive and a chiral Fe(II)-ethylenediamine-pyridine-based complex as catalyst (**Scheme I-19**). Excellent yields and enantioselectivities were achieved in the epoxidation of these substrates, but the same system was not capable of epoxidising terminal olefins.

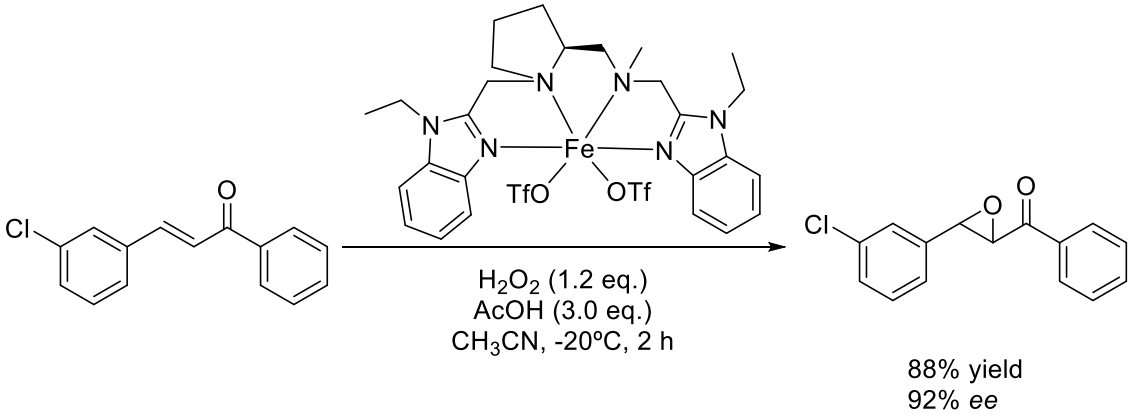

Scheme I-19: Example of enantioselective epoxidation of chalcone derivatives performed by Sun and co-workers.[70]

In 2013, Costas and co-workers[71] presented several aminobipyridine-based iron(II) complexes suitable to epoxidise olefins and α,β-unsaturated ketones, concluding that both effects of (i) functional groups in the pyridyl moiety of the ligands and (ii) the bulkiness of the carboxylic acid additive can influence stereoselectivity and yields obtained for the resulting epoxides. Therefore, the authors confirmed complex **12** as the best catalyst precursor, possessing a *para*-positioned electron-donor substituent in the pyridyl moiety of the ligand (dimethylamino group, -NMe_2, **Scheme I-20**), which was active for a wide range of substrates, with H_2O_2 as oxidant and with addition of catalytic amounts of carboxylic acids. Excellent yields and *ee* values were reported, with (*S*)-ibuprofen and 2-ethylhexanoic acid proving to be the best acid additives. Additional work was reported by the same authors with design perspectives on biologically-inspired non-heme iron catalysts for asymmetric epoxidation of olefins[72] and for enantioselective epoxidation of cyclic aliphatic enones.[73]

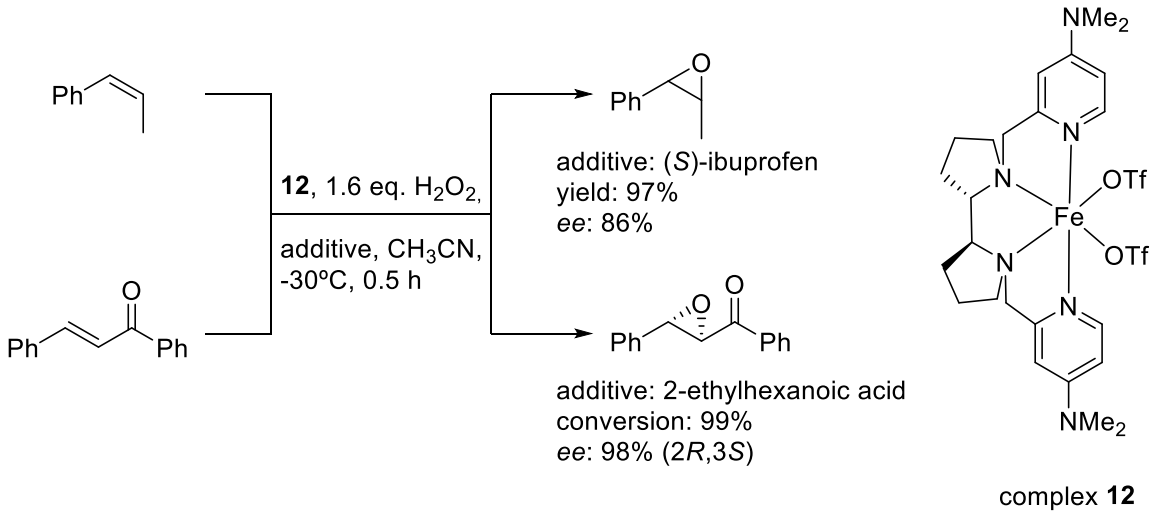

Scheme I-20: Enantioselective epoxidation carried out by Costas and co-workers of olefins and α,β-unsaturated ketones with complex **12**, an aminobipyridine-based iron(II) complex.[71]

I.3.2 – Mukaiyama olefin epoxidations

The Mukaiyama-Yamada or Mukaiyama epoxidation of olefins is a type of aerobic oxygenation which uses molecular dioxygen as oxydant and an aldehyde as co-reagent, with or without the presence of a metal catalyst (**Scheme I-21**).

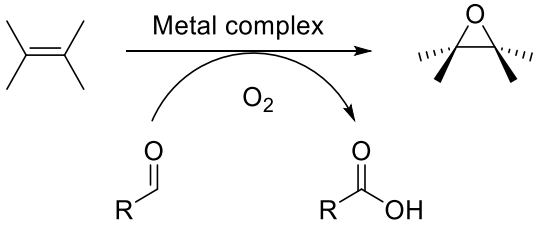

Scheme I-21: Schematic representation of metal-assisted Mukaiyama epoxidation of olefins.

After Mukaiyama-aldol coupling discovery in 1973[15] several Mukaiyama-type reactions appeared especially since the 1990's, such as sylil enol ethers oxigenation,[74] Baeyer-Villiger oxidations[75] and olefin epoxidations,[76,77,78,79] among others.[80,81] Epoxidation reactions under Mukaiyama conditions typically are executed for 2 to 12 hours under mild temperatures, between 25ºC and 40ºC, with molecular oxygen normally bubbled into the reaction mixture containing an aldehyde and the target olefin substrate. The most utilized aldehyde is isobutyraldehyde but other aliphatic or alicyclic aldehydes are also used or tested such as acetaldehyde, pivalaldehyde, cyclohexanocarbaldehyde or long-chained undecanal.

As previously mentioned, Mukaiyama epoxidation of olefins can occur in the absence of metal catalysts,[82] but a large number of examples of metal-mediated epoxidations have been

presented in the literature in the early 1990's.[51] One of the first applications of metal-mediated Mukaiyama-type epoxidations came with the epoxidation of norbonene and trisubstituted or 1,1-disubstituted alkenes catalysed by divalent nickel(II) complexes.[51] Epoxide yield was influenced by the structure of the aldehyde; both olefin conversion and epoxide yield were low when a linear aldehyde (*e.g.* butyraldehyde) was used as reductant, in contrast to the effect observed with the use of isobutyraldehyde or pivalaldehyde. Several other metal-complexes derived from different metal sources also present examples in the literature such as ruthenium(II), molybdenum(V), manganese(III), cobalt(II) and iron(II) compounds.[51]

The Mukaiyama epoxidation occurs through a radical mechanism (**Scheme I-22**). Mechanistic studies of this reaction were carried out in detail by Lassila and collaborators[83] in the metal-free epoxidation of many aliphatic olefins with several aldehydes and by Nam and collaborators[84] in the transition-metal-catalyzed epoxidation of several alkenes using isobutyraldehyde as co-reagent. Nam et al[84] concluded that in both the absence and presence of a metal complex acylperoxy radical, generated *in situ*, is the active epoxidising species (**Scheme I-22**, **A**). This radical can be formed either during an autoxidation process of the aldehyde with molecular O_2 (**Scheme I-22**, step **a**) or with the presence of a metal complex, which (i) plays a role in the initiation step of the radical chain process (**Scheme I-22**, steps **b** and **c**)[84,85] and (ii) in the stabilization of the acylperoxy radical **L**, originating **B** (**Scheme I-22**, step **e**).[84] The olefin then reacts simultaneously with **L** and **M**, yielding the desired epoxide (**Scheme I-22**, steps **d** and **e** respectivelly).

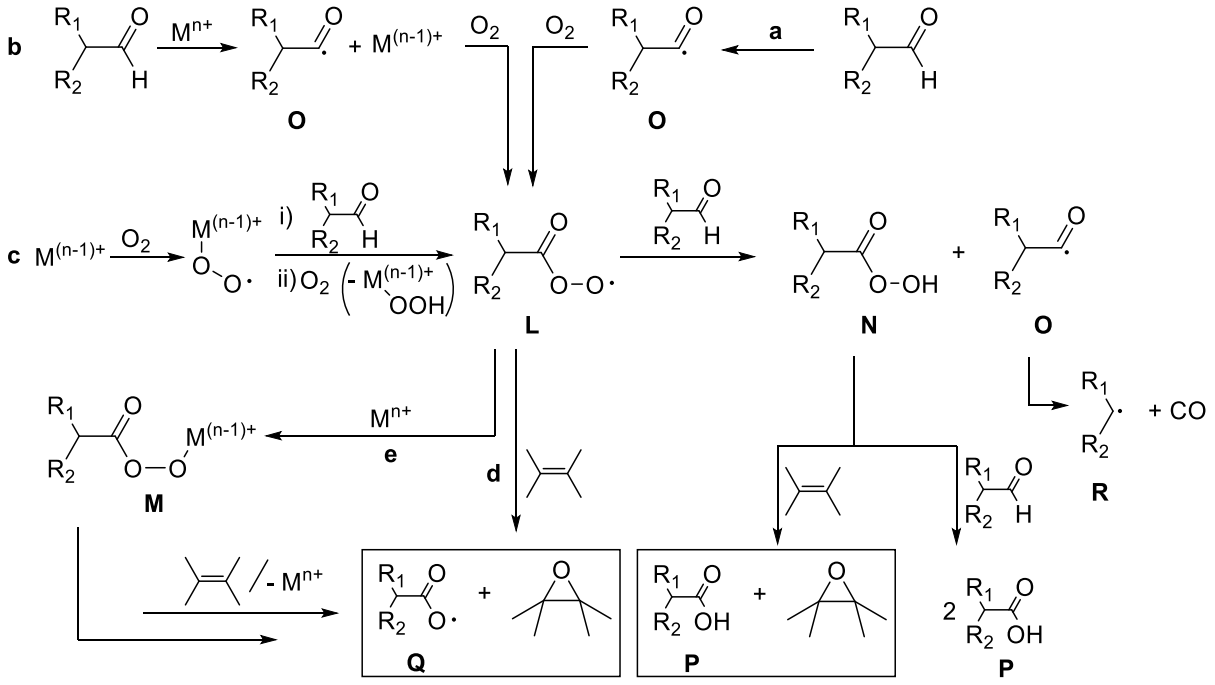

Scheme I-22: Mukaiyama epoxidation reaction mechanism based on studies developed by Nam with collaborators[84] and Feiters with collaborators.[86]

Lassila with collaborators[83] and Feiters with collaborators[86] detected several secondary products in the non-catalyzed and metal-promoted Mukaiyama epoxidation of olefins, respectively. Feiters and collaborators[86] referred a side reaction between **L** and aldehyde (**Scheme I-22**), responsible for the formation of peracid **N** and acyl radical **O**, which can (i) decarboxylate, yielding an alkyl radical **R** and carbon monoxide or (ii) propagate the autoxidation chain reaction **a**. Peracid **N** can either compete with **L** as an oxidising agent of the olefin in a non-radical pathway, or react with an aldehyde, yielding in both cases the respective carboxylic acid **P** (**Scheme I-22**).

Carbon dioxide and aldehyde-derived alcohol and ketone were also detected as side products, resulting from the radicalar propagation reactions presented in **Scheme I-23**.[83,86] Carbon dioxide is originated after the decarboxylation of an unstable carboxyl radical (**Q**, **Scheme I-22** and **Scheme I-23**), formed *in situ* from the reaction between **L** or **M** and the olefin. The resultant alkyl radical **R** from decarboxylation is further oxidised by O_2, yielding an alkyl peroxyradical which forms (i) an alkylhydroperoxide, **S**, after hydrogen abstraction and (ii) the tetroxide **T** by combination with another alkyl peroxyradical unit. This latter intermediate recombines itself, generating the respective ketone **U** and alcohol **V**. If the aldehyde used has no α-hydrogens, only **S** and CO_2 are obtained via this secondary reaction, as observed by Lassila.[83,86]

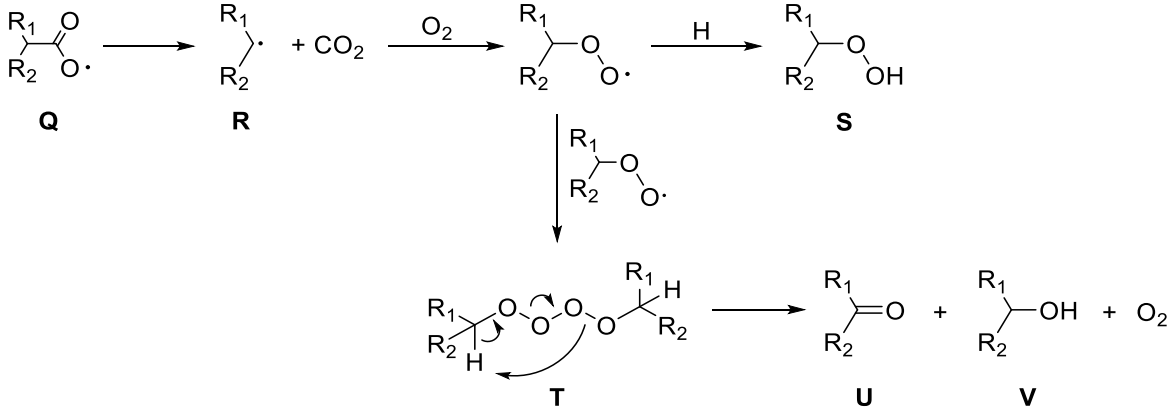

Scheme I-23: Mechanistic formation of side products observed by Lassila and collaborators[83] and Feiters and collaborators.[86]

I.3.3 – Molybdenum-catalyzed olefin epoxidations

Molybdenum(VI) complexes are important catalysts or catalyst precursors for oxygen-transfer reactions in chemical and biological systems.[87] For that reason, coordination chemistry of Mo(VI) has showed a great implementation in academic and industrial catalytic oxidations, as well as in relevant industrial processes such as olefin metathesis, ammoxidation of propene to acrylonitrile and olefin epoxidation.[88] Concerning this last example, these systems have proved to be efficient in the epoxidation of olefins with alkyl hydroperoxides. A very important example

of industrial process is the Halcon-ARCO process, which successfully oxidises propylene to propylene oxide with *tert*-butyl hydroperoxide (TBHP) as oxidant, and because of both economic and scientific importance of this reaction, it has been widely studied since 1970's.

One classical discussion among chemists is concerned with the mechanistic path occurring in these reactions: Mimoun and co-workers[89,90] reported the stoichiometric reaction between molybdenum peroxido complexes and olefins to yield epoxides; mechanistic studies suggested that peroxido complexes could be the active intermediary species in the reaction. The authors also suggested that the olefin directly coordinates to the metal centre, followed by an oxygen transfer from a peroxido group, yielding the final product (**Scheme I-24** a)). Later, in the same decade, Sharpless and co-workers[89,91] suggested four different oxygen-transfer mechanisms, the first one and also the most cited being depicted in **Scheme I-24** b)); they suggested that the active oxidant species is the alkyl hydroperoxide, which is first activated by coordinating to the metal and then promotes oxidation of the olefin, without interaction of the substrate with the Mo centre. The same authors later reported evidence that both peroxido and alkyl hydroperoxide intermediates formation can occur at the reaction medium, depending on the alkyl hydroperoxide and molybdenum source used, initiating the debate about the exact mechanism occurring in these reactions.[89]

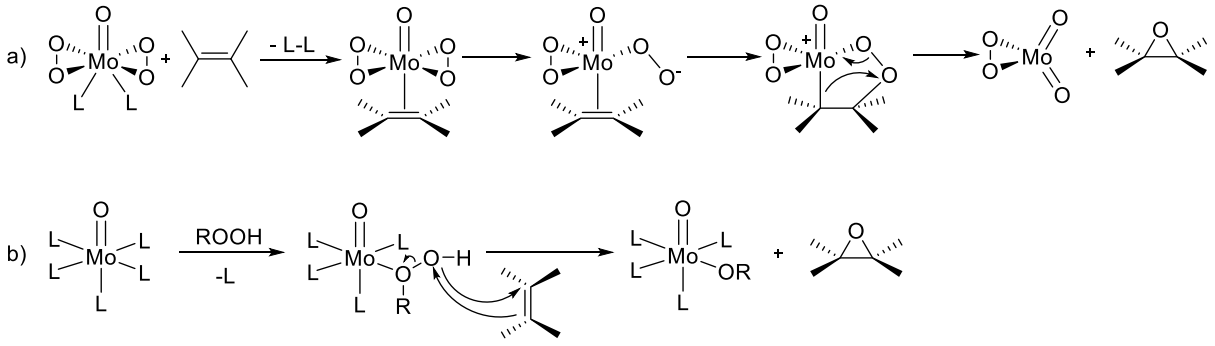

Scheme I-24: Proposed mechanisms for Mo(VI)-catalysed olefin epoxidation: (a) Mimoun proposal, with direct coordination of the olefin to a diperoxido-Mo(VI) complex;[90] (b) Sharpless proposal, where the alkyl peroxide directly coordinates to the Mo center before oxidation step takes place.[91]

Research in this topic followed in the next 20 years focusing on both racemic and enantioselective epoxidation of olefins with alkyl hydroperoxides as oxidants and Mo(VI) complexes as catalyst precursors. In respect to enantioselective procedures, since the early 2000's there was a breakthrough in asymmetric olefin epoxidation mediated by these systems, which is broadly reviewed in the literature.[92,93] The great majority of Mo(VI) complexes active in olefin asymmetric epoxidations hold chiral *N,O*-hetero-donor ligands on their structure, and in this introduction only the more relevant procedures in terms of enantioselectivity will be referred in more detail (**Figure I-3**, complex **13**).[92] Examples of chiral Mo^{II}-cyclopentadienyl-

based complexes have been also applied in asymmetric epoxidation of *trans*-β-methylstyrene, but with poor selectivity comparing with Mo(VI) homologues (**Figure I-3**, complex **14**).[94] Other important examples exist regarding Mo(VI) complexes bearing a cyclopentadienyl (cp) moiety π-coordinated to the metal center (**Figure I-3,** complex **15**), but most concern racemic epoxidation procedures. Therefore, these systems will not be discussed in this work.[88]

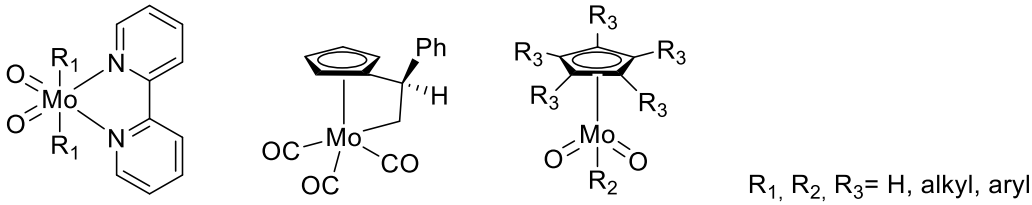

13 **14** **15**

Figure I-3: Representation of distinct molybdenum complexes used as catalysts for epoxidation reactions: **13**: Mo(VI) complex bearing a bis-pyridyl ligand; **14**: Mo(II) complex with a cp ligand; **15**: Mo(VI) complex with a cp ligand.

The first report of chiral active Mo(VI) complexes in enantioselective epoxidation of simple olefins appeared in 1979 by Schurig and co-workers,[95] where the authors reported the synthesis of an oxido-diperoxido-Mo(VI) complex bearing a bidentate chiral ligand ((*S*)-*N,N'*-dimethyl lactamide). Later, the authors explored the same catalytic systems but with several different enantiopure hydroxamides for the enantioselective epoxidation of aliphatic olefins.[96] In 2004, Shi and co-workers[97] reported the enantioselective epoxidation of *cis*-1-propenylphosphonic acid catalysed by three distinct Mo(VI) complexes, differing among them in the chiral ligand coordinated to the metal centre (complexes **16**, **17** and **18**, **Scheme I-25**). The best results were obtained when using complex **18** in CH_2Cl_2 with 30% aqueous H_2O_2 at 0ºC, with 100% conversion of the starting material and 80% *ee* of (**-**)-(*1R,2S*)-(1,2-epoxypropyl)phosphonic acid (fosfomycin), which is a clinically important drug with wide-spectrum of antibiotic activity.[97]

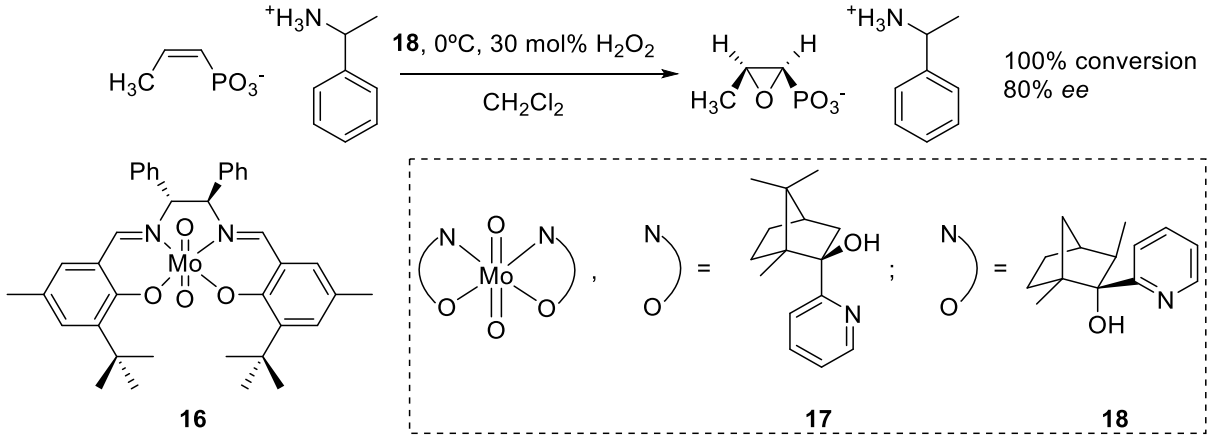

Scheme I-25: Enantioselective epoxidation of *cis*-1-propenylphosphonic acid performed by Shi and co-workers, catalysed by complex **16**. Other complexes used by the same authors are also depicted (**17** and **18**).[97]

Yamamoto and co-workers[98] reported in 2006 *in situ* obtained Mo(VI) complexes bearing chiral hydroxamic acids, which were suitable for the efficient enantioselective catalytic epoxidation of several mono-, di-, and tri-substituted olefins, using TBHP, cumene hydroperoxide (CHP) or tritylhydroperoxide (THP) as oxidants (**Scheme I-26**). It was verified that epoxidations using these systems proceeded smoothly at room temperature (r.t.) under air. The size of the ligands, combined with the degree of substitution of the alkene, played a central role in determining the rate of the oxidation. Yields and *ee* up to 92 and 96%, respectively, were obtained with the substrates used (example of epoxidation of dihydronaphtalene depicted in **Scheme I-26**), and good enantioselectivities were also observed for the epoxidation of squalene, a biological precursor of steroids and terpenoids.

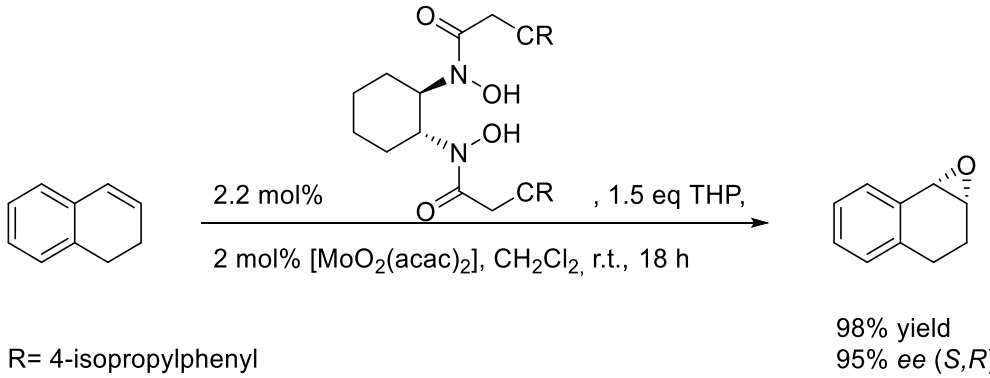

Scheme I-26: Mo-catalysed epoxidation of dihydronaphtalene by Yamamoto and co-workers.[98]

In 2009, Zhou and co-workers[99] presented the first example of *in situ* asymmetric epoxidation of styrene and styrene derivatives by Mo(VI) complexes with chiral aminoalcohols and their derivatives as ligands (**Figure I-4**). Epoxidation of styrene was performed using $MoO_2(acac)_2$ as the Mo(VI) source and a 1.1-fold excess of ligand, with TBHP as oxidant, in CH_2Cl_2 at room

temperature. Yields and *ee* of *ca.* 70% were obtained and these catalytic conditions were extended to other styrene derivatives. The addition of chiral natural amino acids led to low yields and *ee* of the referred substrates in the same conditions.

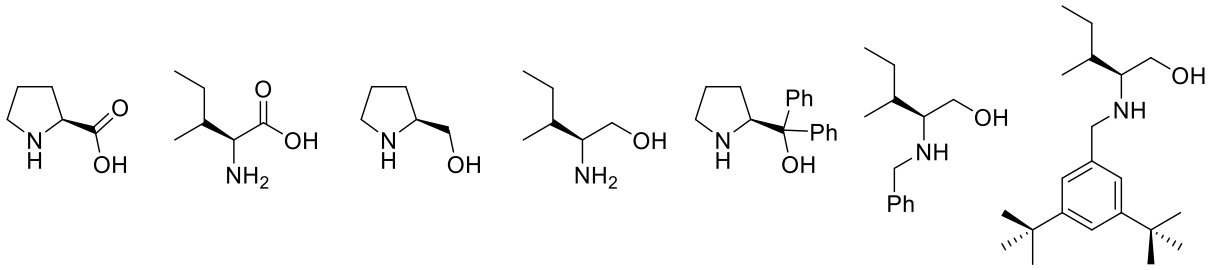

Figure I-4: Aminoacid and aminoalcohol ligands used by Zhou and co-workers.[99]

I.4 – Amino acid-derived complexes in oxidative catalysis

In the field of homogeneous catalysis, there are scarce examples of amino acid-derived complexes applied as catalysts in comparison to other families of coordination compounds. Some reports of these types of complexes appeared recently in oxidation catalysis, and the most relevant will be presented below.

Fujita and co-workers[100] reported in 1989 several aminoacid-derived V(V)=O-Schiff base catalysts for the asymmetric sulfoxidation of thioanisole, using TBHP as the terminal oxidant. The authors reported moderate to high sulfoxide yields but low enantioselectivities.

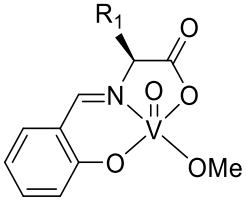

19: R_1= CH_3
20: R_1= Bn
21: R_1= ^{i}Pr

Figure I-5: Structural formulae of the amino acid-derived V(V)=O(Schiff base) compounds reported by Fujita and co-workers.[100]

In 1992, Inoue and co-workers[101] reported amino acid-derived *in situ* Ti(IV)-Schiff base catalysts with compounds **22**, **23**, **24** or **25** as ligands, for the enantioselective epoxidation of terpenoid-class substrates with 1,1-diphenylethyl hydroperoxide (**Figure I-6**). Moderate to high yields and enantioselectivities were obtained in the epoxidation of these substrates.

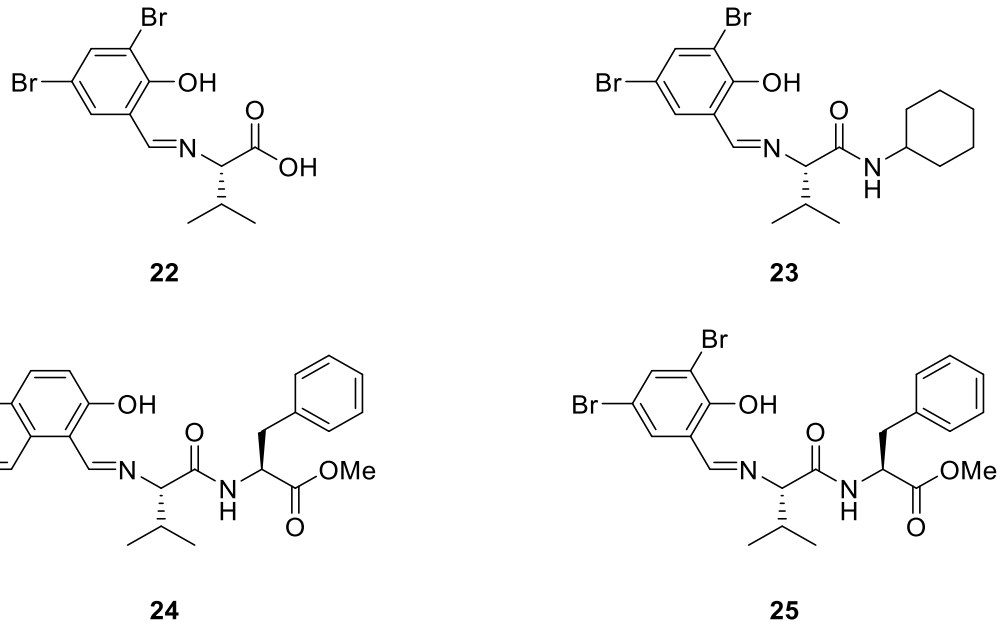

Figure I-6: Amino acid-derived compounds prepared by Inoue and co-workers,[101] further applied as ligands for the *in situ* preparation of Ti(IV)-Schiff base catalysts.

In 2002, Gong and co-workers[102,] reported several L-amino acid-based V(IV)=O complexes for the oxidative coupling of 2-naphthol and substituted derivatives using O_2 as oxidant (compounds **26**-**29**, **Figure I-7**). Moderate to excellent yields of coupling products were obtained with these systems, accompanied with enantioselectivities up to 98%. This system was further improved by Sasai and co-workers.[103,104]

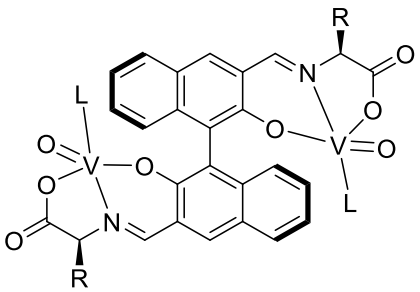

26: R= Bn L= Solvent
27: R= ^{i}Pr
28: R= ^{i}But
29: R= ^{t}But

Figure I-7: Structural formulae of the amino acid-derived V(IV)=O-Schiff base complexes sinthesized by Gong and co-workers[102]

Maeda and co-workers[105] in 2004 synthesized several amino acid-derived V(IV)=O and V(V)=O-Schiff base systems and studied their application in asymmetric thioanisole oxidation (complexes **30**-**38**, **Figure I-8**). Sulfoxide product yields obtained were up to 90%, but enantioselectivities observed were low; the best results were obtained with complex **36** with

20% *ee*. Later, in 2011, Chen and co-workers[106] reported a V(V)=O-Schiff base complex derived from L-*tert*-leucine with catalytic activities in the asymmetric aerobic oxidation of α-hydroxy-ketones to 1,2-diketones, with nearly enantiopure products with complex **39** (**Figure I-8**).

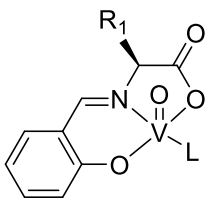

30: R_1= H
31: R_1= ^{i}Pr
32: R_1= CH_3
33: R_1= ^{i}But
34: R_1= ^{sec}-But
35: R_1= $CH_3SCH_2CH_2$
36: R_1= $H_2NCH_2(CH_2)_3$
L= solvent

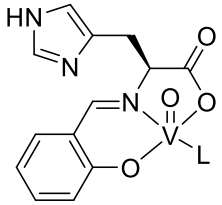

37

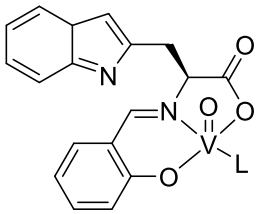

38

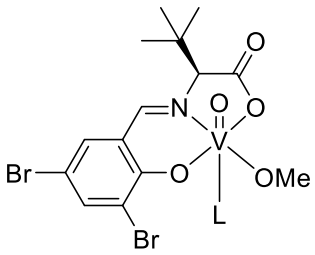

39

Figure I-8: Structural formulae of the amino acid-derived VO(Schiff base) complexes sinthesized by Maeda and co-workers[105] (complexes **30**-**38**) and Chen and co-workers[106] (complex **39**).

More recently, Adão and co-workers[107] synthesized several aminopyridine-L-amino acid derived Cu(II) complexes and studied their performance as catalysts for the oxidative coupling of 2-naphthol, using O_2 as the oxidant (complexes **40**-**44**, **Figure I-9**). Moderate to low enantioselectivities were observed in these catalytic systems in the presence of a basic additive such as morpholine. Addition of inorganic additives such as KI showed a general slight increase in BINOL yield and enantioselectivity.

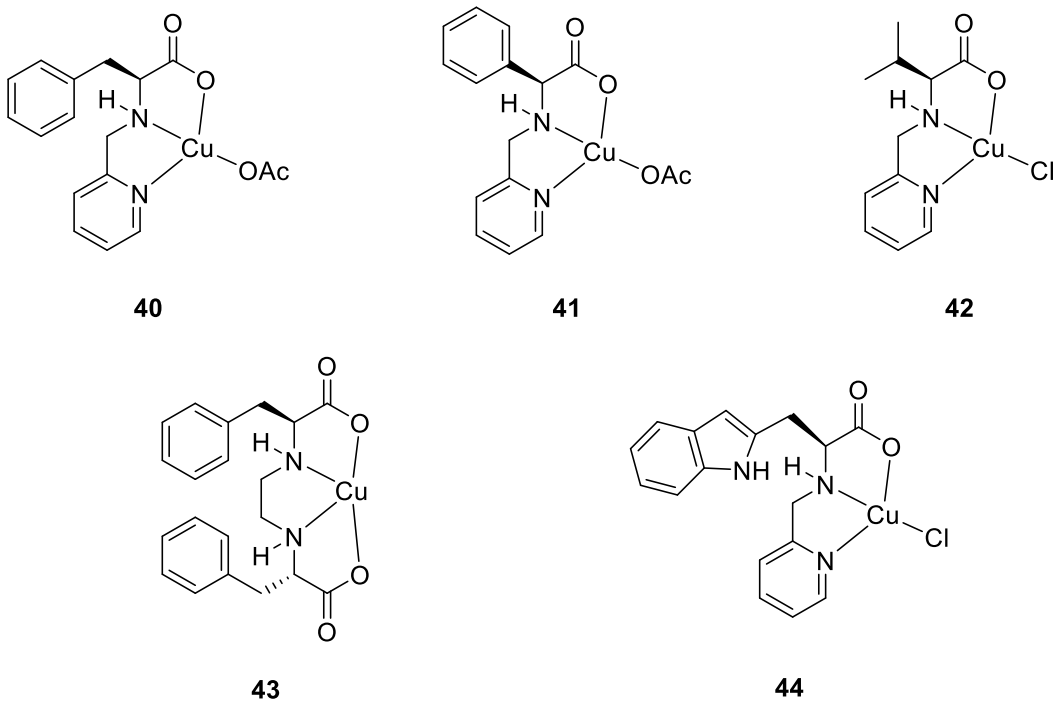

Figure I-9: Structural formulae of the aminopyridine-L-amino acid derived Cu(II) complexes synthesized by Adão and co-workers.[107]

I.5 – Overview and objectives of the present work

The present work intended to design and synthesize several new Fe(III) and Mo(VI) complexes containing chiral amino acid-derived ligands, in order to test these compounds as pre-catalysts in oxidative catalytic reactions such as asymmetric oxidative coupling of 2-naphthol and 3-bromo-2-naphthol, epoxidation of benzalacetophenones and oxidation of 1-phenylethan-1-ol.

The field of iron and molybdenum catalysis in the studied reactions, for the best of knowledge, counts with very few or even no examples in the literature for amino acid-derived catalysts. Most of the catalytic systems reviewed are based on salan- or salen-based metal complexes or complexes with similar ligand structures, often obtained through time-consuming or elaborated synthetic procedures. Hence, the present work intends to contribute to this field of research with the development of amino acid-derived metal complexes with catalytic activity in the referred reactions, respecting Green Chemistry principles such as the utilization of safer solvents and reagents, energy efficiency, usage of renewable feedstocks and preparation of less hazardous chemical products with less hazardous methodologies. Iron is a readily-available transition metal, can exhibit relatively low toxicity and meets economic and environmental appeals normally required for the development of more sustainable synthetic procedures; molybdenum can also be a potential example in sustainable chemistry since it is

an element present in a wide range of important enzymes at a residual level and some of its compounds are important examples in industrial catalysis; amino acids (i) are a cheap natural source of compounds, (ii) possess a great lability in terms of chemical reactivity which allow the insertion of several binding groups with distinct functionalities, ideal to be applied in coordination chemistry for the preparation of tri- and tetra-dentate metal complexes; (iii) comprise a chiral side-chain, which can be explored in asymmetric catalysis.

For the mentioned reasons, this work hopes to contribute with relevant examples of amino acid-derived Fe(III) and Mo(VI) complexes with prospective application as catalysts in oxidative catalysis.

CHAPTER 2

Ligand Precursors

II – Ligand Precursors

II.1 – Preamble

In this chapter will be described the synthesis and characterization of tri- and tetradentate ligand precursors derived from naturally-occurring chiral L-α-amino acids such as L-phenylalanine (L-Phe), L-valine (L-Val) and L-tryptophan (L-Trp) (**Figure II-1**).

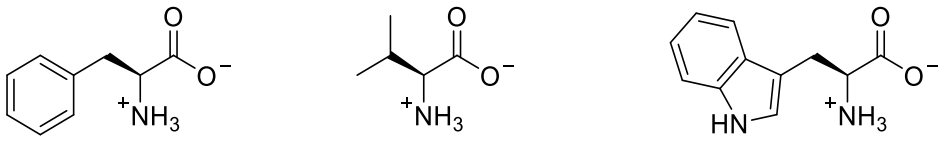

L-Phe L-Val L-Trp

Figure II-1: Structural formulae of the natural amino acid L-Phe, L-Val and L-Trp.

The choice of amino acids lays in the intention of developing sustainable catalytic systems since (i) they are a cheap natural source of compounds, (ii) they depict a versatile reactivity and solubility in environmentally-friendly solvents (*e.g.* water and alcohols) in a wide range of pH values, (iii) they allow the insertion of pendant arms with distinct functionalities by means of simple and effective one-pot reaction procedures, such as condensation reactions. The resulting products can be applied as ligand precursors with a wide range of structural and electronic properties. Additionally, the chirality of the amino acid-derived compounds can be exploited in asymmetric catalysis.

The synthesized ligand precursors were further used in coordination reactions with commercial Fe(III) and Mo(VI) sources for the preparation of the respective complexes, targeting possible applications in catalytic processes.

II.2 – Ligand precursors preparation: Results and discussion

The preparation of the desired ligand precursor compounds could be achieved under one-pot reductive aminations, Mannich reactions and derivatives (Betti reactions), greatly focusing on the application of mild and environmentally-friendly synthetic conditions such as environmentally-friendly solvents and mild temperatures, whenever possible. The resulting ligand precursors were divided into sub-categories based on the condensation reactions performed and products obtained. They are described below in the subsections **II.2.1** to **II.2.4**. All compounds were characterized by Nuclear Magnetic Resonance (NMR, ^{1}H, ^{13}C-{1H} APT, HSQC and HMBC), Infrared Spectroscopy (FT-IR), Electrospray Ionization Mass Spectrometry (ESI-MS) and Elemental Analysis (EA).

II.2.1 – Amino acid-pyridyl and amino acid-imidazolyl ligand precursors

The amino acid-pyridyl compounds **L1**, **L2** and **L3**, depicted in **Figure II-2**, were successfully synthesized according to previously reported procedures.[107,108,109] The amino acid-imidazolyl compound **L4** (**Figure II-2**) is reported for the first time and was prepared by a Mannich-type reaction involving L-Phe and an imidazole-based compound in alkaline medium.

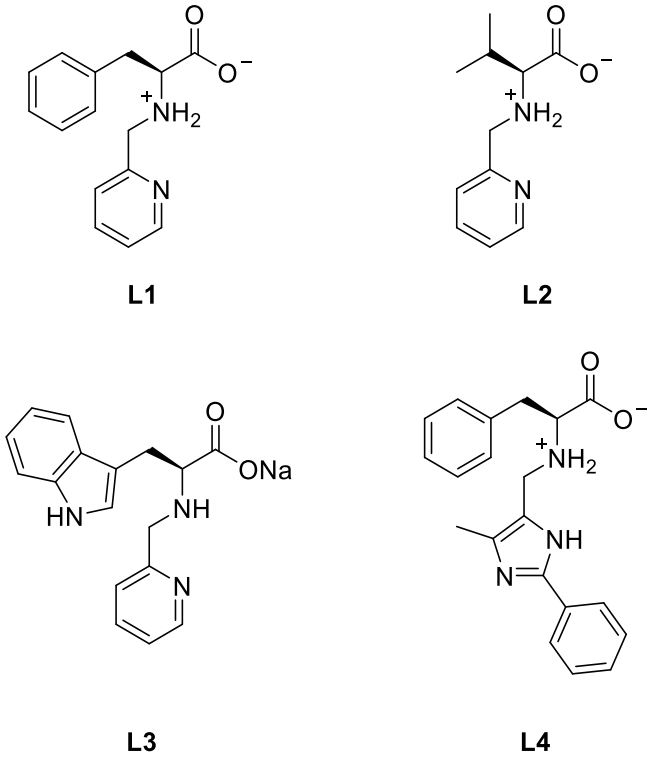

Figure II-2: Structural formulae of the prepared amino acid-pyridyl **L1**-**L3** and amino acid-imidazolyl-based (**L4**) compounds.

The synthesis of **L1**, **L2**, and **L3** was performed after initial dissolution of the respective L-Phe, L-Val and L-Trp precursors in MeOH or MeOH:H_2O mixtures with NaOH at room temperature. One mole equivalent of pyridine-2-carboxaldehyde was then added to the methanolic mixtures, affording a clear orange solution in all cases after 5 minutes of stirring at room temperature. Then, for the preparation of **L1** and **L2**, an excess of $NaBH_4$ was added to the reaction mixture to ensure total reduction of the respective *in-situ* formed Schiff base; for **L3**, concentrated HCl was carefully added dropwise till pH~8-9 was reached. After addition of $NaBH_4$, concentrated HCl was carefully added dropwise in the synthesis of **L1** and **L2** until pH~6-7, affording a white precipitate in both cases. **L1** was obtained in its neutral form in 83% by filtering the resulting precipate and washing it with water and diethyl ether. For **L2** and **L3** the correspondent reaction mixtures were evaporated till dryness, the resulting residue triturated with ethanol and propan-2-ol, respectively, and filtered. To the resulting filtrate was added diethyl ether to induce precipitation of a solid, which was filtered and washed with diethyl ether affording **L2** in its

neutral form and **L3** as a sodium salt in 82% and 71% (**Scheme II-1**). It must be noted that the reaction time of 5 minutes after addition of pyridine-2-carboxaldehyde must be strictly respected, in the preparation of **L3**, to ensure complete selectivity towards the formation of the desired compound and avoid the formation of secondary products derived from intramolecular condensations.

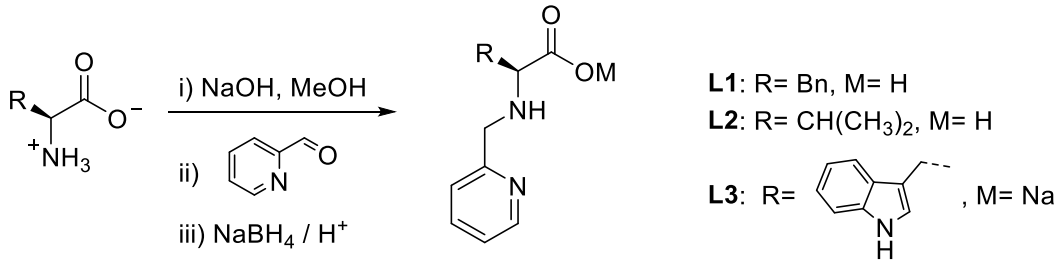

Scheme II-1: Synthetic procedure for the preparation of ligand precursors **L1, L2** and **L3.**

The preparation of **L4** could be achieved by a Mannich-type reaction between L-Phe and 4-methyl-2-phenylimidazole following one of the next methods: Method A, based on a previously reported procedure at room temperature[110] or Method B, using similar procedure but heating under reflux the reaction mixture. Both procedures are outlined in **Scheme II-2**. Method A consisted in the suspension of L-Phe and 4-methyl-2-phenylimidazole in water followed by addition of paraformaldehyde and KOH at room temperature. The white suspension was stirred for 10 days at r.t. Subsequent filtration, acidification to pH~6 of the resulting filtrate with concentrated HCl promoted the formation of a white suspension which was filtered under vacuum and the filtrate despised. The residue was washed with acetone and the resulting filtrate evaporated to dryness, yielding **L4** in its neutral form in 21% (**Scheme II-2**, left reaction). In the attempt to optimize the yield obtained in the reaction, Method B was applied. Compound L-Phe was solubilized in methanolic NaOH at room temperature, followed by addition of paraformaldehyde. After complete solubilization of the reaction mixture, 4-methyl-2-phenylimidazole was added and the solution heated under reflux for 16h, affording a yellow solution. The heating was stopped, the reaction let to cool till room temperature and evaporated to dryness under vacuum. The resulting residue was washed with an aqueous NaOH solution, filtered under vacuum and the obtained filtrate was acidified to pH~6 with concentrated HCl, affording a suspended white solid; sequential filtration, extraction with acetone and evaporation till dryness of the filtrate yielded **L4** in its neutral form in 15% (**Scheme II-2**, right reaction).

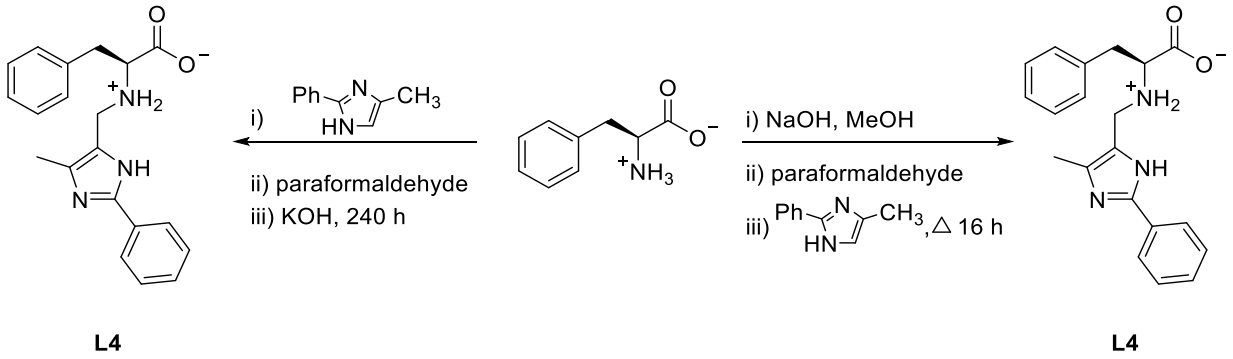

Scheme II-2: Synthetic procedures applied in the preparation of ligand precursor **L4**. Left reaction: Method A[110]; right reaction: Method B.

In both synthetic procedures low yields of **L4** were obtained. This is most probably due to the occurrence of a competing auto-condensation reaction of 4-methyl-2-phenylimidazole with paaformaldehyde. In fact, the auto-condensation product was isolated when using Method A as a white solid in 23% (based on the initial 4-methyl-2-phenylimidazole added) which was analysed by ^{1}H and ^{13}C NMR. Despite Method B afforded lower yield of **L4** than Method A, the former resulted to be more convenient due to the shorter reaction time needed to afford the desired product. Thus, Method B was adopted as the main synthetic procedure for the synthesis of **L4**.

The preparation of ligand precursors analogous to **L4** and derived from L-Val and L-Trp was explored using both synthetic procedures Method A and Method B, but unfortunately the target compounds were not obtained (**Scheme II-3**). The *work-up* procedures at neutral pH enabled only the isolation of the auto-condensation product of 4-methyl-2-phenylimidazole and inorganic impurities. Attempts to isolate the target products in the form of sodium and hydrochloride salts in aqueous alkaline and acidic medium, respectively, were ineffective. The observed difficulties can in part be attributed to higher solubility of the desired compounds in both aqueous and alcoholic medium, in comparison with **L4**, since no precipitation was observed in a wide range of pH values tested. Therefore, the syntheses of these compounds was abandoned.

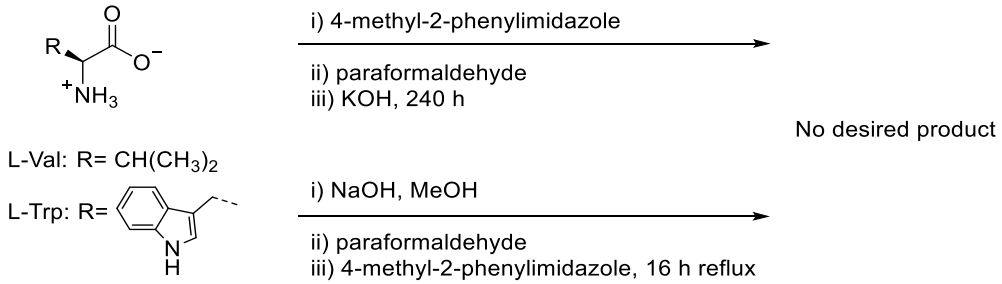

Scheme II-3: Synthetic procedures applied in the attempt to prepare and isolate amino acid-imidazolyl-ligand precursors from L-Val and L-Trp.

All compounds **L1** to **L4** were characterized by ^{1}H-NMR. Spectra of the featured amino acid-derived ligand precursors **L2** and **L3** are presented in **Figure II-3** and **Figure II-4**, respectively. The ligands **L1** to **L4** show some differences according to the amino acid side chain or to the presence of a pyridyl or substituted imidazolyl moiety, particularly in the 6.0-8.5 ppm region. In all cases, the ^{1}H-NMR spectra indicate C_1-symmetry in solution, which is consistent with the chiral nature of the compounds and with the existence of magnetically non-equivalent protons. In all ligand precursors the methylene group bridging the amino and the pyridyl or imidazolyl moieties appears as a doublet of doublet in an AB system, typical of diastereostopic protons (**Figure II-3**, signal **4** and **Figure II-4**, signal **3**). This is an important characteristic on the ^{1}H-NMR spectra of compounds **L1**-**L4**. Other important feature is evident on ligand precursors derived from L-Phe or L-Trp which typically show a doublet of doublet three-spin AMX system attributed to coupling between methylene and CH groups from the amino acid side-chain (**Figure II-4**, signals **1** and **2**).

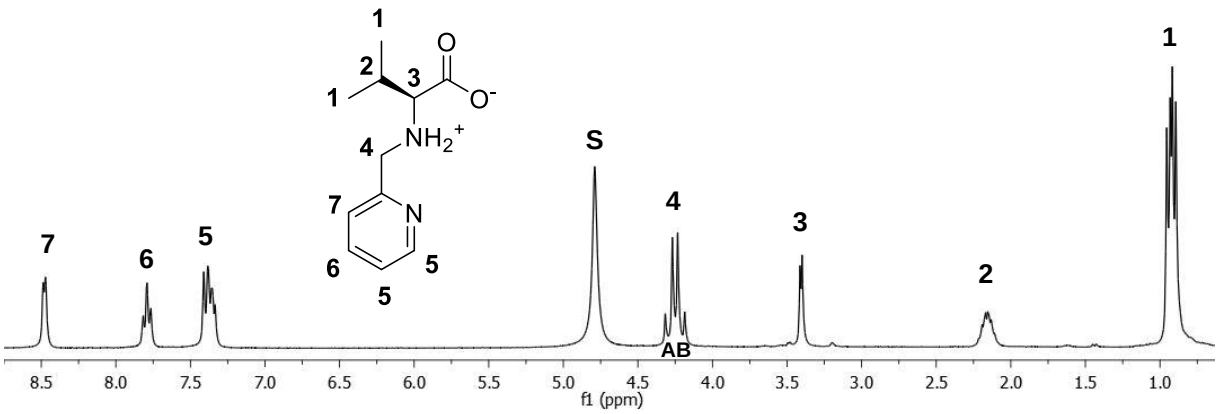

Figure II-3: ^{1}H-NMR spectrum of **L2** indicating C_1-symmetry in D_2O solution. Signal S corresponds to residual H_2O.

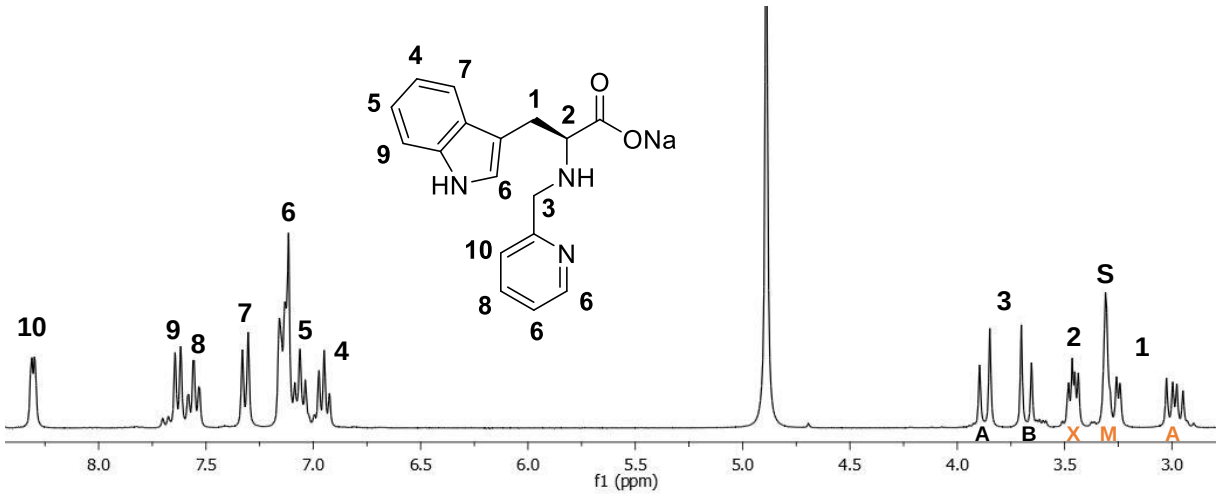

Figure II-4: ^{1}H-NMR spectrum of **L3** indicating C_1-symmetry in CD_3OD solution. The **AMX** doublet of doublet pattern is resolved but the **M** doublet is overlapped with the deuterated solvent signal **S**.

Additional information was obtained by FT-IR spectroscopy, where N-H and C=O stretching bands are detected around 3400-2900 and 1600 cm^{-1}, respectively. The information provided by ESI-MS and EA is consistent with the expected molecular formulas for **L1**-**L4**.

II.2.2 – Amino acid-phenol and amino acid-methoxybenzene ligand precursors

The prepared amino acid-phenol **L5**-**L10** and amino acid-methoxybenzene **L11** and **L12** ligand precursors are depicted in **Figure II-5**. Compounds **L5**-**L10** were successfully synthesized by adapting reported Betti reaction procedures[111] and isolated as zwitterionic amino acid-derived compounds. Ligand precursors **L11** and **L12** were synthesized by adapting the same reported reductive amination procedures[108,109] as in the preparation of **L1**-**L3**, and were isolated as hydrochloride salts. For the best of knowledge, it is the first time compounds **L5**-**L12** are reported.

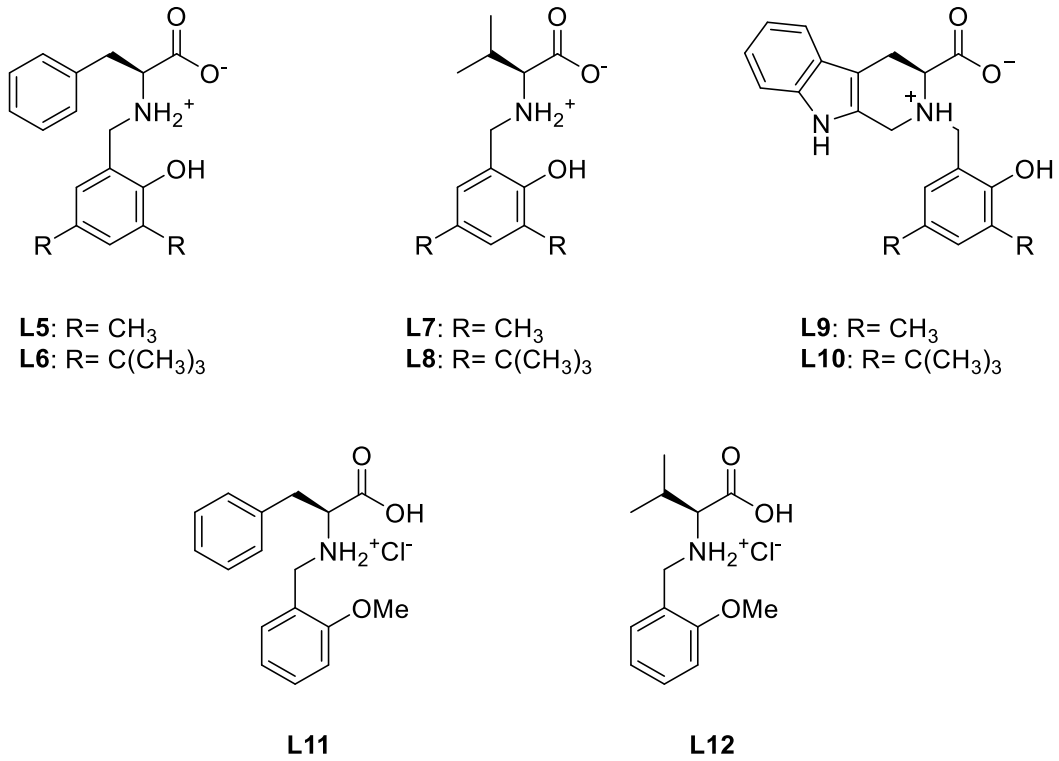

Figure II-5: Structural formulae of the prepared amino acid-phenol **L5-L10** and amino acid-methoxybenzene compounds **L11** and **L12**.

The synthetic pathway used for the preparation of **L5**-**L10** is depicted in **Scheme II-4**. The appropriate amino acid sources L-Phe, L-Val or L-Trp were dissolved simultaneously with NaOH and paraformaldehyde in methanol at room temperature. Then, one mole equivalent of the respective phenol reagent was added to the mixture and the reaction heated under reflux for 16 hours, affording a clear yellow solution. The heating was stopped, the reaction let to cool till r.t. and acidified with concentrated HCl till pH~6, followed by addition of water to induce precipitation of a solid which was filtered under vacuum, washed and the desired compounds isolated on their zwitterionic form in 64, 66, 49, 61, 69 and 66% yields, respectively.

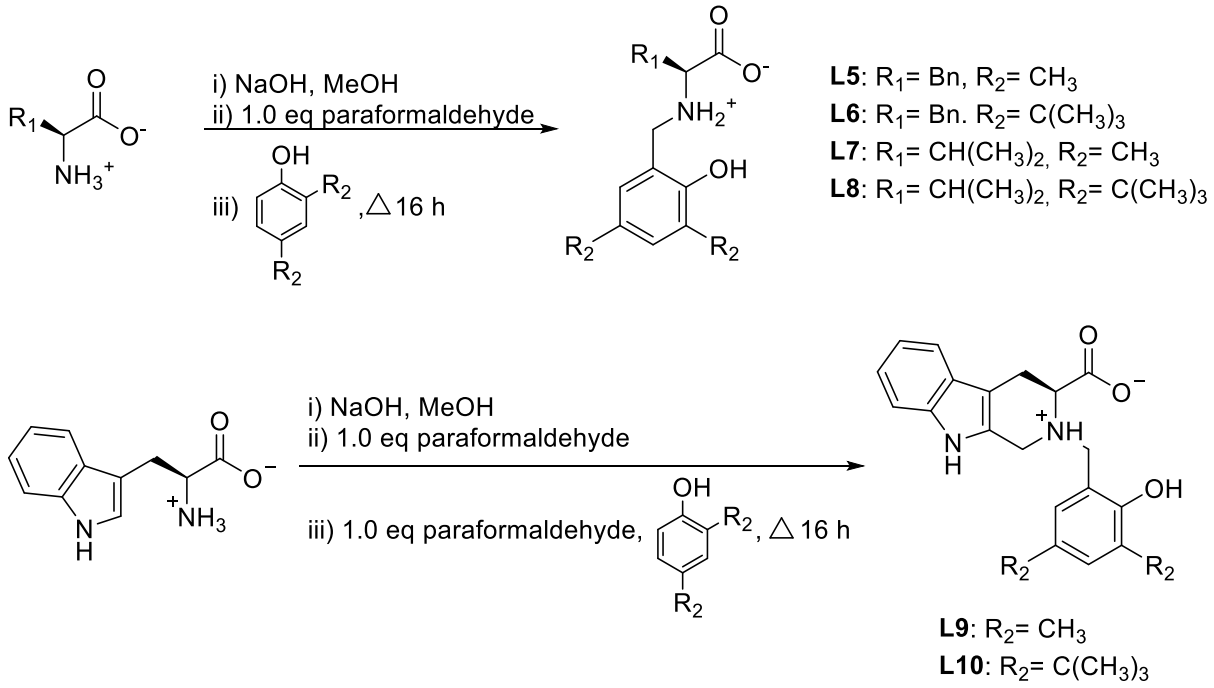

Scheme II-4: Synthesis of ligand precursors **L5-L10**.

The preparation of ligand precursors **L9** and **L10** required two additions of one mole equivalent of paraformaldehyde in different synthetic steps: the first one in the amino acid solubilization and the second simultaneously to the addition of phenol reagent (**Scheme II-4**). The first addition is required to ensure intramolecular condensation (cyclization) between the C1 carbon of the indolyl moiety and the amino group, while the second is responsible for the condensation between the amino group and the phenol unit. This procedure is strictly necessary for the successful preparation of the desired compounds, otherwise competition between the formation of the cyclized and non-cyclized products occurs, and a mixture of products is obtained, as it was observed in synthetic procedures where only one mole equivalent of paraformaldehyde was used (**Scheme II-5**).

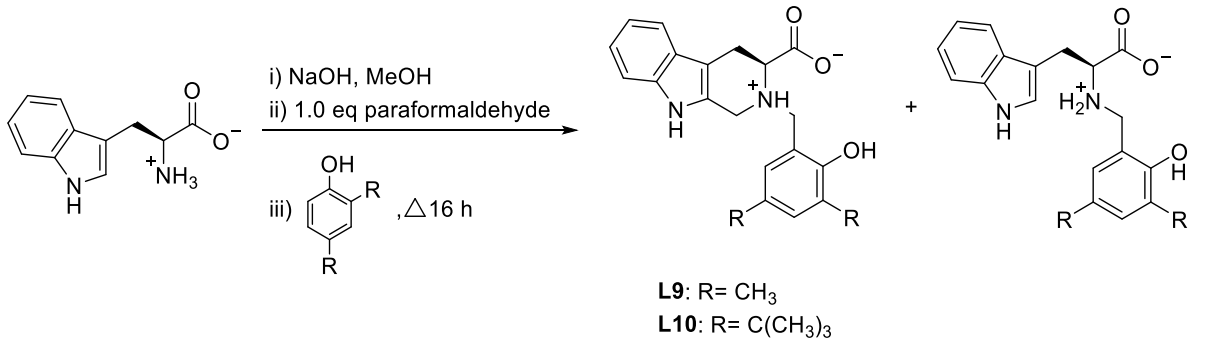

Scheme II-5: Synthetic procedure for the preparation of **L9** and **L10** with one mole equivalent of paraformaldehyde. Further product isolation and NMR analysis showed product mixtures between cyclized (**L9**, **L10**) and non-cyclized products.

Alternatively, the synthesis of **L9** and **L10** was tested in a two-step reaction procedure outlined in **Scheme II-6**, which included preliminary intramolecular cyclization of L-Trp with paraformaldehyde (**CA1, Scheme II-6**), followed by the condensation between this compound and the respective 2,4-dialkylphenol. The intramolecular condensation of L-Trp with paraformaldehyde in acidic water yielded **CA1** in 61% after 3 h under reflux, but Betti condensation between **CA1** and 2,4-dimethylphenol or 2,4-di-*tert*-butylphenol did not afford **L9** and **L10**, respectively, as it was expected. Therefore, this synthetic approach was abandoned for the synthesis of **L9** and **L10**.

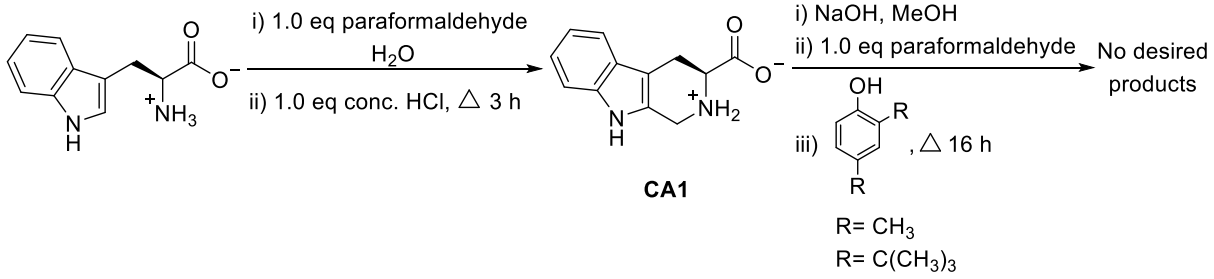

Scheme II-6: Synthetic procedure applied, with no success, for the synthesis of **L9** and **L10**.

The preparation of the amino acid-methoxybenzene ligand precursors **L11** and **L12** is outlined in **Scheme II-7**. The appropriate amino acid sources L-Phe or L-Val were dissolved in methanolic NaOH at room temperature. One mole equivalent of 2-methoxybenzaldehyde was then added to the mixture and stirred for *ca*. 10 minutes, affording a clear colourless solution in both cases. After this period, a slight excess of $NaBH_4$ was added to the reaction to reduce the respective Schiff base. The subsequent suspension was cooled to 5ºC with an external ice bath, carefully acidified with concentrated HCl till pH~2 and the mixture evaporated to dryness. The resulting residue was triturated with propan-2-ol, filtered under vacuum and diethyl ether was added to the filtrate to induce precipitation of a white solid; compound **L11** was isolated as hydrochloride salt in 78% yield after filtration of the referred precipitate. Compound **L12** required manual stirring, decantation and dryness under vacuum being isolated as hydrochloride salt in 83% yield.

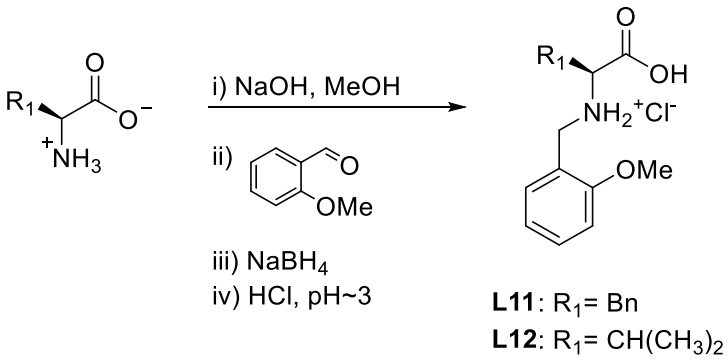

Scheme II-7: Synthesis of ligand precursors **L11** and **L12.**

The ^{1}H-NMR spectra of **L5** and **L11** are presented in **Figure II-6** and **Figure II-7,** respectively. Similarly to **L1**-**L4**, the ^{1}H-NMR spectra of **L5**-**L12** showed C_1-symmetry in solution, consistent with the non-symmetric structure of the compounds and with the existence of magnetically non-equivalent protons. The ^{1}H-NMR spectra of **L5** to **L10** display a doublet of doublet AB system corresponding to the methylene group bridging the amino group and the phenol moiety (**Figure II-6**, signal **5**). The homologous diastereotopic protons in **L11** and **L12** bridging the amino and 2-methoxybenzene moieties appear as a singlet (**L11, Figure II-7**) and a multiplet (**L12**). A doublet of doublet three-spin AMX system is also evident in amino acid-phenol compounds derived from L-Phe and L-Trp, corresponding to coupling between side-chain amino acid methylene and CH groups (**Figure II-6**, signals **3** and **4** for compound **L5**).

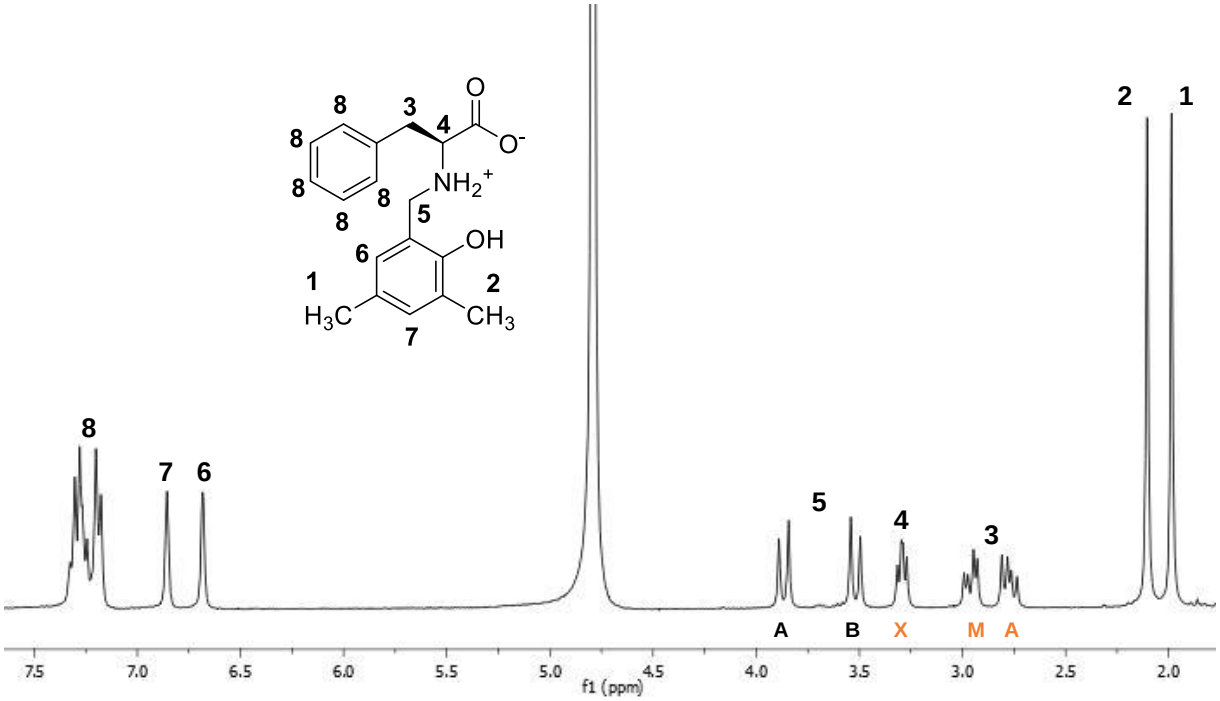

Figure II-6: ^{1}H-NMR spectrum of **L5** indicating C_1-symmetry in D_2O:Na_2CO_3 solution. The **AMX** doublet of doublet pattern is well resolved.

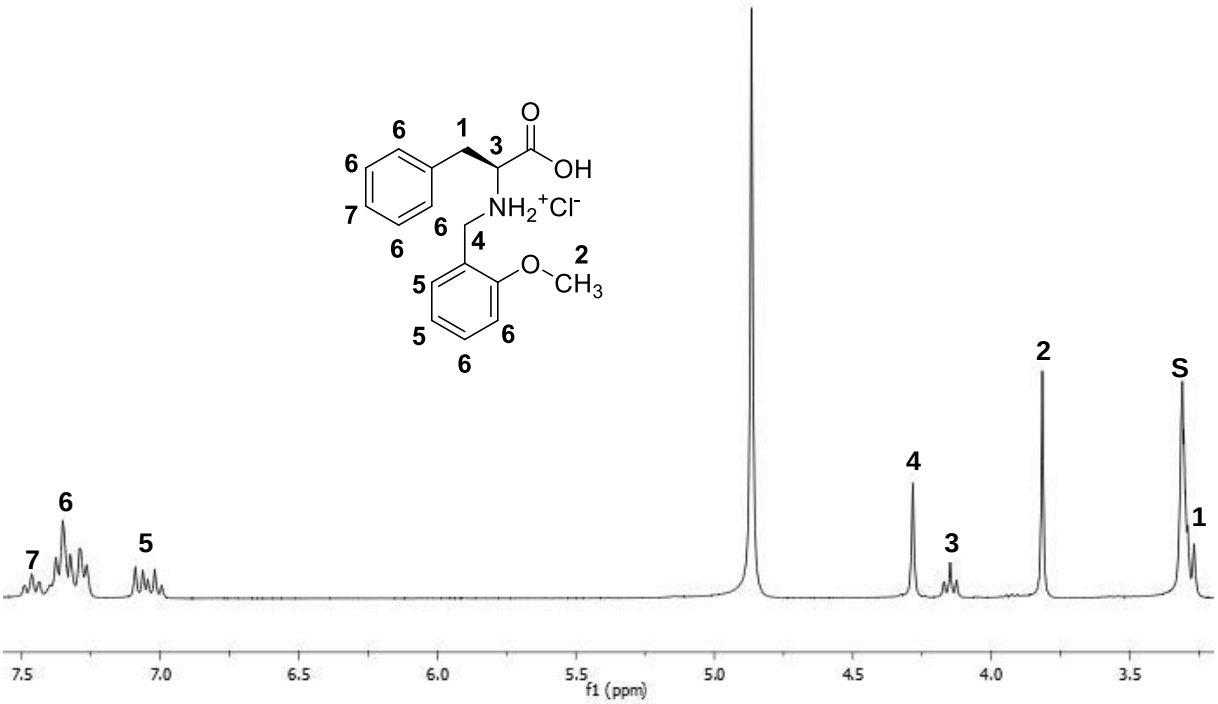

Figure II-7: ^{1}H-NMR spectrum of **L11** indicating C_1-symmetry in CD_3OD solution. Signal **S** is respective to residual MeOH.

FT-IR spectroscopy afforded additional structural information with N-H and C=O stretching bands being detected around 3400-2900 and 1600 cm^{-1}. Phenolic C-O stretching bands were observed around 1200 cm^{-1} for **L5**-**L10** ligand precursors. Information provided by ESI-MS and EA sustain the expected molecular formulas for the prepared ligand precursors. Solvent

molecules were considered in the EA analyses due to the hygroscopic nature of these compounds.

II.2.3 – Amino acid-pyridyl-phenol ligand precursors

The amino acid-pyridyl-phenol **L13**-**L15** ligand precursors synthesized are depicted in **Figure II-8**. All compounds were successfully synthesized by a Betti condensation reaction procedure under alkaline conditions and are reported for the first time.

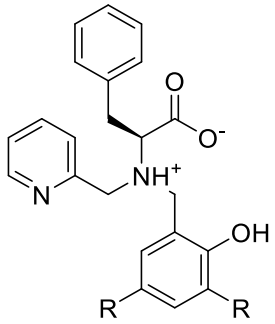

L13: R= CH_3
L14: R= $C(CH_3)_3$

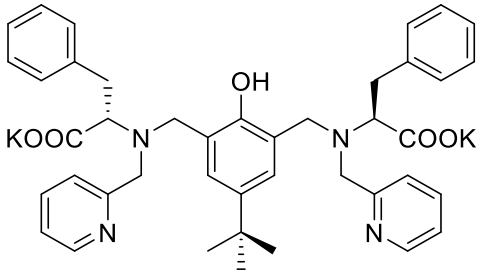

L15

Figure II-8: Structural formulae of amino acid-imidazolyl-phenol-based compounds **L13**-**L15**.

The synthesis of **L13** and **L14** is depicted in **Scheme II-8**. Compound **L1** was firstly suspended in aqueous methanol solution, followed by dropwise addition of an aqueous NaOH solution at room temperature till complete solubilization of the starting material. Afterward, aqueous formaldehyde (formalin) and 2,4-dimethylphenol or 2,4-di-*tert*-butylphenol (depending on the target compound) were added to the solution, which was heated under reflux for 4 h. After this period the reaction heating was stopped, let to cool until room temperature, acidified with concentrated HCl till pH~6 and partially evaporated under vacuum for MeOH removal, affording an aqueous suspension. Compound **L13** was isolated in its zwitterionic form in 43% yield after filtration and washing of the resulting precipitate. The isolation of compound **L14** required acidification of the aqueous suspension with concentrated HCl till pH~2, followed by trituraton and decantation with acidic water and petroleum ether, respectively; further filtration and washing of the resulting precipitate afforded **L14** in its zwitterionic form in 30% yield.

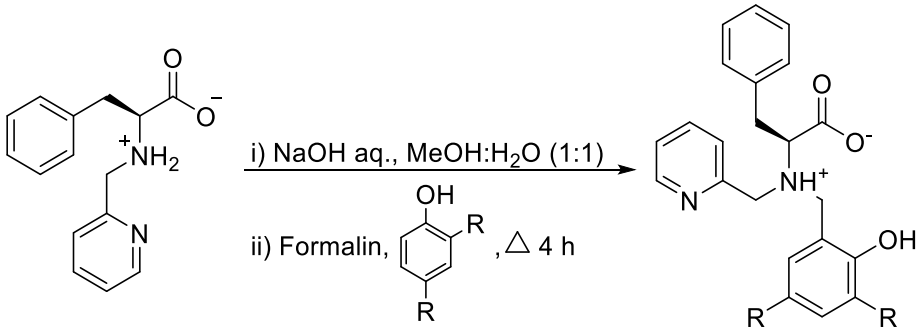

L1

L13: R= CH_3
L14: R= $C(CH_3)_3$

Scheme II-8: Synthesis of ligand precursors **L13** and **L14**.

Preparation of ligand precursors analogous to **L14** and derived from **L2** and **L3** was attempted using the same synthetic procedure. However, the reactions did not afford the desired compounds (**Scheme II-9**). After the reflux step of the processes, the *work-up* procedures followed at different pH values in water, to induce possible precipitation of desired compounds, but with no success. Clear solutions were obtained in both cases, which can be justified by the high solubility of **L2** and **L3** moieties in different pH ranges in water and alcoholic solutions, in comparison to **L1**. The synthesis of these compounds was, therefore, abandoned.

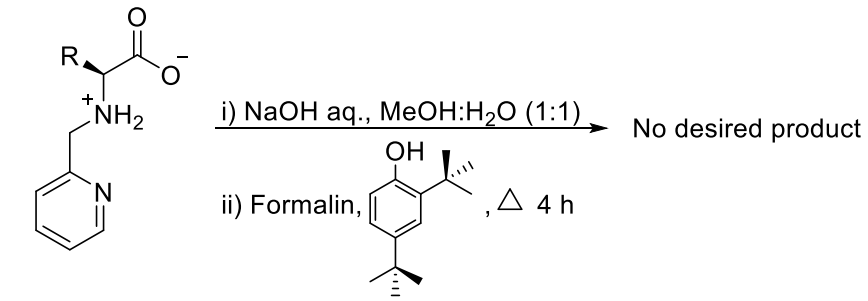

L2: R= $CH(CH_3)_2$

L3: R=

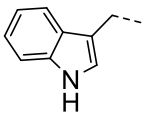

Scheme II-9: Synthetic procedures applied in the attempt to prepare and isolate amino acid-imidazolyl-ligand precursors from **L2** and **L3**.

The preparation of **L15** is outlined in **Scheme II-10**. Compound **L1** and KOH were dissolved in propan-2-ol at r.t., followed by addition of paraformaldehyde and 4-*tert*-buthylphenol. The mixture was heated under reflux for 6 hours, occurring the gradual formation of a white suspension. The reaction heating was stopped, let to cool till room temperature and the suspension filtered under vacuum and washed with propan-2-ol, providind compound **L15** in 18% yield as a potassium salt.

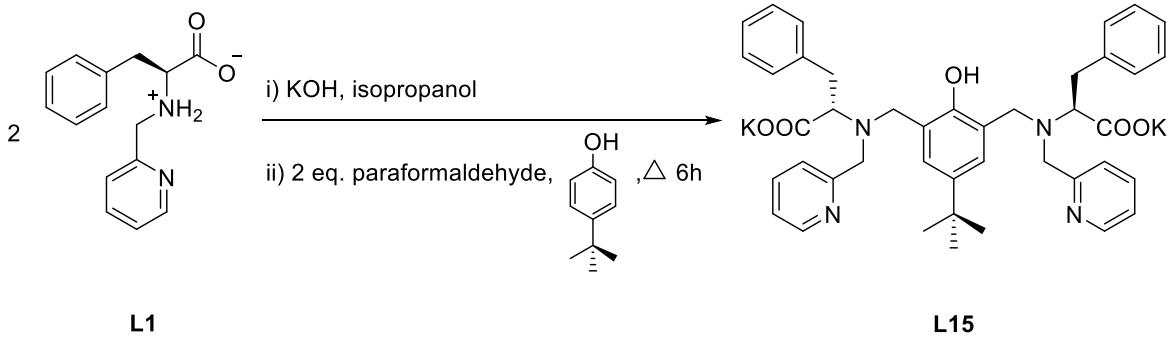

Scheme II-10: Synthesis of ligand precursor **L15.**

The ^{1}H-NMR spectra of **L13** and **L15** are presented in **Figure II-9** and **Figure II-11**, respectively. ^{1}H and ^{13}C NMR spectra of compounds **L13** and **L14** show many similarities, differing mainly on the resonances of the different substitutents present in the phenol unit. ^{1}H-NMR spectra indicate C_1-symmetry in solution for **L13** and **L14**. In contrast, **L15** presents C_2-symmetry, in which protons of each half of the **L15** molecule are magnetically equivalent resulting in a simplified ^{1}H and ^{13}C NMR spectra. In compounds **L13** and **L14** both methylene groups bridging the amino group with the pyridyl and phenol moieties appear as a doublet of doublet in an AB system (**A_1B_1** and **A_2B_2**, respectively, in **Figure II-9** and **Figure II-10**). Also, a doublet of doublet three-spin AMX system is observed and attributed to coupling between the side-chain amino acid methylene and CH groups (**Figure II-9** and **Figure II-10**, for more detail). Similar features are observed for **L15**, with the exception of the magnetic interaction between the side-chain amino acid methylene and CH groups; a doublet of doublet three-spin ABX system is depicted in this case.

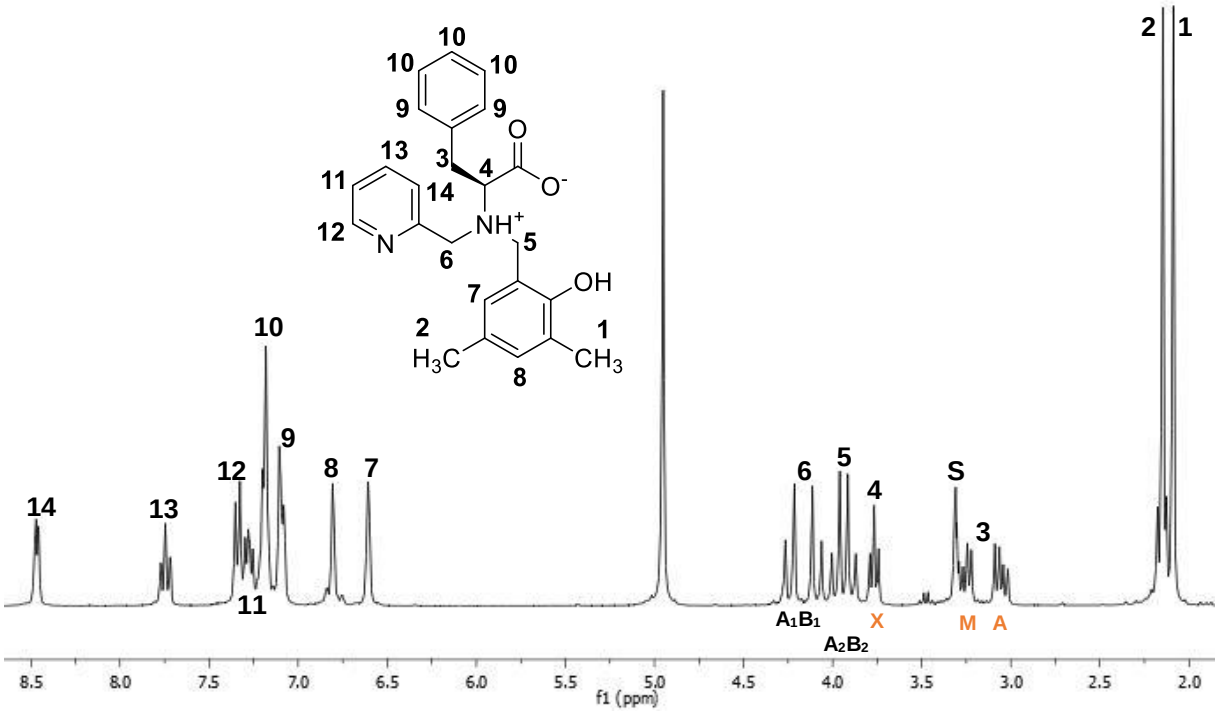

Figure II-9: ^{1}H-NMR spectrum of **L13** indicating *C*$_1$-symmetry in CD_3OD solution. The **AMX** doublet of doublet pattern is resolved but the **M** doublet is overlapped with the deuterated solvent signal **S**.

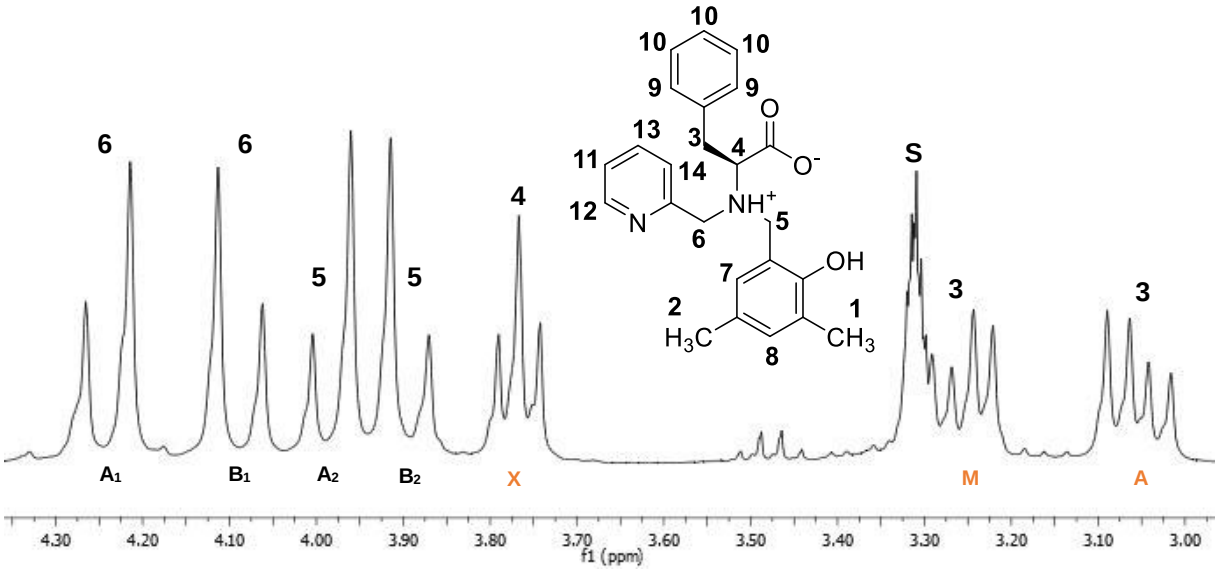

Figure II-10: Amplified ^{1}H-NMR spectrum of **L13** in CD_3OD solution, for better observation of $\mathbf{A_1B_1}$, $\mathbf{A_2B_2}$ and **AMX** signal splitting patterns. Signal **X** appears as a triplet.

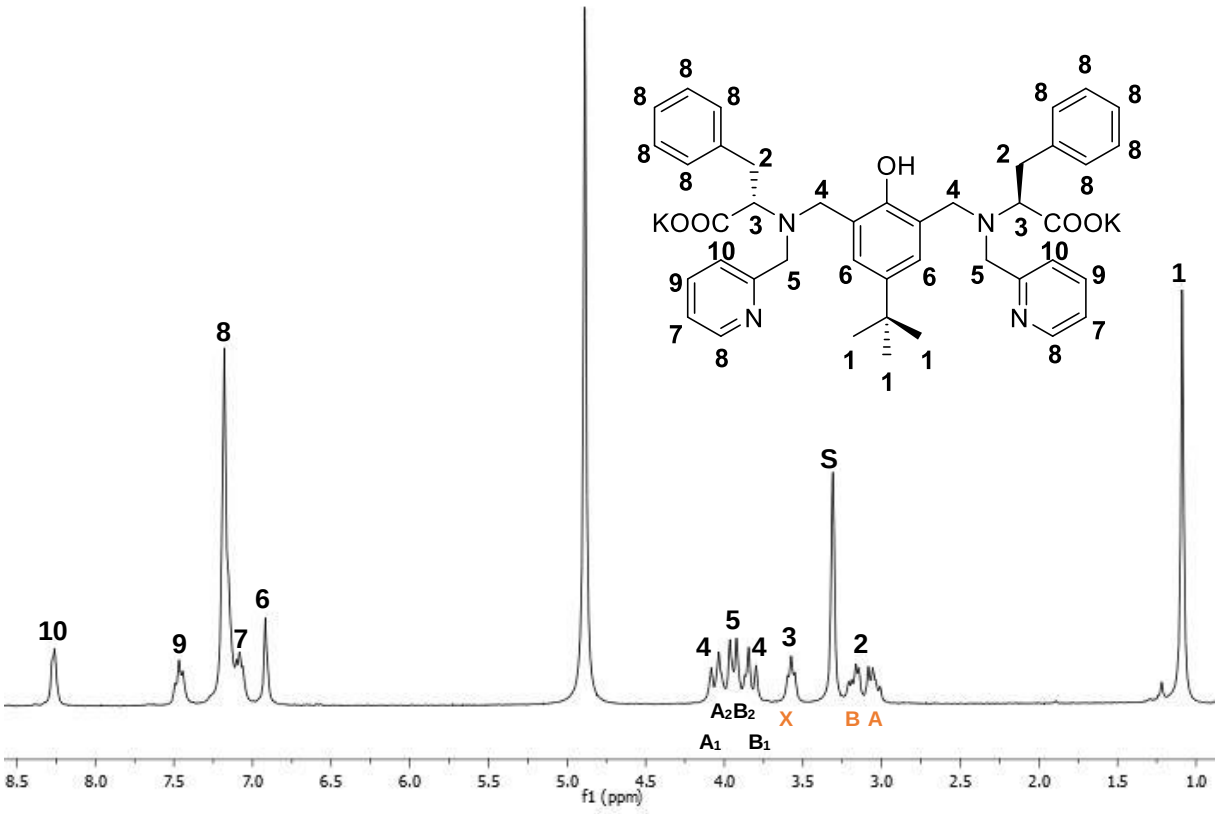

Figure II-11: ^{1}H-NMR spectrum of **L15** indicating C_2-symmetry in CD_3OD solution. The **ABX** doublet of doublet pattern is well resolved. Signal **S** corresponds to the residual solvent MeOH.

FT-IR spectroscopy afforded additional structural information with N-H and C=O stretching bands being detected around 3400-2900 and 1600 cm^{-1}. Phenolic C-O stretching bands were observed around 1200 cm^{-1}. Information provided by ESI-MS support the expected molecular formulae for the prepared ligand precursors, in exception to **L15** where molecular fragmentation seems to occur during sample analysis. EA also confirm the structural formulae of all compounds, but solvent molecules were considered due to the hygroscopic nature of the analysed compounds, especially **L15**.

II.2.4 – *β*-Ketoamino acid ligand precursors

The prepared *β*-ketoamino acid **L16**-**L19** ligand precursors are depicted in **Figure II-12**. For the best of knowledge, all compounds are reported for the first time and were obtained in their neutral form by applying Mannich reaction conditions between L-Phe or L-Val as starting materials, an aromatic ketone and formaldehyde in acidic aqueous medium.

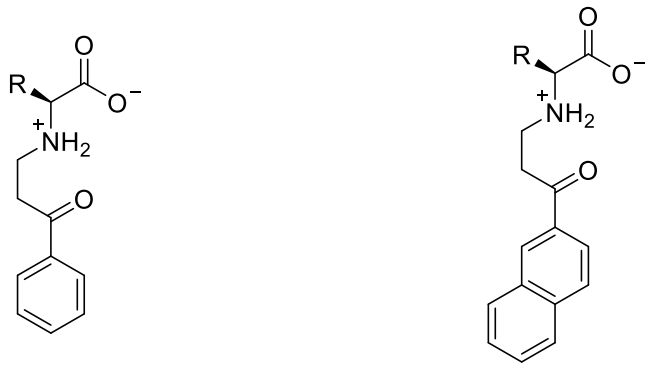

L16: R= Bn
L17: R= $CH(CH_3)_2$

L18: R= Bn
L19: R= $CH(CH_3)_2$

Figure II-12: Structural formulae of β-ketoamino acid-based compounds **L16**-**L19**.

The syntheses of **L16**-**L19** is outlined in **Scheme II-11**. The appropriate amino acid sources L-Phe or L-Val were suspended in distilled water, followed by addition of concentrated HCl and formalin. After solubilization at room temperature of the reaction mixture, acetophenone or 1-(naphthalen-2-yl)ethan-1-one (2-acetonaphthone), depending on the desired product, was added to the reaction, which was heated under reflux for 16 h. After this period the heating was stopped, the reaction cooled to room temperature and an aqueous saturated solution of $NaHCO_3$ was mixed till pH~6, followed by addition of water to induce precipitation of a white solid; further filtration and treatment allowed the isolation of the desired compounds on their neutral form in 30, 36, 29 and 40% yields, respectively.

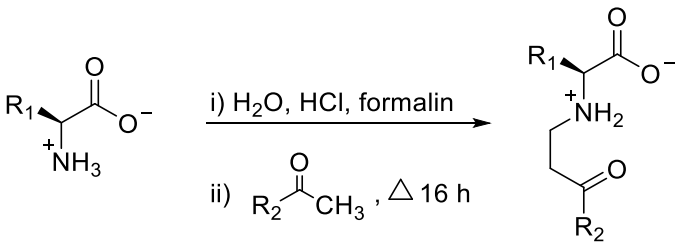

L16: R_1= Bn, R_2= Ph
L17: R_1= $CH(CH_2)_3$, R_2= Ph
L18: R_1= Bn, R_2= 2-Naph
L19: R_1= $CH(CH_2)_3$, R_2= 2-Naph

Scheme II-11: Outline of synthesis of ligand precursors **L16**-**L19**.

The ^{1}H-NMR spectrum of **L17** is presented in **Figure II-13** as an example of this type of ligand precursors. The ^{1}H-NMR spectrum is in accord with a C_1-symmetry for **L17** in solution, consistent with the asymmetric structure of **L17** and with the existence of magnetically non-equivalent protons. In contrast to **L1**-**L15**, **L17** shows two triplets in its ^{1}H-NMR spectrum, each one corresponding to diastereotopic methylene group protons bridging the amino group and the oxo substituent (**Figure II-13**).

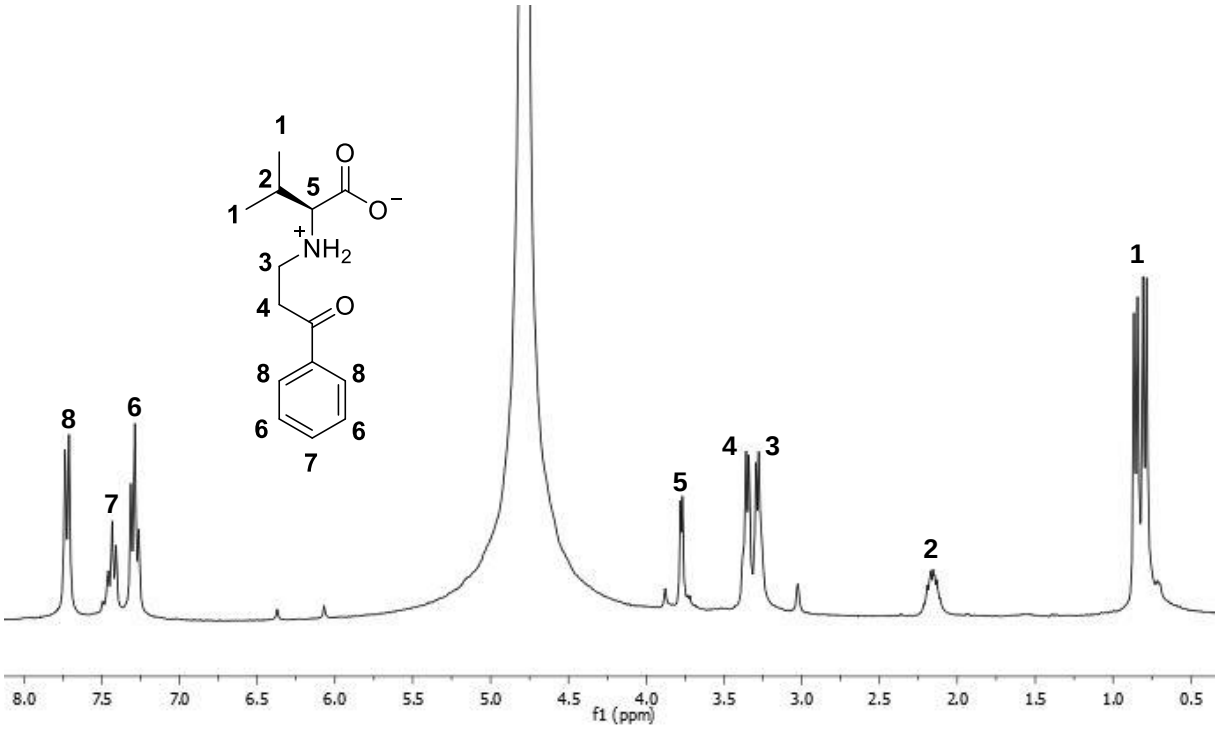

Figure II-13: ^{1}H-NMR spectrum of **L17** indicating C_1-symmetry in CD_3OD:HCl solution.

FT-IR spectroscopy afforded additional structural information of the obtained compounds with N-H stretching bands being detected around 3000-2900 cm^{-1} and two C=O at *ca.* 1600 cm^{-1}. ESI-MS and EA support the expected molecular formulae for the prepared ligand precursors, but solvent molecules were considered (EA) due to the hygroscopic nature of the analysed compounds.

II.3 – Conclusions

A wide array of chiral compounds derived from chiral natural amino acids, containing distinct methylene-bridged pendant arms, were successfully prepared and characterized. The synthesis of all compounds was performed with a great concern on balancing simple and sustainable reaction procedures such as reductive alkylation and Mannich reactions in water, alcohols or mixtures of both solvents. Isolation of new compounds as their carboxylate, hydrochloride or zwitterionic forms simplified general purification and further manipulation of these compounds.

II.4 – Experimental section

II.4.1 – General considerations

All ligand precursor synthesis, isolation and purification were done without air exclusion. All solvents and reagents were purchased from commercial suppliers and used as received.

II.4.2 – Characterization Techniques

II.4.2.1 – Nuclear Magnetic Resonance Spectroscopy (NMR)

1D NMR (^{1}H, ^{13}C-{1H} APT) and 2D NMR (HSQC and HMBC) spectra were recorded on Bruker Advance II+ 300 MHz (UltraShield Magnet) instruments at room temperature. ^{1}H and ^{13}C chemical shifts (δ) are expressed in ppm relative to Me_4Si or the solvent residual peak. Whenever calculation is possible, coupling constants *J* are given in Hz and multiplicities are presented as: s (singlet), d (doublet), dd (doublet of doublet), t (triplet), q (quartet) and m (multiplet). Carbons identified as C_{ipso} by ^{13}C-{1H} APT, HSQC and HMBC are quaternary carbons.

II.4.2.2 – Infrared Spectroscopy (FT-IR)

FT-IR spectra were recorded in KBr disks using a JASCO FT/IR-430 spectrometer. The frequency correspondent to the maximum absorption is presented in cm^{-1}, followed by the molecular group attributed and band intensities: s (strong), m (medium), w (weak) and b (broad).

II.4.2.3 – Electrospray Ionization Mass Spectrometry (ESI-MS)

The ESI mass experiments were made by Prof. Maria da Conceição Oliveira and MSc. Ana Dias at Centro de Química Estrutural of Instituto Superior Técnico. The ESI mass spectra were obtained on a LCQ Fleet ion trap mass spectrometer equipped with an electrospray ion source, operated in the positive and negative mode. The operated parameters were optimized for maximum abundance of the ions of interest, as follows: ion spray voltage, +5 kV; capillary voltage, 5/-20 V; tube lens offset, -125/63 V, sheath gas (N_2), 20 arbitrary units; capillary temperature, 275ºC. Spectra obtained are the average results from 20 to 35 scans, and were saved within the range 100-2000 Da.

II.4.2.4 – Elemental Analysis (EA)

Elemental analyses were carried out at Laboratório de Análises of Instituto Superior Técnico, using a Perkin Elmer EA110 CE automatic analyzer Instrument. The results presented are the average values obtained from two independent determinations.

II.4.3 – Compound Preparation Methods

II.4.3.1 – Amino acid-pyridyl and amino acid-imidazolyl ligand precursors

Synthesis of (*S*)-3-phenyl-2-[(pyridin-2-ylmethyl)ammonio]propanoate (L1):

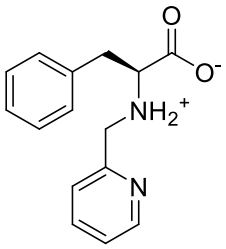

L-phenylalanine (L-Phe, 6.4 g, 38.8 mmol) and NaOH (1.71 g, 42.7 mmol) were dissolved in 80 mL of MeOH. The mixture was stirred at r.t. for 5 minutes and a clear solution was obtained. Pyridine-2-carboxaldehyde (3.70 mL, 38.8 mmol) was added and an orange solution was obtained. After stirring for 5 minutes at r.t., $NaBH_4$ (2.20 g, 58.2 mmol) was added to the reaction mixture and let to stir at r.t. for 1 h. Subsequently, the pH value of the mixture was carefully adjusted to *ca*. 6 with concentrated HCl (dropwise) and a white solid precipitated; the reaction mixture was then poured to *ca.* 300 mL of water, filtered and washed with 3x 100 mL of water and 2x 50 mL of diethyl ether. Yield: 83% (8.2 g) δ_H: (300 MHz, D_2O + Acetone marker, excess Na_2CO_3, ppm) 8.28 (1H, d, Ar<u>H</u>$_{Pyridyl}$, CHCHCHC<u>H</u>N, *J*= 4.4), 7.66 (1H, t, Ar<u>H</u>$_{Pyridyl}$, CHCHC<u>H</u>CHN, *J*= 7.6), 7.29-6.99 (7H, m, Ar<u>H</u>), 3.63 (2H, dd, PyC<u>H</u>$_2$$NH_2^+$, *J*= 54.0, 13.9), 3.25 (1H, t, NH_2^+C<u>H</u>CH_2Ph, *J*= 6.8), 2.81 (2H, d, NH_2^+CHC<u>H</u>$_2$Ph, *J*= 6.6). δ_C (300 MHz, D_2O + Acetone marker, excess Na_2CO_3, ppm) 180.65 (1C, <u>C</u>OO^-), 157.56 (1C, <u>C</u>$_{ipso,Pyridyl}$), 148.24 (1C, Ar<u>C</u>H$_{Pyridyl}$, CHCHCH<u>C</u>HN), 137.98 (1C, Ar<u>C</u>H$_{Pyridyl}$, CHCH<u>C</u>HCHN), 137.60 (<u>C</u>$_{ipso,Phenyl}$), 129.15, 128.47, 126.53, 122.88, 122.79 (7C, Ar<u>C</u>H), 64.43 (NH_2^+<u>C</u>HCH_2Ph) 51.76 (NH_2^+<u>C</u>H_2Py), 38.83 (NH_2^+CH<u>C</u>H_2Ph). ESI-MS (Methanol+AcOH): m/z= 257.13 [$(C_{15}H_{17}N_2O_2)^+$, 100%]. ν_{max}/cm^{-1}: 3021 (<u>N-H</u>, s), 1580 (<u>C=O</u>$_{carboxyl}$, s). Elemental analysis for $C_{15}H_{16}N_2O_2$: calcd. C 70.29, H 6.29, N 10.93; found C 70.25, H 6.36, N 11.05.

Synthesis of (*S*)-3-methyl-2-((pyridin-2-ylmethyl)ammonio)butanoate (L2):

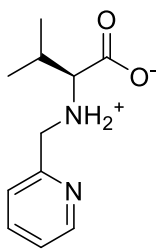

In 40 mL of methanol, L-valine (L-Val, 2.3 g, 20 mmol) and NaOH (0.88 g, 22 mmol) were added and stirred at r.t. for 5 minutes, till a clear solution was obtained. Pyridine-2-carboxaldehyde (1.90 mL, 20 mmol) was added, the reaction mixture stirred for 5 minutes and $NaBH_4$ (1.13 g, 30 mmol) was added. Subsequently, the pH value of the mixture was carefully adjusted to *ca*. 6 with concentrated HCl (dropwise) leading to the precipitation of a white solid. The

mixture was evaporated to dryness and the solid residue was triturated with 50 mL of absolute ethanol, filtered and the insoluble inorganic material washed with additional absolute ethanol. The filtrate was evaporated to nearly one quarter of its initial volume after which diethyl ether was added to induce precipitation of the compound. The precipitate was filtered and washed with Et_2O, yielding a white solid. Yield: 82% (3.43 g) δ_H: (300 MHz, D_2O + CD_3OD marker, ppm) 8.48 (1H, d, Ar<u>H</u>$_{Pyridyl}$, CHCHCHC<u>H</u>N, *J*= 4.3), 7.79 (1H, t, Ar<u>H</u>$_{Pyridyl}$, CHCHC<u>H</u>CHN, *J*= 4.4), 7.46-7.28 (2H, m, Ar<u>H</u>$_{Pyridyl}$, C<u>H</u>C<u>H</u>CHCH), 4.25 (2H, dd, PyC<u>H</u>$_2$NH_2^+, *J*= 25.7, 13.6), 3.41 (1H, d, $^-$OOCC<u>H</u>NH_2^+, *J*= 4.1), 2.30-2.01 (1H, m, C<u>H</u>$(CH_3)_2$), 0.94, 0.91 (3H each, d each, partially overlapped, $^-$OOCCHCH(C<u>H</u>$_3)_2$, *J*= 7.0 each). δ_C (300 MHz, D_2O + CD_3OD marker, ppm) 173.32 (1C, <u>C</u>OO$^-$), 150.99 (1C, <u>C</u>$_{ipso,Pyridyl}$), 150.33 (1C, Ar<u>C</u>H$_{Pyridyl}$, CHCHCH<u>C</u>HN), 139.41 (1C, Ar<u>C</u>H$_{Pyridyl}$, CHCH<u>C</u>HCHN), 125.51 (1C, Ar<u>C</u>H$_{Pyridyl}$, CH<u>C</u>HCHCHN), 125.39 (1C, Ar<u>C</u>H$_{Pyridyl}$, <u>C</u>HCHCHCHN); 68.80 (1C, $^-$OO<u>C</u>CHNH_2^+), 51.39 (1C, Py<u>C</u>H$_2$NH_2^+), 30.26 (1C, <u>C</u>H$(CH_3)_2$), 18.94, 18.38 (1C each, CH(<u>C</u>H$_3)_2$). ESI-MS (Methanol): m/z= 209.10 [$(C_{11}H_{17}N_2O_2)^+$, 35%]. ν_{max}/cm^{-1}: 2960 (<u>N-H</u>, m), 1614 (<u>C=O</u>$_{carboxyl}$, s) Elemental analysis for $C_{11}H_{16}N_2O_2$•0.5H_2O: calcd. C 60.81, H 7.89, N 12.89; found C 61.19, H 7.92, N 12.97.

Synthesis of sodium (*S*)-3-(1H-indol-2-yl)-2-(pyridin-2-ylmethylamino)propanoate (L3):

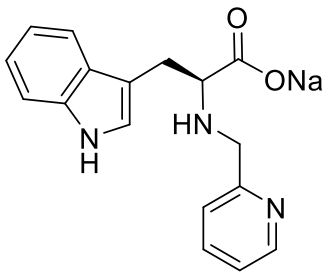

To 20 mL of an EtOH:H_2O (1:1) solution, L-tryptophan (L-Trp, 1 g, 4.9 mmol) and NaOH (0.215 g, 5.4 mmol) were added at room temperature. The reaction mixture was stirred till complete solubilization of the amino acid, and pyridine-2-carboxaldehyde (0.47 mL, 4.9 mmol) was added, yielding a clear orange solution. After 5 minutes of stirring, concentrated HCl was added dropwise to the reaction till pH~9-8, followed by evaporation to dryness, originating a yellow residue which was triturated with 20 mL of warm propan-2-ol. The resulting mixture was filtered, and the insoluble inorganic material washed with additional propan-2-ol. The filtrate was evaporated to nearly one quarter of its volume after which diethyl ether was added to induce precipitation of the compound, which was then filtered and washed with diethyl ether, yielding a yellow-brown solid. Yield: 71% (1.19g, 3.48 mmol). δ_H (300 MHz, CD_3OD, ppm): 8.31 (1H, d, Ar<u>H</u>$_{Pyridyl}$, C<u>H</u>CHCHCHN), *J*= 3.6), 7.63 (1H, d, Ar<u>H</u>$_{Indolyl}$, adjacent to C_{ipso}NH, *J*= 7.9), 7.56 (1H, t, Ar<u>H</u>$_{Pyridyl}$, CHC<u>H</u>CHCHN), *J*= 7.7), 7.32 (1H, d, Ar<u>H</u>$_{Indolyl}$, adjacent to $C_{ipso}C_{ipso}CH_2CHCOONa$, *J*= 8.1), 7.14 (3H, m, overlap between Ar<u>H</u>$_{Pyridyl}$, CHCHC<u>H</u>C<u>H</u>N and NaOOCHCH_2C=C<u>H</u>NH), 7.06 (1H, t, Ar<u>H</u>$_{Indolyl}$, *meta* to NH, *J*= 7.3), 6.95 (1H, t, Ar<u>H</u>$_{Indolyl}$, *para* to NH, *J*= 7.2), 3.87, 3.68 (1H each, d each, NaOOCCHNHC<u>H</u>$_2$Py, *J*= 14.3 each), 3.46 (1H, dd, NaOOCC<u>H</u>CH_2, *J*= 8.6, 5.0), 3.28, 2.99 (1H each, dd each, partially overlapped with CD_3OD signal, NaOOCCHC<u>H</u>$_2$Indolyl, *J*= 17.2, 3.1). δ_C (300 MHz, CD_3OD, ppm): 181.85 (1C, <u>C</u>OONa),

160.60 (1C, $\underline{C}_{ipso,Pyridyl}$), 149.58 (1C, Ar$\underline{C}H_{Pyridyl}$, $\underline{C}$HCHCHCHN), 138.29 (1C, Ar$\underline{C}H_{Pyridyl}$, CH$\underline{C}$HCHCHN), 138.18 (1C, $\underline{C}_{ipso,Indolyl}$, adjacent to NH), 129.01 (1C, $\underline{C}_{ipso,Indolyl}$, adjacent to C=CHNH), 124.38 (1C, NaOOCCHCH$_2$C=$\underline{C}$HNH), 123.85 (1C, Ar$\underline{C}H_{Pyridyl}$, CHCHCH$\underline{C}$HN), 123.33 (1C, Ar$\underline{C}H_{Pyridyl}$, CHCH$\underline{C}$HCHN), 122.19 (1C, Ar$\underline{C}H_{Indolyl}$, *m*eta to NH), 119.77 (1C, Ar$\underline{C}H_{Indolyl}$, adjacent to C_{ipso}NH), 119.49 (1C, Ar$\underline{C}H_{Indolyl}$, *para* to NH), 112.74 (1C, $\underline{C}_{ipso}$C=CHNH), 112.09 (1C, Ar$\underline{C}$H, adjacent to C_{ipso}C=CHNH) 65.12 (1C, NaOOCCH$\underline{C}$H$_2$) 54.07 (1C, NH$\underline{C}$H$_2$Py), 30.91 (1C, NaOOC$\underline{C}$HCH$_2$). ESI-MS (Methanol): m/z= 294.61 [($C_{17}H_{16}N_3O_2$)$^-$, 100%]. ν_{max}/cm^{-1}: 3397 ($\underline{N\text{-}H}$, s,b), 1595 ($\underline{C{=}O}_{carboxyl}$, s). Elemental analysis for $C_{17}H_{16}N_3NaO_2$•1.5H_2O: Calcd. C 60.89, H 5.41, N 12.53; found C 61.40, H 5.43, N 12.38.

Synthesis of (*S*)-2-{[(4-methyl-2-phenyl-1H-imidazol-5-yl)methyl]ammonio}-3-phenylpropanoate (L4)

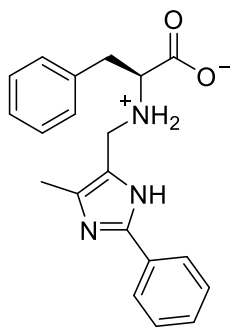

L-phenylalanine (L-Phe, 2.50 g, 15.2 mmol) and NaOH (0.61 g, 19.7 mmol) were weighted into a 100 mL round-bottomed flask and dissolved in 40 mL of methanol at r.t., affording a colourless solution. Paraformaldehyde (0.46 g, 15.15 mmol) was added to the solution and let to dissolve at r.t., followed by the addition of 4-methyl-2-phenylimidazole (2.39 g, 15.2 mmol) and the mixture was heated under reflux for 16 h, gradually affording over time a yellow solution. After this period, the reaction mixture was evaporated till dryness, and the resulting orange residue was suspended in 60 mL of distilled water, filtered under vacuum and washed with 2x50 mL of an aqueous solution of NaOH (1 M). The obtained aqueous filtrate was acidified till pH~6 with concentrated HCl, affording a white suspension which was filtered under vacuum and washed with 3x50 mL of acetone. The resulting solid residue was discarded and the organic filtrate was dried with anhydrous Na_2SO_4, filtered and evaporated to dryness, affording a final white solid. Yield: 15% (0.76 g). δ_H (300 MHz, CD_3OD, ppm): 7.80 (2H, d, Ar$\underline{H}_{Phenyl}$ of imidazolyl moiety, *o*-position, *J*= 7.1), 7.42 (3H, m, Ar$\underline{H}_{Phenyl}$ of imidazolyl moiety, *m*- and *p*- positions) 7.27 (5H, m, Ar$\underline{H}_{Phenyl}$ of phenylalanine), 4.10 (2H, dd, $NH_2^+C\underline{H}_2$Imidazolyl, *J*= 25.2, 14.4), 3.82 (1H, dd,$^-$OOCC$\underline{H}$CH$_2$Ph, *J*= 8.5, 5.4), 3.77, 3.11 (1H each, dd each, $^-$OOCCHC$\underline{H}_2$Ph, partially overlapped with CD_3OD signal, *J*= 14.6, 7.7), 2.26 (3H, s, C$\underline{H}_3$). δ_C (300 MHz, CD_3OD, ppm): 172.78 (1C, $\underline{C}OO^-$), 147.51 (1C, $\underline{C}_{ipso,Phenyl}$ of imidazolyl moiety), 136.91 (1C, $\underline{C}_{ipso,Phenyl}$ of phenylalanine), 130.85 (1C, $\underline{C}_{ipso,Imidazolyl}$, adjacent to CH_3), 130.44 (2C, Ar$\underline{C}H_{Phenyl}$ of phenylalanine, *ortho* to CH_2), 130.04 (1C, partially overlapped, Ar$\underline{C}H_{Phenyl}$ of imidazolyl moiety, *p*-position), 129.99 (2C, partially overlapped, Ar$\underline{C}H_{Phenyl}$ of imidazolyl moiety, *m*-position), 129.90 (2C, Ar$\underline{C}H_{Phenyl}$ of phenylalanine, *meta* to CH_2), 128.41 (1C, Ar$\underline{C}H_{Phenyl}$ of phenylalanine, *para* to CH_2), 127.91 (1C, $\underline{C}_{ipso,Imidazolyl}$, adjacent to $CH_2NH_2^+$), 126.17 (2C, Ar$\underline{C}H_{Phenyl}$ of imidazolyl moiety, *o*-position), 125.88 (1C, $\underline{C}_{ipso,Imidazolyl}$,

adjacent to Ph), 63.31 (1C, $^{-}$OOC<u>C</u>HCH$_2$Ph), 43.45 (1C, NH$_2^+$<u>C</u>H$_2$Imidazolyl), 37.76 (1C, $^{-}$OOCCH<u>C</u>H$_2$Ph), 9.42 (1C, <u>C</u>H$_3$). ESI-MS (Methanol): m/z= 336.04 [(C$_{20}$H$_{22}$N$_3$O$_2$)$^+$, 100%]. ν_{max}/cm^{-1}: 3406 (<u>N-H</u>, w), 1600 (<u>C=O</u>$_{carboxyl}$, m) Elemental analysis for C$_{20}$H$_{21}$N$_3$O$_2$•1.5H$_2$O: Calcd. C 66.28, H 6.67, N 11.59; found C 66.08, H 6.42, N 11.54.

II.4.3.2 – Amino acid-phenol and amino acid-methoxybenzene ligand precursors

II.4.3.2.1 – General synthetic procedure for amino acid-phenol ligand precursors:

L-Phenylalanine, L-valine or L-tryptophan, depending on the desired product, and NaOH (1.2 eq/mmol amino acid) were weighted and introduced in a round bottom flask equipped with a reflux condenser, and dissolved in MeOH (2.50 mL/mmol amino acid) at r.t. To the resulting colourless solution, paraformaldehyde (1.0 eq/mmol amino acid for the synthesis of **L5**-**L8**; 2.0 eq/mmol amino acid for the synthesis of **L9** and **L10,** with 1.0 mole equivalent added before and after addition of phenol) was added to the mixture and let to stir for 1 h at r.t.; a disubstituted phenol (1.0 eq/mmol amino acid) was then added and the reaction took place under reflux for the next 16 h. After this period the heating was stopped and the reaction let to cool till r.t. Concentrated HCl was carefully added dropwise till pH~6, affording a white precipitate. Distilled water was generously added to the mixture and the suspension filtered under vacuum and washed with 3x50 mL of distilled water and 1x50 mL petroleum ether, yielding the desired product.

Synthesis of (*S*)-2-[(2-hydroxy-3,5-dimethylbenzyl)ammonio]-3-phenylpropanoate (L5)

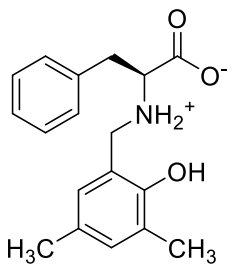

Reagents: L-Phenylalanine (3.30 g, 20.0 mmol), NaOH (0.96 g, 24.0 mmol), paraformaldehyde (0.60 g, 20.0 mmol), 2,4-dimethylphenol (2.42 mL, 20.0 mmol), MeOH (50.0 mL). The compound was obtained as an amorphous white solid. Yield: 64% (3.83 g). δ_H (300 MHz, D$_2$O + Na$_2$CO$_3$ + Acetone-*d*$_6$, ppm) 7.39-7.12 (5H, m, Ar<u>H</u>$_{Phenyl}$), 6.86 (1H, s, Ar<u>H</u>$_{Phenol}$, *para* to CH$_2$NH$_2^+$), 6.68 (1H, s, Ar<u>H</u>$_{Phenol}$, *ortho* to CH$_2$NH$_2^+$), 3.87 (1H, d, NH$_2^+$C<u>H</u>HPhOH, *J*= 13.9), 3.53 (1H, d, NH$_2^+$CH<u>H</u>PhOH, *J*= 14.0), 3.30 (1H, dd, PhCH$_2$C<u>H</u>COO$^-$, *J*= 8.4, 5.7), 2.98 (1H, dd, PhC<u>H</u>HCHCOO$^-$, *J*= 13.7, 5.3), 2.78 (1H, dd, PhCH<u>H</u>CHCOO$^-$, *J*= 13.7, 8.4), 2.11 (3H, s, ArC<u>H</u>$_3$, *ortho* to HO$_{Phenol}$) 1.99 (3H, s, ArC<u>H</u>$_3$, *para* to HO$_{Phenol}$). δ_C (300 MHz, D$_2$O + Na$_2$CO$_3$ + Acetone-*d*$_6$, ppm): 181.30 (1C, <u>C</u>OO$^-$), 153.59 (1C, <u>C</u>$_{ipso,Phenol}$), 138.83 (1C, <u>C</u>$_{ipso,Phenyl}$), 130.56 (1C, Ar<u>C</u>H$_{Phenol}$, *para* to CH$_2$NH$_2^+$), 129.41 (2C, Ar<u>C</u>H$_{Phenyl}$, *ortho* to CH$_2$), 128.84 (2C, Ar<u>C</u>H$_{Phenyl}$, *meta* to CH$_2$), 128.46 (1C, Ar<u>C</u>CH$_3$, *ortho* to HO$_{Phenol}$), 127.23 (1C, Ar<u>C</u>H$_{Phenol}$, *ortho* to CH$_2$NH$_2^+$), 126.90 (1C, Ar<u>C</u>H$_{Phenyl}$, *para* to CH$_2$), 125.63 (1C, Ar<u>C</u>CH$_3$, *para* to HO$_{Phenol}$), 123.68 (1C, Ar<u>C</u>OH$_{Phenol}$), 64.22 (1C, $^{-}$OOC<u>C</u>HCH$_2$Ph), 49.65 (1C, NH$_2^+$<u>C</u>H$_2$PhOH), 39.19 (1C, $^{-}$OOCCH<u>C</u>H$_2$Ph), 19.61 (1C, Ar<u>C</u>H$_3$, *ortho* to HO$_{Phenol}$),

15.27 (1C, Ar<u>C</u>H_3, *para* to HO_{Phenol}). ESI-MS (Methanol+AcOH): m/z= 300.02 [$(C_{18}H_{22}NO_3)^+$, 100%]. ν_{max}/cm^{-1}: 3149 (<u>N-H</u>, w), 1578 (<u>C=O</u>$_{carboxyl}$, w), 1231 (<u>C-O</u>$_{Phenol}$, w). Elemental analysis for $C_{18}H_{21}NO_3$: Calcd. C 72.22, H 7.07, N 4.68; found C 72.10, H 7.19, N 4.66.

Synthesis of (*S*)-2-[(3,5-di-*tert*-butyl-2-hydroxybenzyl)ammonio]-3-phenylpropanoate (L6)

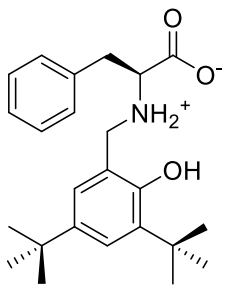

Reagents: L-Phenylalanine (1.65 g, 10.0 mmol), NaOH (0.48 g, 12.0 mmol), paraformaldehyde (0.30 g, 10.0 mmol), 2,4-di-*tert*-buthylphenol (2.06 g, 10.0 mmol), MeOH (25.0 mL). The compound was obtained as a white solid. Yield: 66% (2.54 g). δ_H (300 MHz, CD_3OD, ppm): 7.40-7.25 (6H, m, Ar<u>H</u>), 7.04 (1H, s, Ar<u>H</u>$_{Phenol}$, *para* to $CH_2NH_2^+$), 4.15, 3.97 (1H each, d each, $NH_2^+C\underline{H_2}PhOH$, *J*= 13.0 each), 3.84 (1H, dd, $NH_2^+C\underline{H}CH_2Ph$, *J*= 8.5, 5.0), 3.35 (1H, dd, $NH_2^+CHC\underline{H}HPh$, partially overlapped with CD_3OD signal, *J*= 14.5, 8.6), 3.07 (1H, dd, $NH_2^+CHCH\underline{H}Ph$, *J*= 14.5, 8.6) 1.39 (9H, s, C(C<u>H</u>$_3$)$_3$, *ortho* with HO_{Phenol}), 1.27 (9H, s, C(C<u>H</u>$_3$)$_3$, *para* to HO_{Phenol}). δ_C (300 MHz, CD_3OD, ppm): 173.39 (1C, <u>C</u>OO^-), 153.87 (1C, <u>C</u>$_{ipso,Phenol}$, adjacent to CH_2), 143.98 (1C, <u>C</u>$_{ipso,Phenol}$, *para* to HO_{Phenol}), 139.65 (1C, <u>C</u>$_{ipso,Phenol,}$ *ortho* to HO_{Phenol}), 137.34 (1C, <u>C</u>$_{ipso,Phenyl}$), 130.42, 130.00 (2C each, Ar<u>C</u>H$_{Phenyl}$, *ortho* and *meta* to CH_2), 128.44 (1C, Ar<u>C</u>H, *para* to CH_2), 127.00 (1C, Ar<u>C</u>H$_{Phenol}$, *para* to $CH_2NH_2^+$), 126.35 (1C, Ar<u>C</u>H$_{Phenol}$, *ortho* to $CH_2NH_2^+$), 121.22 (1C, Ar<u>C</u>OH), 64.28 (1C, $NH_2^+\underline{C}HCH_2Ph$), 49.61 (1C, $NH_2^+\underline{C}H_2PhOH$), 37.88 (1C, $NH_2^+CH\underline{C}H_2Ph$), 35.98 (1C, <u>C</u>$(CH_3)_3$, *ortho* to HO_{Phenol}), 35.15 (1C, <u>C</u>$(CH_3)_3$, *para* to HO_{Phenol}), 31.93 (3C, C(<u>C</u>$H_3)_3$, *para* to HO_{Phenol}), 30.33 (3C, C(<u>C</u>$H_3)_3$, *ortho* with HO_{Phenol}). ESI-MS (Methanol): m/z= 384.09 [$(C_{24}H_{34}NO_3)^+$, 100%]. ν_{max}/cm^{-1}: 2955 (<u>N-H</u>, m), 1733 (<u>C=O</u>$_{carboxyl}$, w), 1227 (<u>C-O</u>$_{Phenol}$, m). Elemental analysis for $C_{24}H_{33}NO_3 \bullet 0.5H_2O$: Calcd. C 73.44, H 8.73, N 3.57; found C 73.12, H 8.79, N 3.29.

Synthesis of (*S*)-2-[(2-hydroxy-3,5-dimethylbenzyl)ammonio]-3-methylbutanoate (L7)

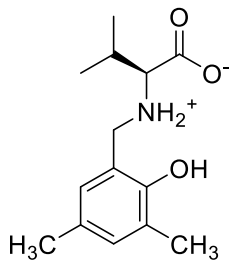

Reagents: L-Valine (2.35 g, 20.0 mmol), NaOH (0.96 g, 24.0 mmol), paraformaldehyde (0.60 g, 20.0 mmol), 2,4-dimethylphenol (2.42 mL, 20.0 mmol), MeOH (50.0 mL). The compound was obtained as a white solid. Yield: 49% (2.45 g). δ_H (300 MHz, CD_3OD, ppm): 6.98 (1H, s, Ar<u>H</u>, *para* to $CH_2NH_2^+$), 6.93 (1H, s, Ar<u>H</u>, *ortho* to $CH_2NH_2^+$), 4.17 (2H, dd, $NH_2^+C\underline{H_2}PhOH$, *J*= 29.6, 12.9), 3.38 (1H, d, $NH_2^+C\underline{H}COO^-$, *J*= 3.8), 2.30-2.20 (1H, m, C<u>H</u>$(CH_3)_2$, partially overlapped with $ArCH_3$), 2.22 (6H, s, respective to all Ar<u>C</u>H_3), 1.05, 1.02 (3H each, d each, CH(C<u>H</u>$_3$)$_2$, partially overlapped, *J*= 7.1 and 7.0 respectively). δ_C (300 MHz, CD_3OD, ppm): 172.46 (1C, <u>C</u>OO^-), 153.05 (1C, Ar<u>C</u>OH), 134.12 (1C, Ar<u>C</u>H, *para* to $CH_2NH_2^+$), 130.76 (1C, Ar<u>C</u>CH_3, *para* to HO_{Phenol}), 130.56 (1C, Ar<u>C</u>H, *ortho* to $CH_2NH_2^+$),

126.17 (1C, Ar<u>C</u>CH$_3$, *ortho* to HO$_{Phenol}$), 119.41 (1C, <u>C</u>$_{ipso,Phenol}$, adjacent to $CH_2NH_2^+$), 68.46 (1C, NH_2^+<u>C</u>HCOO$^-$), 49.40 (1C, $NH_2^+CH_2$PhOH), 30.60 (1C, <u>C</u>H(CH$_3$)$_2$), 20.39 (1C, Ar<u>C</u>H$_3$, *ortho* to HO$_{Phenol}$), 18.80, 18.62 (1C each, CH(<u>C</u>H$_3$)$_2$), 16.43 (1C, Ar<u>C</u>H$_3$, *para* to HO$_{Phenol}$). ESI-MS (Methanol+AcOH): m/z= 386.04 [($C_{14}H_{22}NO_3$•4 MeOH)$^+$, 100%], m/z= 252.03 [($C_{14}H_{22}NO_3$)$^+$, 62%]. ν_{max}/cm^{-1}: 2964 (<u>N-H</u>, s,b), 1564 (<u>C=O</u>$_{carboxyl}$, s), 1229 (<u>C-O</u>$_{Phenol}$, s). Elemental analysis for $C_{14}H_{21}NO_3$: Calcd. C 66.91, H 8.42, N 5.57; found C 66.71, H 8.04, N 5.39.

Synthesis of (*S*)-2-[(3,5-di-*tert*-butyl-2-hydroxybenzyl)ammonio]-3-methylbutanoate (L8)

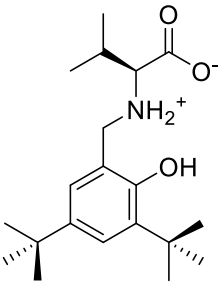

Reagents: L-Valine (1.18 g, 10.0 mmol), NaOH (0.48 g, 12.0 mmol), paraformaldehyde (0.30 g, 10.0 mmol), 2,4-di-*tert*-buthylphenol (2.06 g, 10.0 mmol), MeOH (25.0 mL). The compound was obtained as a white solid. Yield: 61% (2.57 g). δ_H (300 MHz, CD_3OD, ppm): 7.33 (1H, s, Ar<u>H</u>, *para* to $CH_2NH_2^+$), 7.14 (1H, s, Ar<u>H</u>, *ortho* to $CH_2NH_2^+$), 4.19, 4.01 (1H each, d each, NH_2^+C<u>H$_2$</u>PhOH, *J*= 13.2 each), 3.31 (1H, m, HO_2C<u>H</u>CH(CH$_3$)$_2$, totally overlapped by CD_3OD signal, determined by HSQC), 2.18 (1H, m, HOOCCHC<u>H</u>(CH$_3$)$_2$), 1.42 (9H, s, ArC(C<u>H$_3$</u>)$_3$, *ortho* to HO$_{Phenol}$) 1.29 (9H, s, ArC(C<u>H$_3$</u>)$_3$, *para* to HO$_{Phenol}$), 1.06, 1.03 (3H each, d each, CH(C<u>H$_3$</u>)$_2$, partially overlapped, *J*= 9.8 each). δ_C (300 MHz, CD_3OD, ppm): 174.41 (1C, <u>C</u>OO$^-$), 154.30 (1C, Ar<u>C</u>OH), 143.64 (1C, Ar<u>C</u>(^{t}Butyl), *para* to HO$_{Phenol}$), 139.16 (1C Ar<u>C</u>(^{t}Butyl), *ortho* to HO$_{Phenol}$), 126.73 (1C, Ar<u>C</u>H, *ortho* to $CH_2NH_2^+$), 125.83 (1C, Ar<u>C</u>H, *para* to $CH_2NH_2^+$), 121.86 (1C, <u>C</u>$_{ipso,Phenol}$, adjacent to $CH_2NH_2^+$), 69.15 (1C, NH_2^+<u>C</u>HCH(CH$_3$)$_2$), 50.79 (1C, NH_2^+<u>C</u>H$_2$PhOH), 35.98 (1C, <u>C</u>(CH$_3$)$_3$, *ortho* to HO$_{Phenol}$), 35.16 (1C, <u>C</u>(CH$_3$)$_3$, *para* to HO$_{Phenol}$), 31.99 (3C, C(<u>C</u>H$_3$)$_3$, *para* to HO$_{Phenol}$), 31.24 (1C, NH_2^+CH<u>C</u>H(CH$_3$)$_2$), 30.33 (3C, C(<u>C</u>H$_3$)$_3$, *ortho* to HO$_{Phenol}$), 19.15 (2C, NH_2^+CHCH(<u>C</u>H$_3$)$_2$). ESI-MS (Methanol): m/z= 359.28 [($C_{20}H_{33}NO_3Na$)$^+$, 17%], m/z= 336.08 [($C_{20}H_{34}NO_3$)$^+$, 13%]. ν_{max}/cm^{-1}: 2956 (<u>N-H</u>, s), 1622 (<u>C=O</u>$_{carboxyl}$, m), 1203 (<u>C-O</u>$_{Phenol}$, m). Elemental analysis for $C_{20}H_{33}NO_3$•0.5MeOH: Calcd. C 70.05, H 10.04, N 3.98; found 70.16, H 10.33, N 3.87.

Synthesis of (*S*)-2-(2-hydroxy-3,5-dimethylbenzyl)-2,3,4,9-tetrahydro-1H-pyrido[3,4-b]indol-2-ium-3-carboxylate (L9)

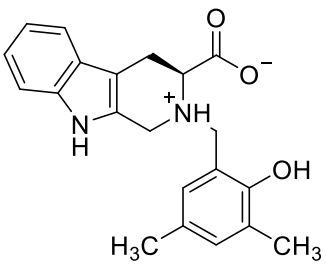

Reagents: L-Tryptophan (2.53 g, 10.0 mmol), NaOH (0.48 g, 12.0 mmol), paraformaldehyde (2 additions, 0.30 g each, 10.0 mmol each, one before and one after addition of 2,4-dimethylphenol), 2,4-dimethylphenol (1.21 mL, 10.0 mmol), MeOH (25.0 mL). The compound was obtained as an amorphous white solid. Yield: 69% (2.53 g). δ_H (300 MHz, CD_3OD + a drop of D_2O/NaOH, ppm): 7.41

(1H, d, Ar<u>H</u>$_{Indolyl,}$ adjacent to $C_{ipso}C_{ipso}CH_2CHCOO^-$, *J*= 7.1), 7.26 (1H, d, Ar<u>H</u>$_{Indolyl}$, adjacent to $C_{ipso}NHC_{ipso}$, *J*= 7.3), 7.10-6.91 (2H, m, Ar<u>H</u>$_{Indolyl}$), 6.80 (1H, s, Ar<u>H</u>$_{Phenol}$, *para* to CH_2NH^+), 6.58 (1H, s, Ar<u>H</u>$_{Phenol}$, *ortho* to CH_2NH^+), 4.03 (1H, d, $^-$OOCCHC<u>H</u>H, *J*= 14.8), 3.90 (2H, s, NHC<u>H$_2$</u>PhOH), 3.74 (1H, d, $^-$OOCCHCH<u>H</u>, *J*= 14.8), 3.58 (1H, t, $^-$OOCC<u>H</u>CH$_2$, *J*= 6.0), 3.11 (2H, s, NH^+C<u>H$_2$</u>$C_{ipso}NH_{Indolyl}$), 2.15 (6H, s, ArC<u>H$_3$</u>). δ_C (300 MHz, CD_3OD + gota D_2O com NaOH, ppm): 180.87 (1C, <u>C</u>OO$^-$), 156.08 (1C, Ar<u>C</u>CH$_3$, *para* to HO_{Phenol}), 137.93 (1C, <u>C</u>$_{ipso,Pyrrolyl,\ position\ 3}$, adjacent to $CH_{Benzene\ ring}$), 132.29 (1C, <u>C</u>$_{ipso,Pyrrolyl,\ position\ 5}$, adjacent to CH_2NH^+), 131.57 (1C, Ar<u>C</u>H$_{Phenol}$, *para* to CH_2NH^+), 129.45 (1C, Ar<u>C</u>H$_{Phenol}$, *ortho* to CH_2NH^+), 128.41 (1C, <u>C</u>$_{ipso,Pyrrolyl,\ position\ 2}$, adjacent to $CH_{benzene\ ring}$), 127.29 (1C, Ar<u>C</u>OH), 125.87 (1C, Ar<u>C</u>CH$_3$, *ortho* to HO_{Phenol}), 123.62 (1C, Ar<u>C</u>CH_2NH^+), 121.74, 119.59 (1C each, Ar<u>C</u>H$_{Indolyl}$ each), 118.43 (1C, Ar<u>C</u>H$_{Indolyl}$, adjacent to $C_{ipso}C_{ipso}CH_2CHCOO^-$), 111.81 (1C, Ar<u>C</u>H$_{Indolyl}$, adjacent to $C_{ipso}NHC_{ipso}$), 107.58 (1C, <u>C</u>$_{ipso,Pyrrolyl,\ position\ 4}$, adjacent to CH_2CHCOO^-), 65.38 (1C,$^-$OOC<u>C</u>HCH$_2$), 54.9 (1C, NH^+<u>C</u>H$_2$PhOH), 47.99 (1C, $^-$OOCCH<u>C</u>H$_2$), 24.33 (1C, NH^+<u>C</u>$H_2C_{ipso}NH_{Indolyl}$), 20.54 (1C, Ar<u>C</u>H$_3$, *para* to HO_{Phenol}), 16.57 (1C, Ar<u>C</u>H$_3$, *ortho* to HO_{Phenol}). ESI-MS (Methanol+AcOH): m/z= 383.05 [$(C_{21}H_{23}N_2O_3$•MeOH$)^+$, 100%], m/z= 351.06 [$(C_{21}H_{23}N_2O_3)^+$, 72%]. ν_{max}/cm^{-1}: 1633 (<u>C=O</u>$_{carboxyl}$, s), 1226 (<u>C-O</u>$_{Phenol}$, s). Elemental analysis for $C_{21}H_{22}N_2O_3$•0.5H_2O: Calcd. C 70.89, H 6.40, N 7.87; found C 70.82, H 6.25, N 8.11.

Synthesis of (*S*)-2-(3,5-di-*tert*-butyl-2-hydroxybenzyl)-2,3,4,9-tetrahydro-1H-pyrido[3,4-b]indol-2-ium-3-carboxylate (L10)

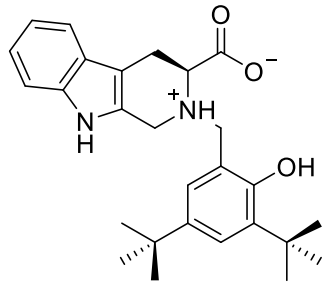

Reagents: L-Tryptophan (2.53 g, 10.0 mmol), NaOH (0.48 g, 12.0 mmol), paraformaldehyde (2 additions, 0.30 g each, 10.0 mmol each, one before and one after addition of 2,4-di-*tert*-buthylphenol), 2,4-di-*tert*-buthylphenol (2.06 g, 10.0 mmol), MeOH (25.0 mL). The compound was obtained as a yellow solid. Yield: 66% (2.85 g). δ_H (300 MHz, Acetone-d_6, ppm): 7.46 (1H, d, Ar<u>H</u>$_{Indolyl}$, adjacent to $C_{ipso}C_{ipso}CH_2CHCOO^-$, *J*= 7.1), 7.28 (1H, d, Ar<u>H</u>$_{Indolyl}$, adjacent to $C_{ipso}NHC_{ipso}$, *J*= 7.3), 7.11-6.89 (2H, m, Ar<u>H</u>$_{Indolyl}$), 6.86 (1H, s, Ar<u>H</u>$_{Phenol}$, *para* to CH_2NH^+), 6.75 (1H, s, Ar<u>H</u>$_{Phenol}$, *ortho* to CH_2NH^+), 5.46 (2H, s, NH^+C<u>H$_2$</u>$C_{ipso,}NH_{Indolyl}$), 4.62 (2H, s, NHC<u>H$_2$</u>PhOH), 4.20 (1H, d, $^-$OOCCHC<u>H</u>H, *J*= 14.8), 4.07 (1H, t, $^-$OOCC<u>H</u>CH$_2$, *J*= 5.9), 3.92 (1H, d, $^-$OOCCHCH<u>H</u>, *J*= 15.7), 1.40 (9H, s, ArC(C<u>H$_3$</u>)$_3$, *para* to HO_{Phenol}), 1.26 (9H, s, ArC(C<u>H$_3$</u>)$_3$, *ortho* to HO_{Phenol}). δ_C (300 MHz, Acetone-d_6, ppm): 174.70 (1C, <u>C</u>OO$^-$), 155.18 (1C, Ar<u>C</u>CH$_3$, *para* to HO_{Phenol}), 141.20 (1C, <u>C</u>$_{ipso,Pyrrolyl,\ position\ 3}$, adjacent to $CH_{Benzene\ ring}$), 137.39 (1C, <u>C</u>$_{ipso,Pyrrolyl,\ position\ 5}$, adjacent to CH_2NH^+), 136.20 (1C, Ar<u>C</u>H$_{Phenol}$, *para* to CH_2NH^+), 132.70 (1C, Ar<u>C</u>H$_{Phenol}$, *ortho* to CH_2NH^+), 127.96 (1C, <u>C</u>$_{ipso,Pyrrolyl,\ position\ 2}$, adjacent to $CH_{benzene\ ring}$), 124.87 (1C, Ar<u>C</u>OH), 124.11 (1C, Ar<u>C</u>CH$_3$, *ortho* to HO_{Phenol}), 122.00 (1C, Ar<u>C</u>CH_2NH^+), 121.87, 119.66 (1C each, Ar<u>C</u>H$_{Indolyl}$

each), 118.45 (1C, Ar<u>C</u>H$_{Indolyl}$, adjacent to C$_{ipso}$C$_{ipso}$CH$_2$CHCOO$^-$), 111.74 (1C, Ar<u>C</u>H$_{Indolyl}$, adjacent to C$_{ipso}$NHC$_{ipso}$), 104.30 (1C, <u>C</u>$_{ipso,Pyrrolyl,\ position\ 4}$, adjacent to CH$_2$CHCOO$^-$), 74.97 (1C, NH$^+$<u>C</u>H$_2$PhOH), 66.54 (1C, NH$^+$<u>C</u>H$_2C_{ipso}NH_{Indolyl}$), 59.56 (1C,$^-$OO<u>C</u>CHCH$_2$), 45.98 (1C, $^-$OOCCH<u>C</u>H$_2$), 35.43 (1C, <u>C</u>(CH$_3$)$_3$, *para* to HO$_{Phenol}$), 34.66 (1C, <u>C</u>(CH$_3$)$_3$, *ortho* to HO$_{Phenol}$), 32.01 (3C, C(<u>C</u>H$_3$)$_3$, *ortho* to HO$_{Phenol}$), 30.00 (3C, C(<u>C</u>H$_3$)$_3$, *para* to HO$_{Phenol}$). ESI-MS (Methanol): m/z= 457.07 [(C$_{27}$H$_{34}$N$_2$O$_3$Na)$^+$, 62%], m/z= 434.25 [(C$_{27}$H$_{35}$N$_2$O$_3$)$^+$, 53%]. ν_{max}/cm^{-1}: 1628 (<u>C=O</u>$_{carboxyl}$, m), 1229 (<u>C-O</u>$_{Phenol}$, m). Elemental analysis for C$_{27}$H$_{34}$N$_2$O$_3$•MeOH: Calcd. C 71.65, H 8.02, N 6.19; found C 71.69, H 8.21, N 5.70.

II.4.3.2.2 – General synthetic procedure for amino acid-methoxybenzene ligand precursors:

L-Phenylalanine or L-valine (depending on the desired product) and NaOH (1.3 eq./mmol amino acid) were weighted in a round bottom flask and suspended in EtOH (3 mL/mmol amino acid). After complete solubilization at r.t., 2-methoxybenzaldehyde (1.3 eq./mmol amino acid) was added to the mixture, accompanied with immediate solubilization, affording a colourless solution. After 10 minutes of stirring at r.t., NaBH$_4$ (1.5eq./mmol amino acid) was added and stirred for additional 30 minutes. The resulting suspension was cooled with the aid of an external ice bath to 5ºC and carefully acidified with concentrated HCl (dropwise) till pH~2. The mixture was evaporated to dryness, yielding a white residue which was suspended and vigorously stirred manually with 80 mL of isopropanol and filtered under vacuum. The filtrate was evaporated under vacuum till removal of *ca.* 80% of isopropanol total volume, being then poured into 150 mL of diethyl ether.

Synthesis of (*S*)-1-carboxy-*N*-(2-methoxybenzyl)-2-phenylethanaminium chloride (L11)

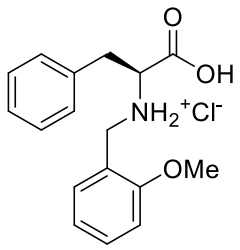

Reagents: L-Phenylalanine (1.65 g, 10.0 mmol), NaOH (0.500 g, 13.0 mmol), 2-methoxybenzaldehyde (1.77 g, 13.0 mmol), NaBH$_4$ (0.54 g, 15.0 mmol), EtOH (30.0 mL). After addition to diethyl ether, a white precipitate formed, which was filtered under vacuum and washed with 2x30 mL of diethyl ether, yielding the desired compound as a white solid. Yield: 78% (2.63 g). δ_H (300 MHz, CD$_3$OD, ppm): 7.51-7.42 (1H, m, Ar<u>H</u>$_{Phenyl}$, *para* to CH$_2$), 7.39-7.24 (6H, m, Ar<u>H</u>), 7.11-6.97 (2H, m, Ar<u>H</u>$_{MeOPhenyl}$, one *ortho* to CH$_2$NHCl and one *para* to OMe), 4.28 (2H, s, NH$_2$ClC<u>H$_2$</u>Ar(OCH$_3$)), 4.14 (1H, t, NH$_2$ClC<u>H</u>CH$_2$Ph, *J*= 6.9), 3.81 (3H, s, ArOC<u>H$_3$</u>), 3.27 (2H, d, NH$_2$ClCHC<u>H$_2$</u>Ph, *J*= 7.1, partially overlapped with MeOH). δ_C (300 MHz, CD$_3$OD, ppm): 170.44 (1C, <u>C</u>OOH), 159.47 (1C, <u>C</u>$_{ipso,MeOPhenyl}$, adjacent to OMe), 135.41 (1C, <u>C</u>$_{ipso,Phenyl,Phenylalanine}$), 132.99 (2C, Ar<u>C</u>H$_{Phenyl}$, *para* to CH$_2$ and Ar<u>C</u>H$_{MeOPhenyl}$, *ortho* to OMe, both overlapped) 130.42 (2C, Ar<u>C</u>H$_{Phenyl}$, *ortho* to CH$_2$) 130.14 (2C, Ar<u>C</u>H$_{Phenyl}$, *meta*

to CH_2), 128.97 (1C, Ar<u>C</u>H$_{MeOPhenyl}$, *para* to CH_2NHCl), 122.17 (1C, Ar<u>C</u>H$_{MeOPhenyl}$, *ortho* to CH_2NHCl), 119.42 (1C, <u>C</u>$_{ipso,MeOPhenyl}$, adjacent to CH_2NH_2Cl), 112.12 (1C, Ar<u>C</u>H$_{MeOPhenyl}$, *para* to CH_2NHCl), 61.47 (1C, NH_2Cl<u>C</u>HCH_2Ph), 56.10 (1C, O<u>C</u>H_3), 47.51 (1C, NH_2Cl<u>C</u>$H_2Ar(OMe)$), 36.81 (1C, NH_2ClCH<u>C</u>H_2Ph). ESI-MS (Methanol): m/z= 321.72 [$(C_{17}H_{20}ClNO_3)^-$, 100%], m/z= 286.05 [$(C_{17}H_{20}NO_3)^+$, 57%]. ν_{max}/cm^{-1}: 3086 (<u>N-H</u>, w), 1741 (<u>C=O</u>$_{carboxyl}$, s). Elemental analysis for $C_{17}H_{20}ClNO_3$•0.5MeOH: Calcd. C 62.22, H 6.56, N 4.15; found C 62.35, H 6.43, N 4.09.

Synthesis of (*S*)-1-carboxy-*N*-(2-methoxybenzyl)-2-methylpropanaminium chloride (L12)

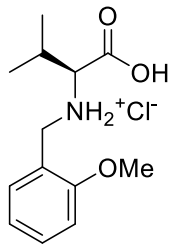

Reagents: L-Valine (2.35 g, 20.0 mmol), NaOH (1.00 g, 26.0 mmol), 2-methoxybenzaldehyde (3.54 g, 26.0 mmol), $NaBH_4$ (1.08 g, 30.0 mmol), EtOH (30.0 mL), EtOH (60.0 mL). After addition to diethyl ether, a white viscous residue formed at the bottom of the flask, which was consecutively decanted and washed with additional diethyl ether (2x30 mL). The resulting residue was dried at 50ºC under vacuum for 24 h and triturated manually, yielding the desired compound a white solid. Yield: 83% (4.83 g). δ_H (300 MHz, CD_3OD, ppm): 7.52-7.44 (1H, m, Ar<u>H</u>, *para* to CH_2NH_2Cl), 7.43-7.37 (1H, m, Ar<u>H</u>, *ortho* to OMe), 7.10 (1H, d, Ar<u>H</u>, *ortho* to CH_2NH_2Cl, *J*= 8.3), 7.03 (1H, t, ArH, *para* to OMe, *J*= 7.5), 4.39-4.23 (2H, m, NH_2ClC<u>H$_2$</u>PhOMe), 3.92 (3H, s, ArOC<u>H$_3$</u>), 3.70 (1H, d, NH_2ClC<u>H</u>$CH(CH_3)_2$, *J*= 3.5), 2.43-2.27 (1H, m, NH_2ClCHC<u>H</u>$(CH_3)_2$), 1.12 and 1.04 (3H each, d each, $CH(C$<u>H$_3$</u>$)_2$, *J*= 7.0 and 6.9, respectively). δ_C (300 MHz, CD_3OD, ppm): 169.95 (1C, <u>C</u>OOH), 159.68 (1C, Ar<u>C</u>OMe), 133.34 (1C, Ar<u>C</u>H, *ortho* to OMe), 133.03 (1C, Ar<u>C</u>H, *para* to CH_2NH_2Cl), 122.13 (1C, Ar<u>C</u>H, *para* to OMe), 119.40 (1C, <u>C</u>$_{ipso}$, adjacent to CH_2NHCl), 112.09 (1C, Ar<u>C</u>H, *ortho* to CH_2NH_2Cl), 65.47 (1C, NH_2Cl<u>C</u>$HCH(CH_3)_2$), 56.07 (1C, ArO<u>C</u>H_3), 47.59 (1C, NH_2Cl<u>C</u>H_2PhOMe), 30.53 (1C, NH_2ClCH<u>C</u>$H(CH_3)_2$), 19.31, 17.55 (2C each, $CH(\underline{C}H_3)_2$). ESI-MS (Methanol): m/z= 238.03 [$(C_{13}H_{20}NO_3)^+$, 62%]. ν_{max}/cm^{-1}: 2965 (<u>N-H</u>, s), 1711 (<u>C=O</u>$_{carboxyl}$, m). Elemental analysis for $C_{13}H_{20}ClNO_3$•0.5MeOH: Calcd. C 55.96, H 7.65, N 4.83; found C 56.20, H 7.89, N 4.62.

Synthesis of (S)-2,3,4,9-tetrahydro-1H-pyrido[3,4-b]indol-2-ium-3-carboxylate (CA1)

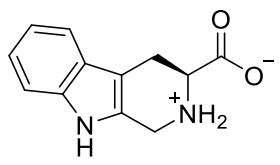

L-Tryptophan (4.09 g, 20.0 mmol) was weighted to a 250 mL round-bottom flask equipped with a reflux condenser and suspended in H_2O (5.00 mL/mmol amino acid), followed by the addition of concentrated HCl (33% in water, 2.80 mL, 30.0 mmol). After complete solubilization at r.t., formalin (36.5% formaldehyde in H_2O, 1.53 mL, 20.0 mmol) was added to the mixture, which was heated under reflux for 2 h, affording a white suspension. The heating was stopped, the reaction cooled to room temperature and the precipitate was filtered under vacuum and

washed with distilled water (4x100 mL) and diethyl ether (2x 50 mL), affording a pale yellow solid. Yield: 61% (3.08 g). δ_H (300 MHz, CD_3OD + drop of HCl, ppm): 7.49 (1H, d, Ar<u>H</u>, adjacent to C_{ipso}NH, *J*= 7.6), 7.36 (1H, d, Ar<u>H</u>, adjacent to C_{ipso}C=C, *J*= 8.0), 7.15 (1H, t, ArH, adjacent to ArHC_{ipso}NH, *J*= 7.4), 7.06 (1H, t, Ar<u>H</u>, adjacent to ArHC_{ipso}C=C, *J*= 7.4), 4.50 (3H, m, $HO_2CC\underline{H}CH_2$ and $NH_2ClC\underline{H}_2$, overlapping), 3.47, 3.19 (1H each, dd each, $HOOCCHC\underline{H}_2$, *J*= 16.0, 4.9). δ_C (300 MHz, CD_3OD + gota HCl, ppm): 171.15 (1C, <u>C</u>OOH), 138.43 (1C, $\underline{C}_{ipso,Aryl}$, adjacent to $NH_{Pyrrolyl}$), 127.26 (1C, $\underline{C}_{ipso}$, adjacent to $NH_{Pyrrolyl}$ and CH_2NH_2Cl), 126.08 (1C, $\underline{C}_{ipso,Aryl}$, adjacent to $C_{ipso}CH_2CH$), 123.46 (1C, Ar<u>C</u>H, adjacent to ArHC_{ipso}NH) 120.60 (1C, Ar<u>C</u>H, adjacent to ArHC_{ipso}C=C), 118.86 (1C, Ar<u>C</u>H, adjacent to C_{ipso}NH), 112.37 (1C, Ar<u>C</u>H, adjacent to C_{ipso}C=C), 106.19 (1C, $\underline{C}_{ipso}$, adjacent to CH_2CH), 56.81 (1C, NH<u>C</u>HCOOH), 41.83 (1C, $\underline{C}H_2NH_2Cl$), 23.37 (1C, $\underline{C}H_2CHCOOH$). Elemental analysis for $C_{12}H_{12}N_2O_2$•0.5H_2O: Calcd. C 63.99, H 5.82, N 12.44; found C 64.10, H 5.63, N 12.27.

II.4.3.3 – Amino acid-pyridyl-phenol ligand precursors

Synthesis of (*S*)-2-[(2-hydroxy-3,5-dimethylbenzyl)(pyridin-2-ylmethyl)ammonio]-3-phenylpropanoate (L13)

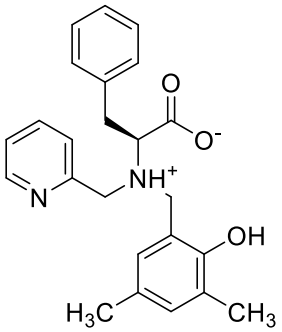

In 60 mL of a MeOH:H_2O (1:1) solution, **L1** (2 g, 7.81 mmol) was added, followed by the dropwise addition of aqueous NaOH (1M, 7 mL, $7x10^{-3}$ mmol) till the complete solubilization of **L1**. After 5 minutes of stirring at r.t., formalin (36.5% formaldehyde in H_2O, 0.589 mL, 7.81 mmol) and 2,4-dimethylphenol (0.98 g, 0.96 mL, 7.81 mmol) were added to the reaction, which was then heated under reflux for 4 h yielding a clear yellow solution. The mixture was then cooled to r.t. and concentrated HCl was added till pH~6 and a white suspension was obtained, which was then partially evaporated to MeOH removal. The resulting white precipitate was filtered, triturated and washed with petroleum ether (2x 20 mL), distilled water (2x 20 mL), saturated aqueous solution of $NaHCO_3$ (2x 20 mL) and distilled water (2x 20 mL), yielding a white-grey solid. Yield: 43% (1.31 g) δ_H (300 MHz, CD_3OD, ppm): 8.47 (1H, m, $NH^+CH_2Ar\underline{H}_{pyridyl}$, C<u>H</u>CHCHCHN), 7.75 (1H, m, $NH^+CH_2Ar\underline{H}_{pyridyl}$, CHC<u>H</u>CHCHN), 7.34 (1H, d, $NH^+CH_2Ar\underline{H}_{pyridyl}$, CHCHCHC<u>H</u>N, *J*= 7.5), 7.28 (1H, dd, $NH^+CH_2Ar\underline{H}_{pyridyl}$, CHCHC<u>H</u>CHN, *J*= 7.4, 5.0), 7.24-7.15 (3H, m, Ar<u>H</u>$_{Phenyl}$, *meta* and *para* to CH_2), 7.09 (2H, dd, Ar<u>H</u>$_{Phenyl}$, *ortho* to CH_2), 6.81 (1H, s, Ar<u>H</u>$_{Phenol,}$ *para* to CH_2NH^+), 6.61 (1H, s, Ar<u>H</u>$_{Phenol}$, *ortho* to CH_2NH^+), 4.17 (2H, dd, $^-OOCCHNH^+C\underline{H}_2$Py, *J*= 46.5, 15.3), 3.94 (2H, dd, $^-OOCCHNH^+C\underline{H}_2$PhOH, *J*= 28.9, 13.2), 3.77 (1H, t, $^-OOCC\underline{H}CH_2$Ph, *J*= 7.2), 3.26 (1H, dd, $^-OOCCHC\underline{H}$HPh, partially overlapped with CD_3OD signal, *J*= 14.2, 6.8), 3.05 (1H, dd, $^-OOCCHCH\underline{H}$Ph, *J*= 14.2, 7.7), 2.15 (3H, s, C<u>H</u>$_3$, *para* to HO$_{Phenol}$), 2.09 (3H, s, C<u>H</u>$_3$, *ortho* to HO$_{Phenol}$). δ_C (300 MHz, CD_3OD, ppm): 174.60 (1C, <u>C</u>OO^-), 158.00 (1C, $\underline{C}_{ipso,Pyridyl}$),

153.59 (1C, Ar<u>C</u>OH$_{Phenol}$), 149.42 (1C, Ar<u>C</u>H$_{Pyridil}$, <u>C</u>HCHCHCHN), 139.46 (1C, <u>C</u>$_{ipso,Phenyl}$), 138.77 (1C, Ar<u>C</u>H$_{Pyridil}$, CH<u>C</u>HCHCHCHN), 132.50 (1C, Ar<u>C</u>H$_{Phenol}$, *para* to CH_2NH^+), 130.29 (2C, Ar<u>C</u>H$_{Phenyl}$, *ortho* to CH_2), 129.88 (1C, Ar<u>C</u>H$_{Phenol}$, *ortho* to CH_2NH^+), 129.43 (2C, Ar<u>C</u>H$_{Phenyl}$, *meta* to CH_2), 129.29 (1C, Ar<u>C</u>CH$_3$, *para* to HO$_{Phenol}$), 127.52 (1C, Ar<u>C</u>H$_{Phenyl}$, *para* to CH_2), 125.71 (1C, Ar<u>C</u>CH$_3$, *ortho* to HO$_{Phenol}$), 124.57 (1C, Ar<u>C</u>H$_{Pyridil}$, CHCHCH<u>C</u>HN), 124.07 (1C, Ar<u>C</u>H$_{Pyridil}$, CHCH<u>C</u>HCHN), 121.68 (1C, Ar<u>C</u>$_{Phenol}$, adjacent to CH_2NH^+), 65.93 (1C, $^-$OO<u>C</u>CHCH$_2$Ph), 56.27 (1C, NH$^+$<u>C</u>H$_2$Py), 55.36 (1C, NH$^+$<u>C</u>H$_2$PhOH), 35.71 (1C, $^-$OOCCH<u>C</u>H$_2$Ph), 20.48 (1C, <u>C</u>H$_3$, *para* to HO$_{Phenol}$), 16.21 (1C, <u>C</u>H$_3$, *ortho* to HO$_{Phenol}$). ESI-MS (Methanol): m/z= 389.38 [$(C_{24}H_{25}N_2O_3)^-$, 100%]. ν_{max}/cm^{-1}: 1576 (<u>C=O</u>$_{carboxyl}$, s), 1227 (<u>C-O</u>$_{Phenol}$, s). Elemental analysis for $C_{24}H_{26}N_2O_3 \bullet H_2O$: Calcd. C 70.57, H 6.91, N 6.86; found C 70.41, H 6.53, N 6.78.

Synthesis of (*S*)-2-[(3,5-di-*tert*-butyl-2-hydroxybenzyl)(pyridin-2-ylmethyl)ammonio]-3-phenylpropanoate (L14)

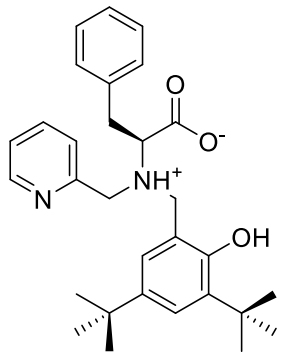

L1 (2 g, 7.81 mmol) was suspended in 60 mL of a MeOH:H_2O (1:1) solution and aqueous NaOH (1M, 7 mL, 7x10^{-3} mmol) was added dropwise to the suspension till the complete solubilization of **L1** was achieved. After 5 minutes of stirring at r.t., formalin (36.5% formaldehyde in H_2O, 0.589 mL, 7.81 mmol) and 2,4-di-*tert*-butylphenol (1.61 g, 7.81 mmol) were added to the mixture, which was then heated under reflux for 4 h yielding a clear yellow solution. The reaction mixture was cooled to r.t. and concentrated HCl was added till pH~6, followed by evaporation to remove the excess of MeOH. Again, concentrated HCl was added to the mixture till pH~2 and the resulting grey precipitate was carefully stirred and decanted, triturated and decanted with petroleum ether (2x 20 mL), filtered and the residue was washed with distilled water (2x 20 mL), saturated aqueous solution of $NaHCO_3$ (2x 20 mL) and distilled water (2x 20 mL), yielding a white-grey solid. Yield: 30 % (1.1g) δ_H (300 MHz, CD_3OD, ppm): 8.42 (1H, d, Ar<u>H</u>$_{Pyridyl,\ C\underline{H}CHCHCHN}$, *J*= 5.5), 8.13 (1H, t, Ar<u>H</u>$_{Pyridyl}$, CHC<u>H</u>CHCHN, *J*= 7.8), 7.65 (1H, t, Ar<u>H</u>$_{Pyridyl}$, CHCHC<u>H</u>CHN, *J*= 6.6), 7.42 (1H, d, Ar<u>H</u>$_{Pyridyl}$, CHCHCHC<u>H</u>N, *J*= 8.0), 7.38-7.23 (5H, m, Ar<u>H</u>$_{Phenyl}$), 7.07 (1H, s, Ar<u>H</u>$_{Phenol,}$ *para* to CH_2NH^+), 6.89 (1H, s, Ar<u>H</u>$_{Phenol}$, *ortho* to CH_2NH^+), 4.41 (1H, d, NH$^+$C<u>H</u>HPy, *J*= 16.5), 4.20 (1H, t, $^-$OOCC<u>H</u>CH$_2$Ph, *J*= 5.1, partially overlapped with NH$^+$<u>CH$_2$</u>Py), 4.16 (1H, d, NH$^+$CH<u>H</u>Py, *J*= 6.1, partially overlapped with $^-$OOCC<u>H</u>CH$_2$Ph), 4.04 (2H, dd, NH$^+$C<u>H$_2$</u>PhOH, *J*= 32.1, 13.0), 3.41 (1H, dd, $^-$OOCCHC<u>H</u>HPh, *J*= 14.6, 6.4), 3.23 (1H, dd, $^-$OOCCHCH<u>H</u>Ph, *J*= 14.6, 9.1), 1.28 (9H, s, C(C<u>H$_3$</u>)$_3$), *para* to HO$_{Phenol}$), 1.23 (9H, s, C(C<u>H$_3$</u>)$_3$), *ortho* to HO$_{Phenol}$). δ_C (300 MHz, CD_3OD, ppm): 175.37 (1C, <u>C</u>OO$^-$), 156.08 (1C, <u>C</u>$_{ipso,Pyridyl}$), 153.40 (1C, Ar<u>C</u>OH$_{Phenol}$), 146.32 (1C, Ar<u>C</u>H$_{Pyridil}$,

CHCHCHCHN), 143.31 (1C, ArC(^{t}Butyl), *ortho* to HO_{Phenol}), 142.16 (1C, $ArCH_{Pyridil}$, CHCHCHCHN), 139.02 (1C, $C_{ipso,Phenyl}$), 137.68 (1C, ArC(^{t}Butyl), *para* to HO_{Phenol}), 130.34 (2C, $ArCH_{Phenyl}$, *ortho* to CH_2), 129.89 (2C, $ArCH_{Phenyl}$, *meta* to CH_2), 128.01 (1C, $ArCH_{Phenyl}$, *para* to CH_2), 127.30 (1C, $ArCH_{Pyridil}$, CHCHCHCHN), 126.58 (1C, $ArCH_{Phenol}$, *ortho* to CH_2NH^+), 126.19 (1C, $ArCH_{Pyridil}$, CHCHCHCHN), 125.14 (1C, $ArCH_{Phenol}$, *para* to CH_2NH^+), 123.64 (1C, ArC_{Phenol}, adjacent to CH_2NH^+), 67.72 (1C, $^-OOCCHCH_2Ph$), 57.18 (1C, NH^+CH_2PhOH), 54.65 (1C, NH^+CH_2Py), 36.08 (1C, $^-OOCCHCH_2Ph$), 35.74 (1C, $C(CH_3)_3$, *ortho* to HO_{Phenol}), 34.99 (1C, $C(CH_3)_3$, *para* to HO_{Phenol}), 31.99 (3C, $C(CH_3)_3$, *ortho* to HO_{Phenol}), 30.26 (3C, $C(CH_3)_3$, *para* to HO_{Phenol}). ESI-MS (Methanol): m/z= 475.12 [$(C_{30}H_{39}N_2O_3)^+$, 100%]. ν_{max}/cm^{-1}: 1733 ($C{=}O_{carboxyl}$, s), 1227 ($C\text{-}O_{Phenol}$, m). Elemental analysis for $C_{30}H_{38}N_2O_3 \cdot 2H_2O$: Calcd. C 70.31, H 8.30, N 5.47; found C 70.25, H 7.90, N 5.22.

Synthesis of potassium (2*S*,2'*S*)-2,2'-({[5-(*tert*-butyl)-2-oxido-1,3-phenylene]bis(methylene)}bis[(pyridin-2-ylmethyl)azanediyl])bis(3-phenylpropanoate) (L15)

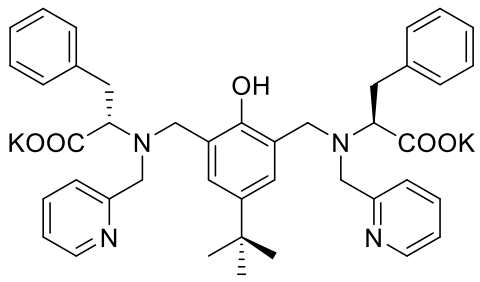

L1 (2 g, 7.81 mmol) and KOH (0.44 g, 7.81 mmol) were weighted to a 50 mL round-bottomed flask and dissolved in 20 mL of isopropanol at r.t. Paraformaldehyde (0.469 g, 15.6 mmol) was added to the reaction mixture and stirred till complete solubilization, followed by the addition of 4-*tert*-butylphenol (0.587 g, 3.91 mmol). The mixture was heated under reflux for 6 h, gradually affording a white suspension over time. The reaction mixture was cooled to r.t., the residue filtered under vacuum and washed with 3x50 mL isopropanol, yielding the desired product as a white solid. Yield: 18 % (1.19 g). δ_H (300 MHz, CD_3OD, ppm): 8.26 (2H, d, $ArH_{Pyridyl}$, CHCHCHCHN, *J*= 4.3), 7.47 (2H, t, $ArH_{Pyridyl}$, CHCHCHCHN, *J*= 7.3), 7.18 (12H, m, ArH), 7.08 (2H, t, $ArH_{Pyridyl}$, CHCHCHCHN, *J*= 6.0), 6.92 (2H, s, ArH_{PhOH}), 4.06 (2H, d, NCHHPhOH, partially overlapped with NCH_2Py, *J*= 14.0), 3.94 (4H, dd, NCH_2Py, *J*= 31.2, 15.4, partially overlapped with NCH_2PhOH) 3.84 (2H, d, NCHHPhOH, partially overlapped with NCH_2Py, *J*= 14.0), 3.57 (2H, t, KOOCCHCH$_2$Ph, *J*= 6.7), 3.18, 3.05 (2H each, dd each, KOOCCHCH_2Ph, *J*= 13.6, 5.9 each), 1.09 (9H, s, $C(CH_3)_3$). δ_C (300 MHz, CD_3OD, ppm): 179.83 (2C, COOH), 161.69 (2C, $C_{ipso,Pyridyl}$), 154.31 (2C, $C_{ipso,PhOH}$, *ortho* to COH), 148.84 (2C, $ArCH_{Pyridyl}$, CHCHCHCHN), 141.92 (1C, $C_{ipso,PhOH}$, *para* to COH), 141.80 (2C, $C_{ipso,Phenyl}$), 138.11 (2C, $ArCH_{Pyridyl}$, CHCHCHCHN), 130.57 (4C, $ArCH_{Phenyl}$, *meta* to $CH_2CHCOOH$), 129.17 (4C, $ArCH_{Phenyl}$, *ortho* to $CH_2CHCOOH$), 126.87 (2C, $ArCH_{PhOH}$), 126.83 (2C, $ArCH_{Phenyl}$, *para* to $CH_2CHCOOH$), 124.87 (1C, ArCOH), 124.50 (2C, $ArCH_{Pyridyl}$, CHCHCHCHN), 123.05 (2C,

Ar<u>C</u>H$_{Pyridyl}$, CH<u>C</u>HCHCHN), 69.42 (2C, KOOC<u>C</u>HCH$_2$Ph), 57.99 (2C, N<u>C</u>H$_2$Pyridyl), 52.98 (2C, N<u>C</u>H$_2$PhOH), 36.82 (2C, KOOCCH<u>C</u>H$_2$Ph), 34.72 (1C, <u>C</u>(CH$_3$)$_3$), 32.08 (3C, C(<u>C</u>H$_3$)$_3$). ESI-MS (Methanol): m/z= 762.93 [$(C_{42}H_{45}K_2N_4O_5)^+$, 100%]. ν_{max}/cm^{-1}: 1562 (<u>C=O</u>$_{carboxyl}$, s), 1241 (<u>C-O</u>$_{Phenol}$, w). Elemental analysis for $C_{42}H_{44}K_2N_4O_5$•3H$_2$O: Calcd. C 61.74, H 6.17, N 6.86; found C 61.46, H 6.16, N 6.60.

II.4.3.4 – *β*-Ketoamino acid ligand precursors

General synthetic procedure: L-Phenylalanine or L-valine, depending on the desired product, was weighted to a round bottom flask equipped with a reflux condenser and suspended with 1.25 mL/mmol of water. To the resulting white suspension, 0.12 mL/mmol of formalin (36.5% formaldehyde in H_2O, 1.58 eq.) and 0.125 mL/mmol of concentrated HCl were added, leading to a colourless solution after 10 minutes of magnetic stirring at r.t. After this period, 1 mole equivalent of the corresponding ketone was added to the reaction mixture, which was then heated under reflux for 24 h yielding a dark-yellow solution. The heating was stopped after this period, the reaction cooled till r.t. and an aqueous saturated solution of $NaHCO_3$ was carefully mixed until pH~6, originating a white-yellow suspension. Distilled water was generously added to the reaction mixture, the suspension filtered under vacuum and washed with 3x50 mL of distilled water and 3x50 mL of acetone, yielding the desired product.

Synthesis of (*S*)-2-[(3-oxo-3-phenylpropyl)ammonio]-3-phenylpropanoate (L16)

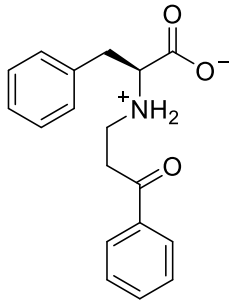

Reagents: L-Phenylalanine (3.30 g, 20.0 mmol), formalin (36.5% formaldehyde in H_2O, 2.37 mL, 31.6 mmol), concentrated HCl (2.50 mL, 219 mmol), acetophenone (2.34 mL, 20.0 mmol), water (25.0 mL). The compound was obtained as a white solid. Yield: 30% (1.79 g). δ_H (300 MHz, CD_3OD+HCl, ppm): 8.00 (2H, t, Ar<u>H</u>$_{ketone,}$ *meta* to C=O, *J*= 7.7), 7.70-7.59 (1H, m, Ar<u>H</u>$_{ketone}$, *para* to C=O), 7.52 (2H, m, Ar<u>H</u>$_{ketone}$, *ortho* to C=O), 7.46-7.22 (5H, m, Ar<u>H</u>$_{Phenylalanine}$), 4.39 (1H, t, NH_2^+C<u>H</u>CH$_2$Ar$_{Phenylalanine}$, *J*= 6.3), 3.59 (2H, t, NH_2^+CH$_2$C<u>H$_2$</u>C(O)Ph, *J*= 5.6), 3.51 (2H, t, NH_2^+C<u>H$_2$</u>CH$_2$C(O)Ph, *J*= 5.3), 3.38 (2H, dd, NH_2^+CHC<u>H$_2$</u>Ph$_{Phenylalanine}$, *J*= 14.6, 6.3). δ_C (300 MHz, CD_3OD+HCl, ppm): 198.68 (1C, CH$_2$<u>C</u>(O)Ph), 170.5 (1C, <u>C</u>OO$^-$), 137.1 (1C, <u>C</u>$_{ipso,Phenyl,\ ketone}$), 135.27 (1C, <u>C</u>$_{ipso,Phenyl,\ Phenylalanine}$), 134.97 (1C, Ar<u>C</u>H$_{ketone}$, *para* to C=O), 130.55, 129.99 (2C each, Ar<u>C</u>H$_{Phenylalanine}$) 129.86 (2C, Ar<u>C</u>H$_{ketone}$, *ortho* to C=O), 129.22 (2C, Ar<u>C</u>H$_{ketone}$, *meta* to C=O), 128.81 (1C, Ar<u>C</u>H$_{Phenylalanine}$, *para* to CH$_2$), 62.80 (1C, NH_2^+<u>C</u>HCH$_2$Ph$_{Phenylalanine}$), 43.71 (1C, NH_2^+<u>C</u>H$_2$CH$_2$C(O)Ph), 36.58 (1C, NH_2^+CH<u>C</u>H$_2$Ph$_{Phenylalanine}$), 35.72 (1C, NH_2^+CH$_2$<u>C</u>H$_2$C(O)Ph). ESI-MS (Methanol+AcOH): m/z= 298.14 [$(C_{18}H_{20}NO_3)^+$, 100%]. ν_{max}/cm^{-1}: 2985 (<u>N-H</u>, m), 1680 (<u>C=O</u>$_{carbonyl}$, s), 1578 (<u>C=O</u>$_{carboxyl}$, s). Elemental analysis for $C_{18}H_{19}NO_3$: Calcd. C 72.71, H 6.44, N 4.71; found C 72.10, H 6.47, N 4.60.

Synthesis of (*S*)-3-methyl-2-[(3-oxo-3-phenylpropyl)ammonio]butanoate (L17)

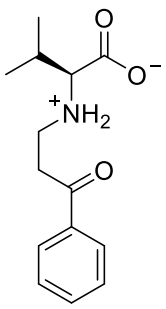

Reagents: L-Valine (2.47 g, 21.0 mmol), formalin (36.5% formaldehyde in H_2O, 2.5 mL, 33.2 mmol), concentrated HCl (2.63 mL, 230 mmol), acetophenone (2.50 mL, 21.0 mmol), water (26.3 mL). The compound was obtained as a white solid. Yield: 36% (1.90 g). δ_H (300 MHz, CD_3OD+HCl, ppm): 8.02 (2H, d, ArH, *ortho* to C=O, *J*= 7.6), 7.65 (1H, t, ArH, *para* to C=O, *J*= 7.3), 7.53 (2H, t, ArH, *meta* to C=O, *J*= 7.6), 4.03 (1H, d, $^-OOCCHNH_2^+$, *J*= 3.2) 3.68 (2H, t, $NH_2^+CH_2CH_2C(O)Ph$, *J*= 6.1), 3.53 (2H, t, $NH_2^+CH_2CH_2C(O)Ph$, *J*= 5.7), 2.57-2.37 (1H, m, $CH(CH_3)_2$), 1.19, 1.10 (3H each, d each, $CH(CH_3)_2$, *J*= 7.0 and 6.9, respectively). δ_C (300 MHz, CD_3OD+HCl, ppm): 198.69 (1C, $CH_2C(O)Ph$), 170.2 (1C, COO^-), 137.15 (1C, $C_{ipso,Phenyl}$), 134.97 (1C, ArCH, *para* to C=O), 129.88 (2C, ArCH, *meta* to C=O), 129.24 (2C, ArCH, *ortho* to C=O), 67.34 (1C, $HOOCCHNH_2^+$), 44.27 (1C, $NH_2^+CH_2CH_2C(O)Ph$), 35.71 (1C, $NH_2^+CH_2CH_2C(O)Ph$), 30.46 (1C, $CH(CH_3)_2$), 19.59, 17.47 (1C each, $CH(CH_3)_2$). ESI-MS (Methanol+AcOH): m/z= 250.06 [$(C_{14}H_{20}NO_3)^+$, 100%]. ν_{max}/cm^{-1}: 2964 (N-H, m), 1682 ($C{=}O_{carbonyl}$, s), 1577 ($C{=}O_{carboxyl}$, s). Elemental analysis for $C_{14}H_{19}NO_3$: Calcd. C 67.45, H 7.68, N 5.62; found C 67.39, H 7.81, N 5.47.

Synthesis of (*S*)-2-{[3-(naphthalen-2-yl)-3-oxopropyl]ammonio)-3-phenylpropanoate (L18)

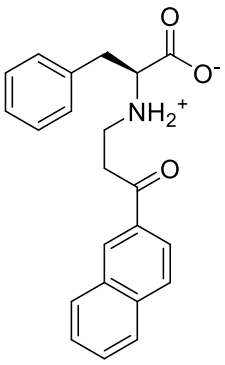

Reagents: L-Phenylalanine (3.30 g, 20.0 mmol), formalin (36.5% formaldehyde in H_2O, 2.37 mL, 31.6 mmol), concentrated HCl (2.50 mL, 219 mmol), 2-acetonaphthone (3.40 g, 20.0 mmol), water (25.0 mL). The compound was obtained as a white solid. Yield: 29% (2.04 g). δ_H (300 MHz, CD_3OD+HCl, ppm): 8.64 (1H, s, ArH, $C1_{Naphthyl}$), 8.14-7.85 (4H, m, ArH, C5-$C8_{Naphthyl}$) 7.72-7.52 (2H, m, ArH, C3-$C4_{Naphthyl}$) 7.48-7.24 (5H, m, ArH_{Phenyl}), 4.43 (1H, t, $NH_2^+CHCH_2Ph$, *J*= 6.3), 3.72 (2H, t, $NH_2^+CH_2CH_2C(O)Naph$, *J*= 6.2), 3.56 (2H, t, $NH_2^+CH_2CH_2C(O)Naph$, *J*= 6.1), 3.40 (2H, dd, $NH_2^+CHCH_2Ph$, *J*= 13.6, 6.3). δ_C (300 MHz, CD_3OD+HCl, ppm): 198.50 (1C, $CH_2C(O)Naph$), 170.53 (1C, COO-), 137.29 (1C, $C2_{Naphthyl}$, adjacent to C=O), 135.32 (1C, $C_{ipso,Phenyl}$), 134.44, 133.9 (1C each, C9 and $C10_{Naphthyl}$), 131.56 (1C, ArCH, $C1_{Naphthyl}$), 130.79 (1C, ArCH, C5 or $C8_{Naphthyl}$), 130.58, 130.02 (2C each, $ArCH_{Phenyl}$, *ortho* and *meta* to CH_2), 129.6 (1C, ArCH, C5 or $C8_{Naphthyl}$), 128.84 (1C, ArCH, $C4_{Naphthyl}$), 128.81 (1C, $ArCH_{Phenyl}$, *para* to CH_2), 128.09, 128.01 (1C each, ArCH, C5 and $C8_{Naphthyl}$), 124.36 (1C, ArCH, $C3_{Naphthyl}$), 62.79 (1C, $NH_2^+CHCH_2Ph$), 43.80 (1C, $NH_2^+CH_2CH_2C(O)Naph$), 36.61 (1C, $NH_2^+CHCH_2Ph$), 35.73 (1C, $NH_2^+CH_2CH_2C(O)Naph$). ESI-MS (Methanol+AcOH): m/z= 348.15 [$(C_{22}H_{22}NO_3)^+$, 100%].

ν_{max}/cm^{-1}: 3032 (N-H, w), 1679 (C=O$_{carbonyl}$, s), 1578 (C=O$_{carboxyl}$, s). Elemental analysis for $C_{22}H_{21}NO_3$•$0.5H_2O$: Calcd. C 74.14, H 6.22, N 3.93; found C 73.71, H 5.97, N 3.87.

Synthesis of (*S*)-3-methyl-2-{[3-(naphthalen-2-yl)-3-oxopropyl]ammonio}butanoate (L19)

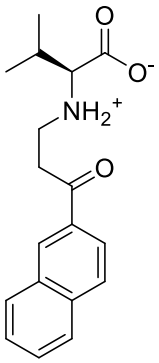

Reagents: L-Valine (4.94 g, 42.0 mmol), formalin (36.5% formaldehyde in H_2O, 5.00 mL, 66.4 mmol), concentrated HCl (5.00 mL, 438 mmol), 2-acetonaphthone (7.16 g, 42.0 mmol), water (42.5 mL). The compound was obtained as a white solid. Yield: 40% (5.04 g). δ_H (300 MHz, CD_3OD+HCl, ppm): 8.66 (1H, s, ArH, C1$_{Naphthyl}$), 8.11-8.04 (1H, m, ArH), 8.02 (1H, s, ArH, C3$_{Naphthyl}$) 7.99-7.90 (2H, m, ArH), 7.69-7.55 (2H, m, ArH), 4.07 (1H, d, NH_2^+CHCH$(CH_3)_2$, *J*= 3.4) 3.78 (2H, t, $NH_2^+CH_2CH_2C(O)$Naph, *J*= 6.3), 3.57 (2H, t, $NH_2^+CH_2CH_2C(O)$Naph, *J*= 6.2), 2.58-2.48 (1H, m, $NH_2^+CHCH(CH_3)_2$), 1.21, 1.12 (3H each, d each, $CH(CH_3)_2$, *J*= 7.0 and 6.9, respectively). δ_C (300 MHz, CD_3OD+HCl, ppm): 198.52 (1C, $CH_2C(O)$Naph), 170.21 (1C, COO^-), 137.28 (1C, C2$_{Naphthyl}$, adjacent to C=O), 134.49, 133.91 (1C each, C9$_{Naphthyl}$ and C10$_{Naphthyl}$) 131.56 (1C, ArCH, C3$_{Naphthyl}$), 130.79 (1C, ArCH, C4$_{Naphthyl}$), 130.01, 129.6, 128.81, 128.08 (4C, ArCH, C5-C8$_{Naphthyl}$), 124.37 (1C, ArCH, C1$_{Naphthyl}$), 67.36 (1C, NH_2^+CHCH$(CH_3)_2$), 44.37 (1C, $NH_2^+CH_2CH_2C(O)$Naph), 35.71 (1C, $NH_2^+CH_2CH_2C(O)$Naph), 30.5 (1C, NH_2^+CHCH$(CH_3)_2$), 19.58, 17.46 (1C each, $CH(CH_3)_2$). ESI-MS (Methanol+AcOH): m/z= 300.09 [$(C_{18}H_{22}NO_3)^+$, 100%]. ν_{max}/cm^{-1}: 2963 (N-H, m), 1684 (C=O$_{carbonyl}$, s), 1576 (C=O$_{carboxyl}$, s). Elemental analysis for $C_{18}H_{21}NO_3$: Calcd. C 72.22, H 7.07, N 4.68; found C 71.82, H 7.12, N 4.51.

CHAPTER 3

Amino acid-Derived Iron(III) Complexes

III – Amino acid-Derived Iron(III) Complexes

III.1 – Preamble

In this Chapter the synthesis and characterization of novel Fe(III) amino acid complexes derived from the compounds prepared in Chapter 2 will be presented. The preparation of these complexes was highly focused on the application of simple and sustainable one-pot reactions, using commercial $FeCl_3 \bullet 6H_2O$ as the Fe(III) source. After the successful synthesis and characterization of these compounds, their application as pre-catalysts was tested in asymmetric oxidative coupling of 2-naphthol, epoxidation of benzalacetophenones and oxidation of 1-phenylethan-1-ol, using mild and environmentally-friendly conditions as much as possible.

III.2 – Preparation of iron(III) amino acid complexes: Results and discussion

The structural formulae of the synthesized Fe(III) amino acid complexes are presented in **Figure III-1**, based on their elemental analyses.

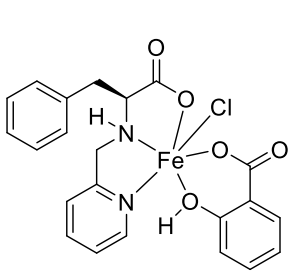

FeL1A

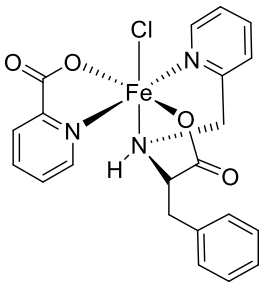

FeL1B

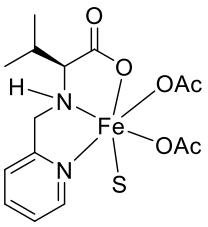

FeL2
S= solvent

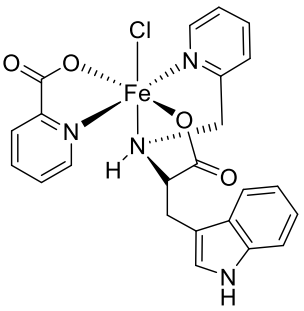

FeL3

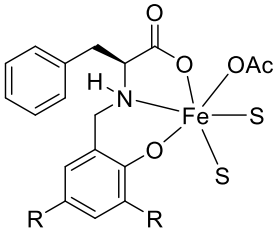

FeL5: R= CH_3
FeL6: R= $C(CH_3)_3$
S= solvent

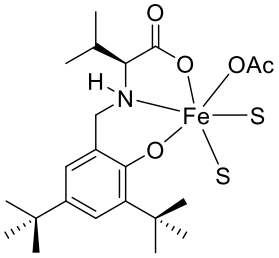

FeL8
S= solvent

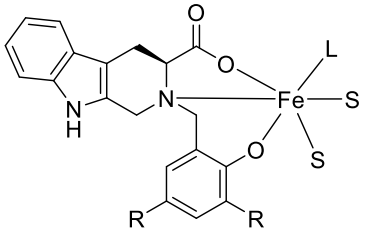

FeL9: R= CH_3, L= Cl
FeL10: R= $C(CH_3)_3$, L= OAc
S= solvent

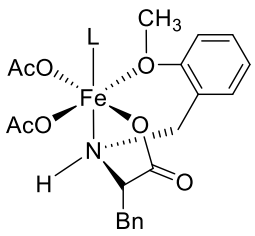

FeL11
S= solvent

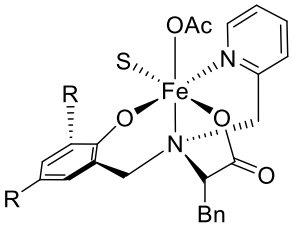

FeL13: R= CH_3
FeL14: R= $C(CH_3)_3$
S= Solvent

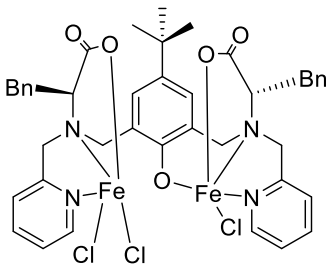

FeL15

Figure III-1: Structural formulae of the prepared Fe(III) amino acid compounds based on their elemental analyses.

The synthesis of the desired Fe(III) amino acid complexes was achieved with one-pot reactions under mild conditions by reacting $FeCl_3 \cdot 6H_2O$ with the corresponding amino acid-derived ligand precursor at room temperature in alcoholic medium, without the requirement of inert atmosphere. A base such as sodium salycilate, sodium picolinate or sodium acetate was therefore subsequently added to the reaction mixture to ensure the adjustment of pH to *ca.* 6-7 and subsequent precipitation of the desired complex (**Scheme III-1**).

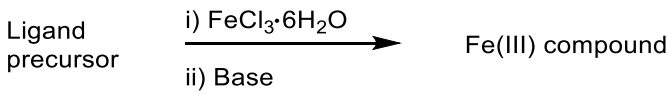

Scheme III-1: General synthetic procedure for the synthesis of the desired Fe(III) amino acid complexes.

The direct utilization of strong inorganic bases such as NaOH or KOH was avoided to prevent the formation of Fe(III) hydroxide species, which would interfere with the isolation of the desired compounds. The compounds were obtained as amorphous solids with different colours, depending on the ligand precursor and the used base for precipitation and on subsequent *work-up* procedures for isolation and purification. All compounds are air-stable and after isolation were stored at room temperature in a dry environment, considering the great stability of Fe(III) compounds in such conditions. All complexes were divided in this Chapter into subsections **III.2.1** to **III.2.4** based on the ligand precursors used in their preparation. The characterization of the Fe(III) complexes was performed by UV-Vis spectroscopy (UV-Vis) and Circular Dichroism (CD), Electrospray Ionization Mass Spectrometry (ESI-MS), Infrared Spectroscopy (FT-IR) and Elemental Analysis (EA). Suitable crystals for single-crystal X-ray diffraction were obtained for **FeL1B**, **FeL3** and **FeL14**. Redox measurements were executed by Cyclic Voltammetry (CV). Magnetic susceptibility of these compounds was determined by the Evans method.

III.2.1 – Fe(III) complexes with amino acid-pyridyl and amino acid-imidazolyl ligands

The synthesis of Fe(III) complexes **FeL1A**, **FeL1B**, **FeL2** and **FeL3** will be presented herein and their structural formulae are depicted in **Figure III-2**. All synthetic procedures entailed the suspension or solubilization of the corresponding ligand precursor in the reaction solvent, followed by the addition of $FeCl_3 \bullet 6H_2O$ in an open vessel at room temperature. After complete solubilization of the reagents, an appropriate base was added to the reaction, which was let to stir till precipitate formation. Subsequent *work-up* treatment of the reaction mixture will be described for each case and afforded the desired complexes.

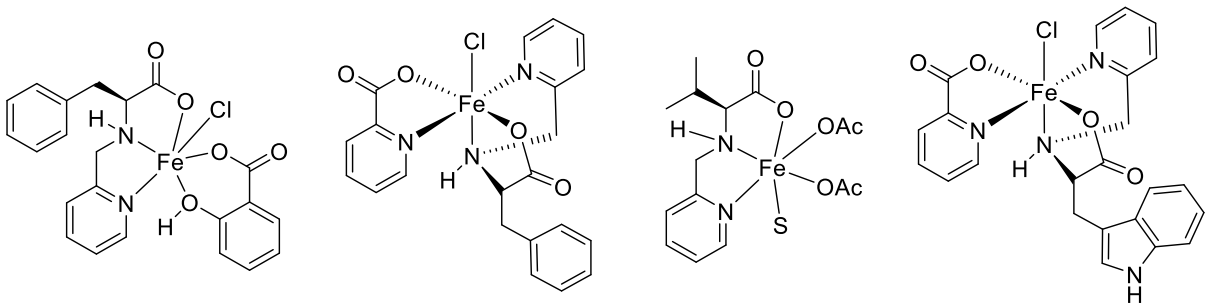

FeL1A **FeL1B** **FeL2** **FeL3**

S= solvent

Figure III-2: Structural formulae of the prepared Fe(III) amino acid compounds **FeL1A**, **FeL1B**, **FeL2** and **FeL3**, based on their elemental analyses.

Fe(III) complexes **FeL1A** and **FeL1B** used **L1** as ligand precursor and the synthetic procedures applied for their preparation differ on the solvent used and on the organic salt added. The synthesis of **FeL1A** is presented in **Scheme III-2** and started with the suspension of **L1** in water, followed by the addition of one mole equivalent of $FeCl_3 \bullet 6H_2O$, affording a clear orange solution after 5 minutes of stirring at room temperature. Separately, an aqueous solution of one mole equivalent of sodium salicylate was prepared and added to the mixture, immediately originating the formation of a purple precipitate which was filtered under vacuum. The resulting residue was dissolved in acetone, dried with anhydrous Na_2SO_4, filtered and the filtrate evaporated to dryness, affording **FeL1A** as a dark-purple solid in 63%.

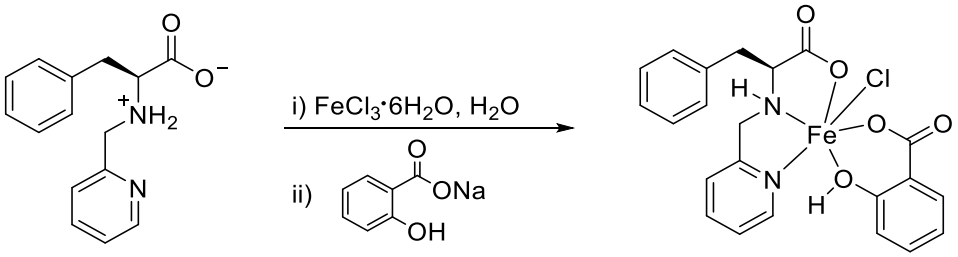

L1 **FeL1A**

Scheme III-2: Synthetic procedure for the preparation of Fe(III)complex **FeL1A**.

The preparation of Fe(III) complex **FeL1B** followed the same initial synthetic step of suspending **L1** and $FeCl_3 \bullet 6H_2O$, but in an water/ethanol mixture (**Scheme III-3**). After complete solubilization of the mixture, an aqueous solution of one mole equivalent of sodium picolinate was added to the reaction, immediately inducing precipitation of a yellow solid which was filtered and washed with distilled water and acetone, affording **FeL1B** as a yellow solid in 85%. The same synthetic procedure was applied with **L3** as ligand precursor for the preparation of **FeL3**, affording the desired Fe(III) complex as an light orange solid in 82% (**Scheme III-3**).

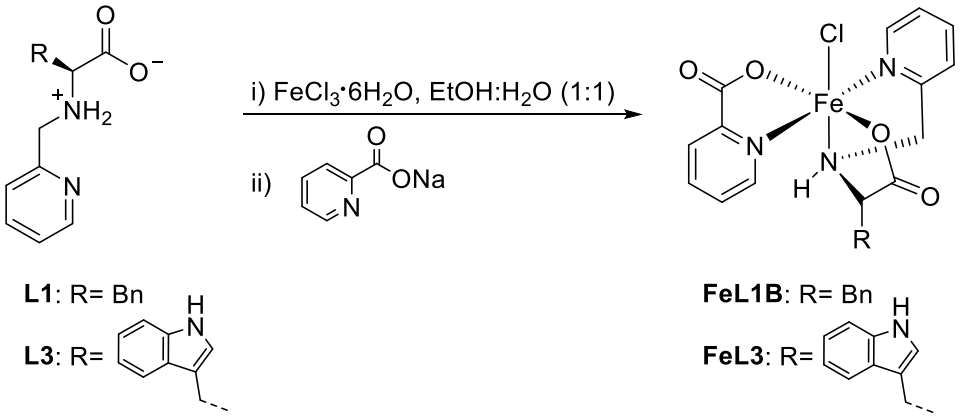

Scheme III-3: Synthesis of the Fe(III) complexes **FeL1B** and **FeL3**.

For the synthesis of **FeL2,** the ligand precursor **L2** was firstly solubilized in EtOH:H_2O (1:1) at room temperature, followed by addition of $FeCl_3$•$6H_2O$ which afforded an orange solution similar to the previous cases. Afterwards, three mole equivalents of sodium acetate (NaOAc) were added, and the resulting dark green solution was evaporated to dryness. The residue was dissolved in acetone and dried with anhydrous Na_2SO_4, filtered and the filtrate evaporated to dryness under vacuum, yielding **FeL2** as a dark green solid in 78% (**Scheme III-4**).

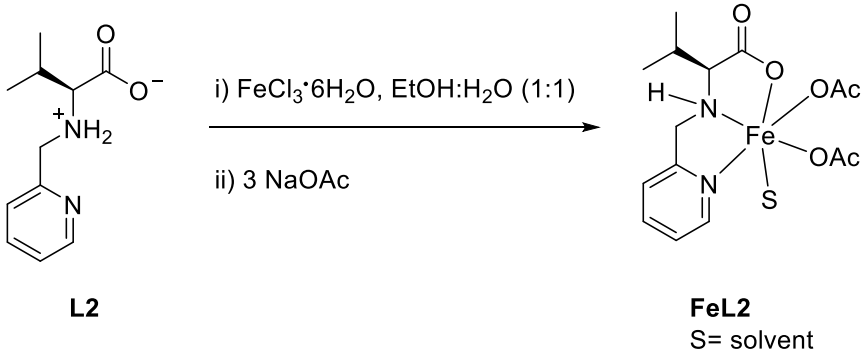

Scheme III-4: Synthetic procedure for the preparation of Fe(III) compond **FeL2**.

The synthesis of an Fe(III) complex derived from ligand precursor **L4** was attempted in an aqueous ethanolic solution within the same reaction conditions for the preparation of **FeL1A**, **FeL2B** and **FeL2**, but with no success (**Scheme III-5**). The use of sodium salicylate, sodium picolinate or NaOAc was not effective for the successful synthesis of the respective Fe(III) complex; elemental analyses of the isolated solids obtained after the *work-up* procedures were not consistent with mononuclear or oligonuclear Fe(III) compounds. In the attempt to purify or extract the desired compounds, the referred solids were suspended in water, filtered, dissolved in acetone, dried with Na_2SO_4, filtered and the resulting filtrate evaporated to dryness under vacuum. Again, the isolated solids were not consistent, by elemental analysis, with the desired compounds and therefore the synthesis of an Fe(III) complex correspondent to **L4** was abandoned.

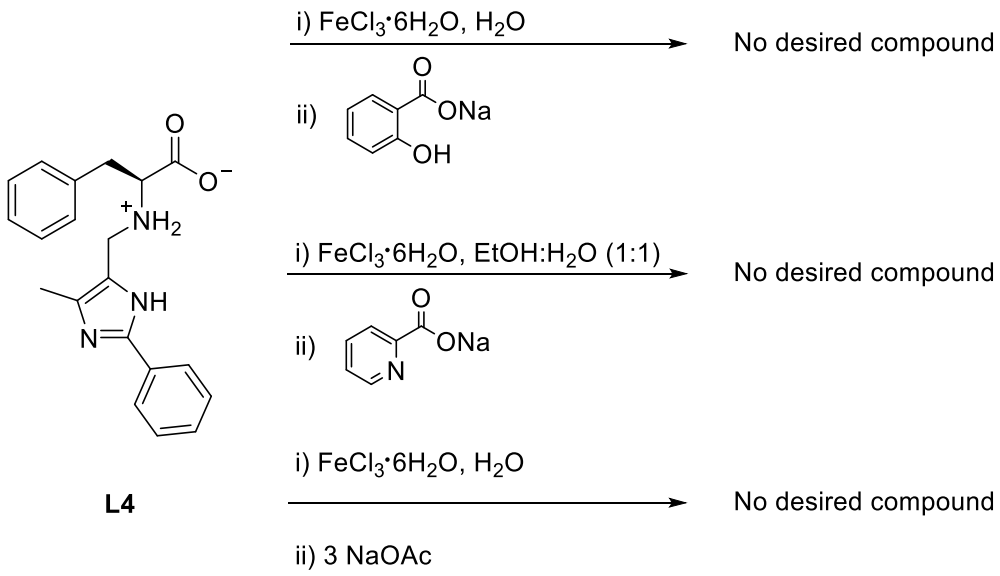

Scheme III-5: Synthetic procedures applied in the attempt of synthesis of an Fe(III) compound derived from ligand precursor **L4**.

The synthesis of an Fe(III) complex bearing **L1** and using NaOAc as a basic additive was also tested to obtain the respective Fe(III) complex (**Scheme III-6**, top reaction). With this procedure, the elemental analysis of the isolated solid obtained after reaction completion was not consistent with a mononuclear or oligonuclear Fe(III) compound, which also contained inorganic impurities. In the attempt to purify the desired compound, the resulting solid was subject to the extraction process mentioned earlier. Again, the elemental analysis of the isolated solid was not consistent with the desired Fe(III) compound and this synthetic line was abandoned. Similar results were observed in the attempt of preparing an Fe(III) complex bearing **L2** and utilizing sodium salicylate or sodium picolinate as organic salt additive (**Scheme III-6**, middle and bottom reations, respectively). The isolated solids obtained in each case at the end of the synthetic procedures did not correspond to the desired mononuclear or oligonuclear Fe(III) compound, by elemental analysis. For this reason the utilization of the referred carboxylate salts in the preparation of the respective Fe(III) complexes was precluded.

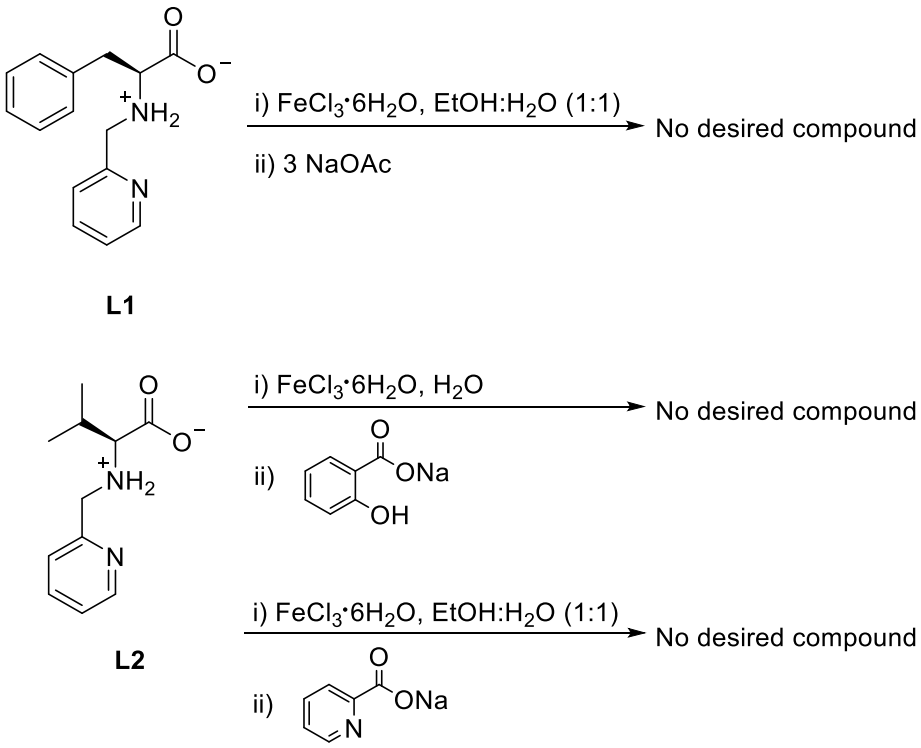

Scheme III-6: Attempt on synthesize the corresponding Fe(III) compound from ligand precursors **L1** and **L2** with different carboxylate co-ligands.

For otimization purposes the synthesis of an Fe(III) complex bearing **L2** as ligand was also tried based on a previously reported dry-milling procedure[112], consisting on the solvent-free mechanical treatment of a solid mixture of **L2** and $FeCl_3$•$6H_2O$. After 1 hour of mechanical stirring a light-yellow solid was obtained, but the respective elemental analysis was not in agreement with the desired Fe(III) complex, therefore this synthetic procedure was abandoned.

III.2.1.1 – Characterization by UV-Vis and CD spectroscopy

The obtained UV-Vis and CD spectra of the Fe(III) compounds **FeL1A**, **FeL1B**, **FeL2** and **FeL3** are presented in **Figure III-3** and **Figure III-5**, respectively, with the relevant maximum absorption wavelenght (λ_{max}), molar absorptivity (ε) and molar circular dichroism ($\Delta\varepsilon$) values listed in **Table III-1**. Compound **FeL1A** exhibit an intense and broad band at 514 nm, assigned to a ligand-to-metal charge transfer (LMCT) between the phenolate oxygen pπ orbitals and the dπ* orbitals of the Fe(III) centre (phenolate→ Fe(III) *p*π-*d*π*).[113] Compounds **FeL1B**, **FeL2** and **FeL3** do not show this band behaviour in the visible region due to the absence of a phenolate ligand in their structure.[114] Instead, very low intensity bands can be observed for these compounds in the 400-650 nm region (see **Figure III-4** for more detail). **FeL1B** and **FeL3** both exhibit a great similarity in their electronic spectra profiles, with one partially allowed *d-d*

transition band appearing at *ca.* 555 and one pyridyl→ Fe(III) *p*π-*d*π* charge transfer (CT) band at *ca.* 480 nm. Compound **FeL2** depict in the visible region one partially allowed *d-d* transition band at 641 nm and several low ε bands at 523, 484, 442 and 412 nm. The band appearing at *ca.* 484 nm might be resultant from a pyridyl→ Fe(III) *p*π-*d*π* CT, while the remaining absorption bands can be assigned to compound interactions with the solvent used[115] or to other LMCT transitions.[114] In the 300-400 nm region, compounds **FeL1B** and **FeL3** exhibit one shoulder at *ca.* 307 nm, attributed to intraligand π→π* transitions ocurring at the amino acid side chain and pyridyl moiety[116] and other shoulder at 340 nm, corresponding to an amine-to-iron CT band.[117] Compound **FeL2** show also one bands in this region at 328 nm correspondent to intraligand π-π* transitions occurring in the pyridyl moiety.

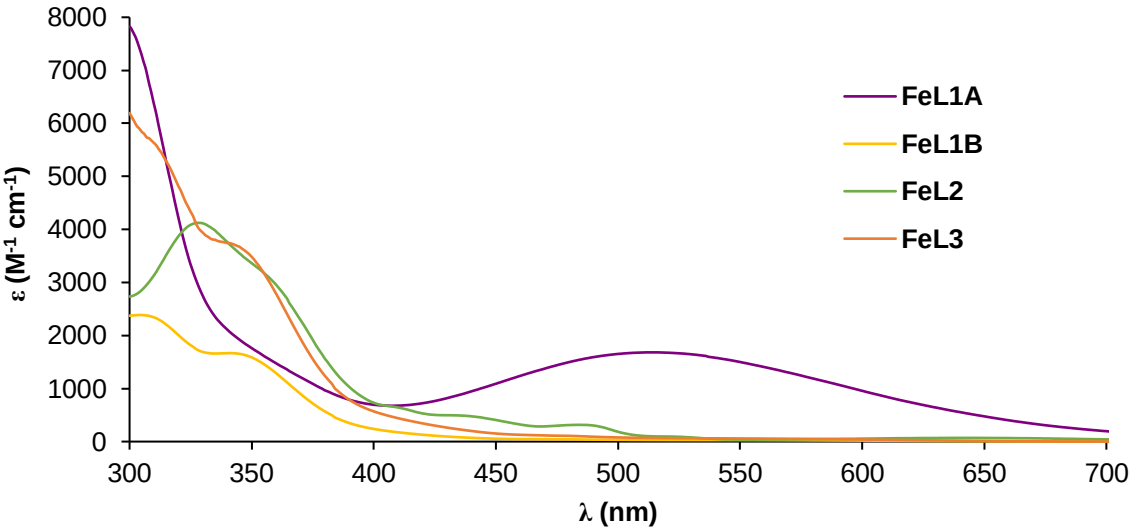

Figure III-3: Electronic absorption (UV-Vis) spectra of compounds **FeL1A** (EtOH, 1.99 mM), **FeL1B** (MeCN:H_2O (1:1), 0.398 mM), **FeL2** (EtOH, 2.01 mM), and **FeL3 (**MeCN:H_2O (1:1), 0.400 mM) at room temperature with 1 mm (**FeL1A**, **FeL2**) and 1 cm (**FeL1B**, **FeL3**) optical path quartz cells.

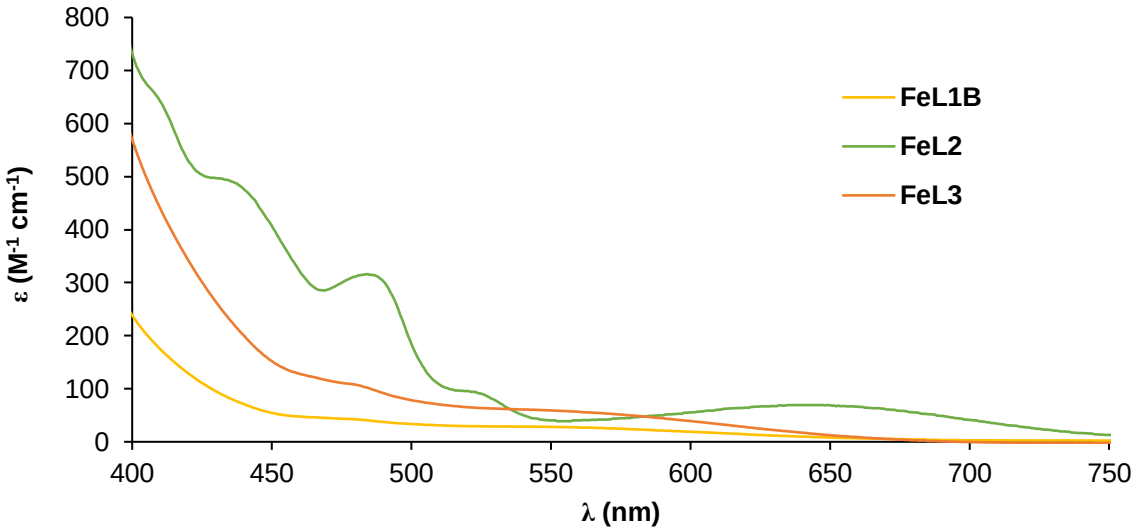

Figure III-4: Close-up of the electronic absorption (UV-Vis) spectra of compounds **FeL1B** (MeCN:H_2O (1:1), 0.398 mM), **FeL2** (EtOH, 2.01 mM), and **FeL3 (**MeCN:H_2O (1:1), 0.400 mM) at room temperature with 1 mm (**FeL1A**, **FeL2**) and 1 cm (**FeL1B**, **FeL3**) optical path quartz cells.

The CD spectra of compounds **FeL1A**, **FeL1B**, **FeL2** and **FeL3** indicate chirality in solution and were complemented with the respective UV-Vis spectra to facilitate identification of the relevant absorption bands. Compounds **FeL1A, FeL1B** and **FeL3** show similar CD spectra profiles with different band intensities at 345, 326 and 319 nm, respectively, yielded by intraligand $\pi \rightarrow \pi^*$ transitions. This observation is an indicator of efficient transmition of chirality from the amino acid ligands, since the amino acid chiral centers are no less than two bonds away from the aromatic benzyl (**FeL1A**, **FeL1B**) and indolyl (**FeL3**) moieties. Noteworthy is the absence of a CD band for **FeL1A** at *ca*. 514 nm, correspondent to the phenolate→ Fe(III) $p\pi$-$d\pi^*$ CT transition, indicating that no chirality transmition occurs from the salycilate co-ligand. Also interesting is the CD spectrum profile of **FeL2** with an opposite pattern in comparison to the other Fe(III) compounds, also showing a series of low intensity CD bands in the 400-500 nm region correspondent to LMCT transitions and a higher intensity CD band at 360 m attributed to intraligand π-π^* transitions occurring in the pyridyl moiety.

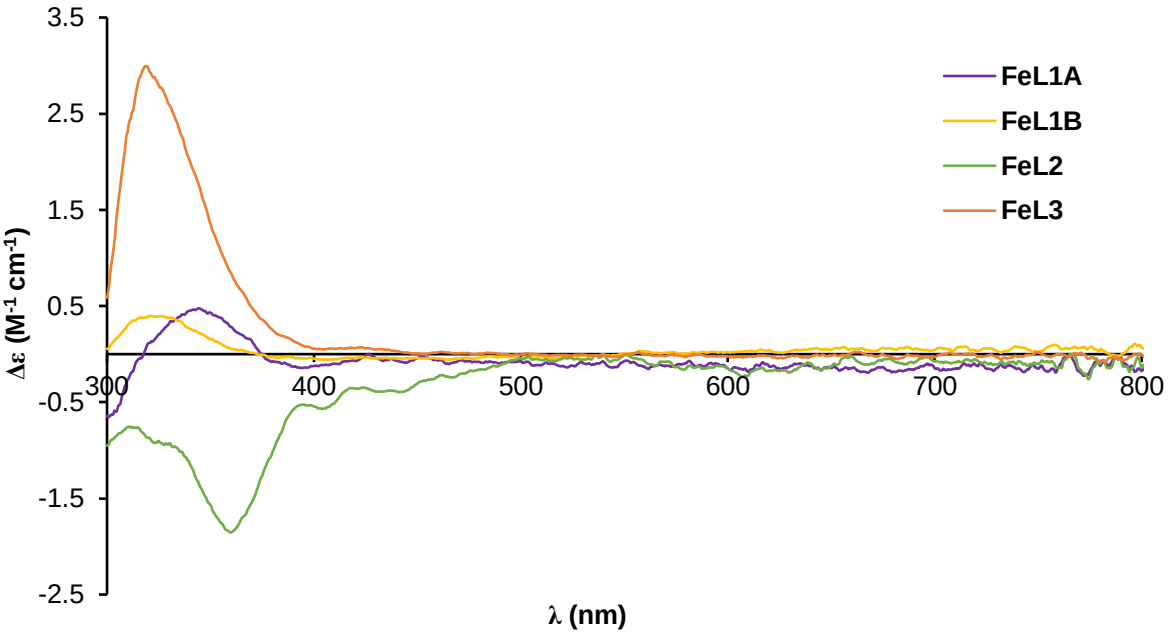

Figure III-5: Circular Dichroism (CD) spectra of compounds **FeL1A** (EtOH, 1.99 mM), **FeL1B** (MeCN:H_2O (1:1), 0.398 mM), **FeL2** (EtOH, 2.01 mM), and **FeL3** (MeCN:H2O (1:1), 0.400 mM) at room temperature with 1 mm (**FeL1A, FeL2**) and 1 cm (**FeL1B, FeL3**) optical path quartz cells**.**

Table III-1: Experimental λ_{max}, ε and $\Delta\varepsilon$ values obtained in the UV-Vis and CD spectra of compounds **FeL1A**, **FeL1B**, **FeL2** and **FeL3**.

	UV-Vis		CD	
Compound	**λ_{max} (nm)**	**ε (M^{-1} cm^{-1})**	**λ_{max} (nm)**	**$\Delta\varepsilon$ (M^{-1} cm^{-1})**
FeL1A	514	1681.9	394 345	-0.144 -0.476
FeL1B	557 480 342 305	45.7 73.9 1667.9 2386.8	326	0.394
FeL2	641 523 484 442 412 328	69.5 93.7 315.9 469.4 628.3 4125.1	445 406 360	-0.376 -0.565 -1.855
FeL3	554 481 340 309	64.1 105.9 3744.3 5647.5	319	2.99

III.2.1.2 – Characterization by X-Ray diffraction

Important structural information was obtained by the X-ray diffraction of single crystals of **FeL1B** and **FeL3**. The ORTEP diagrams are presented below in **Figure III-6** and **Figure III-8**, respectively, and the selected parameters are listed in **Table III-4**. Compound **FeL1B** crystallized in the tetragonal system, space group $P4_32_12$, with a molecule in the asymmetric unit. The molecular structure is depicted in **Figure III-6**. Each molecule is a six-coordinate species, where the metal atom is coordinated to a [N,N,O] ligand (N2, N3 and O1), one chlorine atom (Cl1) and a [N,O] ligand derived from picolinic acid (N1, O3). The coordination geometry around Fe1 is described as distorted octahedral, where the equatorial plane is defined by the atoms N3, O1, N1 and O3, since they are coplanar within a small mean deviation (0.072 Å) from their least square plane. The metal atom lies 0.263(8) Å above the equatorial plane. The remaining axial positions are occupied by the chlorine atom (Cl1) and by a nitrogen atom of the [N,N,O] ligand (N2), with bond lengths of 2.283(5) Å and 2.203(15) Å, respectively. All the bond distances are within the ranges reported for Fe(III) complexes containing N,O ligands.[118] Chiral atoms N2 and C2 have the *R* and *S* configuration, respectively. The supramolecular arrangement of complex **FeL1B** is generated by classic and non-classic N–H···O, C–H···O and C–H···Cl hydrogen bonds being depicted in **Figure III-7**, with the respective bond length and angles listed in **Table III-2**.

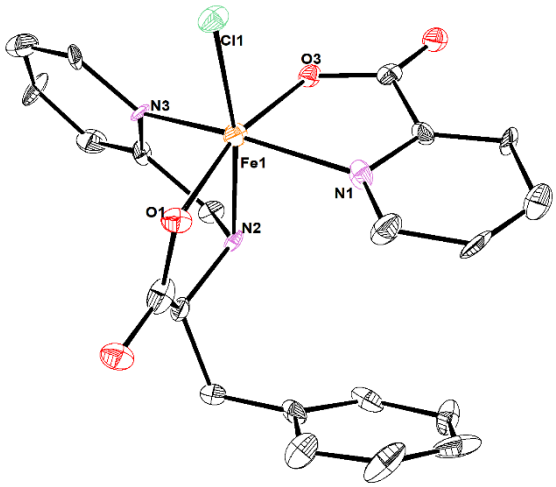

Figure III-6: ORTEP-3 diagram of the asymmetric unit of compound **FeL1B**, using 30% probability level ellipsoids. All H atoms were omitted for clarity.

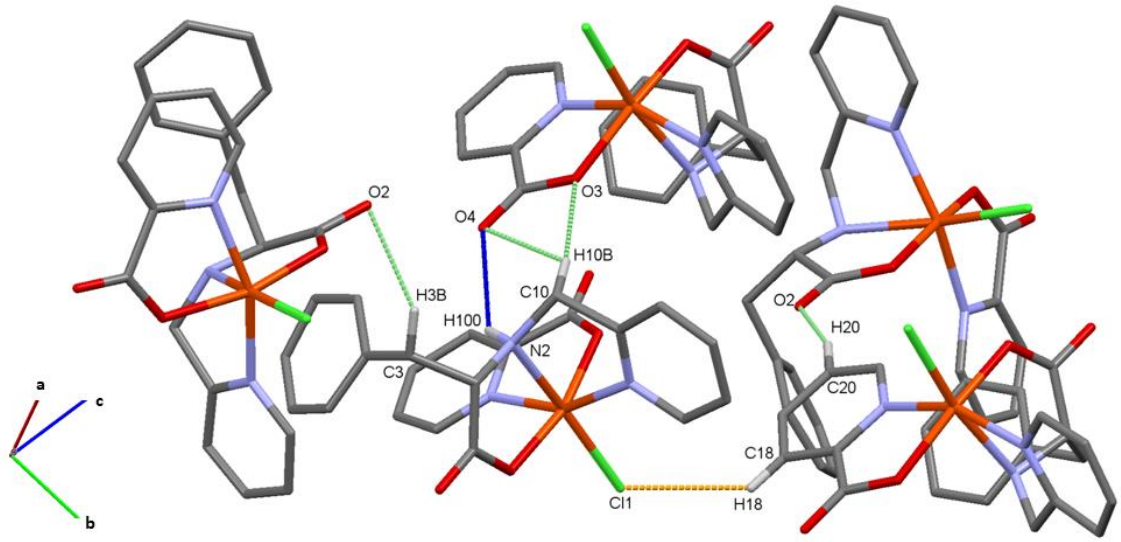

Figure III-7: View of selected hydrogen bonds for complex **FeL1B**. Donor and acceptor atoms are identified. Blue dashed lines represent the N–H···O hydrogen bonds, light-green dashed lines the C–H···O, and orange dashed lines the C–H···Cl assisted non-classical hydrogen bonds. All the hydrogen atoms, except those involved in the interactions, were omitted for clarity.

Table III-2: List of hydrogen bonds for **FeL1B** [Å and °].[a]

D-H...A	***d*(D-H)**	***d*(H...A)**	***d*(D...A)**	**<(DHA)**
C(10)-H(10B)...O(3)#1	0.99	2.29	3.27(2)	173.1
C(10)-H(10B)...O(4)#1	0.99	2.61	3.26(2)	122.9
C(3)-H(3B)...O(2)#2	0.99	2.51	3.41(3)	151.0
C(15)-H(15)...Cl(1)	0.95	2.97	3.542(19)	119.9
C(18)-H(18)...Cl(1)#3	0.95	2.79	3.50(2)	131.9
C(20)-H(20)...O(2)#4	0.95	2.57	3.48(3)	158.6
N(2)-H(100)...O(4)#1	0.87(3)	2.51(12)	3.16(2)	131(13)
N(2)-H(100)...N(1)	0.87(3)	2.53(14)	3.07(2)	120(13)

[a]Symmetry transformations used to generate equivalent atoms: #1 *y,x,-z+2* #2 *-x+1/2,y-1/2,-z+7/4* #3 *y-1,x,-z+2* #4 *-x-1/2,y-1/2,-z+7/4*

Compound **FeL3** crystallized in the orthorhombic system, space group $P2_12_12_1$, with a molecule in the asymmetric unit, and its molecular structure presented in **Figure III-8**. Each molecule is a six-coordinate species, where the metal atom is coordinated to a [N,N,O] ligand (N2, N3 and O2), one chlorine atom (Cl1) and a [N,O] ligand derived from picolinic acid (N1, O4). The coordination geometry around Fe1 is described as slightly distorted octahedral, where the equatorial plane is defined by the atoms N3, O2, N1 and O4, since they are coplanar

within a small mean deviation (0.003 Å) from their least square plane. The metal atom lies 0.2660(17) Å above the equatorial plane. The remaining axial positions are occupied by the chlorine atom (Cl1) and by a nitrogen atom of the [N,N,O] ligand (N2), with a bond lengths of 2.2372(13) Å and 2.160(4) Å, respectively. All the bond distances are within the ranges reported for Fe(III) complexes containing N,O ligands.[118] Chiral atoms N2 and C8 have the *R* and *S* configuration, respectively. The supramolecular arrangement of complex **FeL3** is generated by classic and non-classic N–H···O, C–H···O and C–H···Cl hydrogen bonds, as displayed in **Figure III-9**, with the respective bond length and angles listed in **Table III-3**.

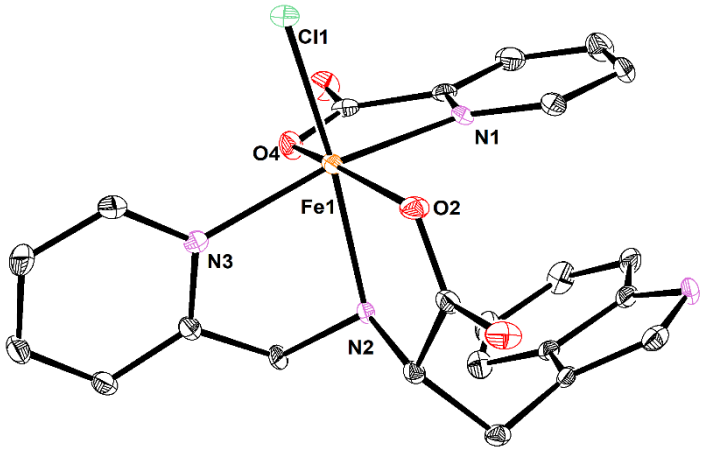

Figure III-8: ORTEP-3 diagram of the asymmetric unit of compound **FeL3**, using 30% probability level ellipsoids. All H atoms were omitted for clarity.

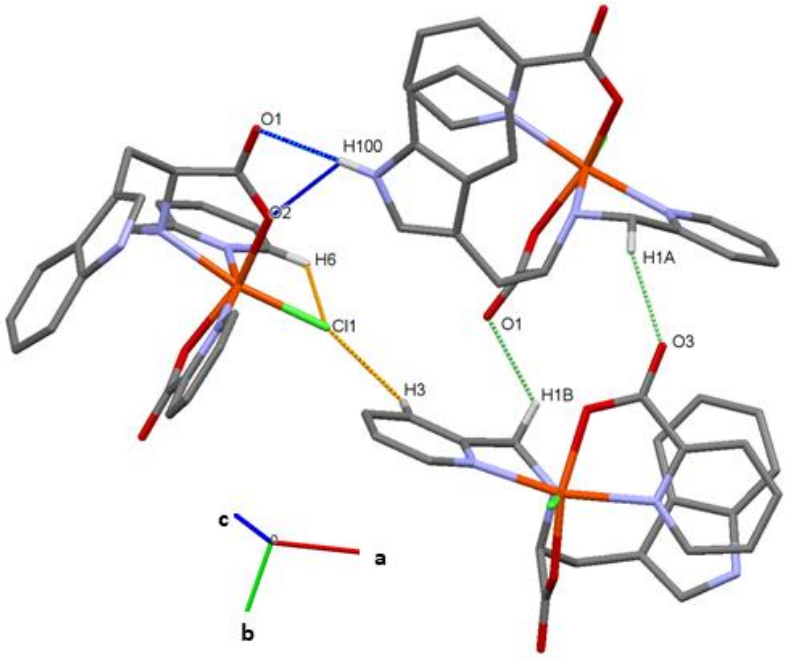

Figure III-9: View of selected hydrogen bonds for complex **FeL3**. Donor and acceptor atoms are identified. Blue dashed lines represent the N–H···O hydrogen bonds, light-green dashed lines the C–H···O, and orange dashed lines the C–H···Cl assisted non-classical hydrogen bonds. All the hydrogen atoms, except those involved in the interactions, were omitted for clarity.

Table III-3: List of hydrogen bonds for **FeL3** [Å and °].[a]

D-H...A	***d*(D-H)**	***d*(H...A)**	***d*(D...A)**	**<(DHA)**
C(3)-H(3)...Cl(1)#1	0.95	2.68	3.408(4)	133.7
C(1)-H(1A)...O(3)#2	0.99	2.37	3.247(5)	147.6
C(1)-H(1B)...O(1)#3	0.99	2.56	3.154(5)	118.3
C(11)-H(11)...Cl(1)#4	0.95	2.96	3.897(4)	168.6
C(23)-H(23)...O(2)	0.95	2.64	3.131(5)	112.3
C(6)-H(6)...Cl(1)	0.95	2.81	3.385(5)	119.6
C(13)-H(13)...Cl(1)#5	0.95	2.97	3.494(5)	116.0
N(4)-H(100)...O(1)#4	0.87(4)	2.15(4)	3.020(5)	178(4)
N(4)-H(100)...O(2)#4	0.87(4)	2.56(4)	3.112(4)	123(3)

[a]Symmetry transformations used to generate equivalent atoms: #1 *-x+3/2,-y+1,z-1/2* #2 *-x+1,y+1/2,-z+3/2* #3 *-x+1,y-1/2,-z+3/2* #4 *x-1/2,-y+3/2,-z+2* #5 *x-1,y,z*

Table III-4: Selected bond lengths (Å) and angles (º) for compounds **FeL1B** and **FeL3**.

Compound	FeL1B	FeL3
Bond lengths (Å)		
Fe1–N1	2.147(17)	2.166(3)
Fe1–N2	2.203(15)	2.160(4)
Fe1–N3	2.149(15)	2.137(4)
Fe1–O1	1.953(13)	
Fe1–O2		1.959(3)
Fe1–O3	2.008(13)	
Fe1–O4		1.991(3)
Fe1–Cl1	2.283(5)	2.2372(13)
Angles (º)		
O1–Fe1–N2		77.35(13)
O3–Fe1–N1	78.8(6)	
O1–Fe1–N1	91.3(6)	
O1–Fe1–N3	100.0(6)	
O3–Fe1–N3	86.4(5)	
N2–Fe1–Cl1	170.6(4)	169.28(11)
O4–Fe1–N3		88.08(12)
N3–Fe1–O2		101.14(12)
N1–Fe1–O2		89.56(13)

III.2.1.3 – Characterization by Mass spectrometry

The Fe(III) compounds **FeL1A**, **FeL1B**, **FeL2** and **FeL3** were studied by negative and positive ESI-MS modes in methanol or in a aqueous acetonitrile solution, depending on their solubility. The mass peaks assignments are for the most probable species having no more than ±1 divergence in m/z from the observed peak.

ESI-MS spectra of **FeL1A** were obtained in methanol and are presented in **Figure III-10**, with the peak assignments indicating dissociation of the amino acid and salycilate ligands under the conditions used for the analyses. In the negative mode spectrum, the main species observed are the mononuclear monoanionic [Fe**L1**(Sal)Cl]$^-$ species (m/z= 482.3) and several other mononuclear species such as the salycilate co-ligand (m/z= 137.7), a [Fe(Sal)$_2$]$^-$ species (m/z=328.1) and a [Fe**L1**(Sal)$_2$]$^-$ species (m/z= 583.9) as the major peak. In the positive mode spectrum the main species observed are the protonated amino acid ligand H**L1**$^+$ (m/z= 257.1), a mononuclear {H[Fe**L1**(Sal)]}$^+$ species (m/z= 448.0) and its sodium adduct {Na[Fe**L1**(Sal)]}$^+$ species (m/z= 470.0), a dinuclear {H[Fe**L1**(Sal)]$_2$}$^+$ species (m/z= 894.9) and its sodium adduct {Na[Fe**L1**(Sal)]$_2$}$^+$ (m/z= 916.9), which holds the major peak value and indicates the formation of Fe**L1**Sal aggregates.

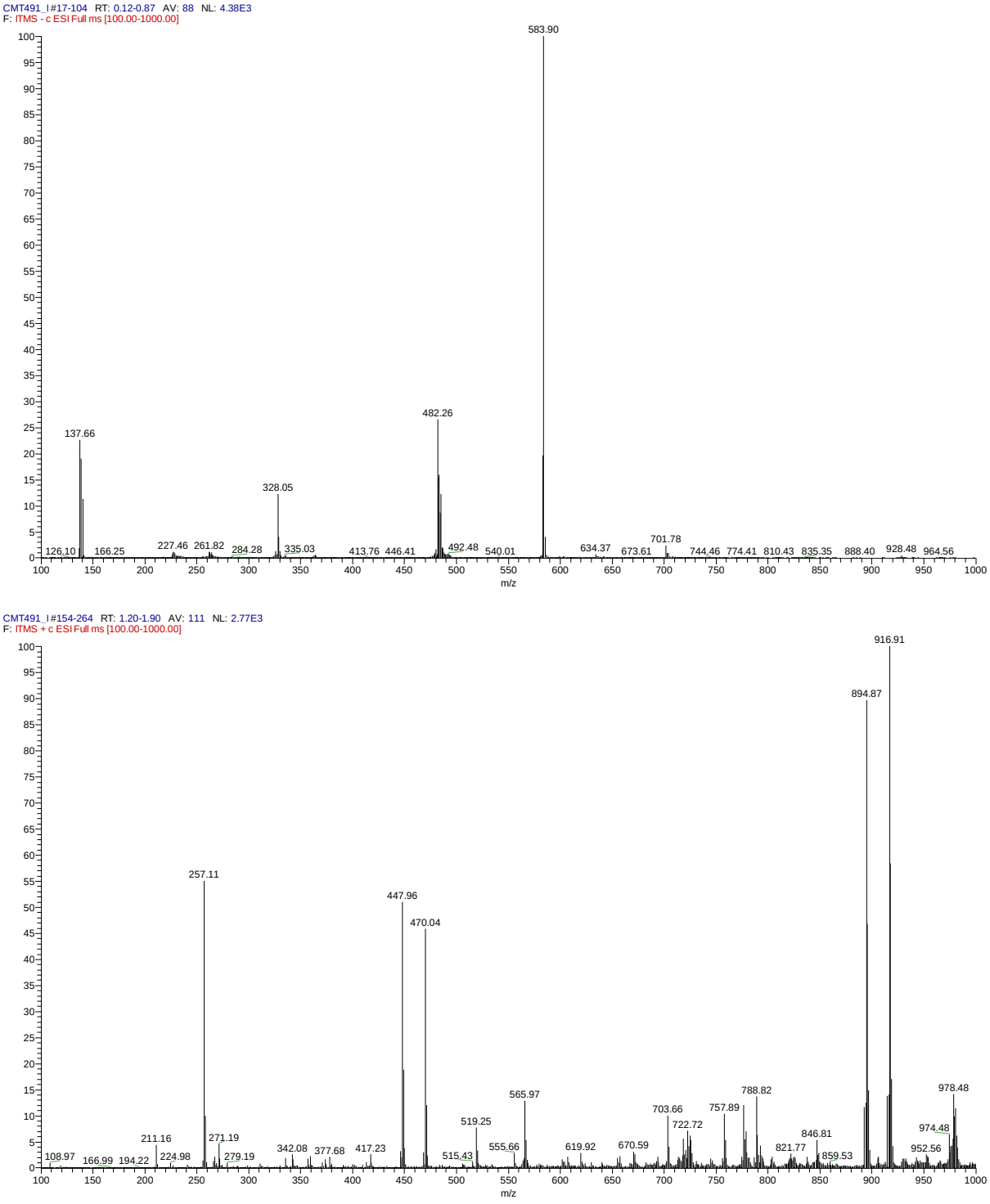

Figure III-10: Negative (up) and positive (down) ESI-MS spectra of **FeL1A** in methanol.

Compound **FeL1B** ESI-MS spectra were obtained in MeCN:H_2O (1:1) and are depicted in **Figure III-11**, also indicating dissociation of the amino acid and picolinate ligands and formation of Fe**L1** μ-hydroxido-bridged aggregates under the conditions used for the analyses. In the negative mode spectrum the major peak is assigned to the solvated monoanionic picolinate ligand $[(Pic)\bullet MeCN]^-$ (m/z= 163.2), followed by several species with lower relative

abundances: the mononuclear $[Fe(Pic)(OH)_2(H_2O)_2]^-$ species (m/z= 248.3), the mononuclear solvated $\{[Fe(Pic)(OH)_2(H_2O)_2]\bullet MeCN\}^-$ species (m/z= 291.3), the mononuclear [Fe**L1**(Pic)Cl]$^-$ species (m/z= 468.2), the mononuclear [Fe**L1**$(Pic)_2Cl]^-$ species (m/z= 589.8) with an additional picolinate molecule, the solvated dinuclear di-μ-hydroxido $\{[Fe\mathbf{L1}(OH)]_2\bullet MeCN\}^-$ species (m/z= 696.8), the solvated dinuclear μ-hydroxido $\{[(Fe\mathbf{L1})_2Cl_2(OH)]\bullet 2H_2O\bullet MeCN\}^-$ species (m/z= 783.6), a possibly solvated dinuclear species $\{[(Fe\mathbf{L1})_2(OH)(Pic)Cl]\bullet 2H_2O\}^-$ with a μ-hydroxido bridge and an extra picolinate molecule (m/z= 829.6) and a possibly solvated dinuclear species $\{[(Fe\mathbf{L1})_2(Pic)_2(OH)]\bullet 2H_2O\}^-$ with a μ-hydroxido bridge and two extra picolinate molecules (m/z= 916.5). In the positive mode spectrum the major peak is assigned to the protonated amino acid ligand H**L1**$^+$ (m/z= 257.1) and other species are observed such as the mononuclear solvated $\{H[Fe\mathbf{L1}(Pic)(OH)]\bullet MeCN\bullet H_2O\}^+$ species (m/z= 510.7), the mononuclear $\{H[Fe\mathbf{L1}_2]\}^+$ and $\{H[Fe\mathbf{L1}_2(Pic)]\}^+$ species (m/z= 565.9 and 688.6, respectively), the dinuclear di-μ-hydroxido $\{[(Fe\mathbf{L1})_2(Pic)(OH)_2(MeCN)(H_2O)]\}^+$ species (m/z= 837.4) and two possibly solvated dinuclear species $\{H[(Fe\mathbf{L1})_2(Pic)_2(Cl)(OH)]\bullet 4H_2O\}^+$ and $\{H[(Fe\mathbf{L1})_2(OH)(Pic)_2]\bullet MeCN\bullet 5H_2O\}^+$, each one with a μ-hydroxido bridge and an extra picolinate molecule (m/z= 990.4 and 1015.6, respectively).

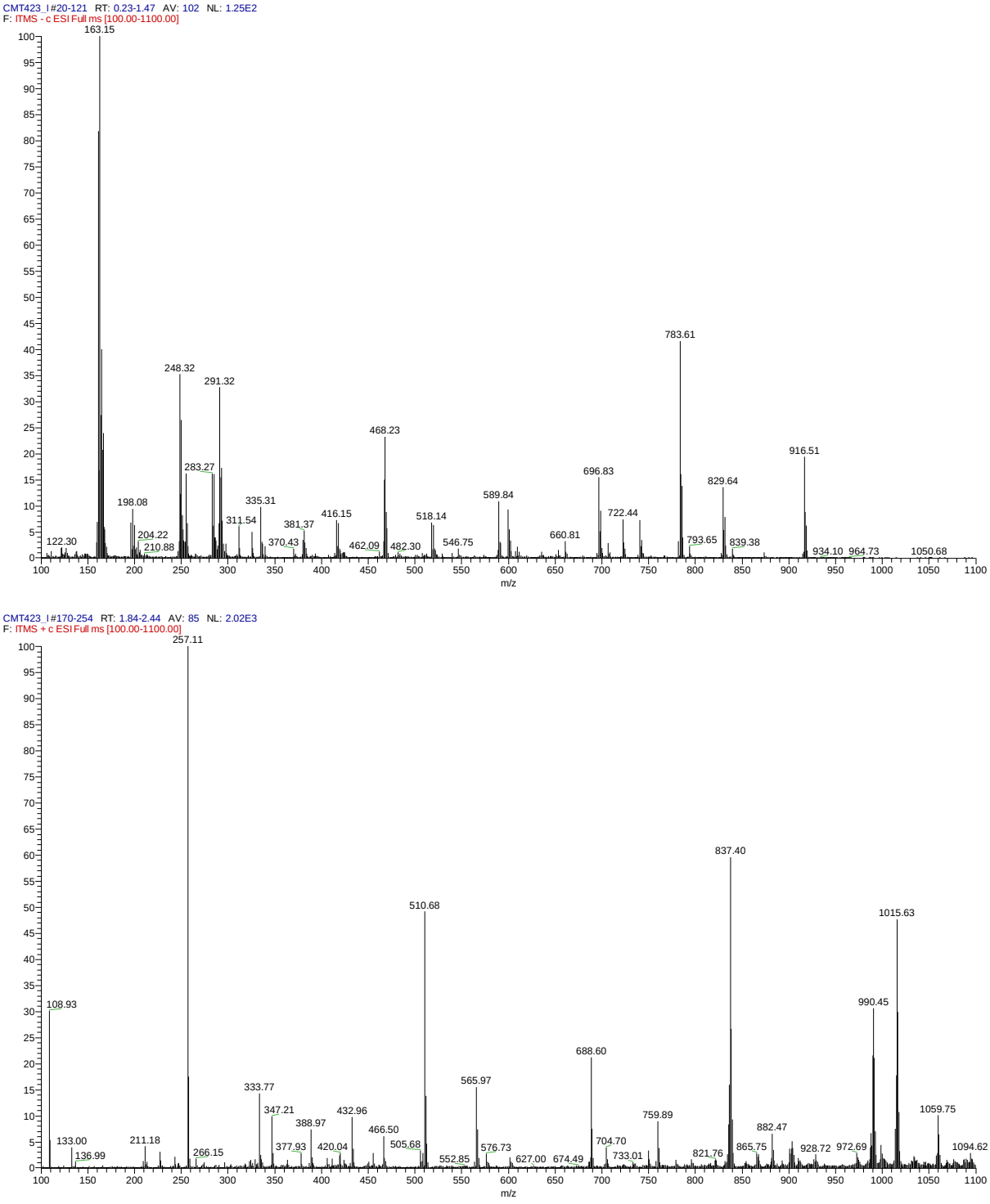

Figure III-11: Negative (up) and positive (down) ESI-MS spectra of **FeL1B** in MeCH:H_2O (1:1). The intense peaks in both modes indicate dissociation of the picolinate and amino acid ligands, respectively, under the conditions used for the analyses.

Compound **FeL2** ESI-MS positive and negative mode spectra were obtained in MeOH and are depicted in **Figure III-12**, clearly indicating the tendency of this compound to form at least dinuclear Fe**L2** aggregates in the conditions applied for these experiments. In the negative mode spectrum it was observed the presence of one solvated mononuclear

{[(Fe**L2**)(MeO)$_2$]•8MeOH•H$_2$O}$^-$ species (m/z= 599.0), one solvated dinuclear {[(Fe**L2**)]$_2$(OH)(AcO)]•MeOH}$^-$ species (m/z= 635.2), one solvated dinuclear di-μ-hydroxido {[(Fe**L2**)]$_2$(OH)$_2$(H$_2$O)$_2$]•2MeOH}$^-$ species (m/z= 659.2), appearing as the major peak, and one solvated dinuclear μ-hydroxido-μ-acetato {[(Fe**L2**)$_2$(AcO)(OH)(H$_2$O)$_2$]•2MeOH•H$_2$O}$^-$ species (m/z= 718.8). The respective spectrum in the positive mode shows a residual peak assigned to the solvated mononuclear {H[Fe**L2**(MeO)$_2$(H$_2$O)]•8MeOH•H$_2$O}$^+$ species (m/z= 601.1) and the peak with higher relative abundance is attributed to a mononuclear sodium adduct {Na[Fe**L2**(MeO)$_2$(H$_2$O)$_2$]•2H$_2$O}$^+$ species (m/z= 682.9), followed by several residual peaks consistent with trinuclear di-μ-acetato-μ-hydroxido species: {H[(Fe**L2**)$_3$(AcO)$_2$(OH)(H$_2$O)$_2$]}$^+$ (m/z= 961.6), {H[(Fe**L2**)$_3$(AcO)$_2$(OH)(H$_2$O)$_3$]•MeOH}$^+$ (m/z= 1012.7), {H[(Fe**L2**)$_3$(AcO)$_2$(OH)(H$_2$O)$_3$]•MeOH•3H$_2$O}$^+$ (m/z= 1063.6) and {Na[(Fe**L2**)$_3$(AcO)$_2$(OH)(H$_2$O)$_3$]•MeOH•4H$_2$O}$^+$ (m/z= 1103.7).

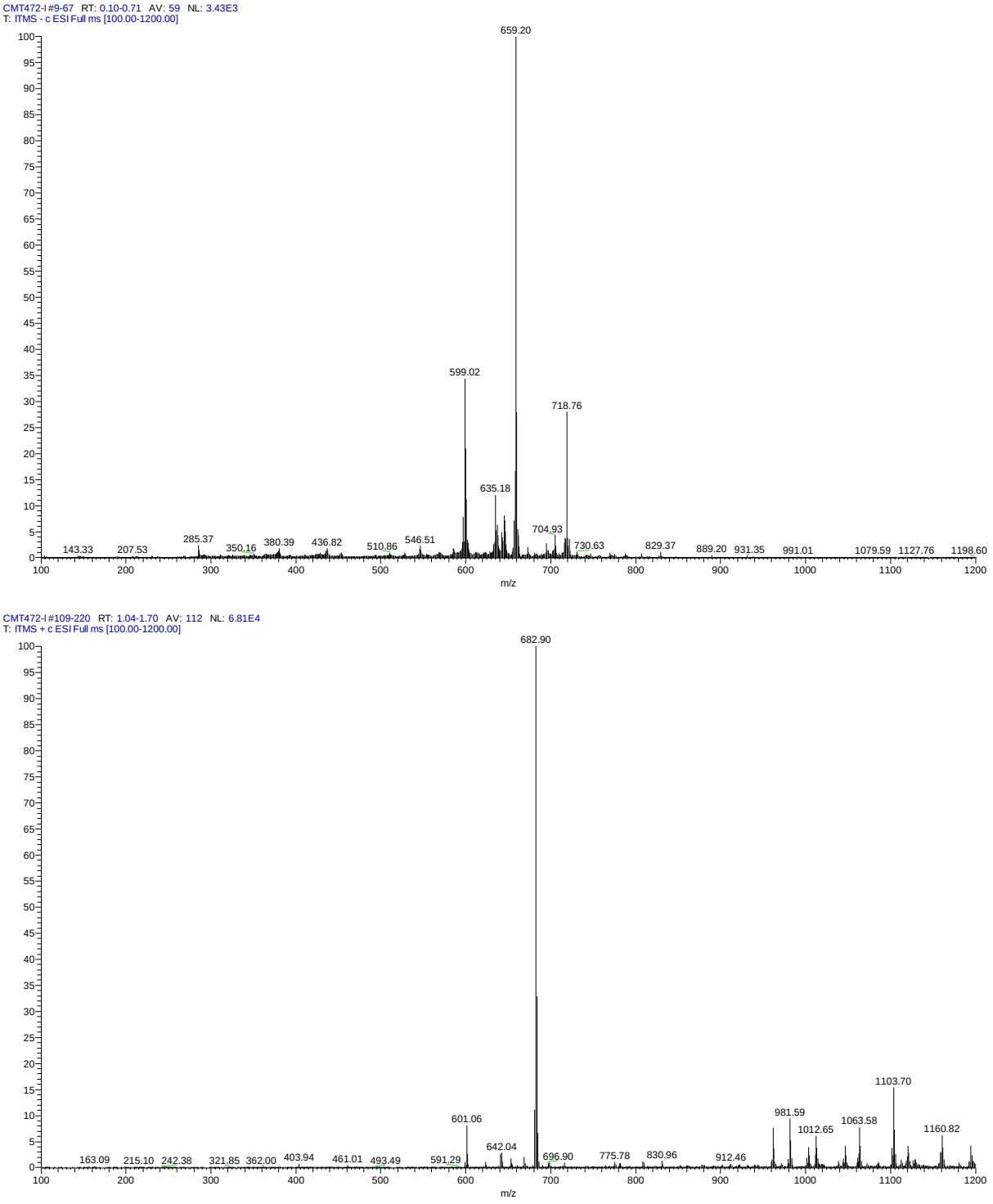

Figure III-12: Negative (up) and positive (down) ESI-MS spectra of **FeL2** in methanol. The intense peaks in both modes indicate the formation of dinuclear Fe**L2** aggregates under the conditions used for the analyses.

ESI-MS spectra of compound **FeL3** were obtained in MeCN:H_2O (1:1) and is presented in **Figure III-13**, indicating dissociation of the amino acid and picolinate ligands, formation of mononuclear Fe**L3** species and aggregation of at least two Fe**L3** μ-hydroxido-bridged units, under the conditions used for the analyses. In the negative mode spectrum the major peak is

assigned to a trianionic solvated dinuclear μ-hydroxido {[(Fe**L3**)(OH)]$_2$•3MeCN}$^{3-}$ species (m/z= 285.6) and it showed the presence of the solvated picolinate [(Pic)•MeCN]$^-$ species (m/z= 163.0), the mononuclear [Fe**L3**(Pic)Cl]$^-$ species in a residual relative abundance (m/z= 507.3) and respective solvated mononuclear {[Fe**L3**(Pic)Cl]•2H$_2$O}$^-$, {[Fe**L3**(Pic)Cl]•3H$_2$O•MeCN}$^-$ and {[Fe**L3**(Pic)Cl]•5MeCN}$^-$ species (m/z= 542.2, 602.2 and 713.7, respectively). In the positive mode spectrum the major peak is assigned to the protonated amino acid ligand H**L3**$^+$ (m/z= 296.1) and it is possible to observe a solvated mononuclear {H[Fe(Pic)$_3$]•MeCN}$^+$ species with three picolinate molecules (m/z= 462.8), a solvated mononuclear {H[Fe**L3**Cl$_2$]•2MeCN•2H$_2$O}$^+$ species without picolinate and two chlorides (m/z= 540.4), a solvated mononuclear sodium adduct {Na[Fe**L3**(Pic)Cl]•H$_2$O}$^+$ species (m/z= 549.6) and a solvated dinuclear {H[(Fe**L3**)$_2$(OH)$_2$]•3H$_2$O}$^+$ species (m/z= 789.4).

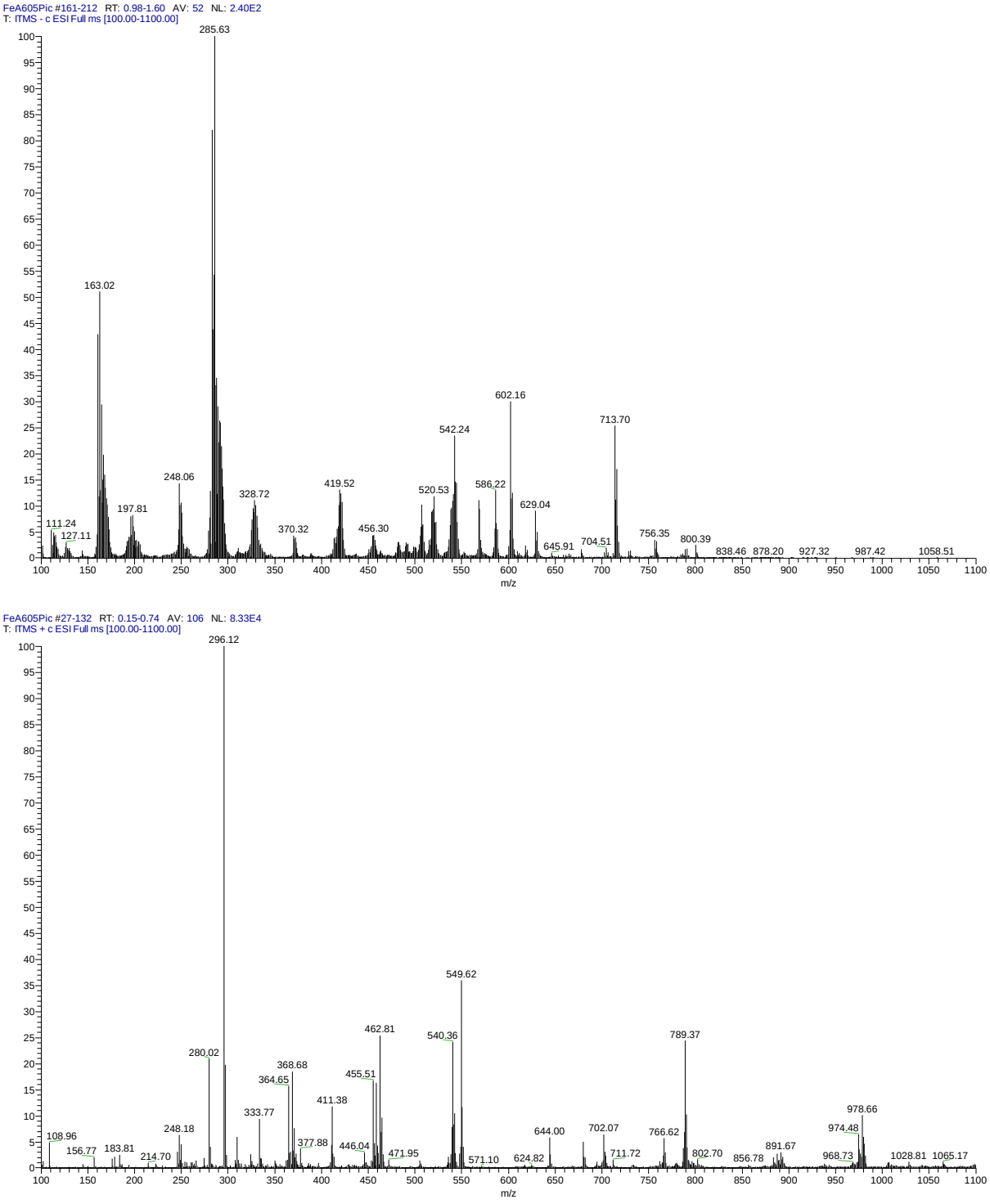

Figure III-13: Negative (up) and positive (down) ESI-MS spectra of **FeL3** in MeCH:H_2O (1:1). The intense peaks in both modes indicate dissociation of the picolinate and amino acid ligands, respectively, under the conditions used for the analyses.

III.2.1.4 – Characterization by Infrared spectroscopy

The FT-IR spectra of solid powered samples of **FeL1A**, **FeL1B**, **FeL2** and **FeL3** were analysed and the most relevant vibrational frequencies are listed in **Table III-5**. All compounds exhibited ν(N-H) and ν(C=O) stretching vibration bands at *ca*. 3000-3200 and 1600 cm^{-1}, respectively. Compound **FeL2** exhibited a strong intensity band at 1454 cm^{-1} and a medium intensity band at 646 cm^{-1}, attributed to symmetric Fe-OAc-Fe stretching vibrations and Fe-OH-Fe bending vibrations, respectively.[119] The presence of these bands in FT-IR spectrum of **FeL2** may indicate the formation of oligonuclear species during the preparation of this compound.

Table III-5: IR stretching frequencies for the prepared Fe(III) compounds **FeL1A**, **FeL1B**, **FeL2** and **FeL3**.

Stretching / bending mode	FeL1A	FeL1B	FeL2	FeL3
	Wavenumber (cm^{-1})			
ν(N-H)	3032	3277	2962	3277
$\nu(C{=}O_{carboxyl,\ aminoacid})$	1598	1656	1610	1590
ν(Fe-OAc-Fe)	-	-	1454	-
ν(Fe-OH-Fe)	-	-	646	-

III.2.1.5 – Elemental analysis

All the prepared Fe(III) compounds afforded elemental analysis results consistent with mononuclear species having water as contaminant.

III.2.2 – Fe(III) complexes bearing amino acid-phenol and amino acid-methoxybenzene ligands

The synthesis of Fe(III) complexes **FeL5**, **FeL6** and **FeL8**-**FeL11** will be presented in this subchapter and their structural formulae are depicted in **Figure III-14**.

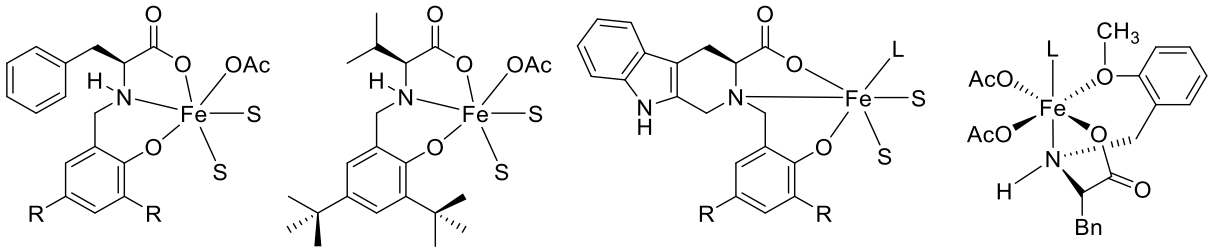

FeL5: R= CH_3
FeL6: R= $C(CH_3)_3$
S= solvent

FeL8
S= solvent

FeL9: R= CH_3, L= Cl
FeL10: R= $C(CH_3)_3$, L= OAc
S= solvent

FeL11
S= solvent

Figure III-14: Structural formulae of the prepared Fe(III) amino acid compounds **FeL5**, **FeL6** and **FeL8**-**FeL11**, based on their elemental analyses.

The preparation of these compounds is ilustrated in **Scheme III-7** and started with the solubilization of the corresponding ligand precursor in MeOH in an open vessel at room temperature, followed by addition of $FeCl_3 \cdot 6H_2O$. After 5 minutes under stirring sodium acetate was added to the mixture, followed by addition of distilled water. A dark purple-blue precipitate appeared in the preparation of **FeL5**, **FeL6**, **FeL8**, and **FeL10**, whereas in the preparation of **FeL9** and **FeL11** brown and orange solutions, respectively, were observed. The isolation of **FeL5**, **FeL6** and **FeL8** required filtration of the formed precipitate and the respective residue was dissolved in acetone, dried with Na_2SO_4, filtered and the resulting filtrate evaporated under vacuum, affording the desired compounds as dark-blue solids in 57, 63 and 68% yields. Compounds **FeL9** and **FeL10** were obtained, respectively, as dark-brown and dark-blue solids in 59 and 42% yields, by filtering the formed precipitate under vaccum and washing it with distilled water and petroleum ether. Compound **FeL11** was obtained as a dark-orange solid in 75% yield after evaporation till dryness of the reaction mixture, trituration of the residue with acetone, drying with anhydrous Na_2SO_4, filtration and evaporation of the resulting filtrate under vaccum.

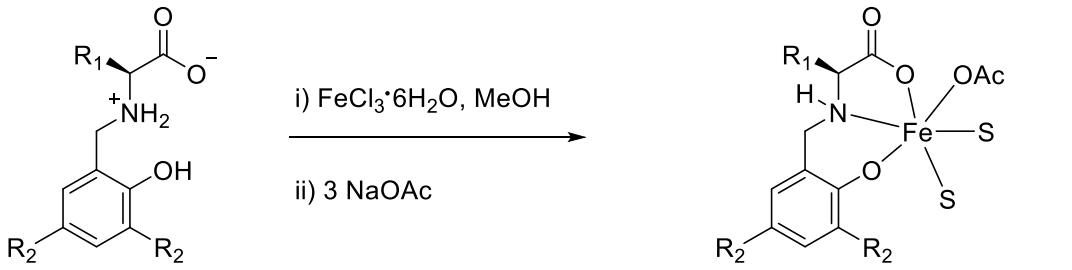

L5: R_1= Bn, R_2= CH_3
L6: R_1= Bn, R_2= $C(CH_3)_3$
L**8**: R_1= $CH(CH_3)_2$, R_2= $C(CH_3)_3$

FeL5: R_1= Bn, R_2= CH_3
FeL6: R_1= Bn, R_2= $C(CH_3)_3$
FeL8: R_1= $CH(CH_3)_2$, R_2= $C(CH_3)_3$
S= solvent

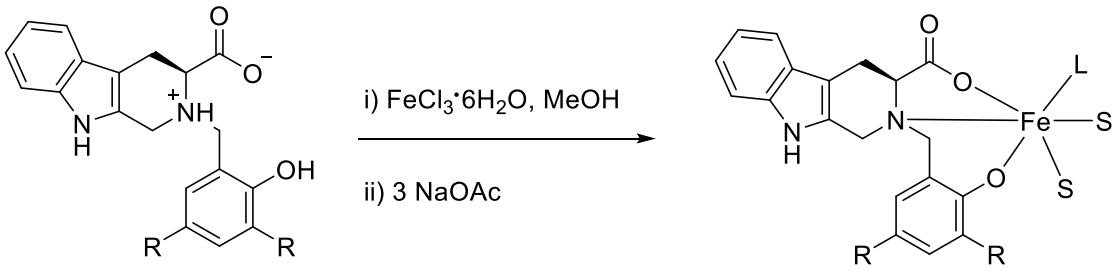

L9: R= CH_3, L= Cl
L10: R= $C(CH_3)_3$, L= OAc
S= solvent

FeL9: R= CH_3, L= Cl
FeL10: R= $C(CH_3)_3$, L= OAc
S= solvent

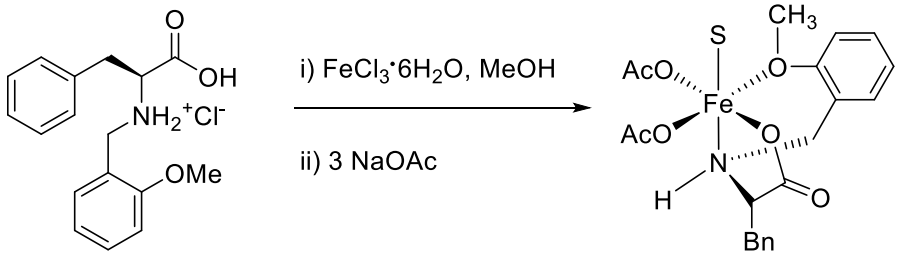

L11

FeL11
S= solvent

Scheme III-7: Synthetic procedure applied in the preparation of Fe(III) complexes **FeL5**, **FeL6**, **FeL8**, **FeL9**, **FeL10** and **FeL11**.

The synthesis of iron(IIII) complexes derived from ligand precursors **L7** and **L12** were also tried in the same reaction conditions described above but with no success (**Scheme III-8**). In both cases it was possible to isolate a solid and the corresponding elemental analyses were not consistent with the desired mononuclear or oligonuclear Fe(III) compound. Attempts to purify these solids by trituration and extraction with acetone was unsuccessful and the preparation of an Fe(III) complex correspondent to **L7** and **L12** was abandoned.

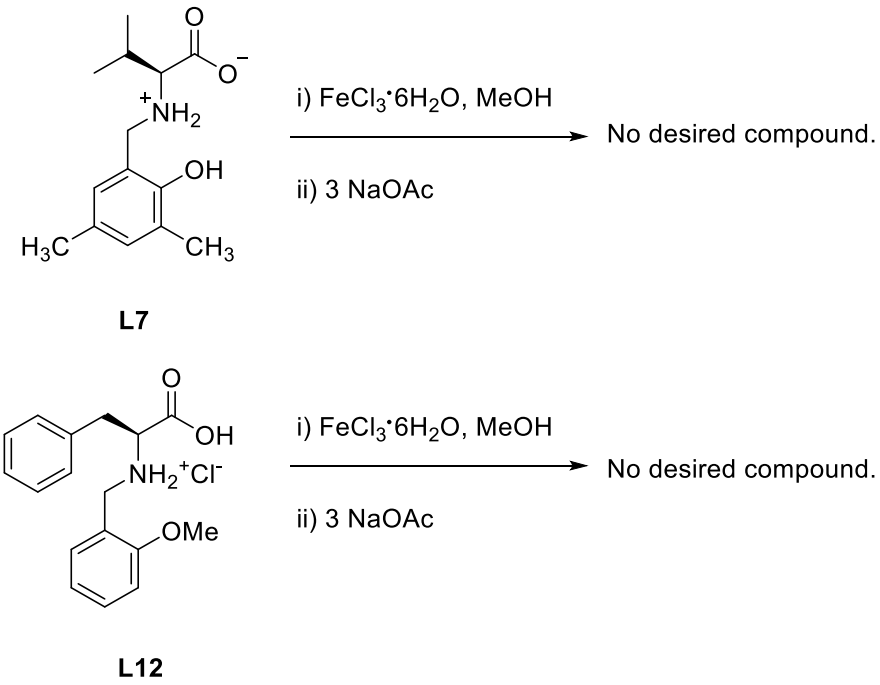

Scheme III-8: Synthetic procedures applied in the attempt of synthesis of Fe(III) compound derived from ligand precursors **L7** and **L12**.

III.2.2.1 – Characterization by UV-Vis and CD spectroscopy

The obtained UV-Vis and CD spectra of the Fe(III) compounds **FeL5**, **FeL6**, and **FeL8**-**11** are presented, respectively, in **Figure III-15** and **Figure III-16** and the most relevant λ_{max}, ε and $\Delta\varepsilon$ values are listed in **Table III-6**. Compounds **FeL5**, **FeL6**, **FeL8** and **FeL10** exhibited intense and broad absorption in the range 556-599 nm, corresponding to phenolate→ Fe(III) $p\pi$-$d\pi^*$ charge transfer (CT) band, thus resulting in the intense dark-blue or dark-purple colours presented by these compounds in solution.[113] Intense bands are also visible in the 322-333 nm range which can be attributed to intraligand π-π^* transitions occurring in the phenolate and amino acid aromatic side-chain systems; in this region, compounds bearing *tert*-butyl groups as substituents in the phenolate ring show more intense bands, which is clear by comparing electronic spectra of **FeL5** and **FeL6**. Compound **FeL9** presents in its electronic spectrum two bands at 501 and 352 nm, also assigned to phenolate-Fe(III) $p\pi$-$d\pi^*$ charge transfer and intraligand π-π^* transitions, respectively. In comparison to **FeL5**, **FeL6**, **FeL8** and **FeL10** compound **FeL9** band profile is quite different by showing less intense bands and a shift of its LMCT band to higher energies, which justifies the brown colour showed by this compound both in solution and in the solid state. Compound **FeL11** exhibits one LMCT band with low intensity at 479 nm and a higher intense band at 322 nm, correspondent to intraligand π-π^* transitions. The absorption at 479 nm can justify the dark-orange colour depicted by this compound in solution and in the solid state.

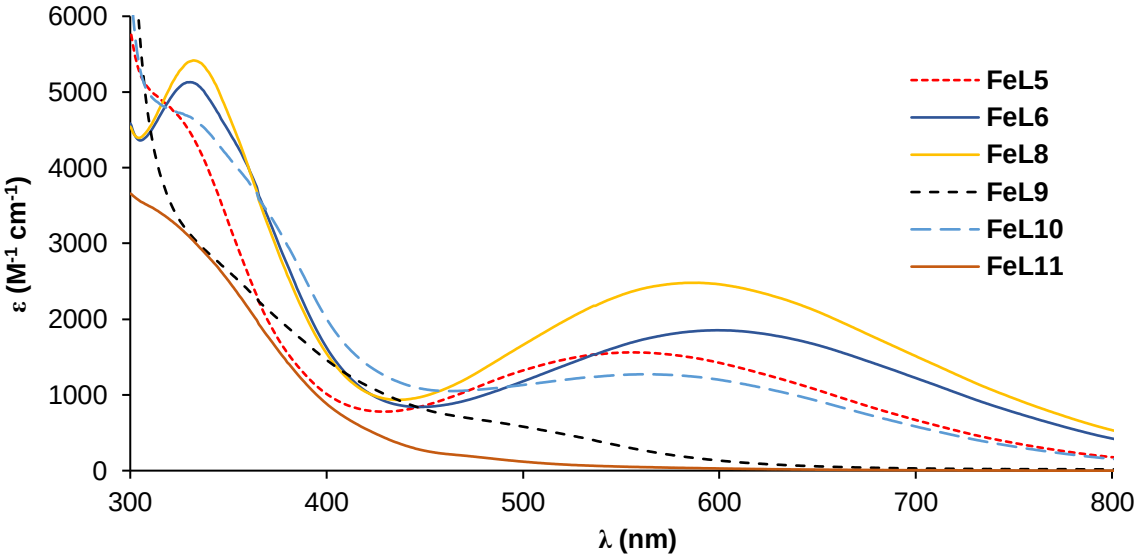

Figure III-15: Electronic absorption (UV-Vis) spectra of compounds **FeL5** (EtOH, 1.99 mM), **FeL6** (EtOH, 1.99 mM), **FeL8** (EtOH, 2.00 mM), **FeL9** (DMSO, 1.99 mM), **FeL10** (EtOH, 2.14 mM) and **FeL11** (EtOH, 1.99 mM) at room temperature with 1 mm optical path quartz cells.

The CD spectra of all compounds indicate chirality in solution and were complemented with the respective UV-Vis spectra to facilitate identification of the relevant absorption bands. Compounds **FeL5**, **FeL9** and **FeL10** show one CD band each near 500 nm and compounds **FeL6** and **FeL8** each depict a similar CD band in the 627-645 nm range, indicating that a chiral induction in the electronic transitions, namely in the phenolate→ Fe(III) $p\pi$-$d\pi^*$ CT transition. Noteworthy is also the near-symmetrical CD spectrum profile of **FeL10** in the visible region in comparison with the other phenolate-containing Fe(III) complexes. In the UV region CD bands are visible in all the referred complexes in the 309-357 nm range, which again indicates efficient transmition of chirality from the amino acid ligands. For **FeL5** and **FeL10** CD bands at 373 and 385 nm, respectively, are observed and may tentatively be assigned to other LMCT transitions, not clearly seen in the UV-Vis spectra. Compound **FeL11** presents a distinct CD spectrum in comparison to the other compounds, with only a faint CD band at 370 nm and it is not clear if this CD band corresponds to a LMCT transition or to an intraligand transition.

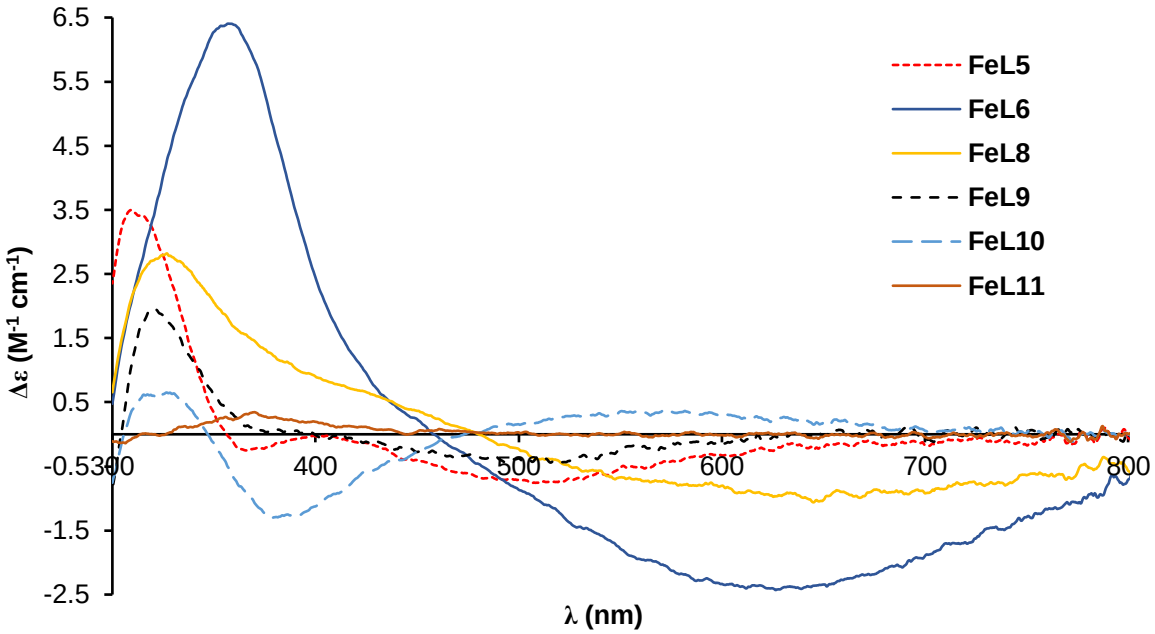

Figure III-16: Circular Dichroism (CD) spectra of compounds **FeL5** (EtOH, 1.99 mM), **FeL6** (EtOH, 1.99 mM), **FeL8** (EtOH, 2.00 mM), **FeL9** (DMSO, 1.99 mM), **FeL10** (EtOH, 2.14 mM) and **FeL11** (EtOH, 1.99 mM) at room temperature with 1 mm optical path quartz cells.

Table III-6: Experimental λ_{max}, ε and $\Delta\varepsilon$ values obtained in the UV-Vis and CD spectra of compounds **FeL5**, **FeL6** and **FeL8**-**11**.

	UV-Vis		CD	
Compound	λ_{max} (nm)	ε (M^{-1} cm^{-1})	λ_{max} (nm)	$\Delta\varepsilon$ (M^{-1} cm^{-1})
FeL5	556	1561.6	512	-0.738
	322	4762.1	373	-0.222
			309	3.397
FeL6	599	1854.2	627	-2.431
	331	5129.9	357	6.405
FeL8	587	2480.2	645	-1.061
	333	5416.3	327	2.819
FeL9	501	579.2	519	-0.435
	352	2584.7	322	1.945
FeL10	563	1273.5	561	0.345
	326	4723.1	385	-1.271
			323	0.568
FeL11	479	174.4	370	0.345
	322	3289.8		

III.2.2.2 – Characterization by Mass spectrometry

The Fe(III) compounds **FeL5**-**6** and **FeL8**-**11** were analysed by ESI-MS negative and positive modes in methanol and DMSO (**FeL9**), and the mass peaks were assigned for the most probable species having no more than ±1 divergence in m/z from the observed peak.

Compound **FeL5** show simple ESI-MS spectra, depicted in **Figure III-17**, clearly indicating dissociation of the amino acid ligand and formation of Fe**L5** aggregates containing two amino acid ligand molecules under the conditions used in the analyses. In the negative mode spectrum the relevant peaks are assigned to a mononuclear $[Fe\mathbf{L5}_2]^-$ species (m/z= 650.2) and the same solvated mononuclear $\{[(Fe\mathbf{L5})_2(\mathbf{L5})(OH)]\bullet H_2O\}^-$ species (m/z= 1038.6), with an extra amino acid ligand molecule, as the major peak. In the positive mode spectrum the peak with higher relative abundance is assigned to the protonated amino acid ligand $H^+\mathbf{L5}$ (m/z= 255.1) and peaks wih lower m/z values are resultant of its fragmentation (*e.g.* m/z= 209.2). A residual mononuclear sodium adduct $\{Na[Fe\mathbf{L5}(OH)]\}^+$ species is assigned to the peak with m/z value of 390.9.

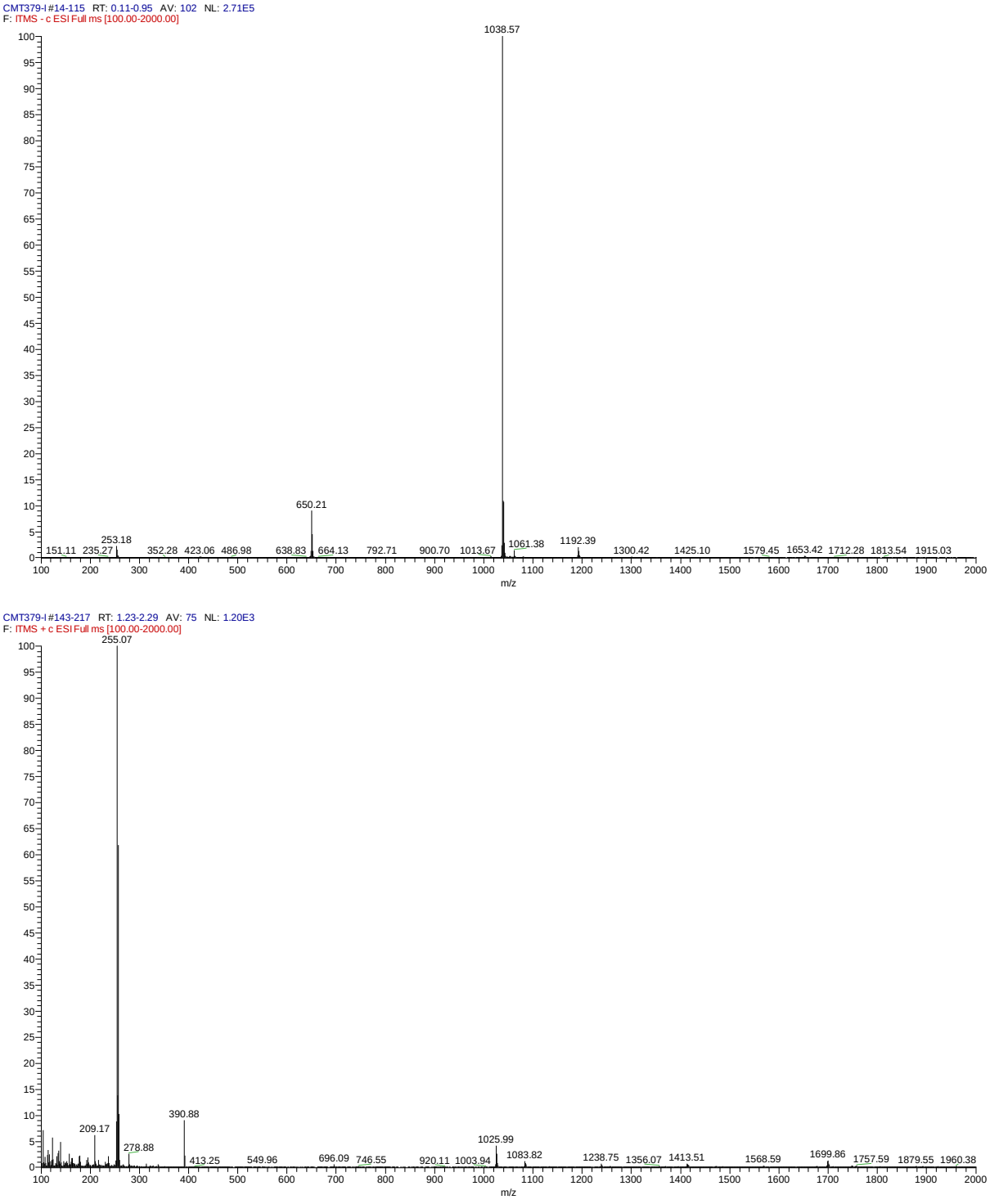

Figure III-17: Negative (up) and positive (down) ESI-MS spectra of **FeL5** in methanol.

The ESI-MS spectra of **FeL6** are presented in **Figure III-18**. The major peak in the negative mode spectrum is assigned to a mononuclear $[Fe\mathbf{L6}_2]^-$ species (m/z= 818.6) with an additional amino acid ligand molecule, and a residual peak possibly corresponds to a solvated trinuclear dianionic tri-μ-hydroxido $\{[(Fe\mathbf{L6})(OH)]_3 \bullet H_2O\}^{2-}$ species (m/z= 689.4). The positive mode spectrum shows a mononuclear dicationic sodium adduct $\{Na_2[Fe\mathbf{L6}] \bullet EtOH\}^{2+}$ species (m/z=

251.2) as the major peak and its respective diprotonated $\{H_2[Fe\mathbf{L6}]\bullet MeOH\}^{2+}$ species (m/z= 262.9). Peaks of m/z values higher than 700 may be due to Fe**L6** aggregates formed under the conditions applied in the ESI-MS analyses.

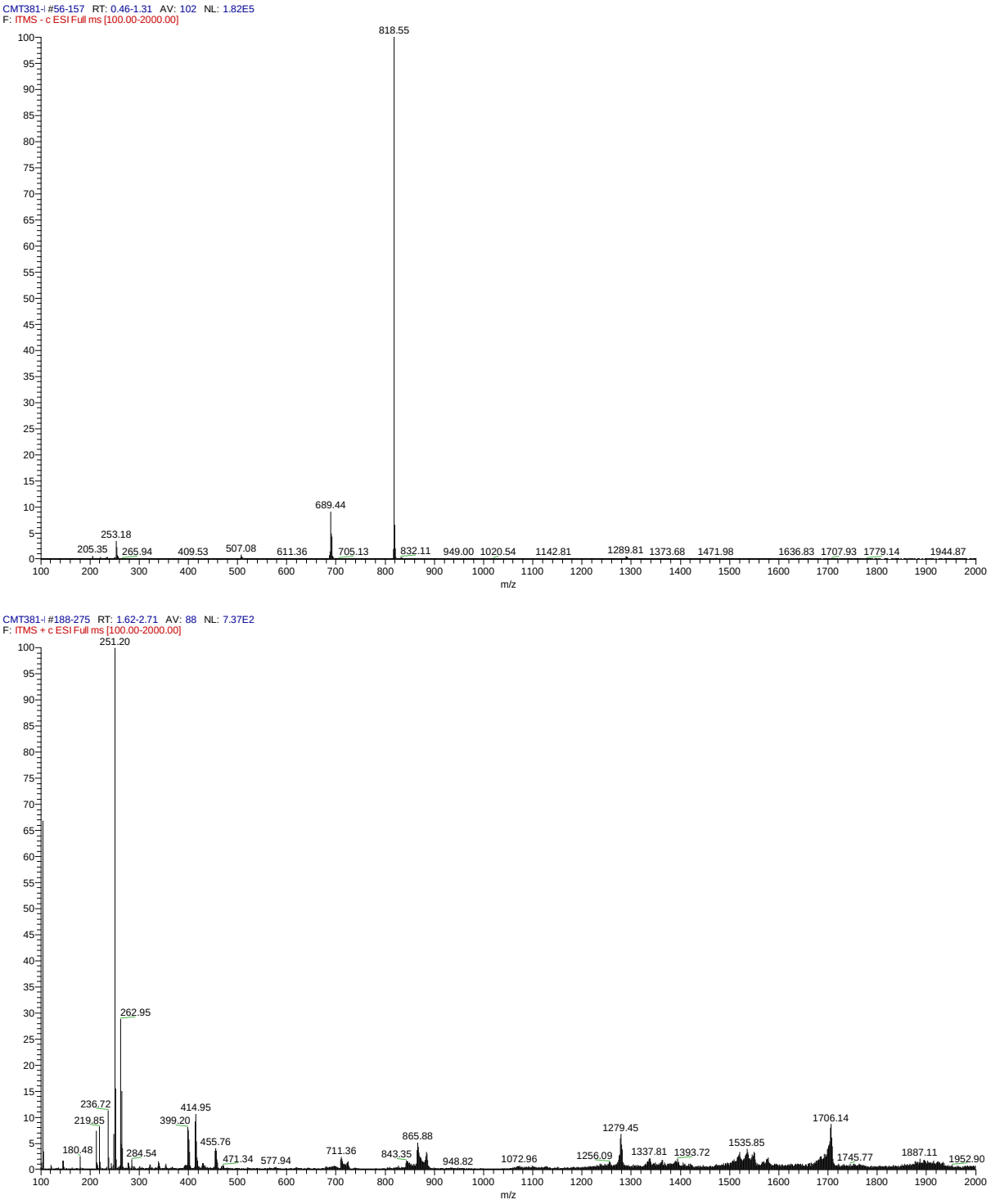

Figure III-18: Negative (up) and positive (down) ESI-MS spectra of **FeL6** in methanol. The residual peaks in the positive mode spectrum indicate formation of Fe**L6** aggregates under the conditions used for the analyses.

ESI-MS spectra of **FeL8** were obtained in methanol and are presented in **Figure III-19**, showing a very simple negative mode spectrum with only one relevant peak assigned to a mononuclear $[Fe\mathbf{L8}_2]^-$ species (m/z= 722.6) containing an additional amino acid ligand molecule. The respective positive mode spectrum is more complex containing several peaks with moderate relative abundances assigned to trinuclear and dinuclear Fe**L8** μ-hydroxido- and μ-methoxido-bridged species, resultant of Fe**L8** aggregation: two possibly solvated trinuclear μ-hydroxido $\{H[(Fe\mathbf{L8})_3(OH)(\mathbf{L8})_2]\bullet 4MeOH\}^+$ and $\{H[(Fe\mathbf{L8})_3(OH)(\mathbf{L8})_2]\bullet MeOH\bullet H_2O\}^+$ species with two additional amino acid ligand molecules each (m/z= 1984.0 and 1906.3, respectively), being the first species corresponding to the major peak, three solvated possibly trinuclear di-μ-methoxido $\{H[(Fe\mathbf{L8})_3(OMe)_2(\mathbf{L8})]\bullet 4MeOH\bullet 2H_2O\}^+$, $\{H[(Fe\mathbf{L8})_3(OMe)_2(\mathbf{L8})]\bullet 4MeOH\bullet H_2O\}^+$ and $\{H[(Fe\mathbf{L8})_3(OMe)_2(\mathbf{L8})]\bullet 2MeOH\}^+$ species (m/z= 1731.7, 1712.6, 1631.7, respectively) with one additional amino acid ligand molecule each, one solvated trinuclear di-μ-hydroxido sodium adduct $\{Na[(Fe\mathbf{L8})_3(OH)_2(\mathbf{L8})]\bullet MeOH\bullet H_2O\}^+$ species (m/z= 1611.4) with one additional amino acid ligand molecule, one solvated dinuclear sodium adduct $\{Na[Fe\mathbf{L8}_2]_2\bullet 2MeOH\bullet 3H_2O\}^+$ species (m/z= 1589.4) with two amino acid ligand molecule coordinated to each metal centre, one solvated dinuclear $\{H[(Fe\mathbf{L8}_2)_2]\bullet 2MeOH\}^+$ species (m/z= 1513.6), one solvated dinuclear $\{H[(Fe\mathbf{L8})_2(\mathbf{L8})]\bullet H_2O\}^+$ species (m/z=) with one additional amino acid ligand molecule and one solvated dinuclear dicationic $\{H_2[(Fe\mathbf{L8}_2)_2]\bullet 5H_2O\}^{2+}$ species (m/z= 1131.2). Mononuclear species were also found in the positive mode spectrum of this compound but with relative abundance lower than 10%: the mononuclear sodium adduct $\{Na[Fe\mathbf{L8}_2]\}^+$ species (m/z= 768.6) with an additional amino acid ligand, the mononuclear sodium adduct $\{Na[Fe\mathbf{L8}(OAc)]\}^+$ species (m/z= 746.3) and the protonated amino acid ligand $H\mathbf{L8}^+$ (m/z= 336.3), indicative of dissociation of the amino acid ligand.

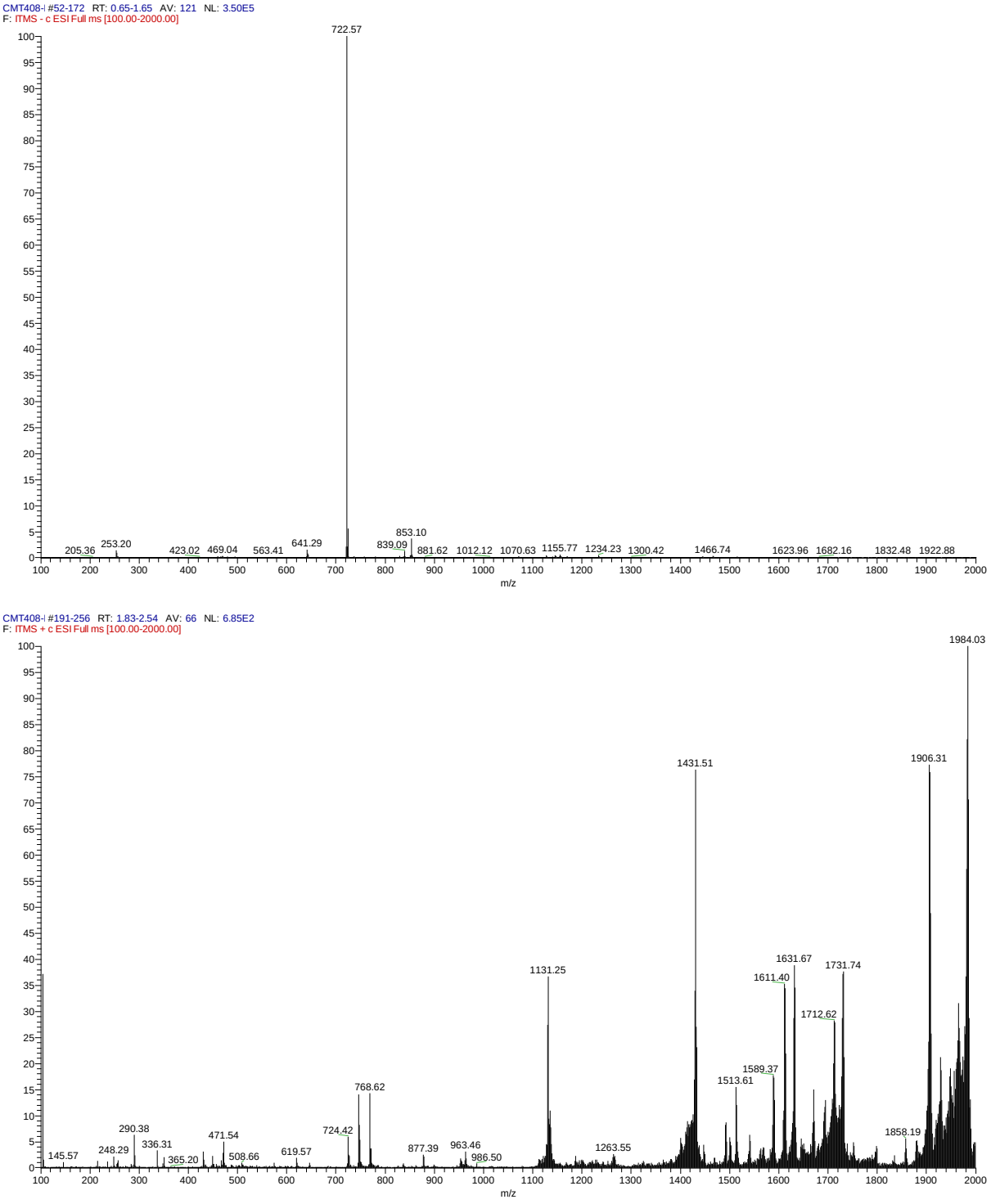

Figure III-19: Negative (up) and positive (down) ESI-MS spectra of **FeL8** in methanol. The intense peaks in the positive mode spectrum indicate the formation of oligonuclear Fe**L8** aggregates under the conditions used for the analyses.

Compound **FeL9** ESI-MS spectra were obtained in DMSO and are presented in **Figure III-20**. In the negative mode spectrum three peaks are assigned to mononuclear species indicating dissociation of the amino acid ligand in the experimental conditions applied: the major species ($[Fe\mathbf{L9}_2]^-$ m/z= 752.4) with an additional amino acid ligand, a possible amino acid ligand adduct

2**L9**$^{-}$ species (m/z= 699.1) and the monoanionic amino acid ligand **L9**$^{-}$ (m/z= 349.4). In the positive mode spectrum dissociation of the amino acid ligand is still evident with mass peaks being assigned to the protonated amino acid ligand H^{+}**L9** (m/z= 351.0), species possibly resultant from amino acid ligand decomposition (decarboxylation, m/z= 303.1) and the diprotonated amino acid ligand H_2**L9**$^{2+}$ (m/z= 178.8), assigned to the major peak. A possible solvated mononuclear dicationic {H_2[Fe**L9**Cl]•MeOH•2H_2O}$^{2+}$ species (m/z= 256.5) is also visible.

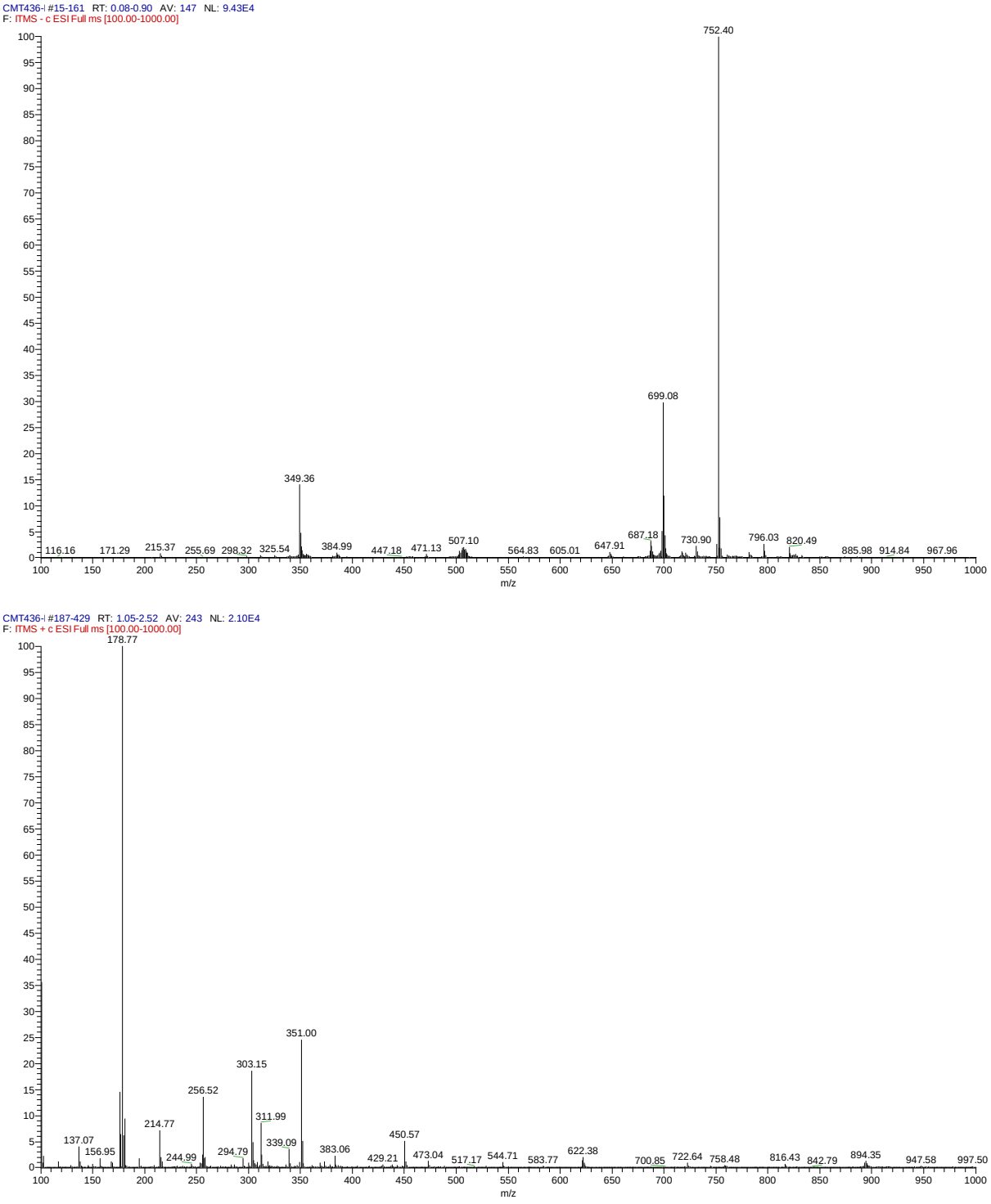

Figure III-20: Negative (up) and positive (down) ESI-MS spectra of **FeL9** in DMSO. The mass peaks evidenced in both negative and positive modes indicate dissociation of the amino acid ligand under the conditions used for the analyses.

The ESI-MS spectra of compound **FeL10** were obtained in methanol and are presented in **Figure III-21**. The negative mode spectrum indicates the presence of several mononuclear species such as the solvated mononuclear $\{[Fe\mathbf{L10}_2]\bullet MeOH\}^-$ species (m/z= 950.4) and the respective unsolvated species $[Fe\mathbf{L10}_2]^-$ (m/z= 920.4), both containing an additional amino acid

ligand and with the last adduct assigned to the major peak, a solvated mononuclear {[Fe**L10**(OH)]•MeOH•3H_2O}$^-$ species (m/z= 592.2) with an hydroxide anion and a solvated mononuclear {[Fe**L10**(OAc)]•MeOH}$^-$ species (m/z= 578.2) with an acetate anion. The positive mode spectrum shows as the major peak assigned to a solvated mononuclear tricationic sodium adduct {Na_3[Fe**L10**$_2$]•MeOH•8H_2O}$^{3+}$ species (m/z= 387.2) with an additional amino acid ligand. Dissociation of the amino acid ligand is also evident with the presence of a solvated diprotonated amino acid ligand (H_2**L10**•2H_2O)$^{2+}$ (m/z= 236.0) and several peaks with m/z values lower than 236, possibly resultant of amino acid ligand decomposition.

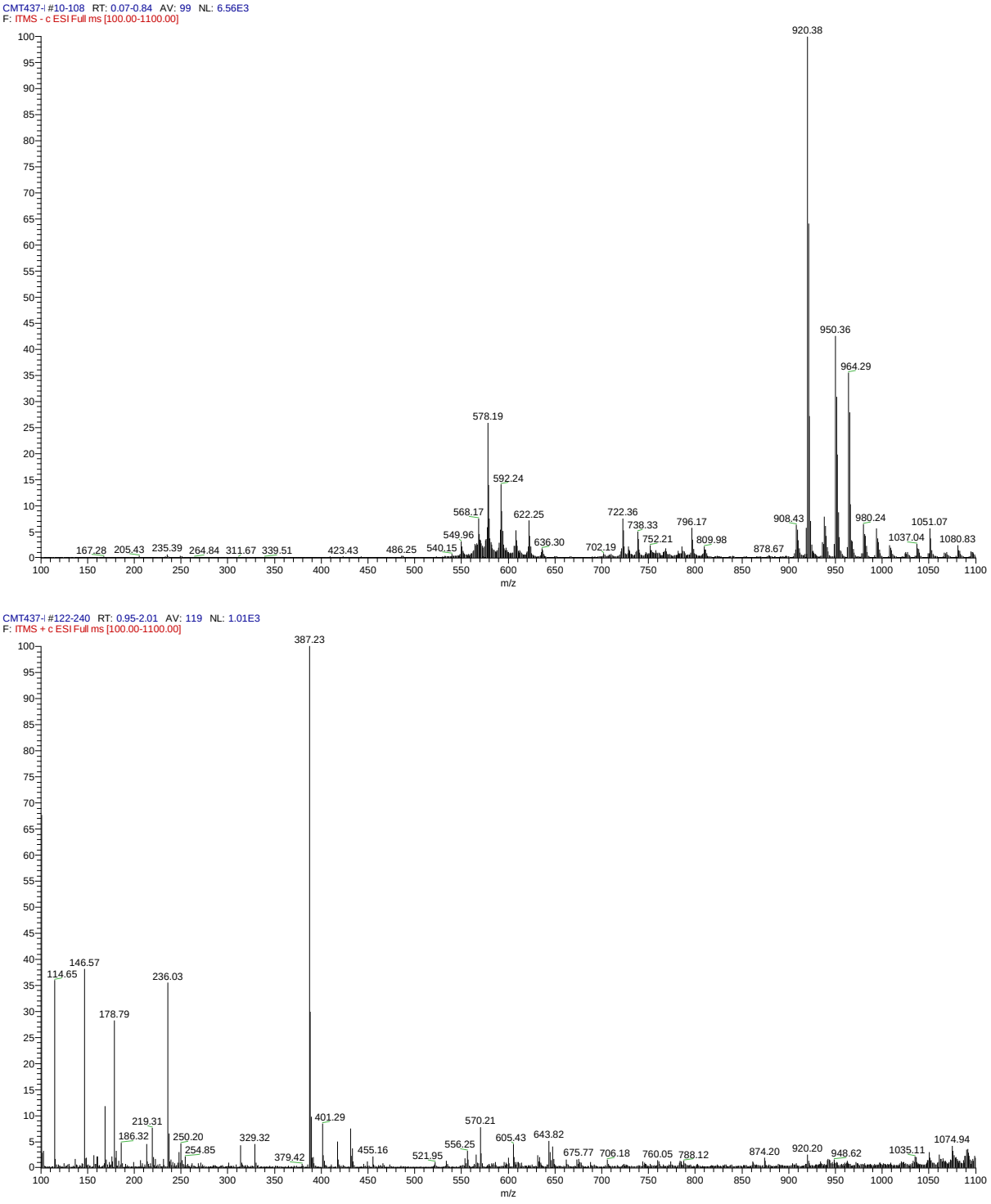

Figure III-21: Negative (up) and positive (down) ESI-MS spectra of **FeL10** in MeOH.

Compound **FeL11** ESI-MS spectra were obtained in methanol and are depicted in **Figure III-22**, showing in the negative mode spectrum the formation of several μ-hydroxido, μ-methoxido and μ-hydroxido-μ-methoxido-bridged Fe**L11** aggregates: three dinuclear di-μ-methoxido $\{[Fe\mathbf{L11}(OMe)]_2 \bullet 7MeOH\}^-$, $\{[Fe\mathbf{L11}(OMe)]_2 \bullet (6MeOH) \bullet (H_2O)\}^-$ and $[Fe\mathbf{L11}(OMe)]_2^-$ species (m/z= 967.1, 953.1, 742.1, respectively) with the first adduct being assigned to the major peak, one dinuclear μ-hydroxido-μ-methoxido $[(Fe\mathbf{L11})_2 \bullet (OH)(MeO)]^-$ species (m/z=

728.2) and one dinuclear di-μ-hydroxido $[Fe\mathbf{L11}(OH)]_2^-$ species (m/z= 714.3). Positive mode spectrum shows solvated mononuclear $\{H[Fe\mathbf{L11}(OH)]\bullet H_2O\}^+$ species (m/z= 394.2) and also species resultant from amino acid ligand dissociation such as two amino acid sodium adduct species $\{Na(\mathbf{L11})\bullet H_2O)\}^+$ and $\{Na(\mathbf{L11})\}^+$ (m/z= 328.2, 308.2, respectively) with the last assigned to the major peak and the protonated amino acid ligand $H\mathbf{L11}^+$ (m/z= 286.1). Several species appear at m/z higher than 580 and might be resultant of formation of Fe**L11** aggregates.

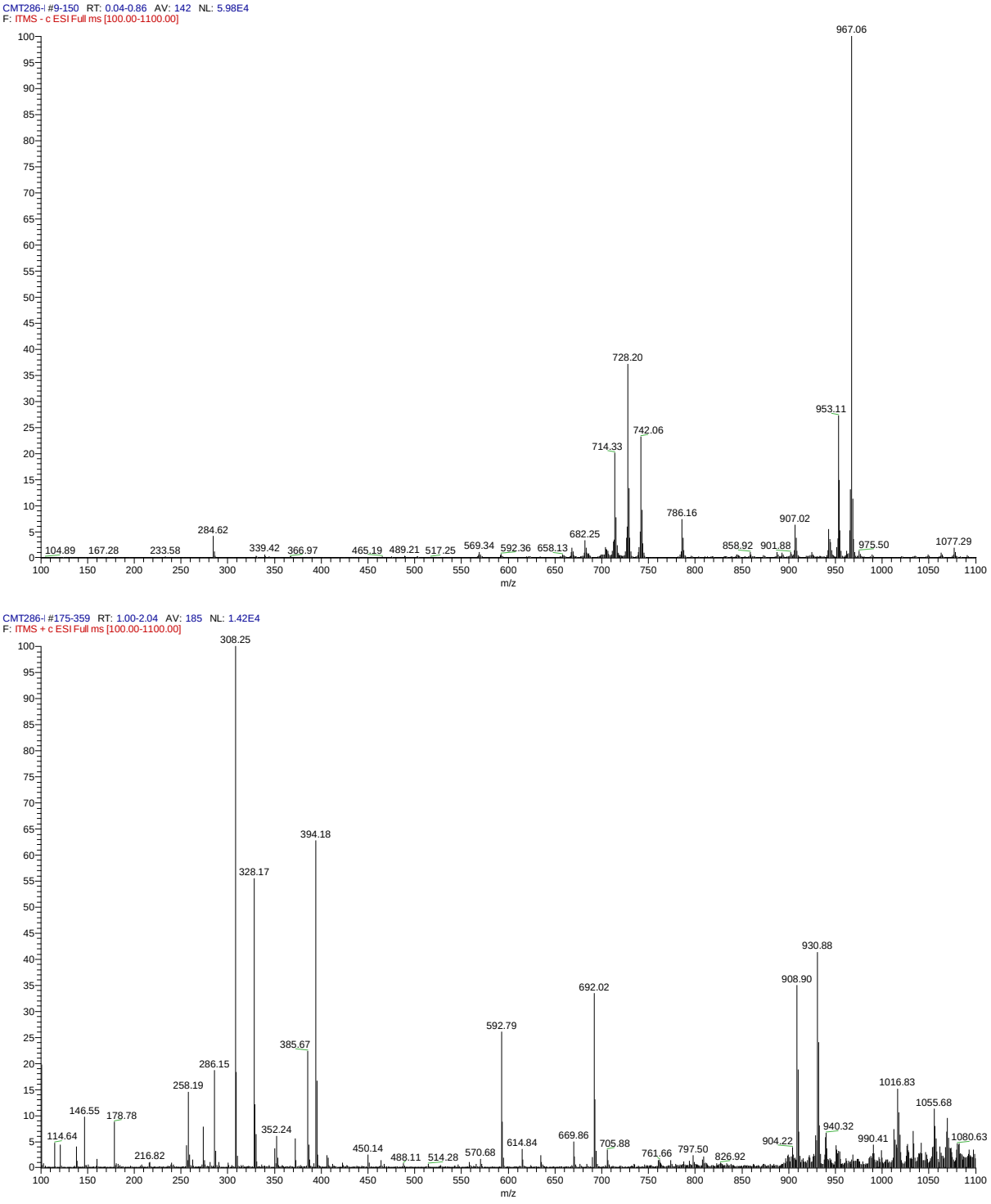

Figure III-22: Negative (up) and positive (down) ESI-MS spectra of **FeL11** in methanol. The low-intense peaks with m/z values higher than 580 in both negative and positive spectra indicate formation of oligonuclear **FeL8** aggregates under the conditions used for the analyses.

III.2.2.3 – Characterization by Infrared spectroscopy

The FT-IR spectra of solid samples of **FeL5**, **FeL6** and **FeL8**-**11** were analysed and the most relevant vibrational frequencies are listed in **Table III-7**. All compounds exhibited a ν(C=O) stretching vibration band at *ca*. 1600 cm^{-1} corresponding to the carboxyl group of the amino acid ligand, and in exception to **FeL11** all compounds depict a ν(C-O) bending vibration band assigned to the phenolate moiety at *ca.* 1220 cm^{-1}. For compounds **FeL5**, **FeL6** and **FeL11** the existence of two bands at *ca.* 1450 and 700 cm^{-1}, corresponding to symmetric Fe-OAc-Fe stretching vibrations and Fe-OH-Fe bending vibrations,[119] possibly indicating the existence of oligonuclear species in these compounds.

Table III-7: IR stretching frequencies for the prepared Fe(III) compounds **FeL5**, **FeL6** and **Fe8**-**11**.

Stretching mode	FeL5	FeL6	FeL8	FeL9	FeL10	FeL11
	Wavenumber (cm^{-1})					
ν(N-H)	3243	2957	2956	-	-	3027
ν(C=$O_{carboxyl,\ aminoacid}$)	1604	1607	1622	1632	1624	1741
ν(Fe-OAc-Fe)	1474	1440	-	-	-	1438
ν(C-O_{Phenol})	1259	1267	1203	1223	1237	-
ν(Fe-OH-Fe)	701	747	-	-	-	659

III.2.2.4 – Elemental analysis

All the prepared Fe(III) compounds afforded elemental analysis results consistent with mononuclear species having water, acetone or ethyl acetate as contaminants. The elemental analysis of **FeL5**, **FeL8** and **FeL11** were also consistent with dinuclear species containing either water or alcohols as vestigial contaminants.

III.2.3 – Fe(III) complexes bearing amino acid-pyridyl-phenol ligands

The preparation of Fe(III) complexes **FeL13** to **FeL15** will be outlined in this Section and their structural formulae are depicted in **Figure III-23**.

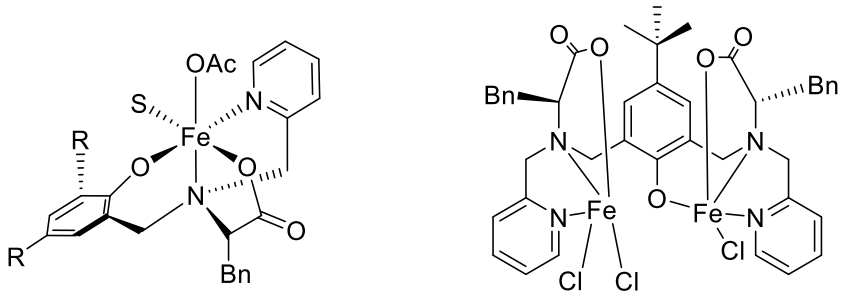

FeL13: R= CH_3
FeL14: R= $C(CH_3)_3$
S= Solvent

FeL15

Figure III-23: Structural formulae of the prepared Fe(III) amino acid compounds **FeL13**-**FeL15** based on their elemental analyses.

The synthesis of these compounds is illustrated in **Scheme III-9.** Ligand precursors **L13**, **L14** or **L15**, depending on the desired Fe(III) compound, were solubilized in MeOH in an open vessel at room temperature, followed by addition of $FeCl_3 \bullet 6H_2O$, which afforded a dark purple-blue solution in the preparation of **FeL13** and **FeL14** and a dark brown solution in the synthesis of **FeL15**. After 5 minutes under stirring sodium acetate was added to the mixture, followed by addition of distilled water, affording a precipitate in all cases. Isolation of compounds **FeL13** and **FeL14** required filtration of the formed precipitate and the resulting residue was dissolved in ethyl acetate, dried with Na_2SO_4, filtered and the filtrate evaporated under vacuum, affording the desired compounds as dark-blue solids in, respectively, 59 and 65% yield, respectively. Compound **FeL15** was obtained as an brown solid in 52% yield after filtration under vacuum of the formed precipitate and washing with distilled water.

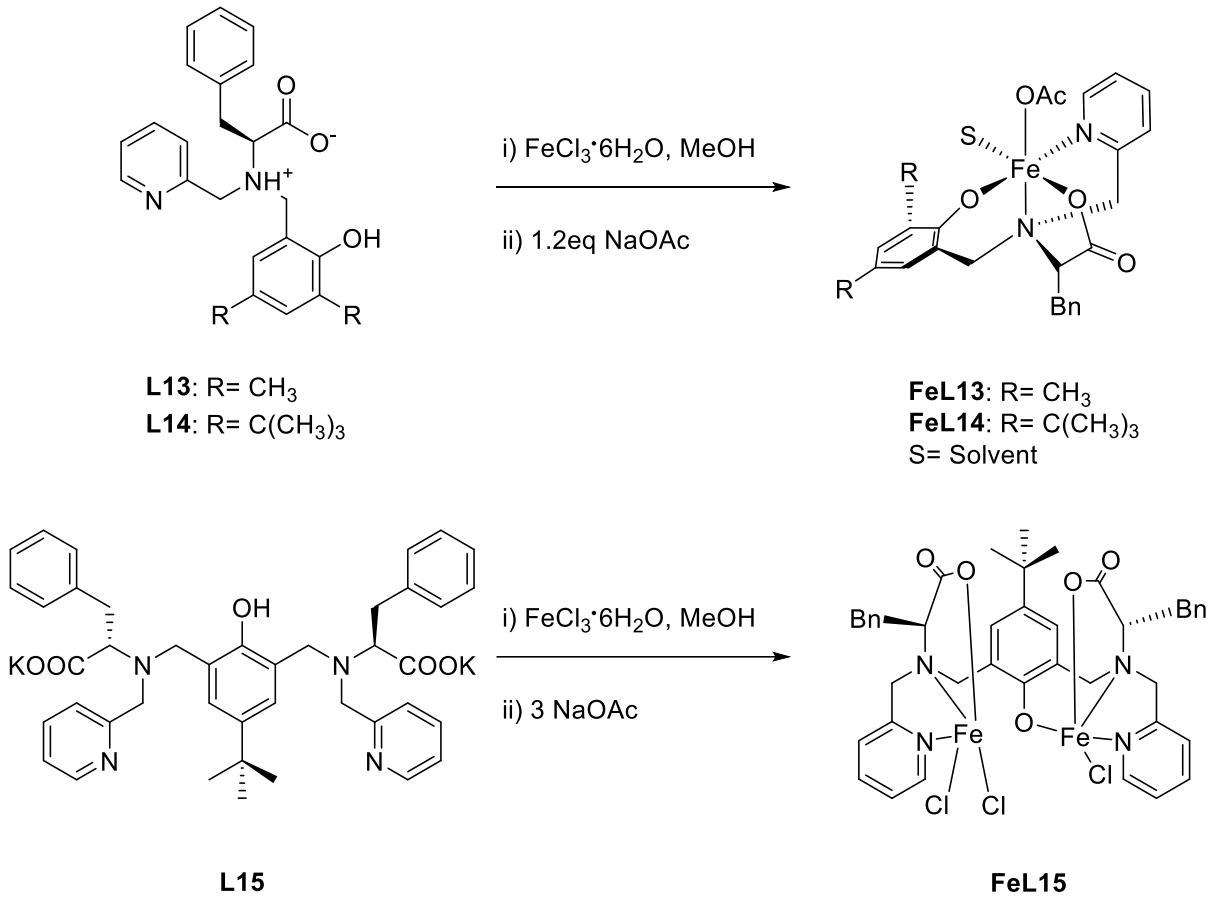

Scheme III-9: Synthesis of Fe(III) compounds derived from ligand precursors **L13**-**L15**.

III.2.3.1 – Characterization by UV-Vis and CD spectroscopy

The electronic and CD spectra obtained for **FeL13**, **FeL14** and **FeL5** are presented in **Figure III-24** and **Figure III-25**, respectively, with the relevant λ_{max}, ε and $\Delta\varepsilon$ values listed in **Table III-8**. Compounds **FeL13** and **FeL14** exhibit similar electronic spectra regarding their band profile. Intense and broad band are exhibited by both complexes at 543 and 572 nm, respectively, assigned to phenolate→ Fe(III) *pπ*-*dπ** CT transitions.[113] The presence of the *tert*-butyl groups in the phenolate moiety of **FeL14** shifts λ_{max} to lower energies, due to the higher electron donating character of these groups when compared to methyl substituents present in the phenol moiety of **FeL13**.[120,121] A second band with higher intensity is observed for both compounds at 335 and 330 nm, respectively, and can be related to intraligand π-π* transitions occurring in the phenolate, pyridyl or benzyl aromatic systems. Compound **FeL15** presents two very low intensity bands at 543 and 483 nm, assigned to partially allowed *d*-*d* transitions. In the 400-300 nm region this compound show two bands at 342 and 305 nm; the less energetic transition is assigned to a phenolate→ Fe(III) $p\pi - d_{x^2-y^2}/d_{z^2}$ CT band[122] while the band at lower wavelength corresponds to intraligand π-π* transitions occurring in the phenolate and pyridyl aromatic systems.

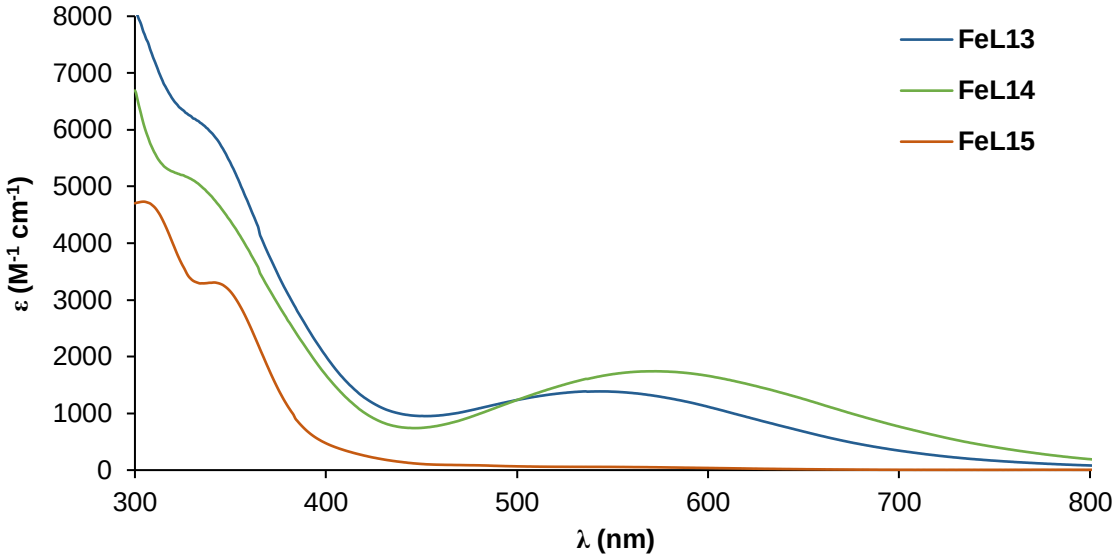

Figure III-24: Electronic absorption (UV-Vis) spectra of compounds **FeL13** (EtOH, 1.99 mM), **FeL14** (EtOH, 1.99 mM) and **FeL15** (EtOH, 2.01 mM) at room temperature with 1 mm optical path quartz cells.

The CD spectra of **FeL13**-**15** indicate chiral induction and were complemented with the respective UV-Vis spectra to facilitate identification of the relevant absorption bands. The first CD band appears at 327 and 410 nm for **FeL13** and **FeL15**, respectively. These bands are assigned to a pyridyl→ Fe(III) *pπ-dπ** CT transition, not evident in the respective UV-Vis spectra; the absence of this transition in the UV-Vis spectra can be attributed to band overlap between this band and intraligand π-π* transitions in **FeL13** and phenolate→ Fe(III) $p\pi - d_{x^2-y^2}/d_{z^2}$ CT transitions in **FeL15**. A second CD band is observed in the 317-360 nm region for compounds **FeL13**-**15,** which is due to intraligand π→π* transitions. These indicate efficient transmition of chirality from the amino acid ligands due to the proximity of the aromatic benzyl side-chain groups and the chiral centers.

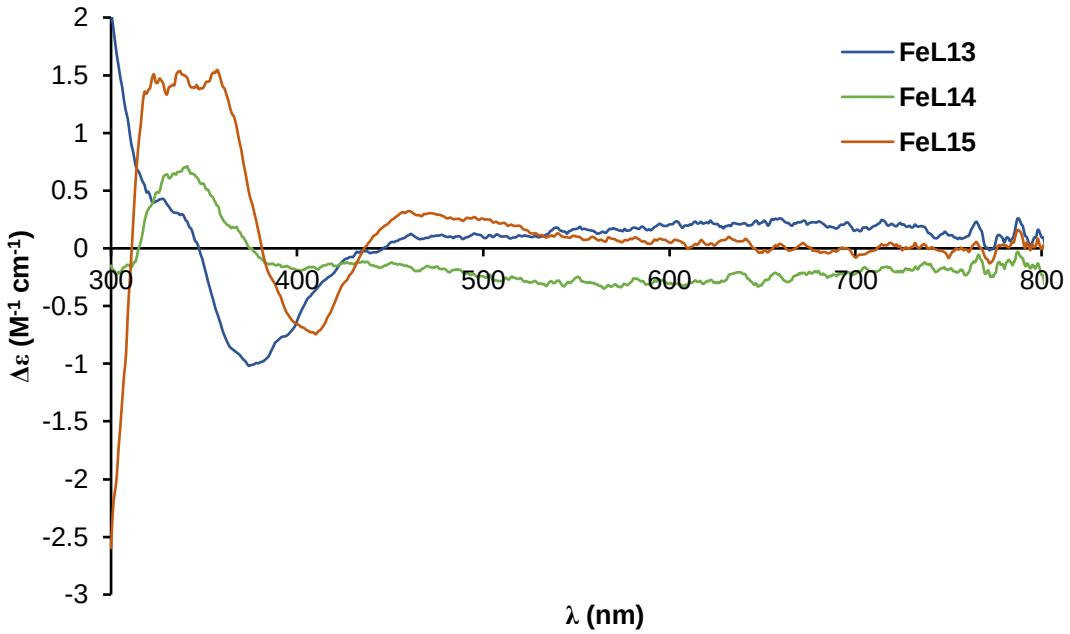

Figure III-25: Circular Dichroism (CD) spectra of compounds **FeL13** (EtOH, 1.99 mM), **FeL14** (EtOH, 1.99 mM) and **FeL15** (EtOH, 2.01 mM) at room temperature with 1 mm optical path quartz cells.

Table III-8: Experimental λ_{max}, ε and $\Delta\varepsilon$ values obtained in the UV-Vis and CD spectra of **FeL13-15**.

	UV-Vis		CD	
Compound	**λ_{max} (nm)**	**ε (M^{-1} cm^{-1})**	**λ_{max} (nm)**	**$\Delta\varepsilon$ (M^{-1} cm^{-1})**
FeL13	543	1387.3	380	-0.988
	335	6105.3	327	0.427
FeL14	572	1741.4	341	0.711
	330	5129.5		
FeL15	543	56.8	472	0.304
	483	81.7	410	-0.745
	342	3306	360-317	1.48
	305	4730.8		

III.2.3.2 – Characterization by X-Ray diffraction

Important structural information was obtained by the X-ray diffraction of single crystals of **FeL14**. The ORTEP diagram is presented below in **Figure III-26** and the selected parameters are listed in **Table III-9**. Compound **FeL14** crystallized in the monoclinic system, space group *C*2/*c*, which is a centrosymmetric space group with a molecule of the complex and a cocrystallized water molecule in the asymmetric unit. Due to the existence of chiral centers (N2, C7, C39 and N4) in complex **FeL14**, the corresponding asymmetric unit cell of **FeL14** shows a racemic mixture, composed by four pairs of (*R,S,S,S*)- and (*S,R,R,R*)-isomers. In the asymmetric unit, chiral atoms N2 (Fe1) have the *S* configuration while atoms C7 (Fe1), C39 (Fe2) and N4 (Fe2) display *R* configuration. Each molecule is composed by two independent Fe(III) atoms, each coordinated to a [O,N,O,N] ligand, one oxygen atom and to an O atom of a acetyl group, giving rise to a solid state structure represented in **Figure III-26**. In **FeL14**, the ligands in both metal centres can be described as *trans* isomers, likely reflecting a better stereochemical arrangement. The dihedral angles between the chelation planes of *cis*-coordinated ligands are close to 90º, whereas the angles between two *trans* O- (or N-) atoms and the metal centre are *ca.* 180º, indicating an octahedral geometry around the iron atoms. The bond distances observed between the metal centres and the donor atoms (1.884(4)–2.248 Å) are within the values observed for Fe(III) complexes with N-, O-donor ligands.[118] The supramolecular arrangement of complex **FeL14** is generated by classic and non-classic O–H···O hydrogen bonds, and C–H···O assisted non-classical hydrogen bonds as depicted in **Figure III-27**, with the respective bond length and angles listed in **Table III-10**.

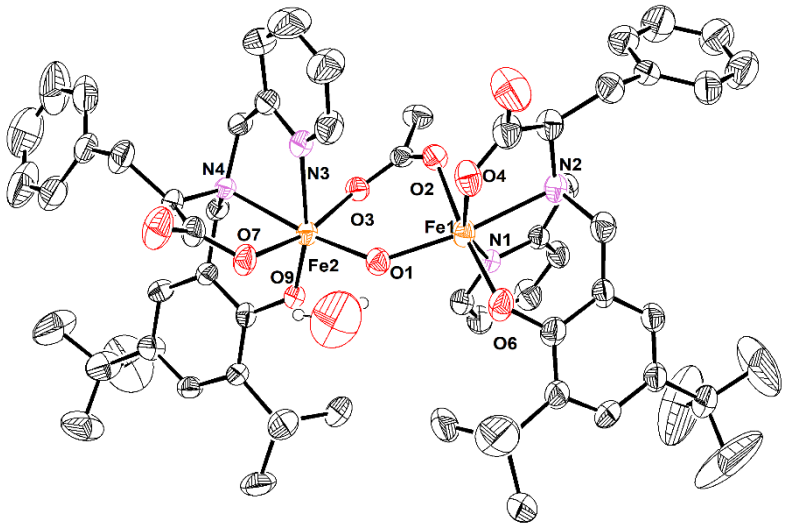

Figure III-26: ORTEP-3 diagram of the asymmetric unit of **FeL14**, using 30% probability level ellipsoids. All calculated H atoms were omitted for clarity.

Table III-9: Selected bond lengths (Å) and angles (º) for compound **FeL14**.

FeL14			
Bond lengths (Å)		**Angles (º)**	
Fe1–N1	2.121(4)	O6–Fe1–O4	97.2(2)
Fe1–N2	2.238(4)	N1–Fe1–O2	80.29(15)
Fe1–O1	1.960(4)	O4–Fe1–O2	89.36(17)
Fe1–O2	2.123(4)	O6–Fe1–N1	90.29(17)
Fe1–O4	1.949(4)	O1–Fe1–N2	171.01(16)
Fe1–O6	1.893(4)	O9–Fe2–O7	96.80(16)
Fe2–O1	1.947(4)	O9–Fe2–O3	92.15(15)
Fe2–N3	2.213(5)	O3–Fe2–N3	84.90(16)
Fe2–N4	2.248(4)	O7–Fe2–N3	83.56(17)
Fe2–O3	2.036(4)	O1–Fe2–N4	167.48(16)
Fe2–O7	1.983(4)		
Fe2–O9	1.884(4)		

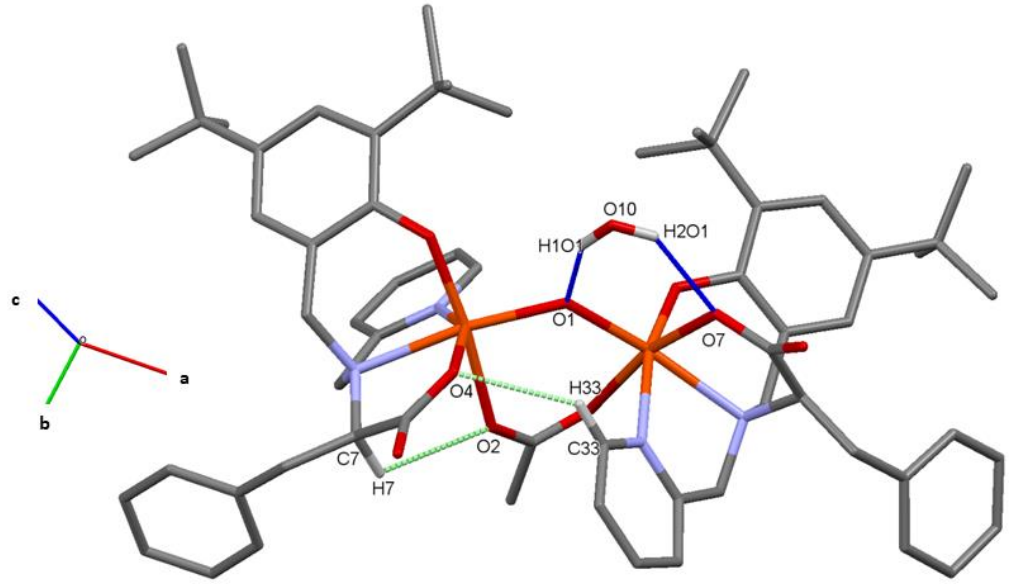

Figure III-27: View of the hydrogen bonds for complex **FeL14**. Donor and acceptor atoms are identified. Blue dashed lines represent the O–H···O hydrogen bonds, light-green dashed lines the C–H···O assisted non-classical hydrogen bonds. All the hydrogen atoms, except those involved in the interactions, were omitted for clarity.

Table III-10: List of hydrogen bonds for **FeL14** [Å and °].

D-H...A	*d*(D-H)	*d*(H...A)	*d*(D...A)	<(DHA)
C(7)-H(7)...O(2)	0.98	2.50	2.992(7)	110.7
C(33)-H(33)...O(4)	0.93	2.47	3.153(8)	130.4
O(10)-H(1O1)...O(1)	0.8474(1)	1.925(3)	2.683(3)	148.17(10)
O(10)-H(2O1)...O(7)	0.8602(1)	2.224(4)	2.968(4)	144.80(10)

III.2.3.3 – Characterization by Mass spectrometry

The Fe(III) compounds **FeL13**-**15** were studied by ESI-MS negative and positive modes in methanol, and the mass assignents are for the most probable species having no more than ±1 divergence in m/z from the observed peak.

The ESI-MS spectra of compound **FeL13** are shown in **Figure III-28** with the mass peaks being majorly atributed to mononuclear Fe**L13** species. In the negative mode spectrum, four mass peaks are observed and are assigned to the following species: [Fe**L13**(AcO)(H_2O)]$^-$, {[Fe**L13**(OH)(H_2O)]•3H_2O}$^-$, {[Fe**L13**(OH)(H_2O)]•MeOH•2H_2O}$^-$ and {[Fe**L13**(OH)(H_2O)]•2MeOH•H_2O}$^-$ (m/z= 519.8, 533.7, 548.6 and 562.4, respectively) with the

third adduct corresponding to the major peak. In the positive mode spectrum the mass peaks are attributed to a mononuclear $\{H[Fe\mathbf{L13}(MeO)]\}^+$ species (m/z= 475.7), a dinuclear μ-methoxido $\{H[(Fe\mathbf{L13})_2(MeO)]\}^+$ species (m/z= 919.2) corresponding to the major peak and a solvated dinuclear μ-hydroxido sodium adduct $\{Na[(Fe\mathbf{L13})_2(OH)]\bullet H_2O\}^+$ species (m/z= 947.1).

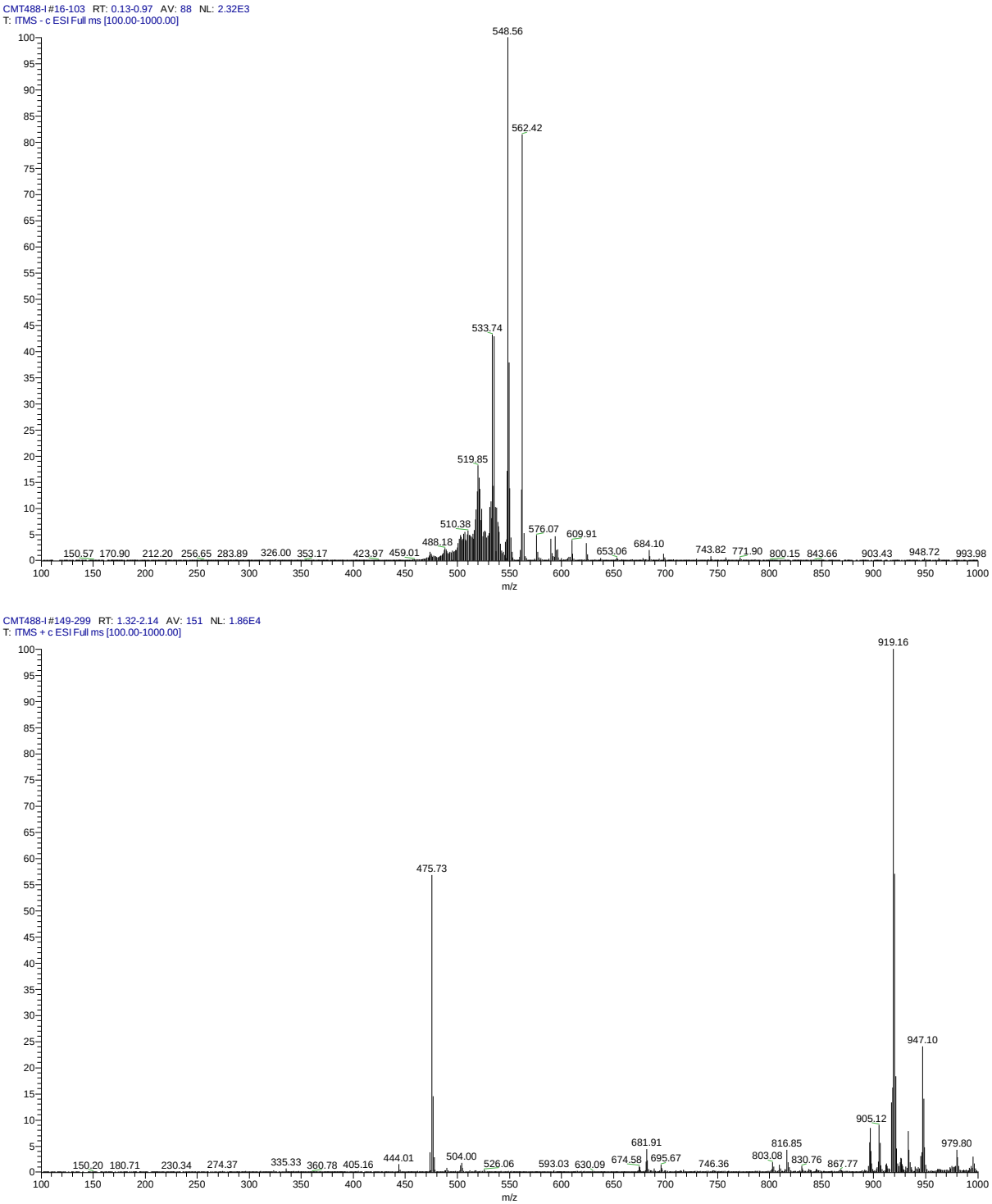

Figure III-28: Negative (up) and positive (down) ESI-MS spectra of **FeL13** in methanol. Peak assignments indicate the formation of mononuclear and dinuclear **FeL13** species.

The ESI-MS spectra of **FeL14** are presented in **Figure III-29**. The negative mode spectrum shows a more complex series of mass peaks in comparison to the previous compound **FeL13**, starting with the presence of the solvated ligand [(**L14**)•5H_2O]$^-$ (m/z= 561.9), several solvated mononuclear species {[Fe**L14**(OH)(H_2O)]•H_2O}$^-$, {[Fe**L14**(OH)(H_2O)]•MeOH}$^-$, {[Fe**L14**(OH)(H_2O)]•MeOH•2H_2O}$^-$ and {[Fe**L14**(OH)(H_2O)]•2MeOH•H_2O}$^-$ (m/z= 580.0, 594.0, 631.8 and 645.7, respectively), all containing and hydroxide ion coordinated to the metal centre, a solvated mononuclear acetate {[Fe**L14**(OAc)(H_2O)]•H_2O}$^-$ species (m/z= 621.8), corresponding to the major peak, a solvated dinuclear di-μ-hydroxido {[(Fe**L14**)$_2$($OH)_2$]•H_2O}$^-$ species (m/z= 1107.1) and a solvated dinuclear μ-acetato-μ-hydroxido [(Fe**L14**)$_2$(OH)(OAc)]$^-$ species (m/z= 1130.9). Mass peaks with m/z values below 560 are assigned to species resultant from amino acid ligand decomposition. The positive mode spectrum shows a simpler profile with peaks attributed to a mononuclear {H[Fe**L14**(MeO)]}$^+$ species (m/z= 559.8), a solvated dinuclear {H[(Fe**L14**)$_2$(**L14**)]•4H_2O}$^+$ major species (m/z= 1601.3) with an additional amino acid ligand molecule, a similar solvated dinuclear {H[(Fe**L14**)$_2$(**L14**)]•3MeOH•H_2O}$^+$ species (m/z= 1645.6) and a solvated dinuclear sodium adduct {Na[(Fe**L14**)$_2$(**L14**)]•6H_2O}$^+$ species (m/z= 1660.2).

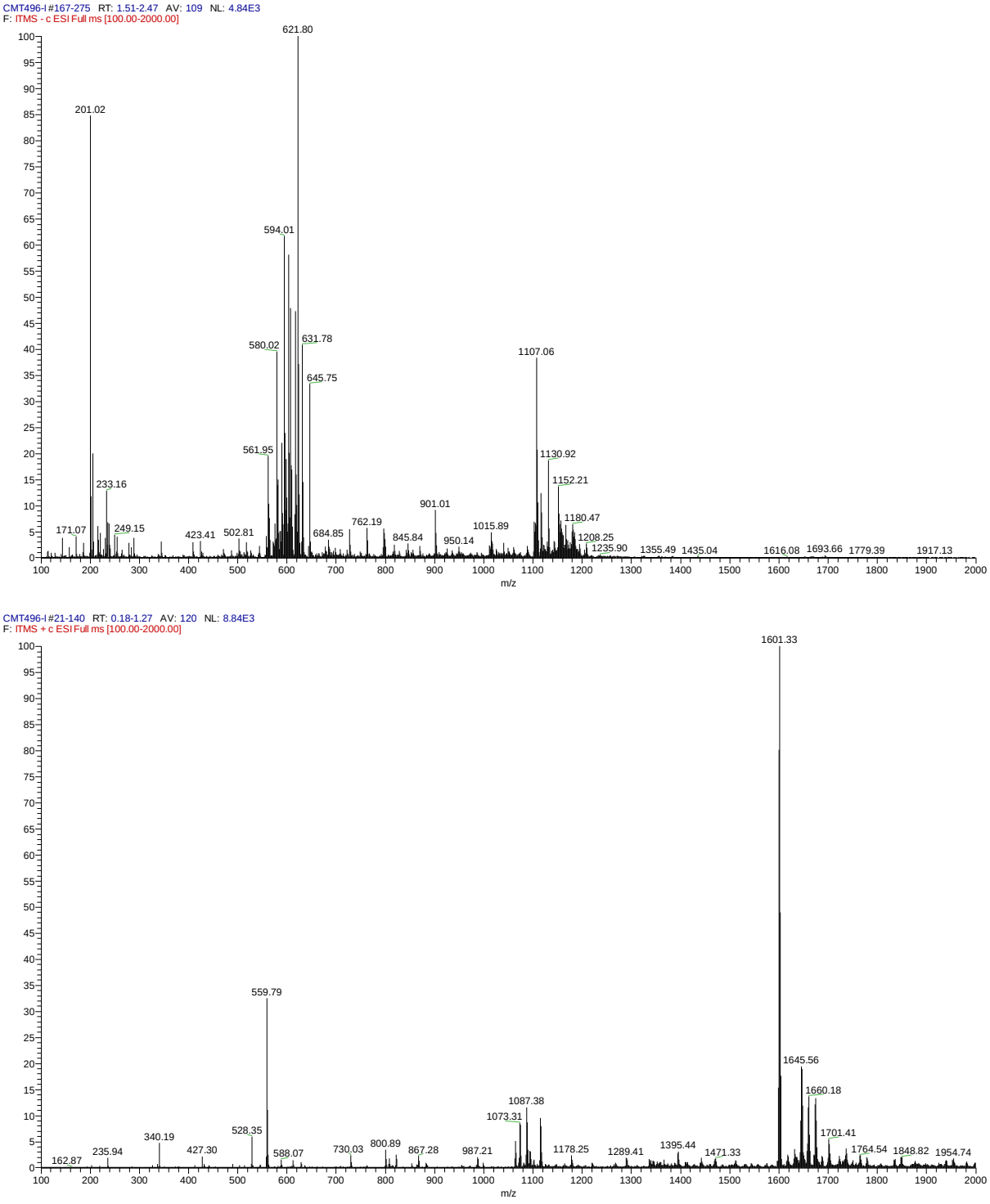

Figure III-29: Negative (up) and positive (down) ESI-MS spectra of **FeL14** in methanol. Negative mode spectrum shows dissociation of the amino acid ligand, but both modes are abundant in mononuclear and dinuclear Fe**L14** aggregates.

Compound **FeL15** ESI-MS spectra is presented in **Figure III-30**. In the negative mode spectrum the presence of amino acid ligand adducts is evident, clearly indicating dissociation of this ligand from the metal centre: a solvated trianionic amino acid ligand $\{\mathbf{L15}\bullet 2MeOH\bullet H_2O\}^{3-}$ species (m/z = 255.2), a trianionic amino acid ligand $\mathbf{L15}^{3-}$ species (m/z= 228.3) and two peaks

assigned to species possibly derived from amino acid ligand decomposition (m/z= 211.3 and 125.3, respectively, the last being respective to the major peak). The peak at m/z= 916.4 is assigned to a solvated mononuclear $\{[Fe_2\mathbf{L15}Cl_3]\bullet H_2O\}^-$ species. In the positive mode spectrum three peaks are assigned to a solvated mononuclear $\{H[Fe_2(\mathbf{L15})Cl_3]\bullet 3MeOH\bullet H_2O\}^+$ major species (m/z= 1015.6), a solvated mononuclear dicationic $\{H_2[Fe_2\mathbf{L15}Cl_3]\bullet 3MeOH\bullet H_2O\}^{2+}$ species (m/z= 510.7) and a sodium adduct $\{Na_3(\mathbf{L15})\bullet H_2O\}^{3+}$ species (m/z= 257.2) of the amino acid ligand.

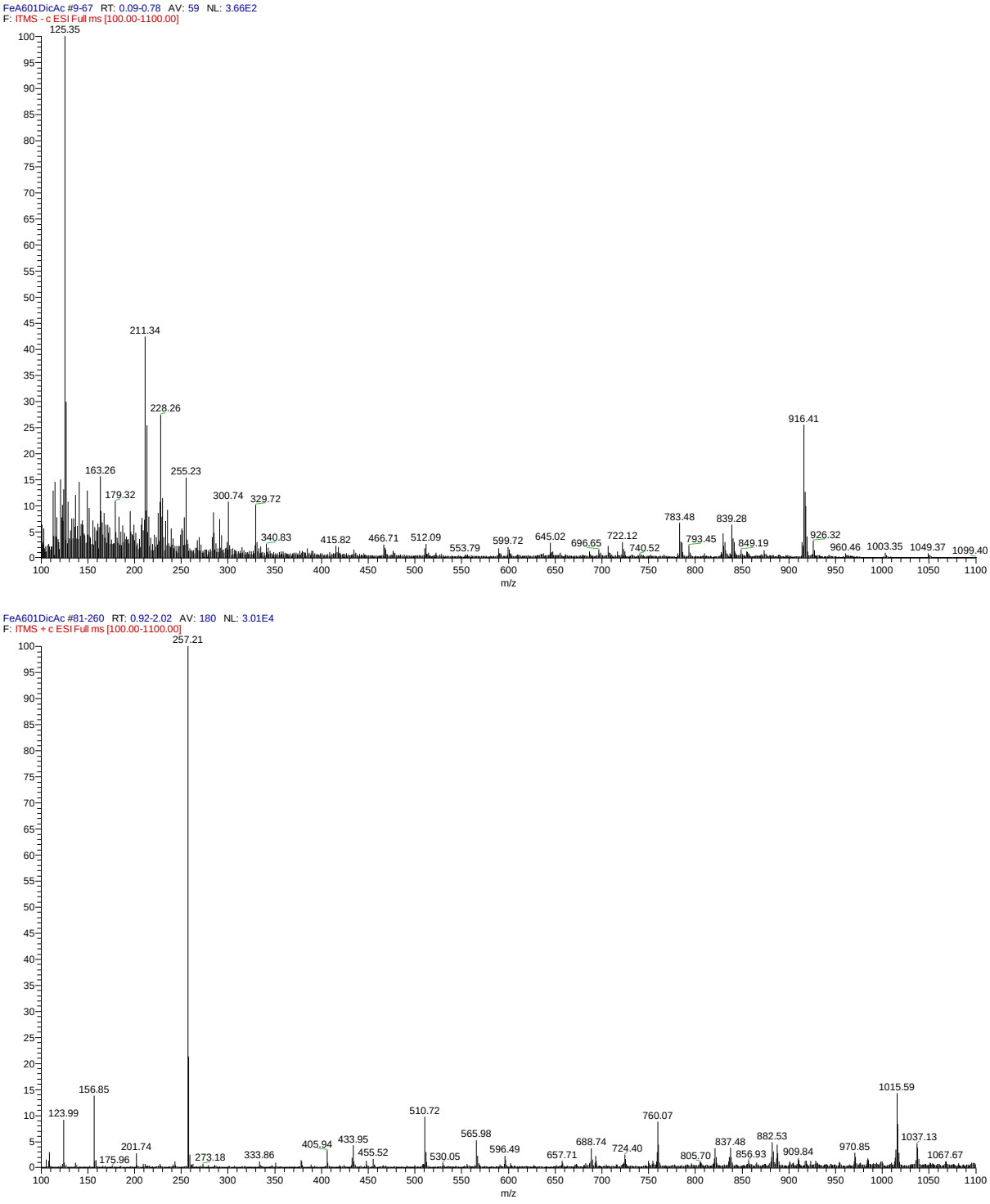

Figure III-30: Negative (up) and positive (down) ESI-MS spectra of **FeL15** in methanol. Dissociation of the amino acid ligand is evident in the negative mode spectrum.

III.2.3.4 – Characterization by Infrared spectroscopy

Solid samples of **FeL13**-**15** were analysed by FT-IR and the most relevant vibrational frequencies are listed in **Table III-11**. All compounds exhibited a ν(C=O) stretching vibration band at *ca*. 1600 cm^{-1} and a ν(C-O) bending vibration band at *ca.* 1270 cm^{-1}, corresponding to the carboxyl and phenolate moieties, respectively. Compounds **FeL13** and **FeL14** show the presence of two bands at *ca.* 1400 and 670 cm^{-1}, respective to symmetric Fe-OAc-Fe stretching vibrations and Fe-OH-Fe bending vibrations,[119] possibly indicating the existence of oligonuclear species in these compounds. In fact, the formation of dinuclear μ-acetato-μ-hydroxido-bridged species was observed by X-Ray diffraction analysis for **FeL14** in **III.2.3.2**, indicating that at least in solution the formation of oligonuclear species occurs for this compound.

Table III-11: IR stretching frequencies for the prepared Fe(III) compounds **FeL13**, **FeL14** and **Fe15**.

Stretching mode	FeL13	FeL14	FeL15
	Wavenumber (cm^{-1})		
$\nu(C{=}O_{carboxyl,\ aminoacid})$	1659	1654	1562
ν(Fe-OAc-Fe)	1437	1438	-
$\nu(C\text{-}O_{Phenol})$	1313	1254	1241
ν(Fe-OH-Fe)	701	647	-

III.2.3.5 – Elemental analysis

Compounds **FeL13**-**15** afforded elemental analysis results consistent with mononuclear species having water as contaminants. The elemental analysis of **FeL13** and **FeL14** were also consistent with dinuclear species containing water as vestigial contaminants.

III.2.4 – Fe(III) complexes bearing β-ketoamino acid ligands

The synthesis of Fe(III) complexes bearing β-ketoamino acid ligands was attempted but with no success. The preparation of these compounds was attempted with the suspension of the respective ligand precursor in methanol, followed by the addition of $FeCl_3 \cdot 6H_2O$ resulting in an orange suspension after 30 minutes of magnetic stirring at room temperature. Sodium acetate (3 mole equivalents) was added to the reaction mixture and the subsequent suspension was filtered and washed with distilled water and diethyl ether, affording orange solids in all cases (**Scheme III-10**, top reaction). Due to the insolubility of the ligand precursors, a different

procedure was tried. The ligand precursors were suspended in water under magnetic stirring and $FeCl_3$•$6H_2O$ was added, resulting in an orange suspension. After 10 minutes the reaction was heated under reflux for one hour, resulting in complete solubilization of the ligand precursor to a light orange solution. The reaction was allowed to cool under stirring till room temperature, with no visible alteration regarding solubility of the reagents. Then, 3 mole equivalents of NaOAc were added and an orange precipitate formed, which was filtered, washed with abundant distilled water and diethyl ether, affording orange solids in all cases (**Scheme III-10**).

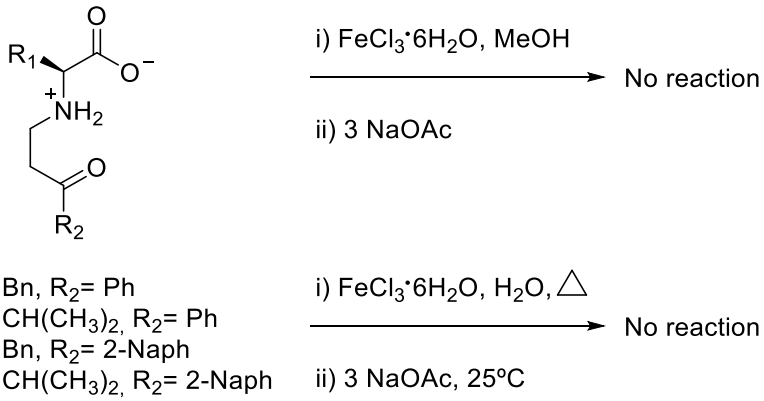

Scheme III-10: Synthetic procedure applied in the preparation of Fe(III) complexes **FeL16**-**FeL19**.

With both synthetic procedures the isolated solids were subjected to elemental analysis which revealed mainly the presence of ligand precursor and therefore the synthesis of an Fe(III) complex correspondent to **L16**-**L19** was abandoned.

III.3 – Cyclic Voltammetry of the Fe(III) complexes

The redox properties of the new Fe(III) complexes were studied by Cyclic Voltammetry and the obtained results will be presented in this Section. Data listed in **Table III-12** shows the redox potentials observed by the Fe(III) complexes for the relevant reduction or oxidation processes. All the Fe(III) complexes, except **FeL2**, display one cathodic quasi-reversible process at potentials in the range -0.16 to -0.68 V.

Table III-12: Cyclic voltammetry data for Fe(III) complexes in Bu_4NBF_4 / Solvent. a) DMSO; b) DMF; c) MeCN.

Compound	E_p^{red} (V)	E_p^{ox} (V)	$E_{1/2}^{Red}$(V)
FeL1A[a]	-0.53	-0.49	-0.51
FeL1B[b]	-0.36	+0.04	-0.16
FeL2[a]	-2.03; -0.92	-	-
FeL3[b]	-0.41	+0.05	-0.18
FeL13[c]	-0.80	-0.40	-0.60
FeL14[c]	-0.70	-0.65	-0.68

Values (±10 mV) measured vs. SCE at 200 mV s^{-1} using ferrocene as an internal reference ($[Fe(\eta^5\text{-}C_5H_5)_2]^{0/+}$, $E_{1/2}^{ox}$=0.440, 0.470 and 0.382 V in DMSO, DMF and MeCN, respectively).

III.3.1 – Fe(III) complexes containing amino acid-pyridyl ligands

The redox behaviour of the Fe(III) complexes **FeL1A**, **FeL1B**, **FeL2** and **FeL3** were studied by Cyclic Voltammetry and the respective cathodic scan voltammograms are presented below. Compound **FeL1A** presents a reduction wave with a quasi-reversible behaviour ($E_{1/2}^{red}$ = -0.51 V) with the cathodic process occurring at E_p^{red} = -0.53 V and its counterpart at E_p^{ox} = -0.49 V (**I** and **II**, respectively, **Figure III-31**) attributable to a Fe(III)→Fe(II) reduction process.[114] The cyclic voltammograms differ upon cathodic and anodic scans. Scanning anodically first, a new cathodic wave at E_p^{red}=-0.04 V appears which is not visible if the cathodic scan is performed first. This new wave (**III**, **Figure III-31**) has some reversible character, and all these observations lead to conclude that new species form upon electron transfer.

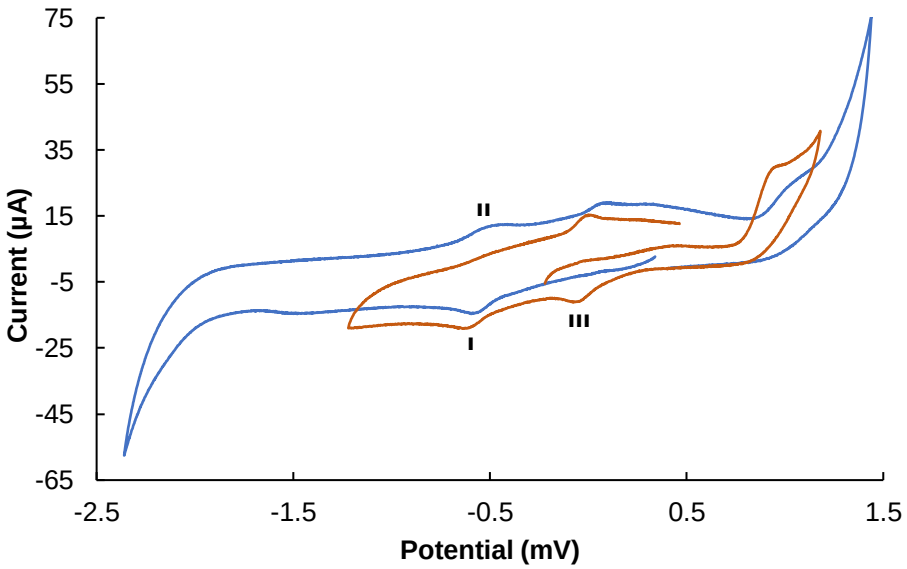

Figure III-31: Cyclic voltammograms of **FeL1A** in Bu_4NBF_4 / DMSO (in blue, cathodic scan; in orange, anodic scan).

Compounds **FeL1B** and **FeL3** both contain in their structure a picolinate ligand, differing between each other in the amino acid-pyridyl ligand precursor used in their synthesis. The main difference between these compounds and **FeL1A** relies on the co-ligand utilized for their preparation: picolinic acid for compounds **FeL1B** and **FeL3** and salicylic acid for **FeL1A**. Compound **FeL1B** display one cathodic wave at E_p^{red} = -0.36 V, with its respective counterpart at E_p^{ox} = +0.04 V (**I** and **II**, respectively, **Figure III-32**). This cathodic process can be attributed to the Fe(III)→Fe(II) reduction process, as described in the literature.[123,124]

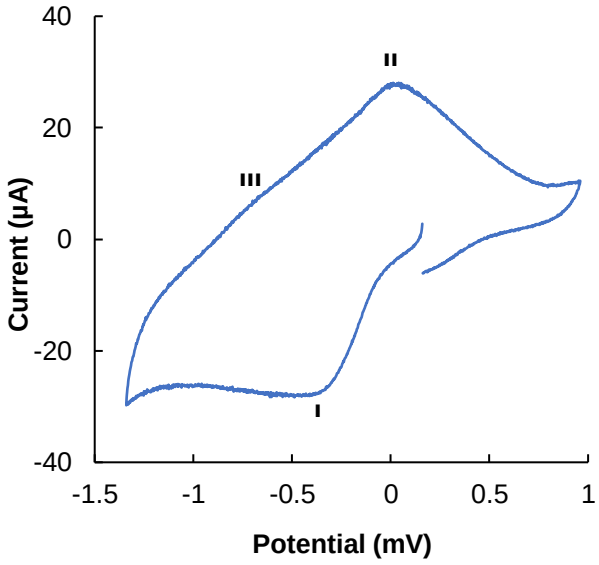

Figure III-32: Cyclic voltammogram (cathodic scan) of **FeL1B** in Bu_4NBF_4 / DMF.

This cathodic redox process seems to induce the formation of an ill-defined chemical species at more negative potentials (**III**, E_p^{red} = -0.72 V, **Figure III-32**) by an Electrochemical-Chemical process (EC); this phenomena is better observed at high scan rates (**Figure III-33**) in agreement with a chemical reaction occurring at moderate rates upon electron transfer.

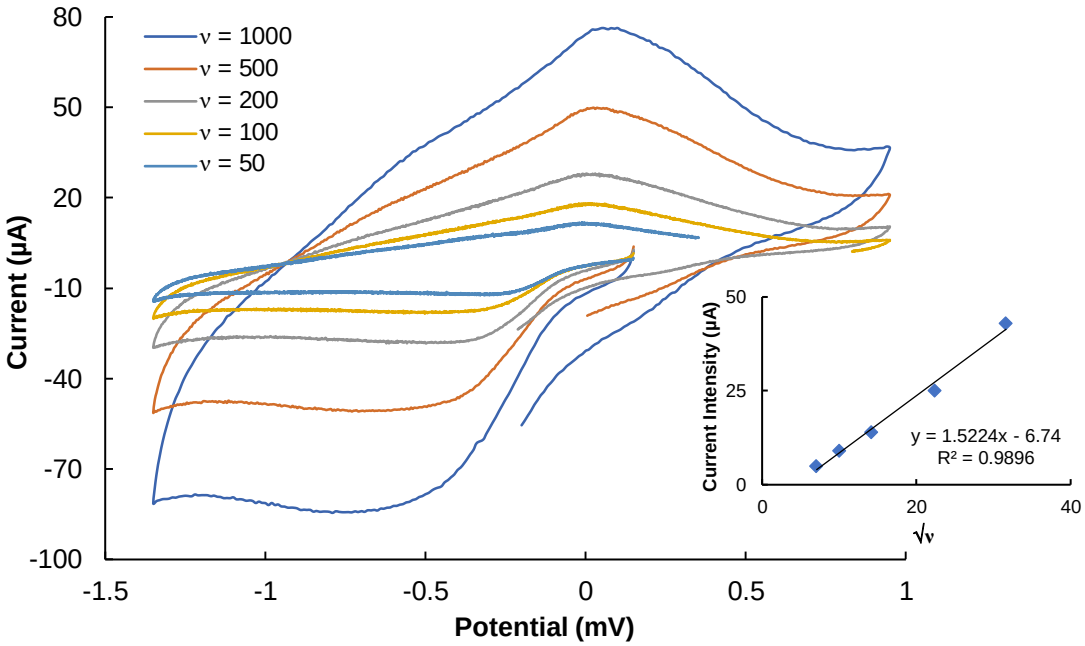

Figure III-33: Cyclic voltammogram (cathodic scan) of **FeL1B** in Bu_4NBF_4 / DMF for different scan rates.

For **FeL1B**, a linear relationship between the current intensity *vs* the square-root of the scan rate is observed, in agreement with the Randles-Sevcik equation:

$$\mathbf{I_p = 268.6\sqrt{n^3}A\sqrt{D}C\sqrt{v}} \qquad \textbf{Eq. III-1}$$

Where I_p is the current intensity (A), n is the number of electrons transferred in the redox process, A is the electrode area (cm^2), D is the diffusion coefficient ($cm^2\ s^{-1}$), C is the concentration ($mol\ cm^{-3}$) and ν is the scan rate ($V\ s^{-1}$). The redox behaviour of **FeL3** is presented in **Figure III-34**. A cathodic wave at E_p^{red}= -0.41 V attributed to a Fe(III)→Fe(II) reduction in the range of values presented in the literature.[114,124] The cathodic process displays an anodic counterpart at E_p^{ox} = +0.05 V.

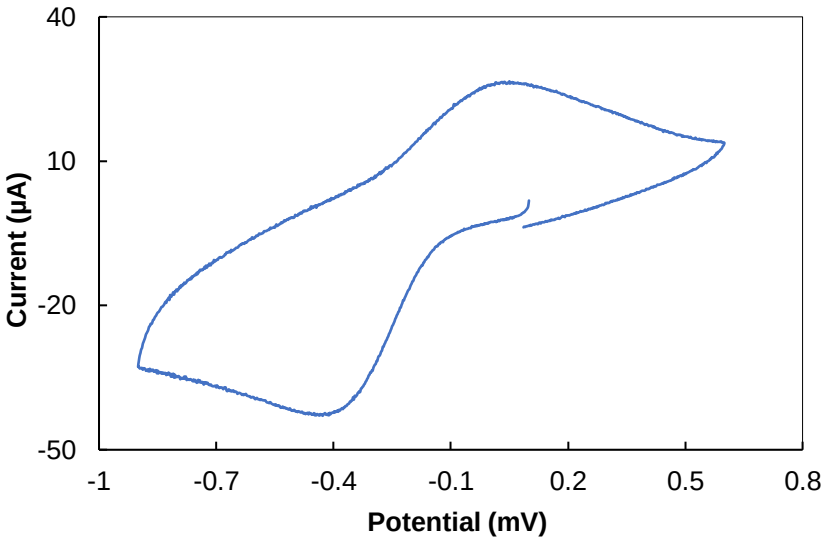

Figure III-34: Cyclic voltammogram (cathodic scan) of **FeL3** in Bu_4NBF_4 / DMF.

The referred redox waves are exclusive of **FeL3**. Both the isolated aminoacid-derived ligand and picolinic acid present redox processes at considerable different potential values as shown in **Figure III-35**.

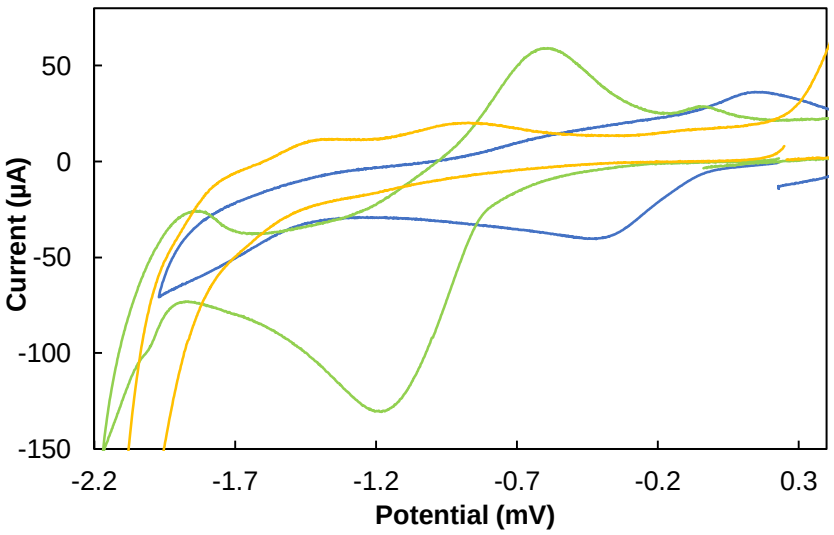

Figure III-35: Cyclic voltammograms (cathodic scan) of **FeL3** (blue), ligand precursor **L3** (orange) and picolinic acid (green) obtained in Bu_4NBF_4 / DMF.

It can also be observed in **Figure III-36**, for compound **FeL3**, a linear relationship between the current intensity *vs* the square-root of the scan rate, in agreement with the Randles-Sevcik equation (**Eq.III-1**). According to the voltammograms in **Figure III-36**, it comes out that the number of electrons transferred in the reduction and the related oxidation process is different $\left(\frac{I_p^{Red}}{I_p^{Ox}} \sim 2\right)$.

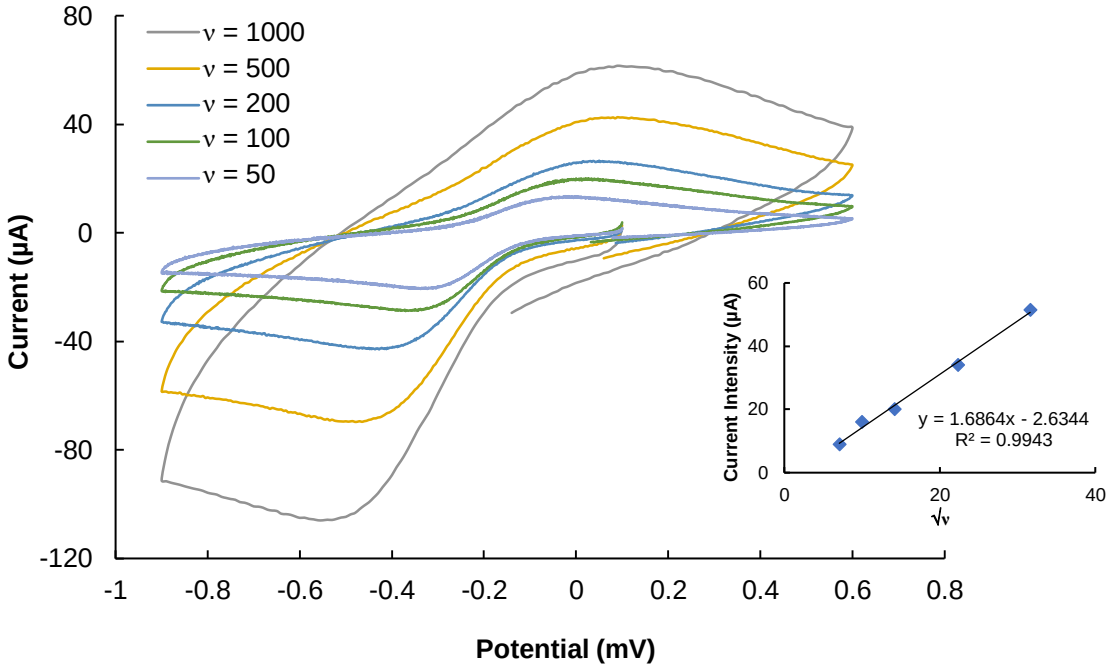

Figure III-36: Cyclic voltammogram (cathodic scan) of **FeL3** in Bu_4NBF_4 / DMF for different scan rates.

Compound **FeL2** display two reduction waves at E_p^{red} = -0.92 V and E_p^{red} = -2.03 V, respectively (**I** and **II**, **Figure III-37** in blue). The first wave (**I**, **Figure III-37**) may be associated (i) to the Fe(III)→Fe(II) reduction process, as described in the literature.[114] The potential of the lower potential irreversible cathodic wave (**II**, -2.03 V, **Figure III-37**) is in the range of the corresponding free amino acid (*ca.* -1.9 V) pointing to a ligand-based process.

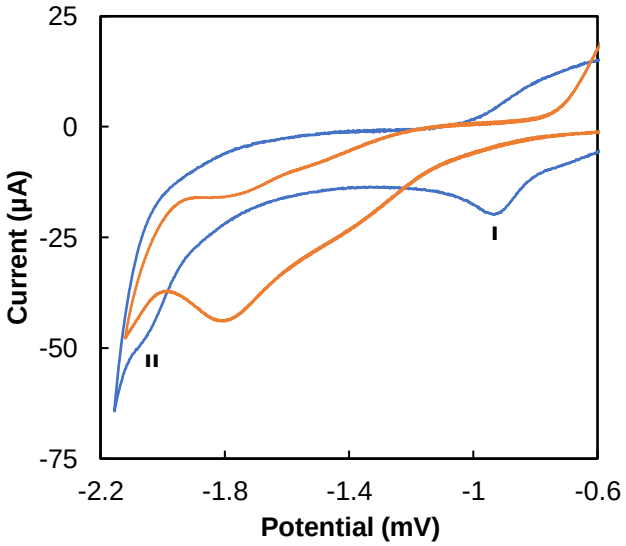

Figure III-37: Cyclic voltammogram (cathodic scan) of **FeL2** (blue line) and ligand precursor **L2** (orange line) in Bu_4NBF_4 / DMSO.

Compounds **FeL1A**, **FeL1B**, **FeL2** and **FeL3** comprise in their structure amino acid-pyridyl ligands and distinct co-ligands utilized for their preparation: salicylate in **FeL1A**, picolinate in

FeL1B and **FeL3** and acetate in **FeL2**. After analysing voltammograms of these compounds it can be concluded that the redox behaviour observed differ from those of the ligand precursors (see **Figure III-37** and **Figure III-35** for **FeL2** and **FeL3**, respectively) and of the isolated co-ligands (see **Figure III-35** for **FeL3**). Also, the iron (III) complexes redox behaviour shows major differences regarding on the co-ligand coordinated to the Fe(III) centre, while the amino acid side chain of the coordinated amino acid ligand does not influence significantly the observed redox potentials. Such can be observed by comparing E_p^{Red} values listed in **Table III-12** for compounds **FeL1B** and **FeL3**.

III.3.2 – Fe(III) complexes containing amino acid-pyridyl-phenol ligands

In this section the redox properties of **FeL13**-**FeL15** will be discussed. Compound **FeL13** presents a cathodic wave at E_p^{red} = -0.80 V attributed to a Fe(III)→Fe(II) reduction, considering the range of values presented in the literature.[110,123] This cathodic process displays an anodic counterpart at E_p^{ox} = -0.40 V (**I**, **Figure III-38**).

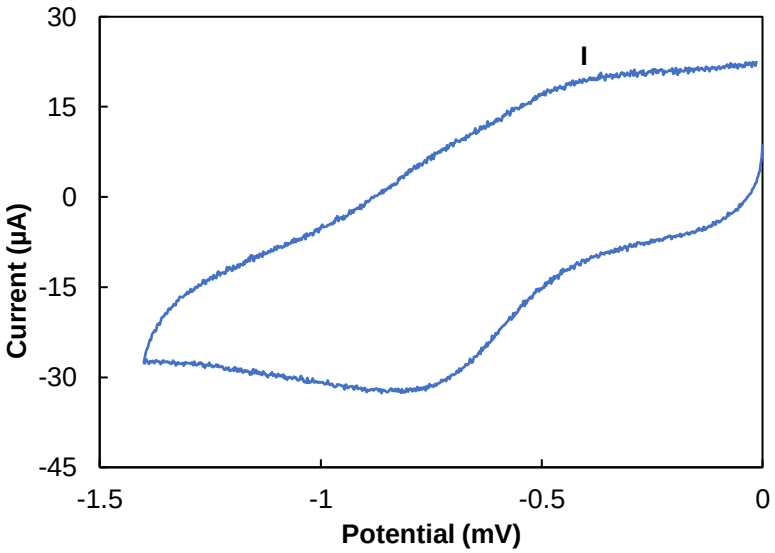

Figure III-38: Cathodic cyclic voltammogram of **FeL13** in Bu_4NBF_4 / MeCN.

A linear relationship between the current intensity and the square-root of the scan rate is observed in **Figure III-39**, in agreement with the Randles-Sevcik equation (**Eq.III-1**). Hence, a relationship can be established between the number of electrons transferred in the electrochemical process. Also, by viewing the voltammograms, it is observable that the number of electrons transferred in the reduction process and its oxidation counterpart is the same $\left(\frac{I_p^{Red}}{I_p^{Ox}} = 1\right)$.

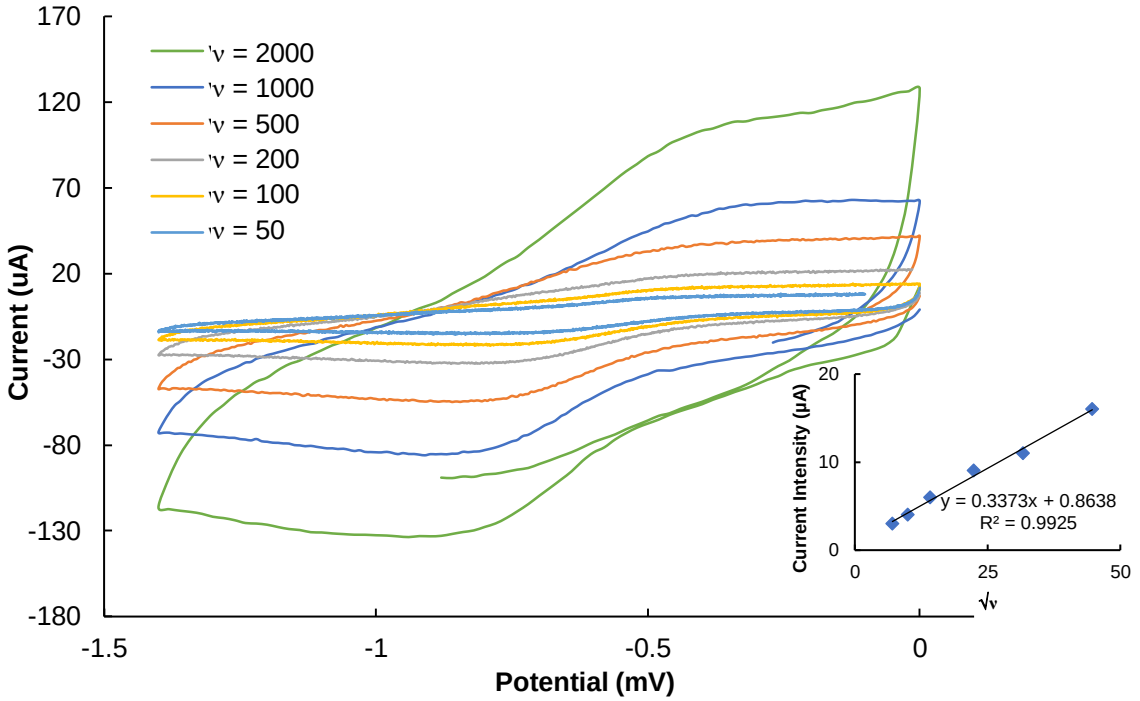

Figure III-39: Cyclic voltammogram (cathodic scan) of **FeL13** in Bu_4NBF_4 / DMF for different scan rates.

Compound **FeL14** presents one cathodic wave at E_p^{red} = -0.70 V attributed to a Fe(III)→Fe(II) reduction, as reported in the literature for Fe(III) complexes.[114,124] This process displays what seems to be its anodic counterpart at E_p^{red} = -0.65 V (**Figure III-40**).

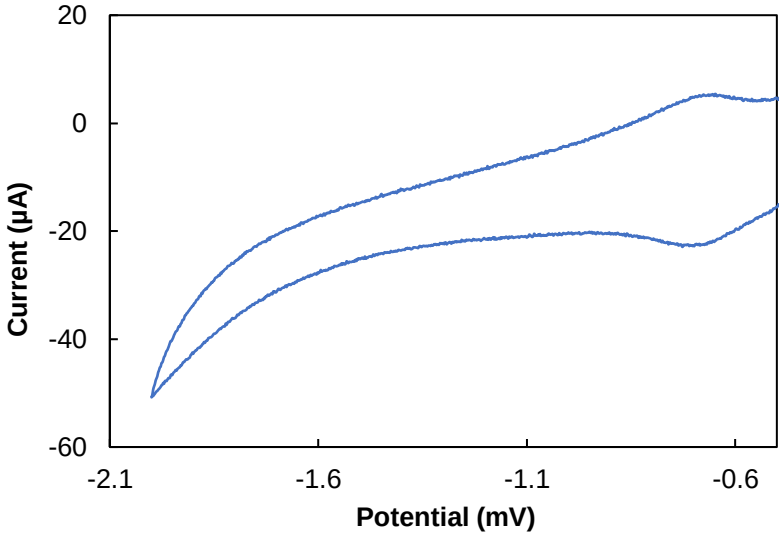

Figure III-40: Cathodic cyclic voltammograms of **FeL14** in Bu_4NBF_4 / MeCN.

The referred redox waves are exclusive of **FeL14**, since the free aminoacid-derived ligand presents redox processes at potentials values quite different as shown in **Figure III-41**.

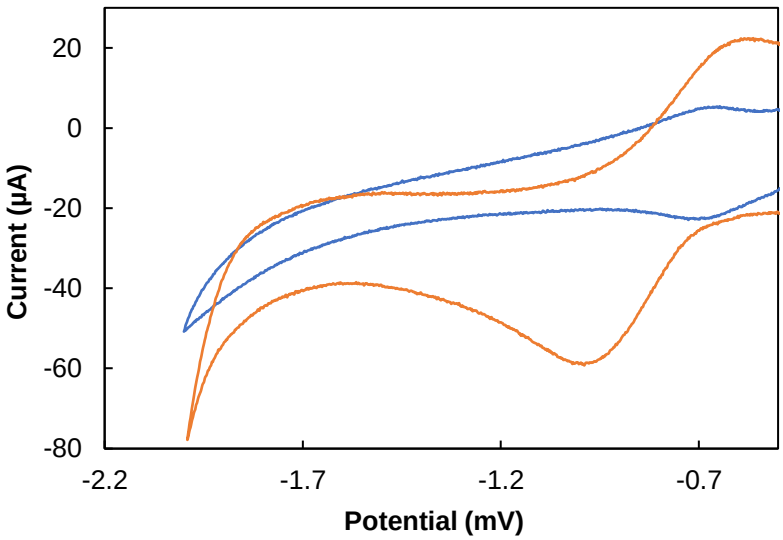

Figure III-41: Cathodic cyclic voltammograms in Bu_4NBF_4 / MeCN for **FeL14** (in blue) and the free aminoacid-derived ligand (in orange).

Comparing both **FeL13** and **FeL14** is was concluded that their $E_{1/2}^{Red}$ values fall in the potential range of -0.60 V with a slightly more negative potential value observed for **FeL14** (-0.68 V *vs* potential of -0.60 V for **FeL13**, **Table III-12**). This small difference is attributed to the more electron-donating effect exerted by the *tert*-butyl groups in the phenolate moiety of **FeL14**.

Compound **FeL15** present very low intensity redox processes when cathodic scans are performed, hence no cyclic voltammograms of these compounds will be displayed.

III.3.3 – Fe(III) complexes containing amino acid-phenol and amino acid-methoxybenzene ligands

Compounds **FeL5**, **FeL6**, and **FeL8**-**11** contain in their structure aminoacid-phenol or amino acid-methoxybenzene based ligands, and very low intensity redox processes were observed when cathodic scans are performed. In most of the examples, no redox processes seem to occur, therefore no cyclic voltammograms of these compounds will be displayed.

III.4 – Magnetic susceptibility of the Fe(III) complexes

The paramagnetic susceptibility of the prepared Fe(III) compounds was determined by the Evans NMR method at room temperature. The calculation of magnetic molar susceptibility χ_M^P in solution (mL/mol) was performed applying the following equation:[125]

$$\chi_{\mathrm{M}}^{\mathrm{P}} = \frac{\delta_{\nu}^{\mathrm{p}} \mathrm{M}^{\mathrm{p}}}{\nu_{\mathrm{o}} \mathrm{S_f} \mathrm{m}^{\mathrm{p}}} - \chi_{\mathrm{M}}^{\mathrm{dia}} \qquad \textbf{Eq. III-2}$$

where δ_ν^p is the shift in frequency for an internal inert reference (CD_2Cl_2 for all compounds with exception to compounds **FeL1B**, **FeL3** and **FeL9** where DMSO-d_6 was used, Hz); M^p is the molecular weight of solute (g/mol); ν_o is the frequency of the NMR spectrometer (3.0013x10^8 Hz); S_f is the shape factor of the NMR spectrometer; $\frac{4\pi}{3}$ sample axis parallel to magnetic field; m^p is the concentration of solute (g/mL) and χ_M^{dia} is the diamagnetic constant (mL/mol). The diamagnetic constant was calculated utilizing the Pascal's constants.[126] The magnetic moment μ_{eff} (μ_B) of the Fe(III) complexes was determined by applying equation **Eq.III-3**:[125]

$$\mu_{\mathbf{eff}} = \mathbf{2.828}\sqrt{\boldsymbol{\chi}_{\mathbf{M}}^{\mathbf{P}}\mathbf{T}} \qquad \textbf{Eq. III-3}$$

where T is the working temperature (298 K). The results obtained are presented in **Table III-13**. Compounds **FeL1A**, **FeL1B**, **FeL3**-**10** and **FeL13**-**15** present μ_{eff} values consistent with those expected for high-spin (S=$^5/_2$) Fe(III) complexes in the range 4.68-6.01 μ_B.[127] Fe(III) complexes containing amino acid-phenol (**FeL5**-**10**) and amino acid-pyridyl-phenol ligands (**FeL13**-**15**) show, in general, lower μ_{eff} values in comparison with **FeL1A**, **FeL1B** and **FeL3**, which can be justified by the possible formation of dinuclear species in solution by these type of amino acid-phenol-based Fe(III) complexes.[128] Such dinuclear formation in solution was observed by X-ray crystallography for **FeL14**. Compounds **FeL2** and **FeL11** show lower μ_{eff} values (2.78 and 3.76 μ_B, respectively) due to antiferromagnetic coupling resultant from the possible formation of oligomers in solution.[128]

Table III-13: Evans NMR method data and parameters for Fe(III) compounds.

Compound	Deuterated solvent	C (x10^{-3} mol/L)	δ_v^p (Hz)	χ_M^p (x10^{-6} mL/mol)	μ_{eff} (μ_B)
FeL1A	CD_2Cl_2	10.11	188.83	257.03	6.01
FeL1B	DMSO-d_6	9.79	165.9	237.85	5.72
FeL2	CD_2Cl_2	9.85	37.87	181.60	2.78
FeL3	DMSO-d_6	9.59	178.99	254.44	5.92
FeL5	CD_2Cl_2	10.02	138.87	256.26	5.19
FeL6	CD_2Cl_2	9.99	142.50	319.42	5.28
FeL8	CD_2Cl_2	9.79	167.15	268.97	5.75
FeL9	CD_2Cl_2	10.05	112.87	259.64	4.68
FeL10	DMSO-d_6	10.13	119.59	369.9	4.83
FeL11	CD_2Cl_2	10.26	73.35	230.4	3.76
FeL13	CD_2Cl_2	10.25	132.66	300.18	5.03
FeL14	CD_2Cl_2	10.18	142.25	389.34	5.24
FeL15	CD_2Cl_2	10.05	133.46	522.47	5.14

III.5 – Catalytic applications

After the successful synthesis and characterization of the referred amino acid-derived Fe(III) complexes, their activity as pre-catalysts was tested in the oxidative coupling of 2-naphthol and 3-bromo-2-naphthol, epoxidation of benzalacetophenones and oxidation of 1-phenylethan-1-ol. The catalytic procedures applied were highly focused, as much as possible, on the usage of environmentally-friendly oxidants such as dioxygen from air or hydrogen peroxide and solvents with a low degree of toxicity, in order to correspond to the expectation of the development of sustainable catalytic processes.

III.5.1 – Asymmetric oxidative coupling of 2-naphthol

The catalytic studies developed in this work in the asymmetric oxidative coupling of 2-naphthol were initially inspired on previous works where air was applied as oxidant.[40,107] Regarding iron-catalyzed processes, Katsuki and co-workers[40] applied several (di-μ-hydroxido)iron-salan complexes as catalysts and used air as oxidant in toluene at 60ºC, without any additives, with a general reaction being schematized in **Scheme III-11**.

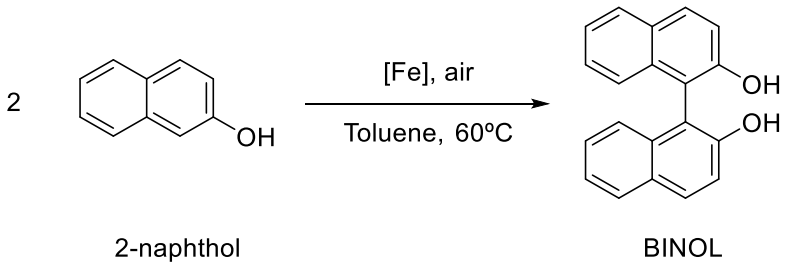

Scheme III-11: Oxidative coupling of 2-naphthol in the preparation of BINOL, using air as oxidant and iron complexes as catalysts.

The catalytic studies in this work started with the application of 1 mol% of **FeL2**, **FeL13** or **FeL14** as pre-catalysts in toluene and the results are presented in **Table III-14**. At a first glance it is observable that the coupling reaction does not occur (i) in the absence of Fe(III) complex or (ii) under air exclusion in the presence of any of the **FeL2**, **FeL13** or **FeL14** compounds. (**Table III-14**, entries 1 to 4). Under aerobic conditions, the reaction time and temperature were varied from 24 to 72 h and 25 to 60ºC, respectively, in order to optimize these parameters, but in all cases low 2-naphthol conversions and BINOL yields were obtained (**Table III-14**, entries 5 to 16). The best general results for BINOL yields were obtained at 60ºC and 72 hours with **FeL2** and **FeL14** in 26 and 29%, respectively (**Table III-14**, entries 14 and 16), and despite the low BINOL yields observed, these preliminary catalytic studies showed a good selectivity towards BINOL formation, especially with **FeL14** (78%, see entry 16 of **Table III-14**). The enantioselectivity obtained in the formation of the (a*S*)-BINOL enantiomer, with *ee* values ranging from 14 to 66% in all cases, should also be highlighted.

Table III-14: Preliminary results obtained in the catalytic oxidative coupling of 2-naphthol.

Entry	[Fe]	T (ºC)	Time (h)	Solvent	Conv. (%)	BINOL (%)	Selectivity (%)	*ee* (%)
1[a]	-	60	72	Toluene	-	-	-	-
2[b]	**FeL2**	60	72	Toluene	-	-	-	-
3[b]	**FeL13**	60	72	Toluene	-	-	-	-
4[b]	**FeL14**	60	72	Toluene	-	-	-	-
5[a]	**FeL2**	25	24	Toluene	18	7	39	66 (a*S*)
6[a]	**FeL13**	25	24	Toluene	15	2	13	25 (a*S*)
7[a]	**FeL14**	25	24	Toluene	7	4	57	20 (a*S*)
8[a]	**FeL2**	25	72	Toluene	13	8	62	26 (a*S*)
9[a]	**FeL13**	25	72	Toluene	14	8	57	15 (a*S*)
10[a]	**FeL14**	25	72	Toluene	5	4	80	14 (a*S*)
11[a]	**FeL2**	60	24	Toluene	41	22	54	22 (a*S*)
12[a]	**FeL13**	60	24	Toluene	17	5	29	14 (a*S*)
13[a]	**FeL14**	60	24	Toluene	21	13	62	16 (a*S*)
14[a]	**FeL2**	60	72	Toluene	43	26	60	20 (a*S*)
15[a]	**FeL13**	60	72	Toluene	22	12	55	14 (a*S*)
16[a]	**FeL14**	60	72	Toluene	37	29	78	17 (a*S*)

Reaction conditions: In a closed 50 mL Schlenk tube, 1 mmol 2-naphthol, 1 mol% [Fe], 4 mL solvent. [a] air as oxidant; [b] under N_2 atmosphere. Conversion of 2-naphthol, BINOL yields and *ee* were determined by HPLC.

After the preliminary studies presented in **Table III-14** the focus was then directed in the attempt to increase BINOL yield, selectivity and enantioselectivity under the optimized temperature and reaction time, 60ºC and 72 h. For this purpose, it was decided to apply iodide salts as additives, based on the work developed by Adão and co-workers[107] in the oxidative coupling of 2-naphthol using amino acid-derived copper(II) complexes as pre-catalysts; the authors reported that the addition of potassium iodide increased the observed 2-naphthol conversion, BINOL yield and *ee* values in the tested catalytic systems. In this work it was decided to use *tert*-butylammonium iodide (TBAI) as additive instead of KI, since KI is insoluble in toluene.

The results obtained with addition of TBAI in the catalytic reactions are presented in **Table III-15**. Initially, it was studied the influence of the proportion of TBAI added relative to 2-naphthol with 1 mol% of **FeL14** as pre-catalyst (**Table III-15**, entries 1 to 6), and the best results were obtained with addition of 5 mol% of TBAI: 46% BINOL yield, 81% selectivity in the formation of BINOL and 19% *ee* in the formation of the (a*S*)-BINOL enantiomer (see entry 2 of **Table III-15**). These results show an improvement of 17% in BINOL yield in comparison to the catalytic results without addition of TBAI, with no significant differences in the BINOL formation selectivity and *ee* values observed (compare entry 16 of **Table III-14** with entry 2 of **Table**

III-15). Addition of TBAI is only effective in the increment of BINOL yield values with an exact amount of 5 mol% relative to 2-naphthol at 60ºC; 25 to 85 mol% of TBAI hampers BINOL formation and reduces reaction selectivity at a rate proportional to the amount of additive used (see entries 3 to 6 of **Table III-15**). Curiously, addition of 5 mol % TBAI at room temperature for 72 hours did afford BINOL in only 3% with also very low 2-naphthol conversion values, suggesting that the TBAI effect in the promotion of BINOL formation is temperature-dependent (entry 7, **Table III-15**).

After these results the remaining Fe(III) complexes were also tested as pre-catalysts with addition of 5 mol% of TBAI in the optimized conditions (see entries 2 and 9 to 20 in **Table III-15**). The most important conclusions were made after observing the BINOL yield values and enantioselectivities: (i) in exception to **FeL13** and **FeL14**, low BINOL yields were obtained with all Fe(III) complexes as pre-catalysts in the range 4-14%; (ii) compounds **FeL13** and **FeL14** promoted BINOL formation in 31 and 46% yield, respectively, with moderate to good selectivities (55 and 81%, respectively, see entries 2 and 19 in **Table III-15**); (iii) the applied catalytic conditions showed to be enantioselective with all Fe(III) complexes towards (a*S*)-BINOL formation in the range 3-32% *ee*, except for **FeL13** (0% *ee*). Within these reaction conditions complex **FeL14** proved to be the best pre-catalyst, and different solvents were tested (see entries 21 to 26 **Table III-15**); the results obtained showed lower values in BINOL yields and selectivities in comparison with the reactions running in toluene, but maintained enantioselectivities in general. In the reactions executed in an aqueous ethanolic mixture or water (entries 22 and 26, **Table III-15**, respectively), no desired coupling product was obtained. No improvements were visible with MeCN, AcOEt, propan-2-ol or THF, therefore the catalytic studies pursued with toluene as solvent.

Table III-15: Preliminary results obtained in the catalytic oxidative coupling of 2-naphthol using air (dioxygen) as oxidant, with addition of different amounts of TBAI.

Entry	[Fe]	T (ºC)	Time (h)	Solvent	mol % TBAI	Conv. (%)	BINOL (%)	Selectivity (%)	*ee* (%)
1	**FeL14**	60	72	Toluene	1	43	32	74	19 (a*S*)
2	**FeL14**	60	72	Toluene	5	57	46	81	19 (a*S*)
3	**FeL14**	60	72	Toluene	25	29	24	83	20 (a*S*)
4	**FeL14**	60	72	Toluene	45	21	14	67	20 (a*S*)
5	**FeL14**	60	72	Toluene	65	19	11	58	26 (a*S*)
6	**FeL14**	60	72	Toluene	85	20	4	20	20 (a*S*)
7	**FeL14**	25	72	Toluene	5	7	3	43	18 (a*S*)
8	**FeL14**	60	24	Toluene	5	36	24	67	20 (a*S*)
9	**FeL1A**	60	72	Toluene	5	21	10	50	11 (a*S*)
10	**FeL1B**	60	72	Toluene	5	17	14	82	9 (a*S*)
11	**FeL2**	60	72	Toluene	5	59	15	25	32 (a*S*)
12	**FeL3**	60	72	Toluene	5	32	6	19	19 (a*S*)
13	**FeL5**	60	72	Toluene	5	18	7	39	7 (a*S*)
14	**FeL6**	60	72	Toluene	5	33	4	12	20 (a*S*)
15	**FeL8**	60	72	Toluene	5	24	5	21	18 (a*S*)
16	**FeL9**	60	72	Toluene	5	29	8	28	24 (a*S*)
17	**FeL10**	60	72	Toluene	5	32	7	22	9 (a*S*)
18	**FeL11**	60	72	Toluene	5	37	9	24	9 (a*S*)
19	**FeL13**	60	72	Toluene	5	56	31	55	0
20	**FeL15**	60	72	Toluene	5	22	8	36	3 (a*S*)
21	**FeL14**	60	24	MeCN	5	12	2	17	21 (a*S*)
22	**FeL14**	60	72	EtOH:H_2O	5	16	1	6	23 (a*S*)
23	**FeL14**	60	72	AcOEt	5	10	6	60	25 (a*S*)
24	**FeL14**	60	72	2-PA	5	12	5	42	10 (a*S*)
25	**FeL14**	60	72	THF	5	4	1	25	15 (a*S*)
26	**FeL14**	60	72	H_2O	5	-	-	-	-
27	**FeL14**	60	72	Toluene	5[a]	59	44	75	12 (a*R*)
28	**FeL14**	60	72	Toluene	5[b]	48	45	94	13 (a*R*)

Reaction conditions: In a closed 50 mL Schlenk tube, 1 mmol 2-naphthol, 1 mol% [Fe], 4 mL solvent. [a] Addition of 1 mol% Et_3N; [b] addition of 1 mol% collidine. Conversion of 2-naphthol, BINOL yields and *ee* were determined by HPLC.

After the results obtained with **FeL14** and TBAI in toluene, the addition of organic bases was tested to observe their effect in the reaction outcome. Such approach was also based on the work developed by Adão and co-workers,[107] where the authors used weak organic bases like morpholine to enhance the 2-naphthol coupling results. For this purpose it was decided to add 1 mol% of triethylamine or 2,4,6-trimethylpyridine (collidine) to the catalytic conditions containing 1 mol% of **FeL14** and 5 mol% of TBAI in toluene, under 60ºC and 72 h (see entries 27 and 28, **Table III-15**). The results observed clearly indicate that addition of an organic weak base greatly increased selectivity towards BINOL formation (up to 94%), maintaining moderate BINOL yield values. Moreover, the enantioselectivity was shifted into the formation of the (a*R*)-BINOL enantiomer, an interesting observation which motivated the application of several other weak organic bases to study their effect in the obtained 2-naphthol coupling results.

To observe the influence of the addition of organic bases to the catalytic reactions, it was decided to use two different Fe(III) complexes. By analysing data obtained without additives in **Table III-14** it was concluded that the best BINOL yields were observed for **FeL2** and **FeL14** (**Table III-14**, entries 14 to 16), therefore these complexes were chosen to study addition of organic bases without any amount of TBAI. Catalytic reactions run at 60ºC for 72 hours in toluene, in opened or closed Schlenk tubes, varying the added amount of Fe(III) complex and base from 1 to 5 mol% relative to 2-naphthol. The organic bases selected for these studies were pyridine (Py), quinoline (Quin), phenanthroline (Phen), collidine (Coll) and triethylamine (Et_3N), and data obtained with **FeL2** and **FeL14** is presented in **Table III-16** and **Table III-17**, respectively.

Low BINOL yield values ranging from 2 to 38% were observed when **FeL2** was applied as pre-catalyst, with the best overall values being obtained on an open Schlenk tube with 5 mol% **FeL2** and 1 mol% base. Addition of Py afforded the best BINOL yield values with 38% in these conditions, which represents a 12% increase in BINOL yield without any additive (compare entry 14 of **Table III-14** with entry 6 of **Table III-16**). Selectivity in BINOL formation was not so straightforward to analyse, but in general these catalytic procedures show to be more prone in BINOL formation with 5 mol% **FeL2** and 1 mol% base on a closed Schlenk tube. The use of Phen afforded selectivities up to 86% in BINOL formation (entries 21 and 22, **Table III-16**). On the other hand, 5 mol% **FeL2** with 5 mol% base in an opened Schlenk tube highly decreased selectivity in BINOL, in general, and with Et_3N in particular (entry 40, **Table III-16**). In fact, analysis of the chromatograms corresponding to reaction samples show the formation of several secondary products with 5 mol% **FeL2** and Et_3N in an opened Schlenk tube, which were not observed with 5 mol% **FeL2** and 1 mol% Phen (**Figure III-42**). Regarding enantioselectivity, this catalytic procedure showed to be very selective in the formation of (a*S*)-

BINOL in all the reactions tested, especially with 5 mol% **FeL2** and 1 mol% Phen in open or closed Schlenk tubes with 38 and 39% *ee*, respectively (see entries 21 and 22, **Table III-16**). It was concluded that so far the best catalytic conditions with **FeL2** were the following: 5 mol% **FeL2**, 1 mol% Phen in an open or closed vessel.

Table III-16: Results obtained in the catalytic oxidative coupling of 2-naphthol using **FeL2** as pre-catalyst, air (dioxygen) as oxidant and organic bases as additives: Pyridine (Py), quinoline (Quin), phenanthroline (Phen), collidine (Coll) and triethylamine (Et_3N).

Entry	FeL2 (mol %)	Closed / Open	mol % Base	Conv. (%)	BINOL (%)	Selectivity (%)	*ee* (%)
1	1%	Closed	1% Py	35	20	57	32 (a*S*)
2	1%	Open	1% Py	43	22	51	31 (a*S*)
3	1%	Closed	5% Py	58	25	43	36 (a*S*)
4	1%	Open	5% Py	52	24	46	30 (a*S*)
5	5%	Closed	1% Py	42	22	52	28 (a*S*)
6	5%	Open	1% Py	83	38	46	27 (a*S*)
7	5%	Closed	5% Py	42	24	57	31 (a*S*)
8	5%	Open	5% Py	48	21	44	34 (a*S*)
9	1%	Closed	1% Quin	55	23	42	18 (a*S*)
10	1%	Open	1% Quin	46	24	52	30 (a*S*)
11	1%	Closed	5% Quin	47	21	45	20 (a*S*)
12	1%	Open	5% Quin	45	17	38	25 (a*S*)
13	5%	Closed	1% Quin	7	2	29	36 (a*S*)
14	5%	Open	1% Quin	66	32	48	29 (a*S*)
15	5%	Closed	5% Quin	30	18	60	35 (a*S*)
16	5%	Open	5% Quin	94	24	26	25 (a*S*)
17	1%	Closed	1% Phen	17	14	82	38 (a*S*)
18	1%	Open	1% Phen	26	18	69	36 (a*S*)
19	1%	Closed	5% Phen	25	7	28	27 (a*S*)
20	1%	Open	5% Phen	9	5	56	27 (a*S*)
21	5%	Closed	1% Phen	32	23	72	38 (a*S*)
22	5%	Open	1% Phen	35	30	86	39 (a*S*)
23	5%	Closed	5% Phen	31	22	71	35 (a*S*)
24	5%	Open	5% Phen	34	16	47	29 (a*S*)
25	1%	Closed	1% Coll	40	21	53	24 (a*S*)
26	1%	Open	1% Coll	47	23	49	29 (a*S*)
27	1%	Closed	5% Coll	42	17	40	35 (a*S*)
28	1%	Open	5% Coll	73	18	25	34 (a*S*)
29	5%	Closed	1% Coll	42	31	74	33 (a*S*)
30	5%	Open	1% Coll	79	31	39	28 (a*S*)
31	5%	Closed	5% Coll	30	15	50	30 (a*S*)
32	5%	Open	5% Coll	79	20	25	27 (a*S*)
33	1%	Closed	1% Et_3N	46	18	39	26 (a*S*)
34	1%	Open	1% Et_3N	51	18	35	31 (a*S*)
35	1%	Closed	5% Et_3N	52	6	12	20 (a*S*)
36	1%	Open	5% Et_3N	68	8	12	21 (a*S*)
37	5%	Closed	1% Et_3N	34	25	74	34 (a*S*)
38	5%	Open	1% Et_3N	88	26	30	29 (a*S*)
39	5%	Closed	5% Et_3N	55	17	31	32 (a*S*)
40	5%	Open	5% Et_3N	84	11	13	26 (a*S*)

Reaction conditions: In a closed or opened 50 mL Schlenk tube, 1 mmol 2-naphthol, 1-5 mol% **FeL2**, 1-5 mol% added base, 4 mL toluene, 60ºC, 72 h. Conversion of 2-naphthol, BINOL yields and *ee* were determined by HPLC.

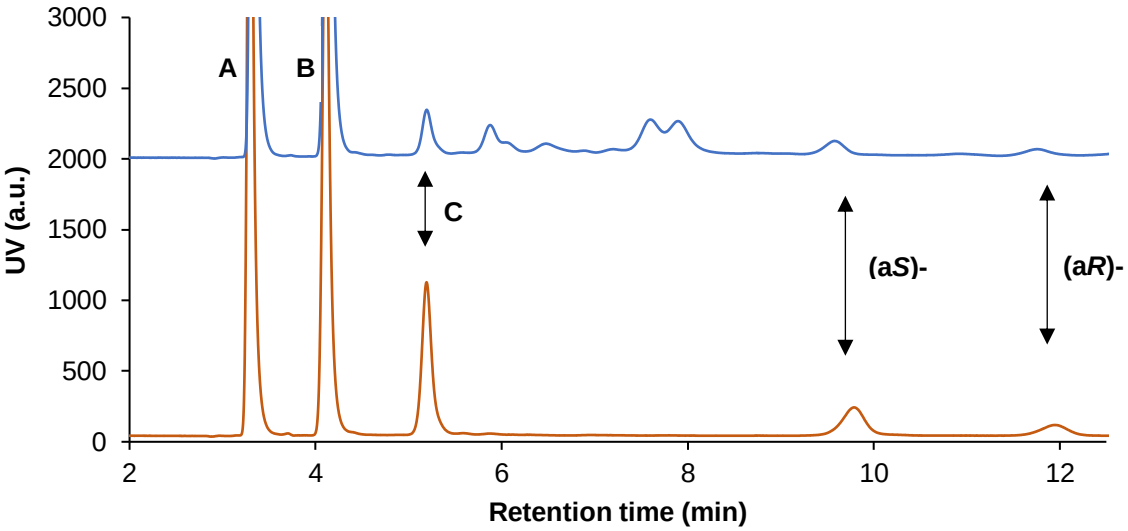

Figure III-42: Chromatograms obtained for the oxidative coupling of 2-naphthol in an open Schlenk tube with toluene at 60ºC for 72 h, with **FeL2** as pre-catalyst. Orange line: 5% **FeL2**, 1% Phen; blue line: 5% **FeL2**, 5% Et_3N. Secondary products were detected in the blue line chromatogram between *ca.* 5:30 and 8 minutes of retention time. **A**: Toluene; **B**: Internal standard (acetophenone); **C**: 2-naphthol.

With **FeL14**, higher BINOL yield values were achieved with 5 mol% **FeL14** and 1 mol% Et_3N (83-84%, see entries 37 and 38 of **Table III-17**) and moderate to good BINOL yields in the range 62-72% with 5 mol% **FeL14** and 5 mol% base, in open Schlenk tubes (entries 8, 16, 24, 32 and 40, **Table III-17**). All the studied reactions showed to be very selective towards BINOL formation: selectivity values up to 97% were obtained with 5 mol% **FeL14** and 1 to 5 mol% of Py, Coll, Phen or Et_3N, and BINOL was the only product with 1 mol% **FeL14** and 5 mol% Py or Coll, but with low BINOL yield values (up to 33%). In contrast to the detected with **FeL2**, reactions catalysed by **FeL14** showed to be enantioselective for (a*R*)-BINOL formation, and in general, catalytic conditions that afford higher BINOL yields and selectivities show lower *ee* values, with the opposite being also true (*e.g.* entry 18 of **Table III-17**: 23% BINOL, 77% selectivity, 17% (a*R*)-BINOL). After this evaluation it was concluded that so far the best catalytic conditions with **FeL14** were those granting higher *ee* values, with 1 mol% of **FeL14** and 1 mol% of any base, except Py.

Table III-17: Results obtained in the catalytic oxidative coupling of 2-naphthol using **FeL14** as pre-catalyst, air (dioxygen) as oxidant and organic bases as additives: Pyridine (Py), quinoline (Quin), phenanthroline (Phen), collidine (Coll) and triethylamine (Et_3N).

Entry	FeL14 (mol %)	Closed / Open	mol % Base	Conv. (%)	BINOL (%)	Selectivity (%)	*ee* (%)
1	1%	Closed	1% Py	17	14	82	8 (a*R*)
2	1%	Open	1% Py	23	15	65	8 (a*R*)
3	1%	Closed	5% Py	34	29	85	2 (a*S*)
4	1%	Open	5% Py	30	30	100	1 (a*S*)
5	5%	Closed	1% Py	29	23	79	15 (a*R*)
6	5%	Open	1% Py	56	54	96	4 (a*R*)
7	5%	Closed	5% Py	48	38	79	0
8	5%	Open	5% Py	74	63	85	2 (a*R*)
9	1%	Closed	1% Quin	35	23	66	12 (a*R*)
10	1%	Open	1% Quin	43	28	65	12 (a*R*)
11	1%	Closed	5% Quin	59	52	88	0
12	1%	Open	5% Quin	58	51	88	2 (a*R*)
13	5%	Closed	1% Quin	36	27	75	15 (a*R*)
14	5%	Open	1% Quin	60	50	83	5 (a*R*)
15	5%	Closed	5% Quin	66	51	77	1 (a*R*)
16	5%	Open	5% Quin	81	68	84	3 (a*R*)
17	1%	Closed	1% Phen	32	27	84	16 (a*R*)
18	1%	Open	1% Phen	30	23	77	17 (a*R*)
19	1%	Closed	5% Phen	36	30	83	3 (a*R*)
20	1%	Open	5% Phen	30	27	90	3 (a*R*)
21	5%	Closed	1% Phen	61	58	95	6 (a*R*)
22	5%	Open	1% Phen	61	54	89	5 (a*R*)
23	5%	Closed	5% Phen	73	59	81	3 (a*R*)
24	5%	Open	5% Phen	64	62	97	6 (a*R*)
25	1%	Closed	1% Coll	49	37	76	14 (a*R*)
26	1%	Open	1% Coll	38	28	74	11 (a*R*)
27	1%	Closed	5% Coll	33	33	100	10 (a*R*)
28	1%	Open	5% Coll	64	44	69	6 (a*R*)
29	5%	Closed	1% Coll	60	58	97	4 (a*R*)
30	5%	Open	1% Coll	67	62	93	5 (a*R*)
31	5%	Closed	5% Coll	80	72	90	9 (a*R*)
32	5%	Open	5% Coll	78	71	91	10 (a*R*)
33	1%	Closed	1% Et_3N	53	40	75	14 (a*R*)
34	1%	Open	1% Et_3N	98	61	62	15 (a*R*)
35	1%	Closed	5% Et_3N	61	23	38	5 (a*R*)
36	1%	Open	5% Et_3N	76	17	22	8 (a*R*)
37	5%	Closed	1% Et_3N	87	84	97	7 (a*R*)
38	5%	Open	1% Et_3N	90	83	92	5 (a*R*)
39	5%	Closed	5% Et_3N	66	49	74	8 (a*R*)
40	5%	Open	5% Et_3N	73	51	70	8 (a*R*)

Reaction conditions: In a closed or opened 50 mL Schlenk tubes, 1 mmol 2-naphthol, 1-5 mol% **FeL14**, 1-5% base, 4 mL toluene, 60ºC, 72 h. Conversion of 2-naphthol, BINOL yields and *ee* were determined by HPLC.

The effect of extending reaction time from 72 to 192 h was evaluated for both **FeL2** and **FeL14** in the optimized conditions and the results are presented in **Table III-18**. In a closed Schlenk tube containing 5 mol% **FeL2** and 1 mol% Phen a significant increment in BINOL yield and selectivity of 17 and 11%, respectively, was observed for the 192 h reaction in comparison to the 72 h experiment, but the *ee* value decreased 11% (compare entry 21 of **Table III-16** with entry 1 of **Table III-18**). With 1 mol% **FeL14** and 1 mol% Et_3N was observed a decrease of 26 and 11% in BINOL yield and BINOL formation selectivity was observed, respectively, in the 192 h reaction, maintaining almost the same *ee* value for (a*R*)-BINOL formation (compare entry 34 of **Table III-16** with entry 4 of **Table III-18**). Therefore, increasing reaction time improved BINOL yield and BINOL formation selectivity values with **FeL2** but revealed to be ineffective in increasing *ee* values with **FeL2** or **FeL14**.

The amount of Fe(III) complex added was also evaluated for different reaction times (see entries 2 to 5 in **Table III-18**). Direct addition of 10 mol% of **FeL2** and 1 mol% Phen for 72 h increased BINOL yield and reduced BINOL selectivity in 15 and 10%, respectively, in comparison with addition of 5 mol% **FeL2** for the same reaction period. Enantioselectivity had no significant increase, *ca.* 2% (compare entry 21 **Table III-16** with entry 3 **Table III-18**). It was also tested a two-step addition of 10 mol% of **FeL2** with 1 mol% Phen: 5 mol% **FeL2** for the first 72 h, followed by 5 mol% more of **FeL2** after this period, prolonging the reaction time til 192 h. An increment of 17% in BINOL yield was observed but BINOL selectivity and *ee* values were lowered by 20 and 10%, respectively (compare entry 21 **Table III-16** with entry 2 **Table III-18**). A two-step addition of 1 mol% **FeL14** was also studied with 1 mol% Et_3N for 192 h: Noteworthy is the significant increase of 23% in BINOL yield obtained in comparison to the 72 h reaction, with no significant changes in selectivity of BINOL formation and *ee* values obtained (compare entry 33 of **Table III-17** with entry 5 **Table III-18**). It can be concluded that direct or two-step 10 mol% of **FeL2** for 72 or 192 h, respectively, and two-step addition of 1 mol% **FeL14** can increase BINOL yield values obtained in all cases but diminishes BINOL selectivity and is unable to significantly improve enantioselectivity.

Since both reaction time extension and additional mol% of **FeL2** or **FeL14** did not afford a significant increase in enantioselectivity, it was decided to test the remaining Fe(III) complexes under the optimal conditions obtained for **FeL2** and **FeL14**, respectively: (i) 5 mol% [Fe], 1 mol % Phen, toluene, 72 h, 60ºC in an opened Schlenk tube; (ii) 1 mol% [Fe], 1 mol % Coll, toluene, 72 h, 60ºC in a closed Schlenk tube. Results are presented in entries 6 to 27 of **Table III-18**. Complexes containing amino acid-pyridyl ligands (**FeL1A**, **FeL1B** and **FeL3**) presented residual BINOL yield values with Phen and up to 20% with collidine. Complex **FeL1A** showed to be more enantioselective for the formation of (a*R*)-BINOL enantiomer in the presence of

collidine, affording 19% *ee*. **FeL1B** and **FeL3** on the other hand showed very low *ee* values or even no enantioselectivities at all under both conditions (see entries 6 to 11 of **Table III-18**). Regarding enantioselectivity, **FeL1A** shows better results than **FeL14** in the presence of Phen, albeit with almost half BINOL yield values (compare entry 25 of **Table III-17** with entry 7 of **Table III-18**). Complexes bearing amino acid-phenol ligands (**FeL5**-**6**, **FeL8**-**10**) and **FeL11** presented very low enantioselectivity towards (a*S*)-BINOL enantiomer in all cases, with the exception to **FeL9** and **FeL10** under both reaction conditions (see entries 12 to 23 of **Table III-18**); no BINOL product was formed with **FeL9** and **FeL10** show to be selective for (a*S*)-BINOL formation in the presence of Phen, affording 10% *ee*. In general, BINOL yields obtained with this class of complexes were below 30% with both Phen and collidine as additives. Compound **FeL8** afforded BINOL yields (35%) comparable with **FeL14** with collidine, but with 11% *ee* towards (a*S*)-BINOL formation (compare entry 25 of **Table III-17** with entry 17 of **Table III-18**). Complexes bearing amino acid-pyridyl-phenol ligands **FeL13** and **FeL15** present different results regarding BINOL yield and enantioselectivities. Compound **FeL13** and **FeL14** show similarity in the results obtained with collidine as additive when compared to all parameters analysed, also showing to be enantioselective for (a*R*)-BINOL formation in 7 to 12% *ee* (compare entry 25 of **Table III-17** with entry 25 of **Table III-18**). Compound **FeL15** show BINOL yield values up to 20% and very poor enantioselectivities (up to 10%) in (a*S*)-BINOL formation with both basic additives.

Data analysed in **Table III-18** confirmed an overall superior catalytic performance of **FeL2**, **FeL13** and and **FeL14** in the presence of Phen and collidine, respectively, when compared to the remaining Fe(III) complexes prepared in this work. This is evidenced by the BINOL yield values obtained with these complexes, varying from moderate to good with the optimized conditions. The E_p^{red} values of these complexes, presented in **Table III-12** and respective to the Fe(III)→Fe(II) reduction process, lie in the range -0.92 to -0.70 V while the remaining compounds present E_p^{red} potentials between -0.53 to -0.36 V (**FeL1A**, **FeL1B**, **FeL3**) or ill-defined to inexistent redox processes (**FeL5-6**, **FeL8-11**, **FeL15**). Thus, there might exist a correlation between E_p^{red} values depicted by **FeL2**, **FeL13** and **FeL14** and the BINOL yields obtained with these complexes, especially **FeL14** where BINOL yields up to 84% were obtained.

Two important features can be highlighted from these catalytic procedures: the first one is that dioxygen from air is used as oxidant, greatly contributing for the development of a more sustainable catalytic system; the second feature is that these catalytic reactions can be tuned to enable higher enantioselectivities towards (a*S*)- or (a*R*)-BINOL, depending on the application of **FeL2** or **FeL14**, respectively.

Table III-18: Extended studies in the oxidative coupling of 2-naphthol within the optimized catalytic conditions.

Entry	mol % [Fe]	Closed / Open	Time (h)	Base	Conv. (%)	BINOL (%)	Selectivity (%)	*ee* (%)
1	5% **FeL2**	Closed	192	Phen	48	40	83	27 (a*S*)
2[a]	2x 5% **FeL2**	Closed	192	Phen	73	41	56	28 (a*S*)
3	10% **FeL2**	Closed	72	Phen	61	38	62	40 (a*S*)
4[b]	1% **FeL14**	Closed	192	Et_3N	66	35	53	17 (a*R*)
5	2x 1% **FeL14**	Closed	192	Et_3N	80	63	79	16 (a*R*)
6	5% **FeL1A**	Open	72	Phen	7	5	71	1 (a*R*)
7	1% **FeL1A**	Closed	72	Coll	38	20	53	19 (a*R*)
8	5% **FeL1B**	Open	72	Phen	8	3	38	7 (a*R*)
9	1% **FeL1B**	Closed	72	Coll	15	13	87	0
10	5% **FeL3**	Open	72	Phen	3	2	67	0
11	1% **FeL3**	Closed	72	Coll	12	11	92	2 (a*S*)
12	5% **FeL5**	Open	72	Phen	14	11	79	2 (a*S*)
13	1% **FeL5**	Closed	72	Coll	18	15	83	9 (a*S*)
14	5% **FeL6**	Open	72	Phen	41	22	54	9 (a*S*)
15	1% **FeL6**	Closed	72	Coll	26	24	92	6 (a*S*)
16	5% **FeL8**	Open	72	Phen	21	16	76	4 (a*S*)
17	1% **FeL8**	Closed	72	Coll	44	35	80	11 (a*S*)
18	5% **FeL9**	Open	72	Phen	-	-	-	-
19	1% **FeL9**	Closed	72	Coll	-	-	-	-
20	5% **FeL10**	Open	72	Phen	11	8	73	10 (a*R*)
21	1% **FeL10**	Closed	72	Coll	-	-	-	-
22	5% **FeL11**	Open	72	Phen	19	12	63	4 (a*S*)
23	1% **FeL11**	Closed	72	Coll	15	14	93	1 (a*S*)
24	5% **FeL13**	Open	72	Phen	59	49	83	7 (a*R*)
25	1% **FeL13**	Closed	72	Coll	62	35	56	12 (a*R*)
26	5% **FeL15**	Open	72	Phen	31	19	61	10 (a*S*)
27	1% **FeL15**	Closed	72	Coll	21	20	95	1 (a*S*)

Reaction conditions: In a closed or open 50 mL Schlenk tube, 1 mmol 2-naphthol, 1-10 mol% [Fe], 1 mol% base, 4 mL toluene, 60ºC, 72-192 h. [a] additional 5 mol% **FeL2** after 72 h of reaction; [b] additional 1 mol% **FeL14** after 72 h of reaction. Conversion of 2-naphthol, BINOL yields and *ee* were determined by HPLC.

The catalytic reaction conditions with Phen and collidine as additives were further tested in the asymmetric oxidative coupling of 3-bromo-2-naphthol with **FeL2** and **FeL14** to obtain 3,3'-dibromo-BINOL (BrBINOL, **Scheme III-12**); During the development of this work it was thought that a bulky substituent in the C3-position could lead to highly enantioselective catalytic reactions with **FeL2** or **FeL14** within the optimized conditions. In addition, 3,3'-substituted binaphthols with electron-withdrawing substituents are usually difficult to synthesize and are

highly valuable compounds as chiral ligands.[40] The choice of 3-bromo-2-naphthol was then natural for the mentioned reasons and also because it was one of the cheapest substrates commercially available.

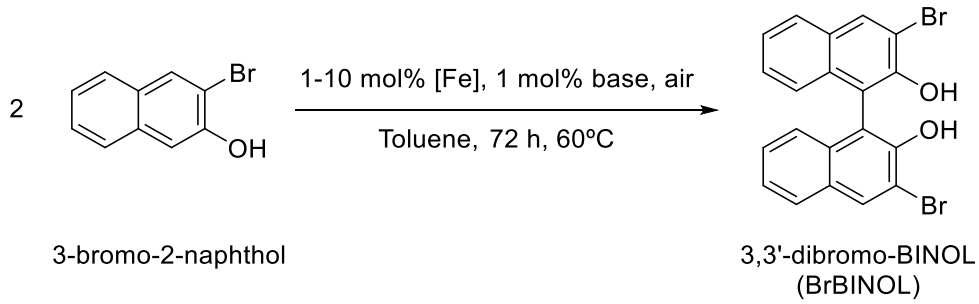

Scheme III-12: Oxidative coupling of 3-bromo-2-naphthol in the preparation of 3,3'-dibromo-BINOL, using air as oxidant under the optimized catalytic conditions.

Results obtained in the oxidative coupling of 3-bromo-2-naphthol are presented in **Table III-19**. Applying **FeL2** with Phen as additive, low BrBINOL yields were obtained but with good selectivity and enantioselectivity values in the formation of (a*S*)-BrBINOL (73 and 39%, respectively, see entry 1 of **Table III-19**). These results were very similar to the presented in the coupling reaction of 2-naphthol (compare with entry 22 of **Table III-16**). Increasing time reaction from 72 to 192 h within the same catalytic conditions decreased BrBINOL values obtained, almost maintaining *ee* values (37%, entry 3 of **Table III-19**). Very interesting were the outputs gathered from the usage of direct and two-step addition of 10 mol% **FeL2**; in both cases very low BrBINOL yields were obtained, up to 15%, but with *ee* values up to 85% in (a*S*)-BrBINOL formation (see entries 2 and 4 of **Table III-19**). Complexes **FeL13** and **FeL14** were tested using collidine as additive and are presented in entries 5 and 6 of **Table III-19**. In both cases moderate BrBINOL yield values were achieved but with good selectivities, up to 89%. Surprisingly, these conditions were also more selective for the formation of (a*S*)-BrBINOL, contrasting with the observed in the oxidative coupling of 2-naphthol which was more selective in affording (a*R*)-BINOL enantiomer. Also worth noting is the lack of enantioselectivity exhibited by **FeL14** as pre-catalyst under these contitions.

Overall, these catalytic systems applied in the oxidative coupling of 3-bromo-2-naphthol are more selective in the formation of (a*S*)-BrBINOL, independently of the Fe(III) complex used. This observation can be related to the bulky nature of bromo- substituents present in the substrate, favouring the formation of the (a*S*)-BrBINOL enantiomer.

Table III-19: Results obtained in the catalytic oxidative coupling of 3-bromo-2-naphthol using air as oxidant and organic bases as additives.

Entry	[Fe]	Time (h)	Base	Conv. (%)	BrBINOL (%)	Selectivity (%)	*ee* (%)
1	5% **FeL2**	72	Phen	41	30	73	39 (a*S*)
2	10% **FeL2**	72	Phen	64	15	23	82 (a*S*)
3	5% **FeL2**	192	Phen	55	21	38	37 (a*S*)
4	2x5% **FeL2**	192	Phen	75	8	11	85 (a*S*)
5	1% **FeL13**	72	Coll	53	47	89	32 (a*S*)
6	1% **FeL14**	72	Coll	51	43	84	0

Reaction conditions: In a closed 50 mL Schlenk tube, 1 mmol 3-bromo-2-naphthol, 1-10 mol% [Fe], 1 mol% base, 4 mL toluene, 60ºC, 72-192 h. Conversion of 3-bromo-2-naphthol, BrBINOL yields and *ee* were determined by HPLC.

III.5.1.1 – Elucidation of the key mechanistic aspects

Some studies were performed in order to understand the interaction between 2-naphthol, iron (III) pre-catalysts and added bases. These studies started with the elucidation of reaction profile over time using the optimal catalytic conditions (5 mol% of **FeL2** and 1 mol% Phen. The profile obtained is presented in **Figure III-43** and reveals that both 2-naphthol conversion and BINOL yield closely increase over time at an apparently constant rate till *ca.* 48 h of reaction, which after this period both parameters slightly increase *ca.* 4% until 72 h. These profiles demonstrate the good selectivity observed towards BINOL formation since the beginning of the reaction, with initial oscillating values but maintaining an apparently constant increase after 30 h of reaction. More interesting was the observed for enantioselectivity, where *ee* values above 60% were detected at the first 2 h, greatly decreasing until between 32 to 40% values till the end of the reaction.

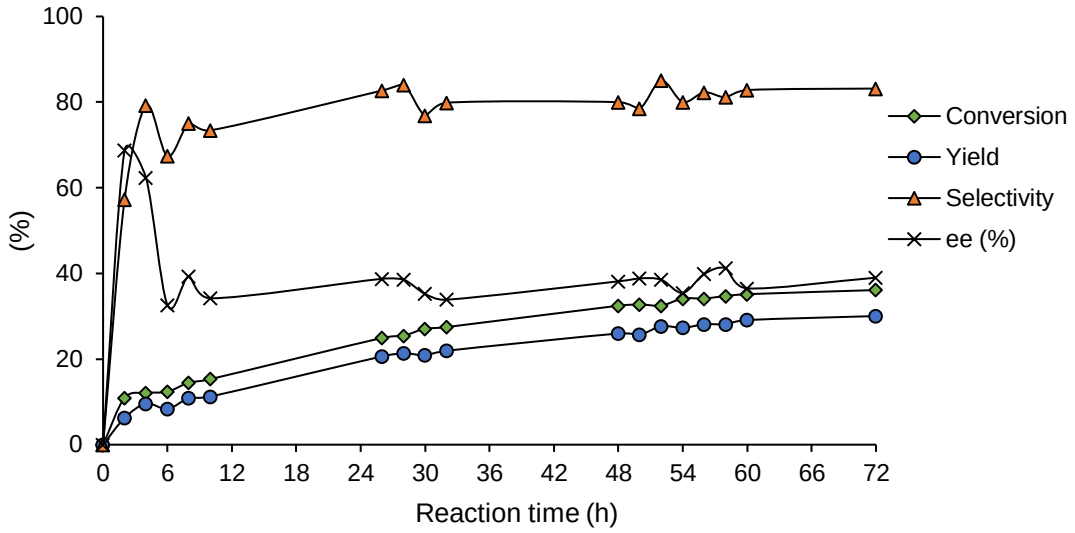

Figure III-43: Reaction profile of the oxidative coupling of 2-naphthol in an open Schlenk tube with 4 mL of toluene, 5 mol% of **FeL2** and 1 mol% Phen at 60ºC for 72 hours.

The interaction of 2-naphthol and collidine with **FeL14** was studied by electronic absorption spectroscopy and the electronic spectra are presented in **Figure III-44**. It is visible an hyperchromic effect on the phenolate→Fe(III) *pπ-dπ** CT band of **FeL14** 24 hours after addition of 2-naphthol (**Figure III-44**, dashed green and blue line), but no significant changes are visible 24 hours after addition of collidine indo a **FeL14** solution (**Figure III-44**, continuous brown and red line). These results suggest that 2-naphthol coordinates to the metal centre of **FeL14** during the reaction time, but no coordination occurs by the added base.

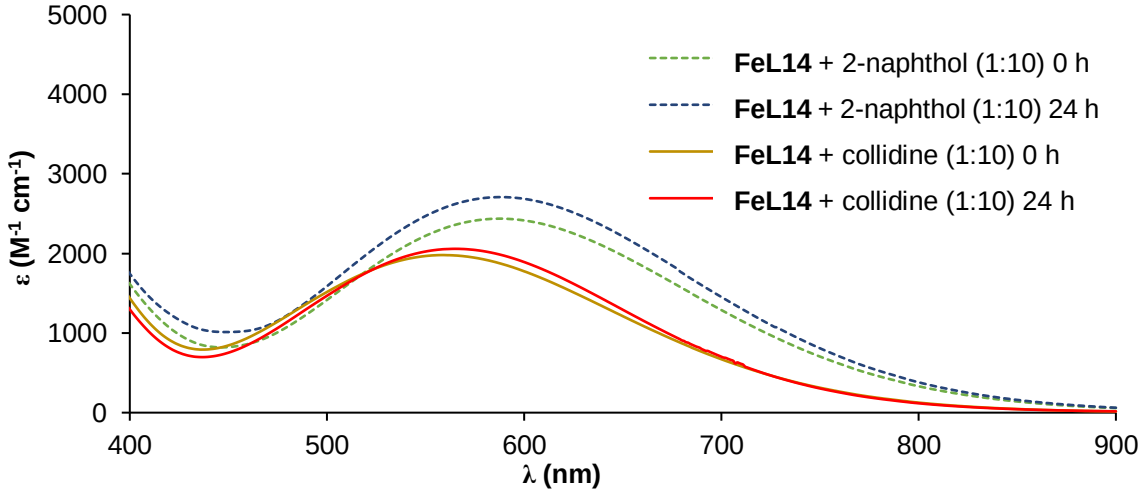

Figure III-44: Electronic absorption (UV-Vis) spectra at room temperature of **FeL14** in toluene (2.00 mM) in a 2 mm optical path quartz cells, after addition of 10 mole equivalents of 2-naphthol (dashed lines) or collidine (continuous lines). Spectra measurements were performed immediately after addition of additives (t= 0 h) and after 24 h.

To elucidate base behaviour, an additional coupling reaction was performed in the following conditions: 1 mol% Coll was added to an opened Schlenk tube containing 1 mol% **FeL14** and the mixture stirred for 24 h at 60ºC. After this period 2-naphthol was added to the mixture and the reaction continued for additional 72 h (conditions A). The results obtained were compared with a reaction occurring for 72 h with 2-naphthol, 1 mol% **FeL14** and 1 mol% Coll (conditions B) and data are presented in **Table III-20**. The BINOL yield values with both conditions are identical, but a slight decrease in *ee* values appeared with conditions A as in BINOL selectivity. This result reinforces the idea that the effect of the base is in assisting the binding of the substrate to the metal centre and not so much on the enhancement of enantioselectivity of the pre-catalyst. Such conclusion is also strengthened by the previously obtained results presented in **Table III-17** with 1 mol% **FeL14** and 1 mol% Et_3N, a non-coordinating base, where *ee* values obtained towards (a*R*)-BINOL formation were up to 15%.

Table III-20: Comparable results obtained in the catalytic oxidative coupling of 2-naphthol using **FeL14** as pre-catalyst, air as oxidant and collidine as additive.

Entry	FeL14 (mol %)	Conv. (%)	BINOL (%)	Selectivity (%)	*ee* (%)
1[a]	1	43	28	65	6 (a*R*)
2[b]	1	38	28	74	11 (a*R*)

Reaction conditions: In an opened Schlenk tube, 1 mmol 2-naphthol, 1 mol% **FeL14**, 1% collidine, 4 mL toluene, 60ºC.[a] mixture of **FeL14** and Coll in the first 24 h, followed by addition of 2-naphthol and prolonging the reaction for more 72 h; [b] 72 h. Conversion of 2-naphthol, BINOL yields and *ee* were determined by HPLC.

The effect of the added base seems to be related to the activation of the substrate, by deprotonation, improving coordination to the metal centre. Adão and co-workers[107] also refered this aspect in the oxidative coupling of 2-naphthol with addition of organic bases and amino acid-derived copper(II) complexes. The authors referred that the pK_a value of the conjugated acid of the used base must not be higher than the pK_a value of 2-naphthol, which is 9.5, otherwise competitive quinone formation might occur. The pK_a values of the conjugated acid of the utilized bases are presented in **Table III-21**. It was observed in the applied conditions of this work that application of Et_3N presented the lowest selectivities towards BINOL formation, especially with 5 mol% Et_3N and 5 mol% **FeL2** (see **Table III-16**, entries 35, 36 and 40) and formation of by-products was detected in the respective chromatogram, as depicted in **Figure III-42**. Application of other bases presented, in general, much higher BINOL selectivities in the same conditions than Et_3N. Hence, the added base should be sufficiently strong to assist in the binding of 2-naphthol to the metal centre, while minimizing the amount of uncoordinated 2-naphthoxide in the reaction, granting higher BINOL selectivities and avoiding the formation of undesired by-products.

Table III-21: Utilized organic bases, their conjugated acids and respective pK_a values.

Entry	Added base	Conjugated acid	pK_a
1	Pyridine	Pyridinium	5.3[129]
2	Quinoline	Quinolinnium	4.9[130]
3	Phenanthroline	Phenanthrolinium	4.8[131]
4	Collidine	Collidinium	7.5[132]
5	Triethylamine	Triethylammonium	10.7[132]

The magnetic susceptibility of **FeL14** in solution, within the applied catalytic conditions, was calculated using Evan's NMR method. For this purpose two NMR samples were prepared, containing a solution of **FeL14**, collidine and 2-naphthol in CD_3CN:toluene (1:1) and the respective reference solution without **FeL14** in the same solvent. The NMR spectrum of one of the samples was measured at inert atmosphere, while the other was determined in aerobic conditions. It was observed after a 72 h period that the sample at inert atmosphere showed an increase in the paramagnetic shift from 37 to 45 Hz relative to the reference signal (methyl group of toluene), while the sample under aerobic conditions presented a decrease in shift from 39 to 35 Hz (see **Figure III-45**). Under the conditions used, the 9 Hz shift corresponds to μ_{eff} = 5.77 μ_B and the 4 Hz deviation to a μ_{eff} = 5.15 μ_B. In both experiments the magnetic moments observed are consistent with those expected for high-spin (S=$^5/_2$) Fe(III) complexes in solution.[127,128] In the inert atmosphere sample, the higher μ_{eff} observed after 72 h can be related to the monomerization of **FeL14** in solution after coordination of 2-naphtholate units.[128] The decrease in magnetic moment observed in the aerobic conditions can lead to other conclusions: although the magnetic moments are not consistent with high-spin (S=2) iron(II) species, if the catalytic mechanism contemplate an Fe(III)→Fe(II) reduction the formed Fe(II) species might react with O_2 from air, leading to the formation of dinuclear μ-hydroxido or μ-oxido species in solution. Anti-ferromagnetic electron spin coupling between μ-hydroxido or μ-oxido bridged Fe(III) centres explains the lower magnetic moment observed in the presence of air. Therefore, a reduction of Fe(III) to Fe(II) is not put aside in these catalytic reactions.

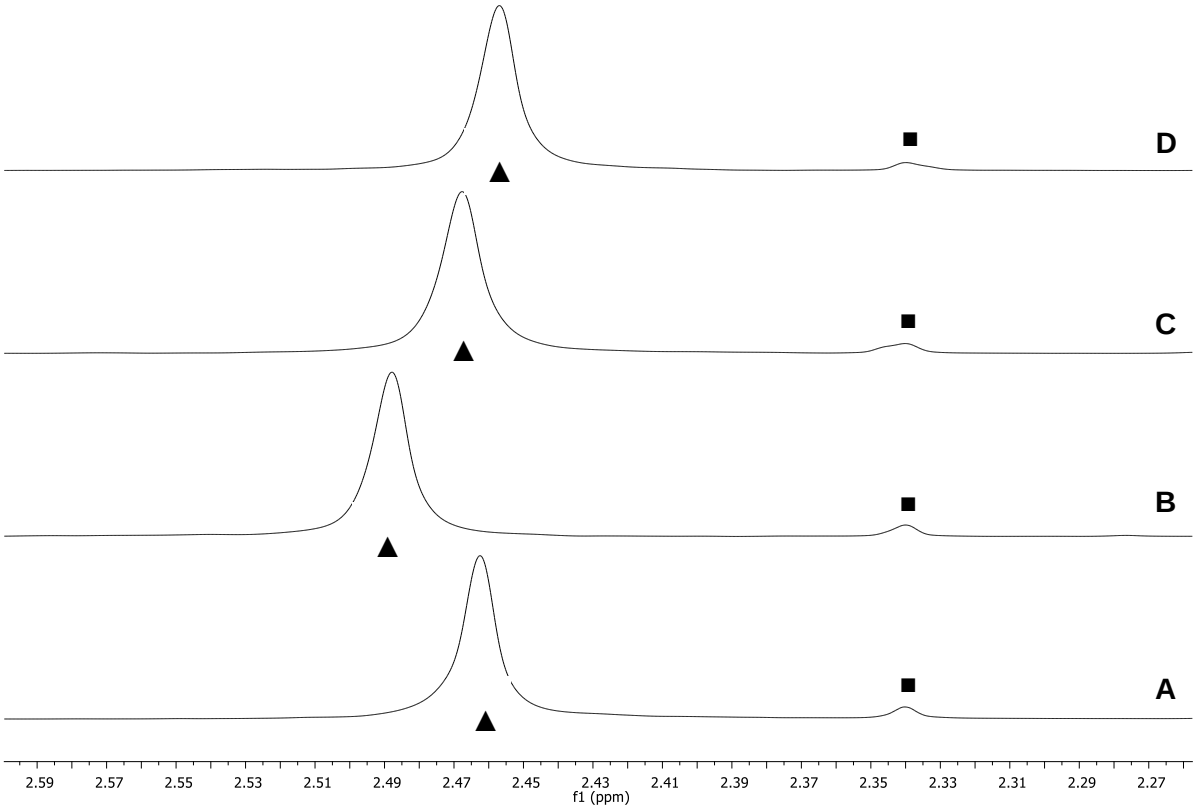

Figure III-45: Solution ^{1}H NMR spectra of **FeL14** (2.5 mM) in the presence of collidine (2.5 mM) and 2-naphthol (250 mM) in CD_3CN:toluene (1:1) at room temperature: (**A**) initial spectrum under N_2 atmosphere; (**B**) spectrum under N_2 atmosphere, measured after 72 hours at 60ºC and cooled to r.t. (**C**) initial spectrum under air; (**D**) spectrum under air, measured after 72 hours at 60ºC and cooled to r.t.. The square indicates the toluene CH_3 signal and the triangle indicates the shifted toluene CH_3 signal.

Several types of metal-promoted oxidative homo- and cross-coupling mechanisms of phenols have been proposed involving radical-radical[133,134] and radical-anion[41,43,135] couplings. In 2015, Pappo and co-workers[136] focused in the development of a more effective catalytic procedure for the asymmetric coupling of several phenols with iron compounds. The authors studied the kinetics of the homocoupling of 2,6-dimethoxyphenol and 2-naphthol with *tert*-butylperoxide (TBP) as oxidant and 1,1,1,3,3,3-hexafluoropropan-2-ol (HFIP) as solvent and compared their results with those achieved by Katsuki and co-workers.[41] Pappo[136] concluded that in his studies the reaction rate with TBP and HFIP was solely dependent on the concentration of the iron pre-catalyst, being zero-order dependent on the oxidant. As for the results obtained the authors proposed a chelated-radical-anion coupling mechanism. In contrast, the conclusions derived from the data developed by Katsuki and co-workers[41] indicate a first-order dependence (i) of the reaction rate on the concentrations of the molecular oxygen and on the coupling substrate and (ii) of the obtained *ee* values on the concentration of the used iron(salan) pre-catalyst;

from the results obtained the authors proposed a radical-anion oxidative coupling mechanism, depicted in **I.2.1.2** – **Scheme I-10**.

In the present work no kinetic studies were carried out but some similarities are found with the work developed by Katsuki:[41] (i) the solvent and oxidant used herein were toluene and air, respectively, not HFIP and TBP; (ii) in the absence of air no coupling products were obtained, indicating that these reactions are dependent on the presence of dioxygen (**Table III-14**, see entries 2 to 4); (iii); a general increase in BINOL yield values was observed for higher amounts of Fe(III) complex added, similarly to data presented in **Table III-16** to **Table III-18** (iv) with 3-bromo-2-naphthol the *ee* values obtained increased with higher mol % of iron complex used (**Table III-19**, see entries 1 to 4). Considering the experimental observation made so far in combination with the data available in the literature[41,136] regarding the oxidative coupling of phenols with Fe(III) complexes, a radical-anion mechanism was proposed and presented below in **Scheme III-13**.

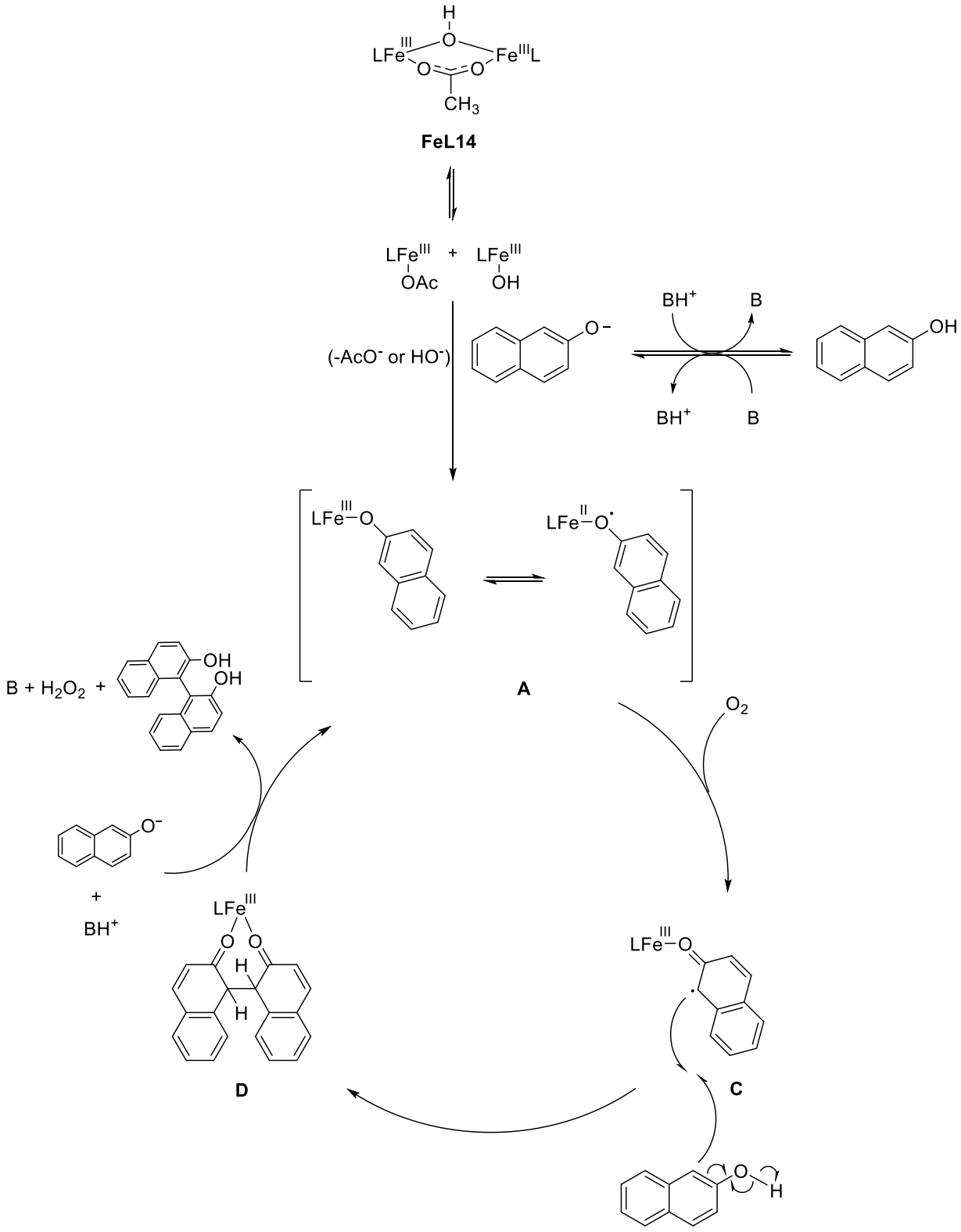

Scheme III-13: Proposed catalytic cycle for the studied oxidative 2-naphthol coupling with added base and **FeL14** as pre-catalyst.

According to the characterization studies, most of the Fe(III) complexes synthesized in this work tend to form dimers or even oligomers in solution. The catalytic cycle was described with **FeL14** since this compound presented interesting catalytic activity in this reaction and also

because it is characterized by X-ray diffraction in Section **III.2.3.2**. Compound **FeL14** may form dinuclear species in solution with partial antiferromagnetic coupling, in equilibrium with its mononuclear species, until the coordination of a 2-naphtholate unit (activated by deprotonation of the added base B) to afford intermediate **A**. The electronic structure of **A**, a Fe-naphtholato complex, may observe one-electron transfer from the naphtholato moiety to the iron centre which in the presence of molecular dioxygen affords intermediate **C**, suitable of radicalar coupling with a 2 naphthol unit, originating intermediate **D**. After a possible proton and hydrogen abstraction and ligand exchange between an activated 2-naphtholate unit, species **A** if formed again, regenerating the catalytic cycle.

Secondary coupling products such as quinones are possibly formed in this final step of the catalytic cycle, especially if a stronger base such as Et_3N is used. BINOL, with a pK_a of 10.28,[137] is easily deprotonated by Et_3N, while weaker bases are more selective in the deprotonation of 2-naphthol. Deprotonation of BINOL can lead to oxidation of the resultant BINOLate, resulting in quinone formation which can justify the formation of the secondary products in **Figure III-42**. Further studies are underway in order to validate this mechanistical suggestion.

III.5.2 – Epoxidation of chalcones

Chalcones are one class of natural and synthetic α-β-unsaturated ketones belonging to the family of flavonoids and possess several important biological activities.[138,139] The respective epoxides, α-β-epoxiketones, also display relevant therapeutical properties and find applications in the preparation of flavouring substances and in the cosmetic industry.[140,141] In the last four decades, chalcone epoxidation have been extensively studied in the field of organocatalysis, with a major effort put forward in the attempt to enhance yields and enantioselectivities obtained.[142,143] Wynberg and co-workers[144] and Vega and co-workers[145] set the starting point of this type of catalytic procedures by studying, respectively, phase-transfer catalysis from alkaloid-derived ammonium salts and peptide-type catalysts in a triphasic toluene-water-polypeptide system. Metal-based catalytic procedures towards chalcones epoxidation are more recent and focused on the influence, for example, of metal *tert*-butyl peroxides[146] or lanthanoid-BINOL derived complexes.[147] Despite the great advancements made in the catalytic epoxidation of chalcones, especially in the organocatalytic field, the past decade saw a shift in emphasis towards more environmentally friendly chemical approaches. The use of more environmentally-benign catalysts, solvents and oxidants has become a major concern in epoxidations in general, with metal-based catalysis playing an important role since the beginning of the century[92,148] Among these, iron-catalyzed epoxidations offer remarkable advantages because iron is abundant, cheap and relatively non-

toxic comparing to other metal sources.[1,15] A great effort has been implemented in modelling the catalytic activity of natural iron-based metalloenzymes by synthetic complexes.[56,72,149] Following this bio-inspired approach, epoxidation of chalcone derivatives find examples in the literature, with non-heme[68] or porphyrin-inspired[150] *in situ* Fe(II) complexes acting as pre-catalysts in the epoxidation of these compounds. The present work intended to test the catalytic activity of the prepared non-heme Fe(III) compounds in the epoxidation of benzalacetophenones, a type of chalcones, using (i) non-heme hydrogen peroxyde-acetic acid epoxidation conditions (ii) Mukaiyama-type epoxidation conditions, using eco-friendly solvents and mild conditions. The substrates chosen for epoxidation were (*E*)-1,3-diphenylprop-2-enone (**HC**) and (*E*)-1-(4-methoxyphenyl)-3-phenylprop-2-enone (**MeOC**).

III.5.2.1 – Epoxidation using the hydrogen peroxyde-acetic acid system

In a first stage, the prepared Fe(III) complexes were employed as pre-catalysts using H_2O_2 as oxidant and acetic acid as additive, inspired on the developed work by Que and co-workers[61,62,63,65] on the non-heme epoxidation of olefins, mimicking the RDO behaviour and reviewed in Section **I.3.1**. A schematic representation of the applied conditions in this work in the epoxidation of **HC** and **MeOC** is presented below in **Scheme III-14**.

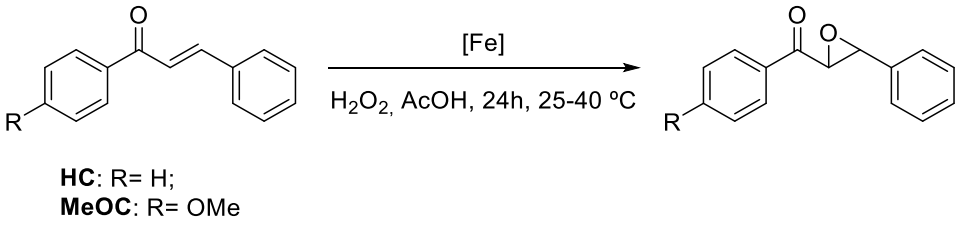

HC: R= H;
MeOC: R= OMe

Scheme III-14: Epoxidation of benzalacetophenones **HC** and **MeOC** with H_2O_2 and AcOH.

The preliminaty studies were performed in the epoxidation of **HC** and **MeOC** with addition of 1 mole equivalent of H_2O_2 and AcOH in acetonitrile, acetone or acetone:H_2O (3:1). Three Fe(III) complexes bearing pyridyl donor groups, **FeL1B**, **FeL2** and **FeL14**, were tested as pre-catalysts. In general, residual epoxide yields and enantioselectivities were observed in reactions running for 24 to 72 h at temperatures ranging from 5 to 40ºC, as shown in **Table III-22**. Increasing the amount of H_2O_2 with 1 mole equivalent of AcOH did not afford better epoxide yields for the epoxidation of **MeOC**, as observed in entries 7 to 21.

Different amounts of H_2O_2 and AcOH were tested to obtain better epoxide yields but with no success. With 7 mole equivalents of AcOH and 6 mole equivalents of H_2O_2 no epoxide was formed as shown in **Table III-23**; selectivity in epoxide formation slightly increased with 10

mol% AcOH and 2 mole equivalents of H_2O_2, but the epoxide yields observed were still very low, as shown in **Table III-24**.

Table III-22: Preliminary results obtained in the non-heme epoxidation of chalcones **HC** and **MeOC**.

Entry	[Fe]	Substrate	H_2O_2 (eq.)	AcOH (eq.)	Solvent	t (h)	T (ºC)	Conv. (%)	Oxirane (%)	Select. (%)	*ee* (%)
1	**FeL2**	**HC**	1	1	MeCN	24	40	36	7	19	3.4
2	**FeL14**	**HC**	1	1	MeCN	24	40	34	5	15	0.9
3	**FeL1B**	**HC**	1	1	MeCN	24	40	41	6	15	0.5
4	**FeL2**	**MeOC**	1	1	MeCN	24	40	49	5	10	1.0
5	**FeL14**	**MeOC**	1	1	MeCN	24	40	28	8	29	0.9
6	**FeL1B**	**MeOC**	1	1	MeCN	24	40	37	5	14	1.4
7	**FeL2**	**MeOC**	2	1	MeCN	72	40	35	6	17	0.7
8	**FeL2**	**MeOC**	2	1	Acetone	72	40	33	14	42	0.7
9	**FeL2**	**MeOC**	2	1	Acetone:H_2O (3:1)	72	40	11	0.6	5	0.7
10	**FeL14**	**MeOC**	2	1	MeCN	72	40	14	6	43	1.3
11	**FeL14**	**MeOC**	2	1	Acetone	72	40	8	3	38	1.4
12	**FeL14**	**MeOC**	2	1	Acetone:H_2O (3:1)	72	40	9	2	22	0.8
13	**FeL1B**	**MeOC**	2	1	MeCN	72	40	29	5	17	1.1
14	**FeL1B**	**MeOC**	2	1	Acetone	24	40	18	8	44	1.6
15	**FeL1B**	**MeOC**	2	1	Acetone:H_2O (3:1)	24	40	15	3	20	2.9
16	**FeL14**	**MeOC**	2	1	MeCN	24	25	19	3	16	1.3
17	**FeL14**	**MeOC**	2	1	Acetone	24	25	17	4	24	1.2
18	**FeL14**	**MeOC**	2	1	Acetone:H_2O (3:1)	24	25	5	2	40	1.1
19	**FeL14**	**MeOC**	2	1	MeCN	24	5	10	4	40	0.6
20	**FeL14**	**MeOC**	2	1	Acetone	24	5	9	3	33	1.3
21	**FeL14**	**MeOC**	2	1	Acetone:H_2O (3:1)	24	5	6	3	50	0.8

Reaction conditions: In a closed 10 mL vessel, 1 mmol chalcone, 1 mol% [Fe], 4 mL solvent. Conversion of chalcone, epoxide yields and *ee* were determined by HPLC.

Table III-23: Results obtained in the non-heme epoxidation of chalcones **HC** and **MeOC** with an excess of H_2O_2 and AcOH.

Entry	[Fe]	Substrate	H_2O_2 (eq.)	AcOH (eq.)	Solvent	t (h)	T (ºC)	Conv. (%)	Oxirane (%)	Select. (%)	*ee* (%)
1	**FeL2**	**HC**	6	7	Acetone:H_2O (3:1)	24	rt	-	-	-	-
2	**FeL1B**	**HC**	6	7	Acetone:H_2O (3:1)	24	rt	-	-	-	-
3	**FeL2**	**MeOC**	6	7	Acetone:H_2O (3:1)	24	rt	-	-	-	-
4	**FeL1B**	**MeOC**	6	7	Acetone:H_2O (3:1)	24	rt	-	-	-	-
5	**FeL2**	**HC**	6	7	MeCN	24	rt	-	-	-	-
6	**FeL1B**	**HC**	6	7	MeCN	24	rt	-	-	-	-
7	**FeL2**	**MeOC**	6	7	MeCN	24	rt	-	-	-	-
8	**FeL1B**	**MeOC**	6	7	MeCN	24	rt	-	-	-	-
9	**FeL2**	**HC**	6	7	Acetone	24	rt	-	-	-	-
10	**FeL1B**	**HC**	6	7	Acetone	24	rt	-	-	-	-
11	**FeL2**	**MeOC**	6	7	Acetone	24	rt	-	-	-	-
12	**FeL1B**	**MeOC**	6	7	Acetone	24	rt	-	-	-	-

Reaction conditions: In a closed 10 mL vessel, 1 mmol chalcone, 1 mol% [Fe], 4 mL solvent. Conversion of chalcone, epoxide yields and *ee* were determined by HPLC.

Table III-24: Results obtained in the non-heme epoxidation of chalcones **HC** and **MeOC**.

Entry	[Fe]	Substrate	H_2O_2 (eq.)	AcOH (eq.)	Solvent	t (h)	T (ºC)	Conv. (%)	Oxirane (%)	Select. (%)	*ee* (%)
1	**FeL2**	**HC**	2	0.10	Acetone	24	40	27	11	41	0.3
2	**FeL2**	**HC**	2	0.10	MeCN	24	40	47	11	23	3
3	**FeL2**	**HC**	2	0.10	Acetone:H_2O (3:1)	24	40	55	13	24	1.5
4	**FeL2**	**MeOC**	2	0.10	Acetone	24	40	27	14	52	1.8
5	**FeL2**	**MeOC**	2	0.10	MeCN	24	40	44	10	23	0.3
6	**FeL2**	**MeOC**	2	0.10	Acetone:H_2O (3:1)	24	40	47	11	23	10
16	**FeL1B**	**HC**	2	-	Acetone	24	40	54	11	20	7
19	**FeL2**	**MeOC**	2	-	Acetone	24	40	12	6	50	1.9
20	**FeL2**	**MeOC**	2	-	MeCN	24	40	29	8	28	2.2
21	**FeL2**	**MeOC**	2	-	Acetone:H_2O (3:1)	24	40	49	9	18	1.3
23	**FeL1B**	**MeOC**	2	-	MeCN	24	40	54	10	19	2.7
24	**FeL1B**	**MeOC**	2	-	Acetone:H_2O (3:1)	24	40	83	5	6	8.9

Reaction conditions: In a closed 10 mL vessel, 1 mmol chalcone, 1 mol% [Fe], 4 mL solvent. Conversion of chalcone, epoxide yields and *ee* were determined by HPLC.

Some points can be raised to justify the residual epoxide yields obtained. The vast majority of the reported iron complexes, applied as pre-catalysts in this type of non-heme epoxidation reactions, contain ligands with four to five *N*- donor atoms and at least one labile coordination site. Neutral donor ligands such as pyridines and tertiary amines are mainly employed, but there also exist examples of ligands containing O- or S- donor atoms.[151,152,153,154] The ligand structure is of great importance for the electronic properties of the iron center, with the type of donor substituents greatly affecting the stabilization of an *in situ*-formed Fe(III)-OOH intermediate, the precursor of the active oxidising species (see Section **I.3.1**).[151,155] Pyridines or other sp^2 hybridised *N*-donor moieties with some π-accepting character tend to increase the Lewis acidity of the Fe centre, leading to stronger stabilization of this intermediate.[155]

The most used technique for detection and characterization of Fe(III)-OOH species in solution is UV/Vis spectroscopy. In the attempt to detect the formation of this intermediate with the complexes applied in this work, the electronic spectrum of **FeL1B** was measured and an excess of H_2O_2 was added to the complex solution. Spectra were measured immediately after addition of H_2O_2, one hour and 24 h after addition and results are presented in **Figure III-46**.

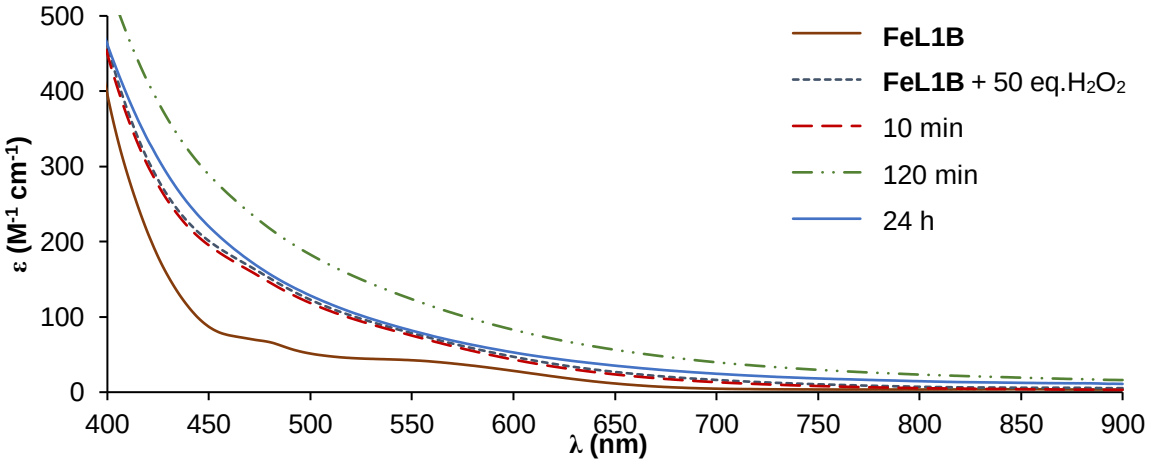

Figure III-46: Electronic absorption (UV-Vis) spectra of compound **FeL1B** (MeCN:H_2O (1:1), 2.6 mM), at room temperature with 1 cm optical path quartz cell, with addition of H_2O_2 (50 eq.).

The absorption profile of **FeL1B** after addition of H_2O_2 slightly increased for the first hour, progressively declining over time after the next 23 hours. The observed results in the absorption intensity of **FeL1B** during this experiment are not in agreement with the reported band behaviour of Fe(III)-OOH intermediates formed *in situ* with Fe(III) complexes bearing *N*-donor ligands (*e.g.* tpa), which typically display an intense absorption band of *ca* 1000 $M^{-1}cm^{-1}$ between 480 and 590 nm, assigned to a HOO→ Fe(III) $p\pi$-$d\pi^*$ CT band.[151] Even considering this observation, the formation of any Fe(III)-OOH species with **FeL1B** should not be discarded, since (i) **FeL1B** and Fe(III) complexes bearing *N*-donor ligands are structuraly different and (ii) it is observed an increase in the absorption spectra of **FeL1B** in the first hour

of experiment, indicating that there exists an interaction with H_2O_2 in solution. Hence, formation of this intermediate, if occurs, may be at a slow rate.

The structure of the amino acid ligand of **FeL1B** may also contribute to the lack or slow formation of Fe(III)-OOH in solution, since it may not efficiently stabilize this intermediate by electron-donation effect to the metal centre, in contrast to the more commonly used *N*-donor ligands derived from pyridines or other sp^2 hybridised moieties.

A final reason for the poor epoxide yields observed can be pointed to the reactivity of benzalacetophenones in the applied catalytic conditions. These substrates typically present a weak nucleophilic character of the conjugated C=C bond, greatly reducing their reactivity with eventual oxidising species formed *in situ*.

For all these reasons, and in accordance with the results obtained, catalytic studies under these conditions were abandoned.

III.5.2.2 – Mukaiyama epoxidation

The catalytic activity of Fe(III) compounds synthesized was tested in the asymmetric epoxidation of **HC** and **MeOC** under Mukaiyama conditions (**Scheme III-15**).

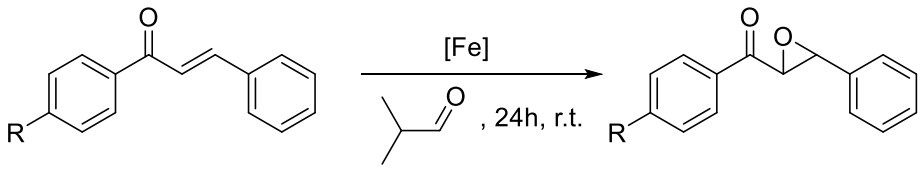

HC: R= H;
MeOC: R= OMe

Scheme III-15: Mukaiyama epoxidation of benzalacetophenones **HC** and **MeOC**.

The first catalytic reactions were carried out in acetone, acetone:H_2O (3:1) and acetonitrile at room temperature for 24 h, using 1 mol% of **FeL1B**, **FeL2** or **FeL3** as pre-catalysts and adding isobutyraldehyde as co-reagent. These catalytic runs allowed to assess the catalytic performance of the Fe(III) complexes used in different solvents and results are summarized in **Table III-25**. Moderate to low yields of epoxide and very low enantioselectivities were observed in all cases. **MeOC** shows to be more prone to catalytic epoxidation in comparison to **HC**. The highest yield of epoxide was obtained when the reaction was carried out in acetonitrile using **FeL1B** as pre-catalyst; 46% and 58% yields were obtained for **HC** and **MeOC**, respectively (**Table III-25**, entries 8 and 11). In the same solvent, residual epoxidation product was obtained with **FeL3**, which can be due to the insolubility of **FeL3** in acetonitrile (**Table III-25**, entries 20

and 23). When the reactions are carried out in acetone, better selectivity towards epoxide formation was achieved in general for both substrates **HC** and **MeOC** and with all pre-catalysts (**Table III-25**, entries 9, 12, 15, 18, 21 and 24), however lower yields of epoxide were obtained in acetone in comparison with acetonitrile (**Table III-25**, see entries 8 and 9 as example of comparison). Propan-1-ol, propan-2-ol and THF are not suitable solvents for these reactions, yielding negligible amounts of epoxide products (**Table III-25**, entries 25 to 27) The Fe(III)-promoted oxidation process of isobutyraldehyde is radicalar and may be compromised in ethers or alcohols, since these solvents are good radical scavengers, which can justify the poor epoxide yields obtained in these solvents.[156] No catalytic reaction was observed when $FeCl_3 \bullet 6H_2O$ was applied as pre-catalyst in acetone (**Table III-25**, entries 5 and 6). Within these Mukaiyama reaction conditions, the presence of an iron complex is necessary for the epoxidation of **HC** and **MeOC**, since the absence of pre-catalyst resulted in very low yields of the respective epoxides (**Table III-25**, entries 1 to 4).

Table III-25: Catalytic epoxidation of **HC** and **MeOC** with Fe(III) compounds **FeL1B** and **FeL3**[a].

Entry	[Fe]	Substrate	Solvent	Conv.[b] (%)	Yield of Oxirane[c] (%)	Selectivity (%)	*ee* (%)
1	-	**HC**	MeCN	18	9	50	-
2	-	**MeOC**	MeCN	33	5	15	-
3	-	**HC**	Acetone	12	4	33	-
4	-	**MeOC**	Acetone	16	3	19	-
5	$FeCl_3$•$6H_2O$	**HC**	Acetone	-	-	-	-
6	$FeCl_3$•$6H_2O$	**MeOC**	Acetone	-	-	-	-
7	**FeL1B**	**HC**	Acetone:H_2O (3:1)	95	18	19	3.3
8	**FeL1B**	**HC**	MeCN	73	46	63	5.6
9	**FeL1B**	**HC**	Acetone	49	28	57	1.6
10	**FeL1B**	**MeOC**	Acetone:H_2O (3:1)	93	26	28	0.0
11	**FeL1B**	**MeOC**	MeCN	79	58	73	2.2
12	**FeL1B**	**MeOC**	Acetone	52	41	79	1.7
13	**FeL2**	**HC**	Acetone:H_2O (3:1)	97	27	28	7.3
14	**FeL2**	**HC**	MeCN	80	39	49	7.5
15	**FeL2**	**HC**	Acetone	37	26	71	2.5
16	**FeL2**	**MeOC**	Acetone:H_2O (3:1)	99	31	31	1.5
17	**FeL2**	**MeOC**	MeCN	83	45	54	3.2
18	**FeL2**	**MeOC**	Acetone	35	34	99	0.3
19	**FeL3**	**HC**	Acetone:H_2O (3:1)	98	18	18	4.1
20	**FeL3**	**HC**	MeCN	2	1	50	0.1
21	**FeL3**	**HC**	Acetone	52	31	60	0.1
22	**FeL3**	**MeOC**	Acetone:H_2O (3:1)	99	22	22	0.1
23	**FeL3**	**MeOC**	MeCN	21	3	14	0.8
24	**FeL3**	**MeOC**	Acetone	56	45	80	0.2
25	**FeL1B**	**MeOC**	Isopropanol	18	-	-	-
26	**FeL1B**	**MeOC**	Propan-1-ol	18	-	-	-
27	**FeL1B**	**MeOC**	THF	37	4	11	-

[a]Reaction conditions: reactions are performed in an open vessel, 1 mmol substrate, 2 eq. isobutyraldehyde, 1 mol% [Fe], 4 mL solvent, r.t., 24 h.[b]Conversions were dertermined by HPLC. [c]Yields of oxirane were determined by HPLC.

The optimization of the catalytic conditions towards epoxide yield was accomplished with **FeL3**, **MeOC** and acetone, and the results are summarized in **Table III-26**. The choice of acetone as solvent for the optimization studies was influenced by the higher selectivity in epoxide formation with this solvent within the catalytic conditions. The first approach focused on the variation of the amount of isobutyraldehyde added with 1 and 2 mol % of **FeL3**, leaving the reaction for 24 h. An increase in epoxide yields was observed when 2 mole equivalents of aldehyde are mixed in the reaction with 2 mol% pre-catalyst (**Table III-26**, entries 2 and 6).

Interestingly, when more than 2 mole equivalents of aldehyde are added, the yields of epoxide decrease when 1 mol % of **FeL3** is used, however, they remain constant with 2 mol % of **FeL3** (**Table III-26**, entries 2 to 4 and 6 to 8). Therefore, the effect of the amount of **FeL3** was evaluated using 2 mole equivalents of isobutyraldehyde. It was concluded that higher yields of epoxide are obtained with 4 mol % of **FeL3**, obtaining an excellent selectivity (**Table III-26**, entries 9, 10 and 11). No significant increase of the epoxide yield was obtained by increasing the reaction temperature and by extending the reaction times under those conditions (**Table III-26**, entries 12 and 13, respectively).

Table III-26: Optimization of the catalytic conditions in the catalytic epoxidation of **MeOC**, using compound **FeL3** as pre-catalyst in acetone.[a]

Entry	FeL3 (mol %)	Isobutyraldehyde (eq.)	T (ºC)	Conv.[d] (%)	Oxirane [e] (%)	Selectivity (%)	*ee* (%)
1[b]	1	1	25	33	27	82	0.3
2[b]	1	2	25	56	45	80	0.2
3[b]	1	3	25	65	38	58	3.8
4[b]	1	4	25	79	35	44	6.0
5[b]	2	1	25	38	27	71	0.2
6[b]	2	2	25	55	43	78	1.0
7[b]	2	3	25	63	43	68	2.1
8[b]	2	4	25	72	42	58	3.1
9[b]	3	2	25	55	45	82	0.4
10[b]	4	2	25	56	51	90	0.2
11[b]	5	2	25	58	45	78	0.2
12[b]	4	2	40	56	48	86	0.1
13[c]	4	2	25	71	46	65	0.2

[a]Reaction conditions: Reactions are performed in an open vessel, 1 mmol **MeOC**, isobutyraldehyde, [Fe], 4 mL acetone. [b]24 h; [c]48 h. [d]Conversions are determined by HPLC. [e]Yields of epoxides are determined by HPLC.

The kinetic profile of the Mukaiyama epoxidation of **MeOC** under the optimized catalytic conditions (4 mol % **FeL3** and 2 eq isobutyraldehyde in acetone) is depicted in **Figure III-47**. The profile revealed that both substrate conversion and product yield achieved their maximum values at the first 12 h of reaction and maintain their values (~60% and ~50%, respectively) with slight oscillations for the next 6 h. (**Figure III-47** and **Table III-27**, entry 4). Addition of 2 mole equivalents of isobutyraldehyde after 12 h of reaction had a positive effect, increasing the conversion to 80%. Epoxide yield, on its turn, saw a slight decrease on its value in the first hour and then continuously increased to 64% for the next 5 h, maintaining this value till the end of the experiment. (see **Figure III-47** and **Table III-27**, entry 9).

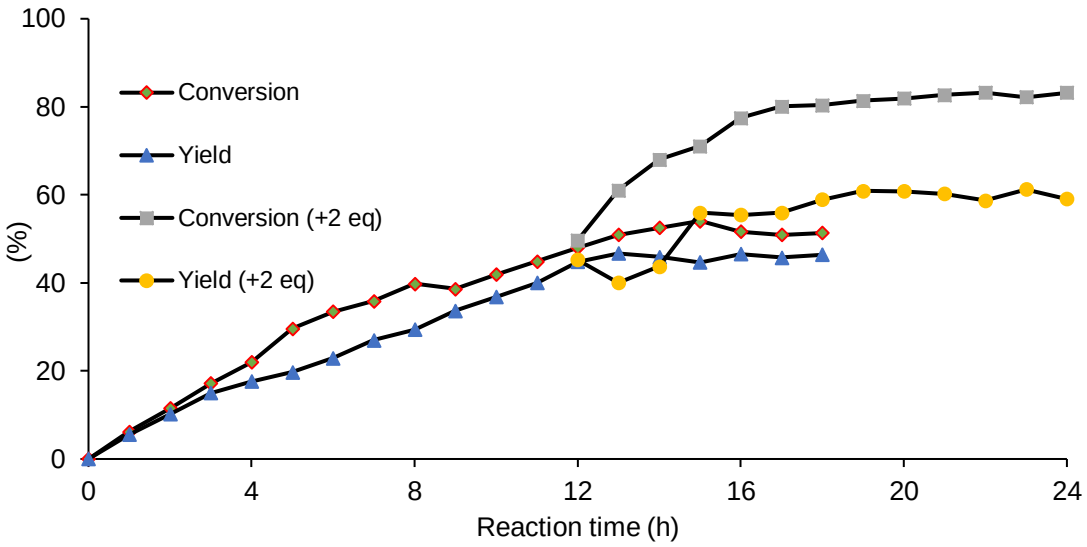

Figure III-47: Reaction profile of the epoxidation of **MeOC** in 4 mL acetone with 4 mol% of **FeL3** as pre-catalyst at 25ºC and [a]2 eq. of isobutyraldehyde, 18h (♦ and ▲); [b]2 eq. of isobutyraldehyde and additional 2 eq. after the first 12 h of reaction (■ and ●).

Under the optimized catalytic conditions **HC** and **MeOC** were epoxidised in acetone and MeCN, with and without additional 2 mole equivalents of isobutyraldehyde after 12 h of reaction. The obtained results are showed in **Table III-27**.

The results observed without further addition of 2 mole equivalents of isobutyraldehyde (**Table III-27**, entries 1 to 8) were firstly compared with the preliminary results presented in **Table III-25** and the following observations were made: (i) no major differences are observed regarding conversion values for both substrates in acetone, but in MeCN there is a decrease of both substrate conversions in 7% for **HC** and 8% for **MeOC** with **FeL1B** as pre-catalyst; (ii) the epoxide yield values have a slight increase in acetone with both **FeL1B** and **FeL3** (4% for **HC**, 6% for **MeOC**) but remained very similar for both substrates in MeCN; (iii) selectivity towards epoxide formation increased between 8 to 15% with the new reaction conditions for both substrates; (iv) *ee* values obtained were very low.

When comparing both substrates uder the optimized conditions, **MeOC** display an overall higher reactivity (see **Table III-25**) with higher substrate conversion, yield of epoxide and selectivity towards epoxide formation, although both **HC** and **MeOC** exhibit similar reactivity in acetone (49% both **HC** and **MeOC**). In general, **FeL1B** showed better performance as pre-catalyst in comparison to **FeL3** with both substrates. Higher epoxide yields were obtained with **FeL1B** in MeCN (48 and 61% for **HC** and **MeOC**, respectively). **MeOC** showed higher selectivity in epoxide formation with **FeL1B** in acetone (94%), even affording a high selectivity in MeCN (85%).

The results obtained by the addition of 2 mole equivalents of isobutyraldehyde after 12 h of reaction (**Table III-27**, entries 9 to 16) were compared with the results observed without additional 2 mole equivalents of isobutyraldehyde (**Table III-27**, entries 1 to 8). A decrease in substrate conversion and epoxide yield was observed with **FeL3** as pre-catalyst in acetone with additional aldehyde (**Table III-27**, entry 10). In contrast to the observed with **FeL3**, epoxidation of **HC** with **FeL1B** showed a major increase in epoxide yield in acetone (from 32 to 52%, **Table III-27** entries 1 and 9), and no apparent change was observed in MeCN (**Table III-27**, entries 5 and 13); epoxidation of **MeOC** has an increase of epoxide yields in acetone of 17 and 9%, respectively, with **FeL1B** and **FeL3**, with no apparent change in activity in MeCN. Overall, the conversion of **HC** and **MeOC** increased between 15 and 32% with additional 1 mole equivalents of aldehyde and selectivity towards epoxide formation decreased, with exception to the previously mentioned example of **HC** catalysed by **FeL3** in acetone.

Table III-27: Application of the optimized catalytic conditions in the epoxidation of **HC** and **MeOC** with **FeL1B** and **FeL3** as pre-catalysts.

Entry	[Fe]	Substrate	Solvent	Conv. (%)	Oxirane (%)	Selectivity (%)	*ee* (%)
1[a]	**FeL1B**	**HC**	Acetone	49	32	65	0.1
2[a]	**FeL3**	**HC**	Acetone	49	35	71	0.2
3[a]	**FeL1B**	**MeOC**	Acetone	50	47	94	0.3
4[a]	**FeL3**	**MeOC**	Acetone	56	51	91	0.2
5[a]	**FeL1B**	**HC**	MeCN	65	48	74	0.2
6[a]	**FeL3**	**HC**	MeCN	2	1	50	0.2
7[a]	**FeL1B**	**MeOC**	MeCN	72	61	85	0.3
8[a]	**FeL3**	**MeOC**	MeCN	9	1	11	0.2
9[b]	**FeL1B**	**HC**	Acetone	64	52	81	0.1
10[b]	**FeL3**	**HC**	Acetone	23	16	70	1.1
11[b]	**FeL1B**	**MeOC**	Acetone	82	64	78	0.9
12[b]	**FeL3**	**MeOC**	Acetone	74	60	81	0.5
13[b]	**FeL1B**	**HC**	MeCN	92	52	57	1.0
14[b]	**FeL3**	**HC**	MeCN	8	1	13	0.2
15[b]	**FeL1B**	**MeOC**	MeCN	98	63	64	0.1
16[b]	**FeL3**	**MeOC**	MeCN	8	1	13	-

Catalytic conditions: In an open vessel, 1 mmol substrate, 2 eq, isobutyraldehyde, 4 mol % [Fe], 4 mL solvent, r.t.. [a] 24 h; [b] addition of 2 more eq. isobutyraldehyde after the first 12 h in a 24 h reaction.

Finally, the catalytic performance of all the prepared Fe(III) complexes was evaluated in the epoxidation of **MeOC** with the addition of 2 mole equivalents of isobutyraldehyde after 12 h of reaction. Results are presented in **Table III-28**.

In general, higher conversions and epoxide yields are detected in MeCN for all Fe(III) compounds, in exception to **FeL3** and **FeL10**. All complexes show maximum selectivity towards epoxide formation in MeCN, with exception for **FeL1B**, **FeL2**, **FeL3**, and **FeL14**. Complexes **FeL1B**, **FeL2**, **FeL11**, **FeL14** and **FeL15** afford the highest epoxide yield values ranging between 58 and 64% in MeCN; the observed yields with these compounds are substantially higher than previous reported values in the literature[157] in metal-free one-pot epoxidation procedures of **MeOC**. Between all complexes, the most active is **FeL11**, with excelent selectivities in both solvents (up to 96% in MeCN), but closely followed by **FeL1B**, **FeL2**, **FeL14** and **FeL15**; very low to non-existent epoxide yields were observed with complexes bearing amino acid-phenol ligands, either in acetone or MeCN (**FeL5**-**6** and **FeL8**-**10**, see entries 9 to 18 in **Table III-28**). This evidence can indicate that amino acid-phenol ligands might exert an inhibitor effect in the epoxidation of **MeOC** under these conditions.

To finalize, the *ee* values for all complexes were very low to non-existent in all the tested conditions. This may be in part justified with the lack of influence of the metal pre-catalyst in inducing chirality to the final epoxide product during the catalytic cycle, since no coordination of the substrate to the metal centre is predicted, judging by the **Scheme I-22** in Section **I.3.2**; the main role of the metal pre-catalyst is in the initiation of the catalytic cycle and in the stabilization of the *in situ*-formed peroxy radical species. The chiral induction might be directly related with the structures of the complex, substrate and aldehyde used.

Table III-28: Application of the optimized catalytic conditions in the epoxidation of **MeOC** with all the prepared Fe(III) complexes as pre-catalysts.

Entry	[Fe]	Solvent	Conv. (%)	Oxirane (%)	Selectivity (%)	*ee* (%)
1	**FeL1A**	Acetone	73	40	55	3.1
2	**FeL1A**	MeCN	71	41	58	0.1
3	**FeL1B**	Acetone	50	47	94	0.9
4	**FeL1B**	MeCN	72	61	85	0.1
5	**FeL2**	Acetone	80	61	76	0.3
6	**FeL2**	MeCN	96	64	67	0.1
7	**FeL3**	Acetone	56	51	91	0.5
8	**FeL3**	MeCN	9	1	11	-
9	**FeL5**	Acetone	5	1	20	0.8
10	**FeL5**	MeCN	14	2	14	0.4
11	**FeL6**	Acetone	0.9	0.2	22	0.9
12	**FeL6**	MeCN	5	4	80	0.2
13	**FeL8**	Acetone	-	-	-	-
14	**FeL8**	MeCN	10	3	30	4.3
15	**FeL9**	Acetone	-	-	-	-
16	**FeL9**	MeCN	13	1	8	1.4
17	**FeL10**	Acetone	-	-	-	-
18	**FeL10**	MeCN	-	-	-	-
19	**FeL11**	Acetone	48	44	92	0.6
20	**FeL11**	MeCN	67	64	96	0.7
21	**FeL13**	Acetone	92	26	28	0.2
22	**FeL13**	MeCN	98	35	36	0.4
23	**FeL14**	Acetone	77	52	68	4.1
24	**FeL14**	MeCN	96	60	63	1.3
25	**FeL15**	Acetone	90	52	58	1.2
26	**FeL15**	MeCN	95	58	61	1.7

Catalytic conditions: In an open vessel, 1 mmol **MeOC**, 4 mol % [Fe], 4 mL solvent, 2 eq isobutyraldehyde and addition of 2 more eq. isobutyraldehyde after the first 12 h in a 24 h reaction.

III.5.3 – Oxidation of 1-phenylethan-1-ol

The oxidation of primary and secondary alcohols to aldehydes and ketones, respectively, has proven to be an important and relevant chemical transformation in biological and industrial reactions. Although apparently simple, alcohol oxidation typically requires the use of selective oxidants, especially in the case of primary alcohols in obtaining the respective aldehydes in detriment of the corresponding carboxylic acid. The dominant chemical processes in classical Organic Chemistry include the use, for example, of pyridinium chlorochromate, potassium

permanganate or hypervalent iodide sulfoxides as terminal oxidants. These are toxic compounds which require specific care in waste treatments resultant from these procedures. Therefore, the use of more economically and ecologically viable procedures has become a subject of interest in the oxidation of alcohols.

More recent work has focused on molecular oxygen as an inexpensive and environmentally benign alternative to the referred terminal oxidants. Palladium-mediated procedures were among the first examples of organometallic catalytic aerobic alcohol oxidation.[158] However, copper[159] and vanadium[38] catalysts have emerged as attractive, inexpensive, and readily-available alternatives. Several other metals such as ruthenium, iridium or cobalt have also been investigated, with varying degrees of success.[50,160] Regarding iron-mediated oxidation of alcohols, some relevant works have been published in the literature, especially in the attempt to develop processes capable of mimicking heme and non-heme oxygenases.[161,162,163,164] In light of the importance of this oxidation process,it was attempted to evaluate the catalytic potential of the Fe(III) complexes in the oxidation of 1-phenylethan-1-ol.

More recently, Royo and co-workers[165] presented the oxidation of 1-phenylethan-1-ol with iron(II) bis-heterocyclic carbene complexes as pre-catalysts precursors. It was decided to reproduce the synthetic conditions applied in the work developed by Royo and co-workers[165] with the Fe(III) complexes prepared in this thesis. To the best of knowledge, this is the first example of amino acid-derived Fe(III) complexes applied as pre-catalysts in oxidation of alcohols.

The oxidation of 1-phenylethan-1-ol (PhEtOH) was studied with all the prepared Fe(III) complexes using TBHP as oxidant, illustrated in **Scheme III-16**.

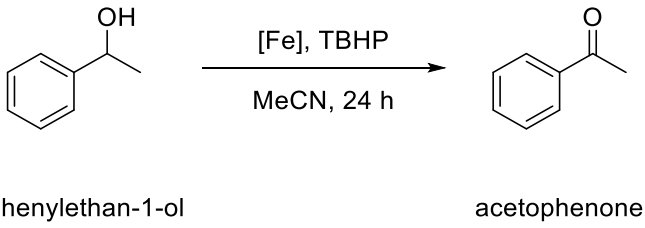

Scheme III-16: Oxidation of 1-phenylethan-1-ol with TBHP and iron complexes.

The preliminary studies were conducted relatively to PhEtOH with 2 mol% **FeL1A**, **FeL1B**, and **FeL2** in MeCN with 0.75 mol% TBHP at 80ºC for 24 h. Results are presented in **Table III-29**. Very good to excelent conversions of PhEtOH were obtained with moderate acetophenone yields (up to 62% with **FeL1A**, **Table III-29** entries 1 to 3). Changing the amount of **FeL2** from 2 to 5 mol% resulted in a decrease of acetophenone obtained in 17% (compare entries 3 and 4 of **Table III-29**), and for this reason a screening was made to all complexes in MeCN with 2

mol% of added complex. In general, good to excelent conversions and low to good ketone yields were observed, with the best results being obtained with **FeL13** (**Table III-29**, entries 5 to 15).

Compound **FeL13** was then applied as pre-catalyst precursor to optimize the reaction conditions. Acetophenone yields obtained with 1 or 2 mol% of **FeL13** were nearly identical, therefore these optimization studies were carried out with 1 mol % **FeL13** (compare entries 12 and 15 of **Table III-29**). The reaction temperature was optimized by varying it from 25 to 80ºC in reactions running for 24 h; excelent conversions of PhEtOH were observed in all the experiments, with the highest yield being obtained at 60ºC (86%, see entry 16 of **Table III-29**). The same experiments were executed with 0.75 mol% H_2O_2 as oxidant, but only low ketone yields were observed (**Table III-29**, entries 19 to 22).

Table III-29: Preliminary catalytic studies in the oxidation of 1-phenylethan-1-ol using TBHP as oxidant.

Entry	[Fe]	Oxidant	T (ºC)	Conv. (%)	Yield (%)	Selectivity (%)
1[a]	**FeL1A**	TBHP	80	99	62	63
2[a]	**FeL1B**	TBHP	80	86	38	44
3[a]	**FeL2**	TBHP	80	98	57	58
4[b]	**FeL2**	TBHP	80	70	40	57
5[a]	**FeL3**	TBHP	80	99	52	53
6[a]	**FeL5**	TBHP	80	98	55	56
7[a]	**FeL6**	TBHP	80	99	59	60
8[a]	**FeL8**	TBHP	80	84	55	65
9[a]	**FeL9**	TBHP	80	79	26	33
10[a]	**FeL10**	TBHP	80	85	37	44
11[a]	**FeL11**	TBHP	80	76	34	45
12[a]	**FeL13**	TBHP	80	99	72	73
13[a]	**FeL14**	TBHP	80	98	48	49
14[c]	**FeL15**	TBHP	80	99	30	30
15[c]	**FeL13**	TBHP	80	99	75	76
16[c]	**FeL13**	TBHP	60	99	86	87
17[c]	**FeL13**	TBHP	40	99	72	73
18[c]	**FeL13**	TBHP	25	95	59	62
19[c]	**FeL13**	H_2O_2	80	30	8	27
20[c]	**FeL13**	H_2O_2	60	38	8	21
21[c]	**FeL13**	H_2O_2	40	24	9	38
22[c]	**FeL13**	H_2O_2	25	45	15	33

Reaction conditions: In a sealed tube, 1 mmol 1-phenylethan-1-ol, 0.75 mol% oxidant, 0.8 mL MeCN, 24 h.[a] 2 mol% [Fe] complex; [b] 5 mol% [Fe] complex; [c] 1 mol% [Fe] complex. Acetophenone yields calculated considering the 1-phenylethan-1-ol converted. Conversion and yield values were determined by GC.

Under the optimized conditions, several complexes with different families of ligands coordinated were tested as pre-catalysts and results are presented in **Table III-30**. The reaction profile over time was studied and is presented in **Figure III-48**, it was observed that after 4 h of reaction, PhEtOH was completely converted with acetophenone yields up to 99% with **FeL3**. Excelent ketone yield values were obtained with **FeL1A**, **FeL2** and **FeL13**, but low yields were observed with **FeL5** and **FeL10**.

Table III-30: Catalytic oxidation of 1-phenylethan-1-ol with TBHP under the optimized conditions.

Entry	[Fe]	T (ºC)	Conv. (%)	Yield (%)	Selectivity (%)
1	**FeL1A**	60	98	95	97
2	**FeL2**	60	97	88	91
3	**FeL3**	60	99	99	100
4	**FeL5**	60	31	26	84
5	**FeL10**	60	9	3	33
6	**FeL13**	60	99	94	95

Reaction conditions: In a sealed tube, 1 mmol 1-phenylethan-1-ol, 1% [Fe] complex, 0.75 mol% TBHP, 0.8 mL MeCN, 60ºC, 4 h. Conversion and yield values were determined by GC.

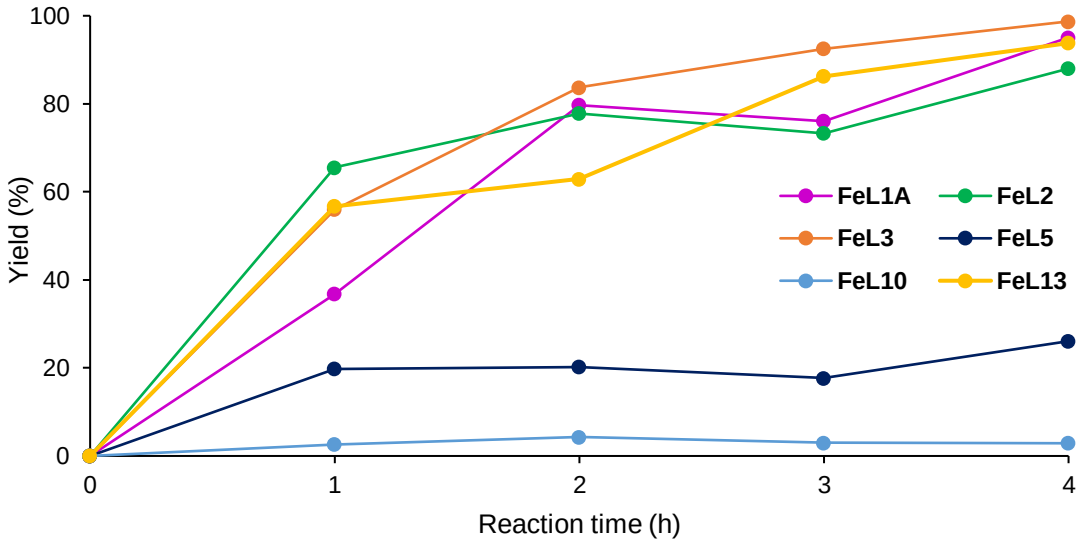

Figure III-48: Reaction profile of the catalytic oxidation of 1-phenylethan-1-ol under the optimized conditions: In a sealed tube, 1 mmol 1-phenylethan-1-ol, 1 mol% [Fe] complex, 0.75 mol% TBHP, 0.8 mL MeCN, 60ºC, 4 h.

The results presented in **Table III-30** and **Figure III-48** show that iron(III) complexes bearing amino acid ligands with pyridyl donor groups to be very active in the oxidation of PhEtOH to acetophenone under the tested conditions. Contrasting with these results, compounds containing amino acid phenol ligands such as **FeL5** or **FeL10** proved to be much less active as pre-catalysts in these reactions in the same conditions.

III.6 – Conclusions

Several Fe(III) complexes containing amino acid-pyridyl, amino acid phenol, amino acid-pyridyl-phenol or amino acid-methoxybenzene ligands were synthesized using simple and mild one-pot conditions, one of the main objectives of this work. All compounds were isolated as solids with distinct colours depending on the coordinating ligands or co-ligands.

Characterization of the Fe(III) complexes was made by UV-Vis and CD spectroscopy, ESI-MS, FTIR, Cyclic Voltammetry and elemental analysis. Compounds **FeL1B**, **FeL3** and **FeL14** afforded crystals suitable for single crystal X-ray diffraction analysis. All the compounds were shown to be chiral and depict CD spectra in solution. The ESI-MS spectra analysis confirmed the existence of the mononuclear Fe(III) species prepared for each complex, but also the presence of oligonuclear species and dissociacion of the amino acid ligand from the metal centre, under the conditions applied in the experiments. In general, compounds containing amino acid-phenol ligands showed simpler spectra, especially in the negative mode. The Infrared spectroscopy data is compatible with the formulations proposed for the Fe(III) complexes; bands assigned to symmetric Fe-OAc-Fe stretching vibrations and Fe-OH-Fe bending vibrations were detected in **FeL2**, **FeL5**, **FeL6**, **FeL11**, **FeL13** and **FeL14**, indicating the presence of μ-hydroxido- and μ-acetato-bridged species in these compounds. Single crystal X-ray diffraction analysis for **FeL1B** and **FeL3** confirmed a chiral mononuclear species, while **FeL14** showed a chiral dinuclear μ-hydroxido-μ-acetato-bridged species. Cyclic Voltammetry showed that Fe(III) complexes display one cathodic quasi-reversible process at potentials in the range -0.16 to -0.68 V, except **FeL2**, **FeL15** and compounds containing amino acid-phenol and amino acid-methoxybenzene ligands. The magnetic susceptibility of the Fe(III) complexes was measured with the Evans NMR method, confirming that all compounds possess μ_{eff} values consistent with those expected for high-spin ($S=^5/_2$) Fe(III) complexes, except **FeL2** and **FeL11** with μ_{eff} values consistent with antiferromagnetic coupling.

All the synthesized Fe(III) complexes were used as pre-catalyst presursors in the asymmetric aerobic oxidative coupling of 2-naphthol and 3-bromo-2-naphthol, epoxidation of benzalacetophenones and oxidation of 1-phenylethan-1-ol.

In the asymmetric aerobic oxidative coupling of 2-naphthol, catalytic reactions were studied regarding BINOL yields obtained, selectivity in BINOL formation and enantioselectivity. No BINOL products were formed in the absence of air or Fe(III) complex and reactions running in other solvents such as MeCN, EtOH:H_2O, AcOEt, propan-2-ol, THF or H_2O did not yield BINOL product. No oxidants other than air were tested. From all the tested catalytic conditions those who afforded better general results were performed in toluene at 60ºC for 72 h, with 1 to 5

mol% of iron complex as pre-catalysts; low BINOL yields (up to 29%) were obtained in the preliminary reactions. Utilization of additives was tested to improve reaction outcomes, and the most relevant results were obtained by adding weak organic bases within the preliminary conditions with **FeL2** and **FeL14** as pre-catalysts. In general, an increase in BINOL yields and selectivity in BINOL formation was detected with both complexes, but the most relevant results in terms of enantioselectivity towards (a*S*)-BINOL were obtained with **FeL2** (up to 39% *ee*) and (a*R*)-BINOL with **FeL14** (up to 17% *ee*). In general, compounds **FeL2** and **FeL14** depicted the best catalytic results with the optimized conditions, with **FeL13** presenting similar results to those obtained with **FeL14**. The effect of the added base was also studied and it was suggested to be due to the activation of the substrate rather than to the coordination to the metal centre. Stronger bases such as Et_3N should be avoided since they can promote the formation of undesired secondary products, greatly decreasing the selectivity in the formation of BINOL. For the asymmetric oxidative coupling of 3-bromo-2-naphthol under the optimized conditions, enantioselectivities up to 85% were obtained for (a*S*)-BrBINOL formation with 10 mol% **FeL2** and 1 mol% Phen, but with only residual BrBINOL yield values of 15%. With this substrate these catalytic conditions proved to be more selective for the formation of (a*S*)-BrBINOL, independently of the Fe(III) compound used, indicating that the substituent present at C3 position of 2-naphthol may contribute to the enantioselectivities observed. A catalytic cycle was proposed considering the observed data in this work as well as the information gathered in the literature. Globally, the catalytic studies developed herein represent a good alternative as a sustainable asymmetric oxidative coupling procedure of 2-naphthol and substituted derivatives, because (i) the iron(III) compounds used as pre-catalysts are synthesized in one-pot procedures with environmentally-friendly conditions and reagents; (ii) the oxidant tested in the catalytic reactions was air; (iii) both **FeL2** and **FeL14** by adding weak organic bases.

In the epoxidation of benzalacetophenones, the prepared Fe(III)-complexes proved to be inefficient in mimicking non-heme oxygenases for the epoxidation of **HC** and **MeOC**, using a hydrogen peroxide-acetic acid system. Under the applied conditions (2 mole equivalents H_2O_2, 10 mol% AcOH in MeCN), very low epoxide yields were obtained and some reasons may justify these result: (i) benzalacetophenones are not very reactive in the applied catalytic conditions; (ii) the formation of Fe(III)-OOH species is not discarded, it might be formed at a slow rate; (iii) the amino acid ligands may not stabilize effectively the Fe(III)-OOH intermediate, if formed. Under Mukaiyama conditions, the Fe(III) complexes proved to be active in the epoxidation of benzalacetophenones. Epoxide yields and conversions were moderate, with good selectivities towards epoxide formation in acetone and MeCN for both substrates after optimization of the catalytic conditions. The presence of water in the reaction medium

drastically decreased epoxide formation and reaction occurring in THF or alcohols yielded poor results. **MeOC** shows higher reactivity than **HC**, which can be related to the higher electron-density of the unsaturated α-β double bond, caused by the resonance-based electron donating effect exerted by the methoxyl group, thus rendering it more reactive (more nucleophilic) in a Sharpless-type epoxidation mechanism. In the optimized conditions without additional aldehyde, substrate conversions and epoxide yields attain their maximum values after 12 h of reaction. Further addition of 2 mole equivalents of aldehyde instead to a general increase in substrate conversion and epoxide yields. This procedure has a more significant impact for **HC** epoxidation in acetone with **FeL1B** as pre-catalyst, increasing in 20% the epoxide yield when compared with the first 12 h of reaction. The same is observed for **MeOC** epoxidation in acetone with **FeL1B** or **FeL3** as pre-catalyst. The optimized conditions were tested to all complexes in the epoxidation of **MeOC**, showing **FeL11** as the best pre-catalyst with good yields and excelent selectivities in both solvents. Complexes bearing amino acid-phenol ligands, **FeL5**-**6** and **FeL8**-**10** present low activities as demonstrated by the low yields of epoxide. Thus, it can be concluded that complexes bearing amino acid-pyridyl and amino acid-pyridyl-phenol ligands are, in general, reliable alternatives as pre-catalysts in the epoxidation of benzalacetophenones under Mukaiyama conditions.

The synthesized Fe(III) complexes proved to be excelent pre-catalysts in the oxidation of 1-phenylethan-1-ol to acetophenone with TBHP as oxidant in MeCN, and to the present knowledge these compounds represent the first examples of amino acid-derived Fe(III) complexes applied in the oxidation of alcohols. At 60ºC, excelent yields of acetophenone (up to 99%) were obtained with **FeL1A**, **FeL2**, **FeL3** and **FeL13** after 4 h of reaction in a closed vessel. Hydrogen peroxide was less effective as oxidant, presenting very low acetophenone yields. Under the optimized conditions with TBHP, compounds **FeL5** and **FeL10** showed lower activity as pre-catalysts, affording only very low acetophenone yields. The observed differences may be related with the ligand structures of both these complexes, containing a phenolate donor group and lacking a pyridyl moiety. These results confirm that, within the applied conditions, the iron(III) complexes bearing pyridyl donor group can be an interesting alternative for the oxidation of 1-phenylethan-1-ol.

III.7 – Experimental section

III.7.1 – General considerations

All Fe(III) compounds synthesis, isolation and purification were done without air exclusion. If not mentioned, all solvents and reagents were purchased from commercial suppliers and used as received.

III.7.1.1 – Target catalytic substrates and desired products

The target catalytic product BrBINOL was synthesized by adapting previously reported procedures,[9] in order to be used in the calibration curve of the product for the control of catalytic reactions. Substrates **HC** and **MeOC** were syntesized by adapting previously reported Claisen-Schmidt condensation procedures.[166] The target catalytic products **HC** oxide and **MeOC** oxide were also prepared according to previously reported Weitz-Scheffer epoxidation procedures,[157] in order to be used in the calibration curve of the products for the control of catalytic reactions. The preparation of all the referred compounds is described in Section **III.7.5**.

III.7.1.2 – Dry milling procedure in the preparation attempt of FeL2

The dry milling technique was executed by MSc. Marta Alexandre at Centro de Química Estrutural of Instituto Superior Técnico in a PM100/200 Retsch GmbH planetary ball mill equipment, equipped with a 250 mL grinding bowl and 10 stainless steel balls of 10 mm size for homogenization. The rotational speed was 450 rpm, with rotational inversions every 5 minutes. **L2** and $FeCl_3$•$6H_2O$ mixture (10 mmol each) was prepared in the absence of any added solvent (dry milling). The amount of **L2** and $FeCl_3$•$6H_2O$ used were previously weighted and directly added to the reactor.

III.7.2 – Characterization Techniques

III.7.2.1 – UV-Vis and CD Spectroscopy

UV-Vis spectra were recorded using a Shimadzu U-2000 spectrophotometer. CD spectra were recorded using a Jasco J-720 Spectropolarimeter.

III.7.2.2 – X-Ray Crystallography

Single crystals suitable for X-ray diffraction crystallography were obtained as described in the ligand preparation methods. Crystals of **FeL1B, FeL3** and **FeL14** were selected, covered with

polyfluoroether oil, and mounted on a nylon loop by PhD Clara Gomes at Centro de Química Estrutural of Instituto Superior Técnico. Crystallographic data was collected using graphite monochromated Mo-Kα radiation (λ=0.71073 Å) on a Bruker AXS-KAPPA APEX II diffractometer, at room temperature. Cell parameters were retrieved using Bruker SMART software and refined using Bruker SAINT on all observed reflections. Absorption correction was applied using SADABS.[167] Structure solution and refinement were performed using direct methods with the programs SHELXT 2014/5[168] and SIR2014[169] included in the package of programs WINGX-Version 2014.1[170] and SHELXL.[167,171] All hydrogen atoms were inserted in idealised positions and allowed to refine riding on the parent carbon atom with C–H distances of 0.93 Å, 0.96 Å, 0.97 Å and 0.98 Å for aromatic, methyl, methylene and methine H atoms, and with Uiso(H) = 1.2Ueq(C). All structures refined to convergence, even though the crystals of **FeL1B** and **FeL14** were of poorer quality displaying high R_{int} and poor diffracting power. Complexes **FeL1B** was refined as a 2-component inversion twin, leading to a BASF parameter of 0.11. Graphic presentations were prepared with ORTEP-III,[170] at the 30% probability level, and with Mercury CSD 3.9.[172]

Table III-31: Crystal data and structure refinement for compounds **FeL1B**, **FeL3** and **FeL14**.

Compound	**FeL1B**	**FeL3**	**FeL14**
Formula	$C_{21}H_{19}ClFeN_3O_4$	$C_{23}H_{20}ClFeN_4O_4$	$C_{62}H_{77}Fe_2N_4O_{10}$
M	468.69	507.73	1149.97
λ (Å)	0.71073	0.71073	0.71073
T (K)	293(2)	293(2)	293(2)
crystal system	Tetragonal	orthorhombic	Monoclinic
space group	$P4_3\,2_1\,2$	$P2_1\,2_1\,2_1$	*C*2/*c*
a (Å)	9.4520(10)	10.8194(5)	35.146(4)
b (Å)	9.4520(10)	11.7722(5)	14.5114(16)
c (Å)	45.144(5)	17.8400(9)	28.365(3)
α (deg)	90	90	90
β (deg)	90	90	108.143(4)
γ (deg)	90	90	90
V (Å^3)	4033.1(10)	2272.25(18)	13747(3)
Z	8	4	8
ρ_{calc} (g cm^{-3})	1.544	1.484	1.111
μ (mm^{-1})	0.914	0.819	0.474
θ_{max} (deg)	25.805	26.083	25.942
total data	77532	12632	266205
unique data	3882	4486	13280
R_{int}	0.2394	0.0654	0.3883
R [I>3σ(I)]	0.1393	0.0389	0.0931
wR_2	0.3298	0.0734	0.2124
Goodness of fit	1.167	0.985	1.045
ρ min	-0.920	-0.274	-0.725
ρ max	2.267	0.308	0.416

III.7.2.3 – Electrospray Ionization Mass Spectrometry (ESI-MS)

The ESI mass experiments were made by Prof. Maria da Conceição Oliveira and MSc. Ana Dias at Centro de Química Estrutural of Instituto Superior Técnico. The ESI mass spectra were obtained on a LCQ Fleet ion trap mass spectrometer equipped with an electrospray ion source, operated in the positive and negative mode. The operated parameters were optimized for maximum abundance of the ions of interest, as follows: ion spray voltage, +5 kV; capillary voltage, 5/-20 V; tube lens offset, -125/63 V, sheath gas (N_2), 20 arbitrary units; capillary temperature, 275ºC. Spectra obtained are the average results from 20 to 35 scans, and were saved within the range 100-2000 Da.

III.7.2.4 – Infrared Spectroscopy (FT-IR)

FT-IR spectra were recorded in KBr disks using a JASCO FT/IR-430 spectrometer. The frequency corresponding to the maximum absorption is presented in cm^{-1}, followed by the molecular group attributed and band intensities: s (strong), m (medium), w (weak), b (broad).

III.7.2.5 – Elemental Analysis

Elemental analyses were carried out at Laboratório de Análises of Instituto Superior Técnico, using a Perkin Elmer EA110 CE automatic analyzer Instrument. The results presented are the average values obtained from two independent determinations.

III.7.2.6 – Cyclic Voltammetry

The redox properties were studied by Cyclic Voltammetry (under nitrogen) using a three-compartment cell, equipped with Pt electrodes using a Radiometer Analytical Voltammetry PST050 VoltaLab equipment, interfaced with a computer. The cyclic voltammograms were obtained in a $[Bu_4N][BF_4]$ solution (0.10 M) of DMSO, DMF or MeCN, depending on the analysed Fe(III) compound. All solvents were distilled and dried with molecular sieves before use. The potentials (±10 mV) are quoted *versus* the saturated calomel electrode (SCE) and measured at 200 mV s^{-1} using ferrocene ($[Fe(\eta^5\text{-}C_5H_5)_2]^{0/+}$, $E_{1/2}^{ox}$=0.440, 0.470 and 0.382 V in DMSO, DMF and MeCN, respectively) as an internal reference.

III.7.2.7 – Magnetic Susceptibility

The magnetic susceptibilities of the prepared Fe(III) compounds were measured applying the Evan's method. To a NMR tube containing a capillary tube with pure deuterated solvent was added a solution of Fe(III) complex, with known concentration (*ca*. 10 mM). ^{1}H-NMR spectra were recorded on a Bruker Advance II+ 300 MHz (UltraShield Magnet) instrument at ambient temperature.

III.7.2.8 – Nuclear Magnetic Resonance Spectroscopy (NMR)

The target catalytic substrates and desired products were characterized by NMR. 1D NMR (^{1}H, ^{13}C-{1H} APT) and 2D NMR (HSQC and HMBC) spectra were recorded on Bruker Advance II+ 300 MHz (UltraShield Magnet) instruments at room temperature. ^{1}H and ^{13}C chemical shifts (δ) are expressed in ppm relative to Me_4Si or the solvent residual peak. Whenever calculation is possible, coupling constants *J* are given in Hz and multiplicities are presented as: s (singlet), d (doublet), dd (doublet of doublet), t (triplet), q (quartet) and m

(multiplet). Carbons identified as C_{ipso} by ^{13}C-{1H} APT, HSQC and HMBC are quaternary carbons.

III.7.3 – Catalytic studies

III.7.3.1 – Techniques applied in the control of catalytic reactions

III.7.3.1.1 – High Performance Liquid Chromatography (HPLC)

The analyses of the products obtained in catalytic oxidative coupling and epoxidation reactions were done by HPLC using a Jasco system equipped with a Daicel Chiralpak IA column, a 870-UV Intelligent UV-Vis detector, two 880-PU Intelligent HPLC Pumps, a 2-line degasser 880-51 and a Rheodyne 725i injector (5 µL). The system uses Borwin software for data acquisition and analysis. The calibration of each reagent and product was performed by single point calibration, using an internal standard. Detection wavelength, eluent mixtures and internal standards used will be specified in each case.

III.7.3.1.2 – Gas Chromatography (GC)

The analyses of the products obtained in catalytic oxidation of 1-phenylethan-1-ol were done by GC using a Thermo Scientific Trace 1300 Gas Chromatograph and a Thermo Scientific AS 3000 auto-sampler injector. The system uses Thermo Xcalibur software for data acquisition and analysis. The calibration of PhEtOH and acetophenone was performed using a calibration curve obtained from different concentrations of each compound.

III.7.3.2 – General procedures for the asymmetric oxidative coupling of 2-naphthol

The catalytic experiments were carried out at constant temperature in an opened or closed 50 mL Schlenck tube, equipped with magnetic stirrer. In a typical run, substrate (2-naphthol or 3-bromo-2-naphthol, 1.0 mmol), Fe(III) complex (1.0 to 5.0 mol %) and additive (1.0 to 85 mol %) were mixed in the respective solvent (4 mL). The reaction mixture was magnetically stirred during the catalytic run (up to 192 h) at the given temperature (25 to 60ºC). Control experiments were carried out in the absence of pre-catalyst. The analysis of coupling products was performed by HPLC with a detection wavelength of 254 nm. The eluent used was *n*-heptane:propan-1-ol (8:2) with a flow rate of 1.0 mL min^{-1}. Before analysis by HPLC, 1 mmol of acetophenone (internal standard) and 4 mL EtOH were added to the reaction mixture.

III.7.3.3 – General procedures for the epoxidation of benzalacetophenones under non-heme hydrogen peroxyde-acetic acid conditions

The catalytic experiments were carried out at constant temperature in a closed 10 mL glass batch reactor, equipped with magnetic stirrer. In a typical run, substrate **HC** or **MeOC** (1.0 mmol), Fe(III) complex (1.0 mol %), H_2O_2 (1.0 to 6.0 mmol) and AcOH (0.1 mol% to 7 mmol) were mixed in the respective solvent (4 mL). The reaction mixture was magnetically stirred during the catalytic run (24 to 48 h) at the given temperature (25 to 40ºC). Control experiments were carried out in the absence of pre-catalyst. The analysis of epoxidation products was performed by HPLC with a detection wavelength of 220 nm. The eluent used was *n*-heptane:propan-1-ol (98:2) and *n*-heptane:propan-2-ol (9:1), respectively, for the catalytic reactions with **HC** and **MeOC**, with a flow rate of 1.0 mL min^{-1}. Before analysis by HPLC, 1 mmol of toluene (internal standard) was added to the reaction mixture.

III.7.3.4 – General procedures for the epoxidation of benzalacetophenones under Mukaiyama conditions

The catalytic experiments were carried out at atmospheric pressure and at constant temperature in an opened 10 mL glass batch reactor, equipped with magnetic stirrer. In a typical run, substrate **HC** or **MeOC** (1.0 mmol), Fe(III) complex (1.0 to 5.0 mol %) and isobutyraldehyde (1.0 to 4.0 mmol) were mixed in the respective solvent (4 mL). The reaction mixture was magnetically stirred during the catalytic run (up to 48 h) at the given temperature (25 to 40ºC). Control experiments were carried out in the absence of pre-catalyst. The analysis of epoxidation products was performed by HPLC with a detection wavelength of 220 nm. The eluent used was *n*-heptane:propan-1-ol (98:2) and *n*-heptane:propan-2-ol (9:1), respectively, for the catalytic reactions with **HC** and **MeOC**, with a flow rate of 1.0 mL min^{-1}. Before analysis by HPLC, 1 mmol of toluene (internal standard) was added to the reaction mixture.

III.7.3.5 – General procedures for the oxidation of 2-phenylethan-1-ol

The catalytic experiments were carried out in a closed 2 mL tube at constant temperature, equipped with magnetic stirrer. In a typical run, substrate PhEtOH (1.0 mmol), Fe(III) complex (1.0 to 5.0 mol %) and oxidant (0.75 mol%) were mixed in MeCN (0.8 mL). The reaction mixture was magnetically stirred during the catalytic run (up to 24 h) at the given temperature (25 to 80ºC). Control experiments were carried out in the absence of pre-catalyst. The analysis of oxidation products was performed by GC. Before analysis by GC, the reaction mixture was cooled to r.t. and 0.75 mol% of MnO_2 were added. Then, a sample of the mixure was filtered and the filtrate dissolved in MeCN.

III.7.4 – Fe(III) Compounds Preparation Methods

III.7.4.1 – Fe(III) complexes bearing amino acid-pyridyl ligands

Synthesis of FeL1A:

To a 50 mL round-bottomed flask containing 20 mL of water were added **L1** (1 g, 1.95 mmol) and $FeCl_3$•$6H_2O$ (0.53 g, 1.95 mmol) and the reaction mixture was stirred at r.t. for 10 minutes, affording a light-orange solution. Separately, salycilic acid (0.27 g, 1.95 mmol) and NaOH (0.16 g, 1.95 mmol) were solubilized in an Erlenmeyer containing 20 mL of distilled water and added to the **L1**/ $FeCl_3$•$6H_2O$ reaction mixture. The formation of a dark-purple precipitate then ensued. After 10 minutes of stirring at room temperature the suspension was filtered, dissolved in acetone, dryed with ahydrous Na_2SO_4 and the resulting mixture again filtered. The obtained filtrate was evaporated till dryness and dried under vacuum, yielding **FeL1A** as a dark-purple solid. Yield: 63% (0.61 g). ESI-MS [Methanol]: m/z= 916.91 ({Na[Fe**L1**(Sal)]$_2$}$^+$, 100%), m/z= 894.87 ({H[Fe**L1**(Sal)]$_2$}$^+$, 88%), m/z= 583.90 ([Fe**L1**(Sal)$_2$]$^-$, 100%), m/z= 482.26 ([Fe**L1**(Sal)Cl]$^-$, 27%), m/z= 470.04 ({Na[Fe**L1**(Sal)]}$^+$, 47%), m/z= 447.96 ({H[Fe**L1**(Sal)]}$^+$, 52%), ν_{max}/cm^{-1}: 3032 (N-H, w), 1598 (C=O$_{carboxyl}$, w). Elemental analysis for $C_{22}H_{20}ClFeN_2O_5$•$0.5H_2O$: calcd. C 53.63, H 4.30, N 5.69; found C 53.88, H 4.17, N 5.47.

Synthesis of FeL1B:

$FeCl_3$•$6H_2O$ (1.30 g, 4.80 mmol) and **L1** (1.23 g, 4.80 mmol) were added to a 50 mL round bottom flask containing 30 mL of an EtOH:H_2O (1:1) solution, and left under stirring at r.t. till complete solubilization. Separately from this mixture, picolinic acid (0.59 g, 4.80 mmol) and NaOH (0.19 g, 4.80 mmol) were added to a beaker containing 10 mL of distilled water, solubilized and added to the **L1**/ $FeCl_3$•$6H_2O$ solution. The resulting mixture was stirred at r.t. for *ca.* 30 minutes, resulting in a yellow suspension. After this period, the suspension was filtered under vacuum and washed with distilled water (1x10 mL) and acetone (3x 10mL), yielding a light-yellow solid. Yield: 85% (1.94g). ESI-MS [MeCN:H_2O (1:1)]: m/z= 1015.63 ({H[(Fe**L1**)$_2$(OH)(Pic)$_2$]•MeCN•$5H_2O$}$^+$, 48%), m/z= 990.45 ({H[(Fe**L1**)$_2$(Pic)$_2$(Cl)(OH)]•$4H_2O$}$^+$, 31%), m/z= 916.51 ({[(Fe**L1**)$_2$(Pic)$_2$(OH)]•$2H_2O$}$^-$, 21%), m/z= 837.40 ({[(Fe**L1**)$_2$(Pic)(OH)$_2$(MeCN)(H_2O)]}$^+$, 58%), m/z= 829.64 ({[(Fe**L1**)$_2$(OH)(Pic)Cl]•$2H_2O$}$^-$, 13%), m/z= 783.61 ({[(Fe**L1**)$_2$Cl$_2$(OH)]•$2H_2O$•MeCN}$^-$, 43%), m/z= 696.83 ({[Fe**L1**(OH)]$_2$•MeCN}$^-$, 17%), m/z= 688.60 ({H[Fe**L1**$_2$(Pic)]}$^+$, 22%), m/z= 589.84 ([Fe**L1**(Pic)$_2$Cl]$^-$, 12%), m/z= 566.97 ({H[Fe**L1**$_2$]}$^+$, 15%), m/z= 510.68 ({H[Fe**L1**(Pic)(OH)]•MeCN•H_2O}$^+$, 50%), m/z= 468.23 ([Fe**L1**(Pic)Cl]$^-$, 23%). ν_{max}/cm^{-1}: 3277 (N-H, s), 1656 (C=O$_{carboxyl}$, s). Elemental analysis for $C_{21}H_{19}ClFeN_3O_4$•$0.5H_2O$: calcd. C 52.80, H 4.22, N 8.80; found C 52.83, H 4.02, N 8.71.

Crystals suitable for single crystal X-ray diffraction analysis were obtained by suspending this compound in acetonitrile, heating under reflux, filtration and slow evaporation of the resulting filtrate.

Synthesis of FeL2:

To 30 mL of a EtOH:H_2O (1:1) solution was added **L2** (1 g, 4.8 mmol) and the mixture was stirred at r.t. $FeCl_3$•$6H_2O$ (1.30 g, 4.80 mmol) was added after complete solubilization of **L2** and the reaction was left under stirring, yielding a dark orange solution. After 20 minutes, sodium acetate (1.18 g, 14.4 mmol) was added to the reaction mixture, which was left under stirring for additional 20 minutes, resulting in a dark green solution. After this period, the mixture was evaporated to dryness and the residue was triturated with acetone, filtered and the inorganic residue washed with additional acetone. The resulting filtrate was dried with anhydrous Na_2SO_4, filtered, evaporated to dryness and dried under vacuum, yielding a dark green solid. Yield: 78% (1.55g). ESI-MS (Methanol): m/z= 1103.70 ({Na[(Fe**L2**)$_3$(AcO)$_2$(OH)(H_2O)$_3$]•MeOH•$4H_2O$}$^+$, 15%), m/z= 1063.56 ({H[(Fe**L2**)$_3$(AcO)$_2$(OH)(H_2O)$_3$]•MeOH•$3H_2O$}$^+$, 9%), m/z= 1012.65 ({H[(Fe**L2**)$_3$(AcO)$_2$(OH)(H_2O)$_3$]•MeOH}$^+$, 7%), m/z= 961.91 ({H[(Fe**L2**)$_3$(AcO)$_2$(OH)(H_2O)$_2$]}$^+$, 10%), m/z= 718.76 ({[(Fe**L2**)(AcO)(OH)(H_2O)]$_2$•2MeOH•H_2O}$^-$, 29%), m/z= 682.90 ({Na[Fe**L2**(MeO)$_2$(H_2O)$_2$]•$2H_2O$}$^+$, 100%), m/z= 659.20 ({[(Fe**L2**)]$_2$(OH)$_2$(H_2O)$_2$]•2MeOH}$^-$, 100%), m/z= 635.18 ({[(Fe**L2**)]$_2$(OH)(AcO)]•MeOH}$^-$, 13%), m/z= 601.06 ({H[Fe**L2**(MeO)$_2$(H_2O)]• 8MeOH•H_2O}$^+$, 7%), m/z= 599.02 ({[(Fe**L2**)(MeO)$_2$]•8MeOH•H_2O}$^-$, 34%). ν_{max}/cm^{-1}: 2962 (N-H, m), 1610 (C=O$_{carboxyl}$, s), 1454 (Fe-OAc-Fe, s) 646 (Fe-OH-Fe, m). Elemental analysis for $C_{15}H_{21}FeN_2O_6$•$2H_2O$: calcd. C 43.29, H 5.81, N 6.73; found C 43.60, H 5.61, N 6.80.

Synthesis of FeL3:

The preparation method for this compound was identical to that used for **FeL1B**. Reagents: **L3** (1.52 g, 4.80 mmol), $FeCl_3$•$6H_2O$ (1.30g, 4.80 mmol) Picolinic acid (0.59 g, 4.80 mmol), NaOH (0.19 g, 4.80 mmol), EtOH:H_2O (1:1) solution (30.0 mL). Obtained as a light orange solid. Yield: 82% (2.00g). ESI-MS [MeCN:H_2O (1:1)]: m/z=789.37 ({H[(Fe(**L3**))$_2$(OH)$_2$]•$3H_2O$}$^+$, 26%), m/z= 713.70 ({[Fe**L3**(Pic)Cl]•5MeCN}$^-$, 27%), m/z=602.16 ({[Fe(**L3**)(Pic)Cl]•$3H_2O$•MeCN}$^-$, 31%), m/z=549.62 ({Na[(Fe(**L3**)(Pic)(Cl)] •H_2O}$^+$, 37%), m/z= 542.24 ({[Fe**L3**(Pic)Cl]•$2H_2O$}$^-$, 24%), m/z= 540.36 ({H[Fe**L3**Cl_2]•2MeCN•$2H_2O$}$^+$, 26%), m/z=507.31 ([Fe(**L3**)(Pic)(Cl)]$^-$, 10%), m/z=285.63 ({[Fe**L3**(OH)]$_2$•3MeCN}$^{3-}$, 100%). ν_{max}/cm^{-1}: 3277(N-H, s,b), 1590 (C=O$_{carboxyl}$, s). Elemental analysis for $C_{23}H_{20}ClFeN_4O_4$•$0.5H_2O$: calcd. C 53.46, H 4.10, N 10.84; found C 53.26, H 4.23, N 10.22. Crystals suitable for single crystal X-

ray diffraction analysis were obtained by suspending this compound in acetonitrile, heating under reflux, filtration and slow evaporation of the resulting filtrate.

III.7.4.2 – Fe(III) complexes bearing amino acid-phenol and amino acid-methoxybenzene ligands

General synthetic procedure: Ligand precursor **L5**, **L6**, or **L8**-**11**, depending on the desired Fe(III) compound, was weighted and introduced in a round bottom flask and dissolved in MeOH (10.0 mL/mmol ligand precursor) at room temperature. To the resulting colourless solution $FeCl_3$•$6H_2O$ (1.0 eq/mmol ligand precursor) was added to the mixture and let to stir for 5 minutes at room temperature. Then, sodium acetate (3.0 eq/mmol ligand precursor) was added to the reaction, followed by addition of distilled water (30.0 mL/mmol ligand precursor). Different *work-up* procedures were performed for each compound preparation and will be specified in each case.

Synthesis of FeL5:

Reagents: **L5** (0.50 g, 1.67 mmol), $FeCl_3$•$6H_2O$ (0.45 g, 1.67 mmol), sodium acetate (0.41 g, 5.01 mmol), MeOH (20.0 mL), water (60.0 mL). After addition of $FeCl_3$•$6H_2O$ the reaction mixture switched from a colourless to a dark-purple solution Addition of NaOAc and water induced precipitation of a dark-purple solid, which was filtered and washed with distilled water (2x50 mL) and petroleum-ether (1x 30 mL). The resulting residue was transferred to an Erlenmeyer, dissolved in acetone, dried with anhydrous Na_2SO_4 and the resulting mixture filtered; the obtained filtrate was evaporated to dryness and dried under vacuum, affording **FeL5** as a dark-purple solid. Yield: 57% (0.42 g). ESI-MS (Methanol): m/z= 1038.57 ($\{[(Fe\mathbf{L5})_2(\mathbf{L5})(OH)]•H_2O\}^-$, 100%), m/z= 650.21 ($[Fe\mathbf{L5}_2]^-$, 10%), m/z= 390.88 ($\{Na[Fe\mathbf{L5}(OH)]\}^+$, 10%). ν_{max}/cm^{-1}: 3243 (N-H, w), 1604, ($C{=}O_{carboxyl}$, s), 1474 (Fe-OAc-Fe, s), 1259 ($C\text{-}O_{Phenol}$, m), 701 (Fe-OH-Fe, m). Elemental analysis for $C_{20}H_{22}FeNO_5$•$1.5H_2O$: calcd. C 54.69, H 5.74, N 3.19; found C 54.72, H 5.54, N 3.23.

Synthesis of FeL6:

Reagents: **L6** (0.50 g, 1.30 mmol), $FeCl_3$•$6H_2O$ (0.35 g, 1.30 mmol), sodium acetate (0.32 g, 3.90 mmol), MeOH (13.0 mL), water (39.0 mL). After addition of $FeCl_3$•$6H_2O$ the reaction mixture aquired a dark-blue colour and the addition of NaOAc and water induced the precipitation of a dark-blue solid, which was filtered and washed with distilled water (2x30 mL). The resulting residue was transferred to an Erlenmeyer, dissolved in acetone, dried with anhydrous Na_2SO_4 and again filtered. The obtained filtrate was evaporated to dryness and dried under vacuum, allowing the isolation of **FeL6** as a dark-blue solid. Yield: 63% (0.50 g).

ESI-MS (Methanol): m/z= 815.55 ([Fe**L6**$_2$]$^-$, 100%), m/z= 689.44 ({[(Fe**L6**)(OH)]$_3$•H_2O}$^{2-}$, 9%), m/z= 262.95 ({Na_2[Fe**L6**]•EtOH}$^{2+}$, 30%), m/z= 251.20 ({H_2[Fe**L6**]•MeOH}$^{2+}$, 100%). ν_{max}/cm^{-1}: 2957 (N-H, m), 1607 (C=O$_{carboxyl}$, m), 1440 (Fe-OAc-Fe, m), 1267 (C-O$_{Phenol}$, m), 747 (Fe-OH-Fe, w). Elemental analysis for $C_{26}H_{34}FeNO_5$•2$(CH_3)_2CO$: calcd. C 62.74, H 7.57, N 2.29; found C 62.42, H 7.54, N 2.13.

Synthesis of FeL8:

Reagents: **L8** (0.70 g, 2.09 mmol), $FeCl_3$•6H_2O (0.56 g, 2.09 mmol), sodium acetate (0.51 g, 6.27 mmol), MeOH (20.9 mL), water (62.7 mL). After addition of $FeCl_3$•6H_2O the reaction mixture aquired a dark-blue colour and addition of NaOAc and water induced precipitation of a dark-purple solid, which was filtered and washed with distilled water (2x50 mL). The resulting residue was transferred to an Erlenmeyer, dissolved in acetone, dried with anhydrous Na_2SO_4, filtered and the obtained filtrate evaporated to dryness and dried under vacuum, yielding **FeL8** as a dark-purple solid. Yield: 68% (0.64 g). ESI-MS (Methanol): m/z= 1984.03 ({H[(Fe**L8**)$_3$(OH)(**L8**)$_2$]•4MeOH}$^+$, 100%), m/z= 1906.31 ({H[(Fe**L8**)$_3$(OH)(**L8**)$_2$]•MeOH•H_2O}$^+$, 80%), 1731.74 ({H[(Fe**L8**)$_3$(OMe)$_2$(**L8**)]•4MeOH•2H_2O}$^+$, 37%), m/z= 1712.62 ({H[(Fe**L8**)$_3$(OMe)$_2$(**L8**)]•4MeOH•H_2O}$^+$, 33%), m/z= 1631.67 ({H[(Fe**L8**)$_3$(OMe)$_2$(**L8**)]•2MeOH}$^+$, 35%), m/z= 1611.40 ({Na[(Fe**L8**)$_3$(OH)$_2$(**L8**)]•MeOH•H_2O}$^+$, 35%), m/z= 1589.37 ({Na[Fe**L8**$_2$]$_2$•2MeOH•3H_2O}$^+$, 20%), m/z= 1513.61 ({H[(Fe**L8**$_2$)$_2$]•2MeOH}$^+$, 18%), m/z= 1131.25 ({H[(Fe**L8**)$_2$(**L8**)]•H_2O}$^+$, 35%), m/z= 768.62 ({H_2[(Fe**L8**$_2$)$_2$]•5H_2O}$^{2+}$, 17%), m/z= 746.03 ({Na[Fe**L8**$_2$]}$^+$, 17%), m/z= 722.57 ([Fe**L8**$_2$]$^-$, 100%), m/z= 471.54 ({Na[Fe**L8**(OAc)]}$^+$, 7%). ν_{max}/cm^{-1}: 2956 (N-H, s), 1622 (C=O$_{carboxyl}$, m), 1203 (C-O$_{Phenol}$, m). Elemental analysis for $C_{22}H_{34}FeNO_5$•0.5AcOEt: calcd. C 58.54, H 7.78, N 2.84; found C 58.65, H 8.19, N 2.97.

Synthesis of FeL9:

Reagents: **L9** (0.50 g, 1.36 mmol), $FeCl_3$•6H_2O (0.37 g, 1.36 mmol), sodium acetate (0.34 g, 4.08 mmol), MeOH (13.6 mL), water (40.8 mL). After addition of $FeCl_3$•6H_2O the reaction mixture switched into a dark-brown solution; addition of NaOAc and water induced precipitation of a dark-brown solid, which was filtered, washed with distilled water (2x30 mL) and petroleum-ether (1x20 mL) and dried under vacuum, affording **FeL9** as a dark-brown solid. Yield: 59% (0.37 g). ESI-MS (DMSO): m/z= 752.40 ([Fe**L9**$_2$]$^-$, 100%), m/z= 256.52 ({H_2[Fe**L9**Cl]•MeOH•2H_2O}$^{2+}$,15%). ν_{max}/cm^{-1}: 1632 (C=O$_{carboxyl}$, m), 1223 (C-O$_{Phenol}$, m). Elemental analysis for $C_{21}H_{20}ClFeN_2O_3$•H_2O: calcd. C 55.11, H 4.84, N 6.12; found C 55.37, H 5.05, N 6.12.

Synthesis of FeL10:

Reagents: **L10** (0.50 g, 1.07 mmol), $FeCl_3$•$6H_2O$ (0.29 g, 1.07 mmol), sodium acetate (0.26 g, 3.21 mmol), MeOH (10.7 mL), water (32.1 mL). After addition of $FeCl_3$•$6H_2O$ the reaction mixture changed from colouress to a dark-blue solution. The addition of NaOAc and water induced precipitation of a dark-blue solid which was filtered, washed with distilled water (2x30 mL), petroleum-ether (1x20 mL) and dried under vacuum, affording **FeL10** a dark-blue solid. Yield: 42% (0.27 g). ESI-MS (Methanol): m/z= 950.36 ({[Fe**L10**$_2$]•MeOH}$^-$, 45%), m/z= 920.38 ([Fe**L10**$_2$]$^-$, 100%), m/z= 592.24 ({[Fe**L10**(OH)]•MeOH•$3H_2O$}$^-$, 15%), m/z= 578.19 ({[Fe**L10**(OAc)]•MeOH}$^-$, 27%), 387.23 ({Na_3[Fe**L10**$_2$]•MeOH•$8H_2O$}$^{3+}$, 100%). ν_{max}/cm^{-1}: 1624 (C=O$_{carboxyl}$, m), 1237 (C-O$_{Phenol}$, w). Elemental analysis for $C_{29}H_{35}FeN_2O_5$•$2.5H_2O$: calcd. C 58.79, H 6.80, N 4.73; found C 58.47, H 6.60, N 4.41.

Synthesis of FeL11:

Reagents: **L11** (1.95 g, 6.06 mmol), $FeCl_3$•$6H_2O$ (1.64 g, 6.06 mmol), sodium acetate (1.49 g, 18.2 mmol), MeOH (60.6 mL), water (181.8 mL). The addition of $FeCl_3$•$6H_2O$ to the reaction mixture yielded a dark-orange solution, which was evaporated till dryness. The resulting residue was suspended and triturated with acetone, dried with anhydrous Na_2SO_4 and again filtered; the obtained filtrate was evaporated to dryness and dried under vacuum, affording **FeL11** as a dark-orange solid. Yield: 75% (2.21 g). ESI-MS (Methanol): m/z= 967.06 ({[Fe**L11**(OMe)]$_2$•7MeOH}$^-$, 100%), m/z= 953.11 ({[Fe**L11**(OMe)]$_2$•6MeOH•H_2O}$^-$, 28%), m/z= 742.06 ([Fe**L11**(OMe)]$_2^-$, 25%), m/z= 728.20 ([(Fe**L11**)$_2$•(OH)(MeO)]$^-$, 35%), m/z= 714.33 ([Fe**L11**(OH)]$_2^-$, 20%), m/z= 394.18 ({H[Fe**L11**(OH)]•H_2O}$^+$, 63%). ν_{max}/cm^{-1}: 3027 (N-H, w), 1741 (C=O$_{carboxyl}$, s, b) 1438 (Fe-OAc-Fe, s, b), 659 (Fe-OH-Fe, m). Elemental analysis for $C_{21}H_{24}FeNO_7$•$1.5H_2O$: calcd. C 51.98, H 5.61, N 2.89; found C 51.61, H 5.41, N 2.75.

III.7.4.3 – Fe(III) complexes bearing amino acid-pyridyl-phenol ligands

General synthetic procedure: Ligand precursor **L13**, **L14** or **L15**, depending on the desired Fe(III) compound, was weighted in a 100 mL round bottomed flask and dissolved in MeOH (12.0 mL/mmol ligand precursor) at room temperature. To the resulting colourless solution $FeCl_3$•$6H_2O$ (1.0 eq/mmol ligand precursor for the preparation of **FeL13** and **FeL14**; 2.0 eq/mmol ligand precursor for the synthesis of **FeL15**) was added to the mixture and let to stir for 5 minutes at room temperature. Then, an aqueous solution of sodium acetate (1M, 1.2 mL/mmol $FeCl_3$•$6H_2O$) was added to the reaction until pH~6 was reached. Distilled water (20.0 mL/mmol ligand precursor) was added to the reaction, leading to the formation of a precipitate: different *work-up* procedures were performed for each compound preparation and will be specified in each case.

Synthesis of FeL13:

Reagents: **L13** (1g, 2.56 mmol), $FeCl_3$•$6H_2O$ (0.692g, 2.56 mmol), aqueous sodium acetate solution (3.112 mL, 1M), MeOH (31.0 mL), distilled water (51.2 mL). The precipitate formed after addition of water was filtered under vacuum. The filtrate was discarded, and the resulting residue was dissolved in 20 mL AcOEt and dried with anhydrous Na_2SO_4; the suspension was filtered, the filtrate was transferred to a 50 mL round-bottomed flask and evaporated till dryness, yielding a dark-purple solid. Yield: 59% (0.78g). ESI-MS (Methanol): m/z= 947.10 ({Na[(Fe**L13**)$_2$(OH)]•H_2O}$^+$, 23%), m/z= 919.16 ({H[(Fe**L13**)$_2$(MeO)]}$^+$, 100%), m/z= 562.42 ({[Fe**L13**(OH)(H_2O)]•2MeOH•H_2O}$^-$, 80%), m/z= 548.46 ({[Fe**L13**(OH)(H_2O)]•MeOH•$2H_2O$}$^-$, 100%), m/z= 533.74 ({[Fe**L13**(OH)(H_2O)]•$3H_2O$}$^-$, 42%), m/z= 529.85 ([Fe**L13**(AcO)(H_2O)]$^-$, 18%), m/z= 475.53 ({H[Fe**L13**(MeO)]}$^+$, 57%). ν_{max}/cm^{-1}: 1659 (C=O$_{carboxyl}$, s), 1437 (Fe-OAc-Fe, s), 1313 (C-O$_{Phenol}$, m), 701 (Fe-OH-Fe, w). Elemental analysis for $C_{26}H_{27}FeN_2O_5$•$0.5H_2O$: calcd. C 60.95, H 5.51, N 5.47; found C 60.72, H 5.25, N 5.44.

Synthesis of FeL14:

Reagents: **L14** (1g, 2.10 mmol), $FeCl_3$•$6H_2O$ (0.57g, 2.10 mmol) aqueous sodium acetate solution (2.52 mL, 1M), MeOH (25.2 mL), distilled water (42.0 mL). The precipitate formed after addition of water was filtered under vacuum and the residue dissolved in 20.0 mL AcOEt, dried with anhydrous Na_2SO_4 and filtered. The filtrate was transferred to a 50 mL round-bottomed flask and evaporated till dryness, yielding a dark-blue solid. Yield: 65% (0.80g). ESI-MS (Methanol): m/z= 1660.18 ({Na[(Fe**L14**)$_2$(**L14**)]•$6H_2O$}$^+$, 14%), m/z= 1645.56 ({H[(Fe**L14**)$_2$(**L14**)]•3MeOH•H_2O}$^+$, 20%), m/z= 1601.33 ({H[(Fe**L14**)$_2$(**L14**)]•$4H_2O$}$^+$, 100%, m/z= 1130.92 ([(Fe**L14**)$_2$(OH)(OAc)]$^-$, 20%), m/z= 1107.06 ({[(Fe**L14**)$_2$(OH)$_2$]•H_2O}$^-$, 37%), m/z= 645.75 ({[Fe**L14**(OH)(H_2O)]•2MeOH•H_2O}$^-$, 37%), m/z= 631.78 ({[Fe**L14**(OH)(H_2O)]•MeOH•$2H_2O$}$^-$, 41%), m/z= 621.80 ({[Fe**L14**(OAc)(H_2O)]•H_2O}$^-$, 100%), m/z= 594.01 ({[Fe**L14**(OH)(H_2O)]•MeOH}$^-$, 62%), m/z= 580.02 ({[Fe**L14**(OH)(H_2O)]•H_2O}$^-$, 39%), m/z= 559.79 ({H[Fe**L14**(MeO)]}$^+$, 33%). ν_{max}/cm^{-1}: 1654(C=O$_{carboxyl}$, s, b), 1438 (Fe-OAc-Fe, s, b), 1254 (C-O$_{Phenol}$, m), 647 (Fe-OH-Fe, w). Elemental analysis for $C_{32}H_{39}FeN_2O_5$: calcd. C 65.42, H 6.69, N 4.77; found C 65.22, H 7.02, N 4.71. Crystals suitable for single crystal X-ray diffraction analysis were obtained for **FeL14** by dissolving this compound in the minimum volume of methanol, dropwise addition of DMSO and slow evaporation of the resulting mixture.

Synthesis of FeL15:

Reagents: **L15** (0.80 g, 10.05 mmol), $FeCl_3$•$6H_2O$ (0.57 g, 2.10 mmol) aqueous sodium acetate (2.5 mL, 1M), distilled water (2.10 mL). The precipitate formed after addition of water was filtered under vacuum and the residue washed with distilled water (2x30 mL) and dried under

vacuum, affording a brown solid. Yield: 52% (0.49 g). ESI-MS (Methanol): m/z= 1015.59 ({H[Fe_2(**L15**)Cl_3]•3MeOH•H_2O}$^+$, 100%), m/z= 510.72 ({H_2[Fe_2**L15**Cl_3]•3MeOH•H_2O}$^{2+}$, 12%), m/z= 916.41 ({[Fe_2**L15**Cl_3]•H_2O}$^-$, 27%). ν_{max}/cm^{-1}: 1562 (C=O$_{carboxyl}$, s), 1241 (C-O$_{Phenol}$, w). Elemental analysis for $C_{42}H_{43}Cl_3Fe_2N_4O_5$•1.5$H_2O$: calcd. C 54.31, H 4.99, N 6.03; found C 54.16, H 5.28, N 5.99.

III.7.5 – Synthesis of target catalytic substrates and desired products

Synthesis of 3,3'-dibromo-[1,1'-binaphthalene]-2,2'-diol (BrBINOL):

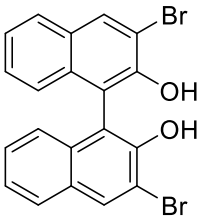

To a 25 mL round-bottomed flask containing 15 mL of EtOH were added 3-bromo-2-naphthol (0.50 g, 2.24 mmol) and $FeCl_3$•6H_2O (0.30 g, 1.12 mmol) and the reaction mixture was stirred at r.t. for 120 hours, affording a dark green solution which was evaporated to nearly one quarter of its initial volume. Then, distilled water was added to induce precipitation of a light brown solid which was filtered and washed with H_2O. Yield: 22% (0.22 g) δ_H (300 MHz, Acetone-d_6, ppm): 8.44 (2H, s, ArOH, partially overlapped with ArH$_{C4}$), 8.33 (2H, s, ArH$_{C4}$, partially overlapped with ArOH), 7.91 (2H, d, ArH$_{C5}$, *J*= 7.4), 7.36 (2H, t, ArH$_{C7}$, partially overlapped with ArH$_{C6}$, *J*= 9.34), 7.30 (2H, t, ArH$_{C6}$, partially overlapped with ArH$_{C7}$, *J*= 9.38), 6.99 (2H, d, ArH$_{C8}$, *J*= 7.7). δ_C (300 MHz, Acetone-d_6, ppm): 151.23 (2C, ArCBr), 134.30 (2C, C$_{ipso,10}$), 133.73 (2C, ArCH$_{C4}$), 130.51 (2C, C$_{ipso,9}$), 128.15 (2C, ArCH$_{C5}$), 127.87 (2C, ArCH$_{C6}$), 125.14 (2C, ArCH$_{C8}$), 124.99 (2C, ArCH$_{C7}$), 115.90 (2C, C$_{ipso,1}$), 114.06 (2C, ArCOH).

Synthesis of (*E*)-1,3-diphenylprop-2-enone (HC):

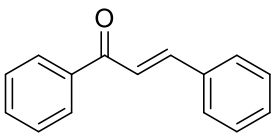

Sodium hydroxide (2.07g, 51.8 mmol) was dissolved in 30 mL of an EtOH:H_2O (2:3) mixture. The temperature was cooled down to 20ºC, and acetophenone (5.25 mL, 40.5 mmol) was added to the aqueous mixture, forming a white suspension. Reaction temperature was kept between 15 and 30ºC and benzaldehyde (4.6 mL, 40.5 mmol) was added to the reaction, resulting in a yellow suspension after 3 h of stirring. The suspension was filtered under vacuum and washed with cold distilled water (till pH~7 was reached) and EtOH (1x 10 mL), affording the desired product as a crystalline light-yellow solid. Yield: 68% (5.7g) δ_H: (300 MHz, Acetone-d_6, ppm): 8.20 (2H, d, ArH, *meta* to C=C), 7.88 (4H, m, both ene C=CH and ArH, *ortho* to C=C, overlapped), 7.67 (1H, dd, ArH *p*-related to carbonyl, partially overlapped with ArH *ortho* to carbonyl, *J*= 13.4, 6.4), 7.59 (2H, t, ArH *ortho* to carbonyl, partially overlapped with ArH *para* to carbonyl, *J*= 7.3), 7.49 (3H, m, ArH *meta* to carbonyl and ArH *para* to C=C, overlapped). δ_C (300 MHz, Acetone-d_6, ppm): 189.91 (1C, C=O), 144.80 (1C, C=CH, adjacent to phenyl), 139.05 (1C, C$_{ipso,Phenyl}$,

adjacent to carbonyl), 135.94 (1C, C*ipso,Phenyl*, adjacent to C=C), 133.61 (1C, ArCH, *para* to carbonyl), 131.26 (1C, ArCH, *para* to C=C), 129.76 (2C, ArCH, *meta* to carbonyl), 129.49 (2C, ArCH, *ortho* to carbonyl), 129.45 (2C, ArCH, *ortho* to C=C), 129.26 (2C, ArCH, *meta* to C=C), 122.84 (1C, C=CH, adjacent to carbonyl).

Synthesis of (*E*)-1-[(4-methoxy)phenyl]-3-phenylprop-2-enone (**MeOC**):

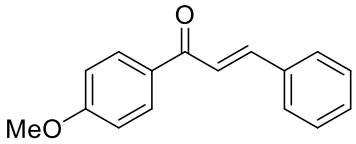

The preparation method for this compound was identical to that used for **HC**. Reagents: NaOH (2.07g, 51.8 mmol), 4-methoxyacetophenone (5.02 mL, 40.5 mmol) benzandehyde (4.6 mL, 40.5 mmol). Was obtained as a white solid. Yield: 73% (7.04g) δ_H: (300 MHz, Acetone-d_6, ppm): 8.16 (2H, m, ArH, *ortho* to OMe), 7.82 (4H, m, both ene =CH and ArH *meta* to C=C overlapped), 7.46 (1H, m, ArH, *para* to C=C and partially overlapped with ArH *ortho* to C=C), 7.44 (2H, m, ArH, *ortho* to C=C and partially overlapped with ArH, *para* to C=C), 7.06 (2H, m, ArH, *meta* to OMe), 3.89 (3H, s, OCH_3). δ_C (300 MHz, Acetone-d_6, ppm): 188.09 (1C, C=O), 164.43 (1C, C*ipso,MeOPhenyl*, adjacent to OMe), 143.92 (1C, C=CH, adjacent to carbonyl), 136.15 (1C, C*ipso,Phenyl*, adjacent to C=C), 131.90 (1C, C*ipso,MeOPhenyl*, adjacent to carbonyl), 131.59 (2C, ArCH, *ortho* to carbonyl), 131.06 (1C, ArCH, *para* to C=C), 129.74 (2C, ArCH, *ortho* to C=C), 129.36 (2C, ArCH, *meta* to C=C), 122.76 (1C, C=CH, adjacent to phenyl), 114.68 (2C, ArCH, *meta* to carbonyl), 55.91 (1C, OCH_3).

Synthesis of Phenyl(3-phenyloxiran-2-yl)methanone (HC oxide):

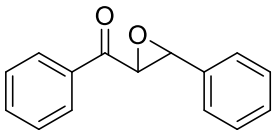

HC (1.02g, 4.91 mmol) was dissolved in 25mL of MeOH at r.t. Hydrogen peroxide (30% in H_2O, 1 mL, 9.82 mmol) was added to the mixture, followed by addition of an aqueous solution of NaOH (4M, 1.64 mL, 6.56 mmol) and the reaction was stirred for 30 minutes at r.t., affording a white suspension. Then, 5 mL of distilled water were added and the mixture was cooled down in an ice bath. After 20 minutes, the white precipitate was filtered and washed with cold distilled water (until pH~7 was reached) and EtOH (1x 10 mL), affording the desired product as a white solid. Yield: 39% (0.43g) δ_H (300 MHz, CD_3OD, ppm): 8.01 (2H, d, ArH, *ortho* to carbonyl, *J*= 7.9), 7.66 (1H, t, ArH, *para* to carbonyl, *J*= 7.3), 7.52 (2H, t, ArH, *meta* to carbonyl, *J*= 7.6), 7.41 (5H, m, ArH Phenyl ring adjacent to oxyrane ring), 4.56 (1H, d, $CH_{Oxyrane}$, adjacent to carbonyl, *J*= 1.0), 4.03 (1H, d, $CH_{Oxyrane}$, adjacent to phenyl ring, *J*= 1.0). δ_C (300MHz, CD_3OD, ppm): 195.24 (1C, C=O), 137.01 (1C, C*ipso,Phenyl*, adjacent to oxyrane ring), 136.70 (1C, C*ipso,Phenyl*, adjacent to carbonyl), 135.26 (1C, ArCH, *para* to carbonyl), 130.09 (1C, ArCH, *para* to oxyrane ring), 130.04 (2C, ArCH, *meta* to carbonyl), 129.72 (2C, ArCH, *ortho* to oxyrane ring), 129.40 (2C,

Ar<u>C</u>H, *ortho* to carbonyl), 127.03 (2C, ArCH, *meta* to oxyrane ring), 61.97 (1C, <u>C</u>H$_{Oxyrane}$, adjacent to carbonyl), 60.43 (<u>C</u>H$_{Oxyrane}$, adjacent to phenyl ring).

Synthesis of [(4-methoxy)Phenyl)]-(3-phenyloxiran-2-yl)methanone (MeOC oxide):

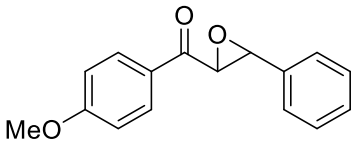

The preparation method for this compound was identical to that used for **HC** oxide. Reagents: **MeOC** (1.17g, 4.91 mmol), H_2O_2 (30% in H_2O, 1.0 mL, 9.82 mmol) NaOH (4M, 1.64 mL, 6.56 mmol). Was obtained as a white solid. Yield: 35% (0.437g) δ_H: (300 MHz, Acetone-d_6, ppm): 8.07 (2H, d, Ar<u>H</u>, *ortho* to carbonyl, *J*= 8.7), 7.42 (5H, m, ArH$_{Phenyl}$, adjacent to oxyrane ring), 7.07 (2H, d, ArH, *ortho* to OMe, *J*= 8.7), 4.53 (1H, d, C<u>H</u>$_{Oxyrane}$, adjacent to carbonyl, *J*= 1.0), 4.08 (1H, d, C<u>H</u>$_{Oxyrane}$, adjacent to phenyl ring, *J*= 1.0), 3.86 (3H, s, OC<u>H</u>$_3$). δ_C (300 MHz, Acetone-d_6, ppm): 191.71 (1C, <u>C</u>=O), 165.13 (1C, <u>C</u>$_{ipso,Phenyl}$, adjacent to OMe), 137.29 (1C, <u>C</u>$_{ipso,Phenyl}$, adjacent to oxyrane ring), 131.48 (2C, Ar<u>C</u>H, *ortho* to carbonyl), 129.80 (1C, <u>C</u>$_{ipso}$, adjacent to carbonyl), 129.60 (1C, ArCH, *para* to oxyrane ring), 129.45 (2C, ArCH, *meta* to oxyrane ring), 126.92 (2C, ArCH, *meta* to oxyrane ring), 114.95 (2C, ArCH, *ortho* to OMe), 61.02 (1C, <u>C</u>H$_{Oxyrane}$, adjacent to carbonyl), 59.35 (1C, <u>C</u>H$_{Oxyrane}$, adjacent to phenyl ring), 56.04 (1C, O<u>C</u>H$_3$).

CHAPTER 4

Amino acid-Derived Molybdenum(VI) Complexes

IV – Amino acid-Derived Molybdenum Complexes

IV.1 – Preamble

In this Chapter will be described the synthesis and characterization of novel Mo(VI) amino acid complexes derived from the compounds prepared in Chapter 2. As in the case of Fe(III) compounds, the preparation of these complexes was highly focused on the application of simple and sustainable one-pot reactions, using commercial $MoO_2(acac)_2$ as the Mo(VI) source. The application of these complexes as pre-catalysts was tested in the epoxidation of benzalacetophenones under mild and environmentally-friendly conditions.

IV.2 – Preparation of molybdenum(VI) amino acid complexes: Results and discussion

The proposed structural formulae of the synthesized Mo(VI) amino acid complexes synthesized are presented in **Figure IV-1**, based on their elemental analyses.

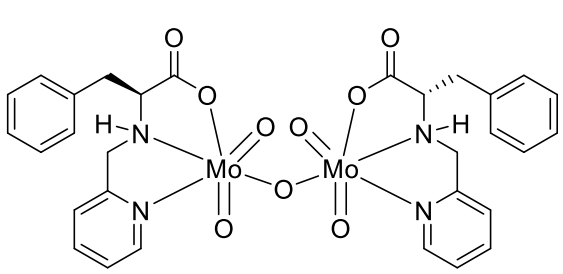

MoL1

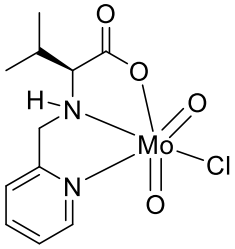

MoL2

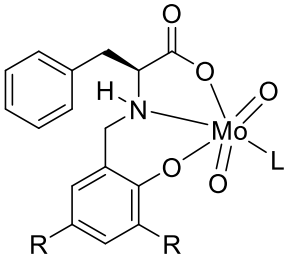

MoL5: R= CH_3
MoL6: R= $C(CH_3)_3$
L= Solvent

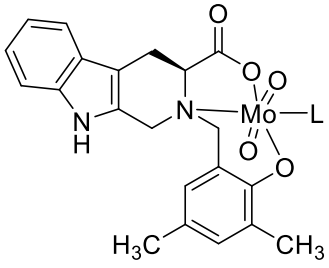

MoL9
L= Solvent

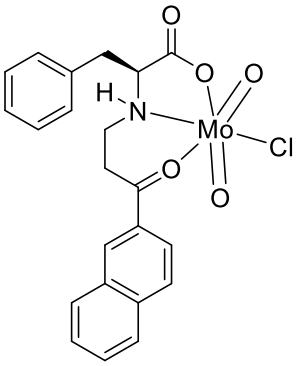

MoL18

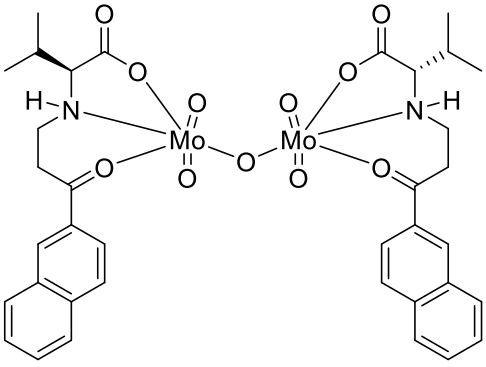

MoL19

Figure IV-1: Structural formulae of the prepared Mo(VI) amino acid compounds based on their elemental analyses.

The preparation of the referred Mo(VI) amino acid complexes was performed in one-pot reactions under mild conditions by reacting $MoO_2(acac)_2$ with the corresponding amino acid-

derived ligand precursor at room temperature in methanol or ethanol, depending on the ligand precursor utilized, under aerobic conditions (**Scheme IV-1**).

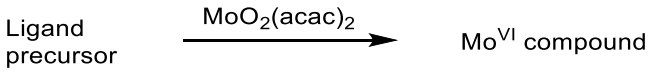

Scheme IV-1: General synthetic procedure for the synthesis of the desired Mo(VI) amino acid complexes.

These compounds were obtained as solids with insolubility in water and apolar organic solvents in general. All compounds are air-stable and were stored at room temperature in a dry environment after isolation. All compounds were characterized by UV-Vis spectroscopy (UV-Vis) and Circular Dichroism (CD), Electrospray Ionization Mass Spectrometry (ESI-MS), Infrared Spectroscopy (FT-IR) and Elemental Analysis (EA). No suitable crystals for single-crystal X-ray diffraction were obtained for these compounds. Redox measurements were carried out by Cyclic Voltammetry (CV).

IV.2.1 – Mo(VI) complexes bearing amino acid-pyridyl and amino acid-imidazolyl ligands

The preparation of Mo(VI) complexes **MoL1** and **MoL2** will be presented herein and their structural formulae are depicted in **Figure IV-2**.

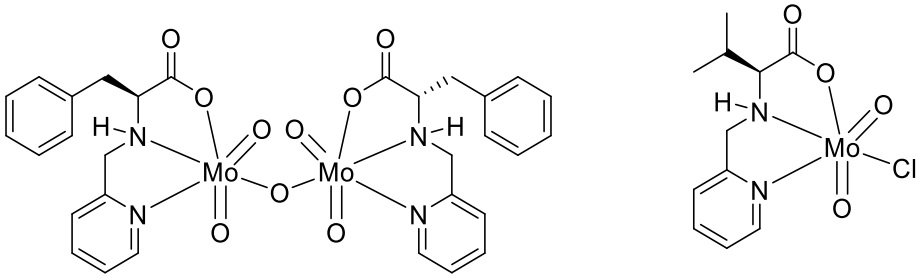

Figure IV-2: Structural formulae of the prepared Mo(VI) amino acid compounds **MoL1** and **MoL2**, based on their elemental analyses.

The synthesis of **MoL1** and **MoL2** utilized compounds **L1** and **L2** as ligand precursors, respectively. The applied synthetic procedure is presented in **Scheme IV-2** and entailed the suspension of the corresponding ligand precursor in EtOH in an open vessel at room temperature, followed by addition of one mole equivalent of concentrated HCl till complete solubilization under stirring. Then, one mole equivalent of $MoO_2(acac)_2$ was added to the mixture and let to stir for *ca.* 10 minutes, followed by addition of diethyl ether which induced the formation of a precipitate. Water was also added to the reaction mixture, after the addition of Et_2O, in order to induce precipitation and facilitate filtration. The precipitate was filtered and

washed with distilled water and petroleum ether, yielding **MoL1** and **MoL2** as white solids in 40 and 25%, respectively.

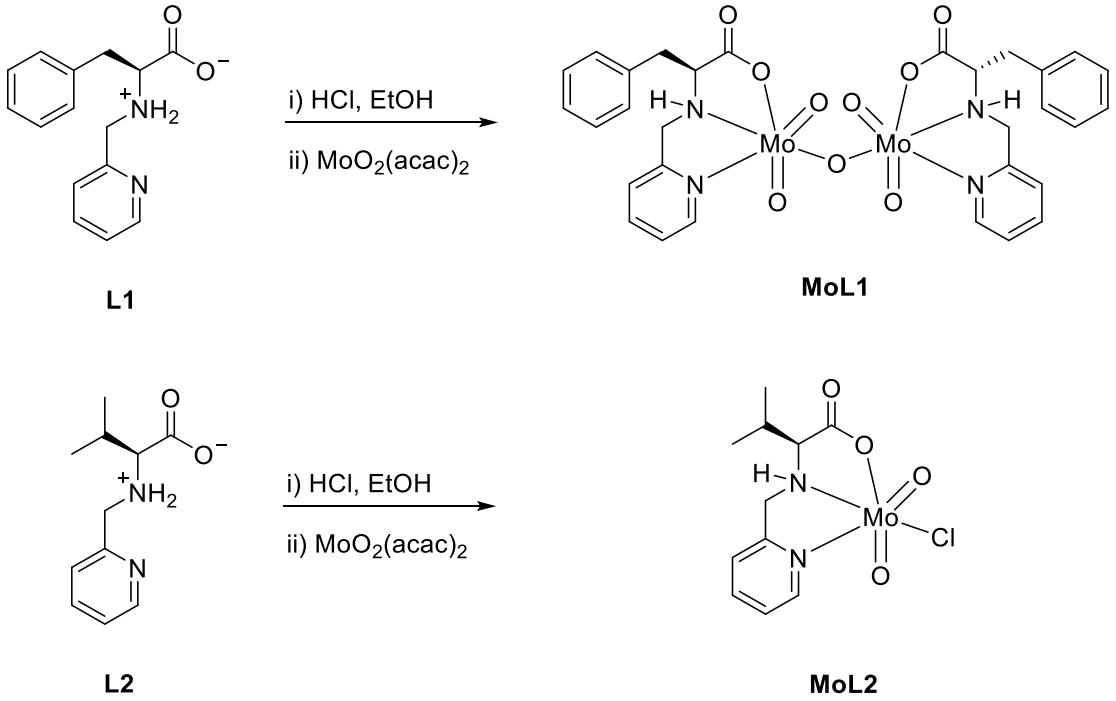

Scheme IV-2: Synthetic procedure for the preparation of Mo(VI) complexes **MoL1** and **MoL2**.

The synthesis of Mo(VI) complexes derived from ligand precursors **L3** and **L4** was attempted by applying the same reaction conditions for the preparation of **MoL1** and **MoL2**, but with no success. The isolated solids obtained in each case did not correspond to the desired mononuclear or dinuclear Mo(VI) compounds, by elemental analysis. Therefore, the preparation of the respective Mo(VI) complexes was abandoned.

IV.2.2 – Mo(VI) complexes bearing amino acid-phenol and amino acid-methoxybenzene ligands

The synthesis of Mo(VI) complexes **MoL5**, **MoL6** and **MoL9** will be presented in this Section and their structural formulae are depicted in **Figure IV-3**.

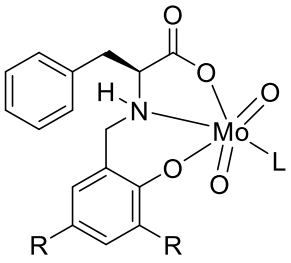

MoL5: R= CH_3
MoL6: R= $C(CH_3)_3$
L= Solvent

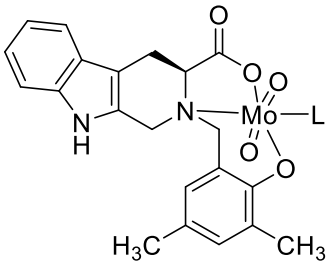

MoL9
L= Solvent

Figure IV-3: Structural formulae of the prepared Mo(VI) amino acid compounds **MoL5, MoL6** and **MoL9**, based on their elemental analyses.

The preparation of these compounds is illustrated in **Scheme IV-3** and started with the solubilization of the respective ligand precursor in MeOH in an open vessel at room temperature, followed by addition of $MoO_2(acac)_2$. After 10 minutes under stirring water was added to the reaction, inducing the formation of a precipitate which was filtered and washed with distilled water and petroleum ether, affording **MoL5**, **MoL6** and **MoL9** as solids in 67, 52 and 71% yields, respectively.

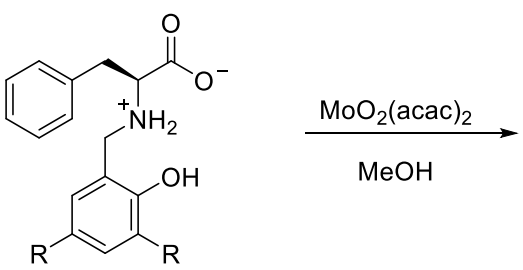

L5: R= CH_3
L6: R= $C(CH_3)_3$

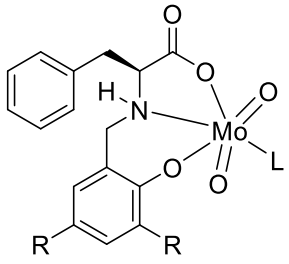

MoL5: R= CH_3
MoL6: R= $C(CH_3)_3$
L= Solvent

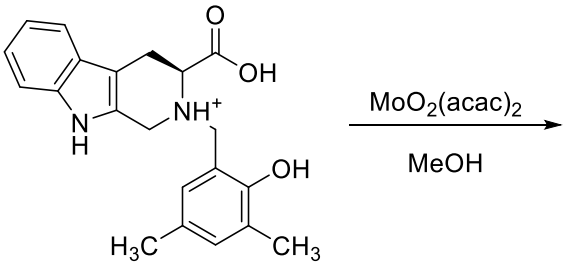

L10

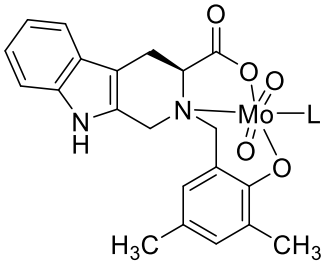

MoL9
L= Solvent

Scheme IV-3: Synthetic procedure for the preparation of Mo(VI) complexes **MoL5**, **MoL6** and **MoL9**.

The preparation of Mo(VI) compounds derived from ligand precursors **L7**, **L8**, **L10**, **L11** and **L12** was also tried within the same reaction conditions but with no success. In all cases the results obtained from elemental analyses of all the isolated solids were not in agreement with the desired Mo(VI) compounds, and the syntheses of such compounds was precluded.

IV.2.3 – Mo(VI) complexes bearing amino acid-pyridyl-phenol ligands

The synthesis of Mo(VI) compounds derived from amino acid-pyridyl-phenol ligand precursors **L13**, **L14** and **L15** was not attempted. The main reason behind this decision is based on the tetradentate nature of these ligand precursors, which could lead to the preparation of Mo(VI) compounds without labile coordination sites, hampering the application of such compounds as pre-catalysts.

IV.2.4 – Mo(VI) complexes bearing β-ketoamino acid ligands

The preparation of Mo(VI) complexes **MoL18** and **MoL19** will be resumed herein and their structural formulae are depicted in **Figure IV-4**.

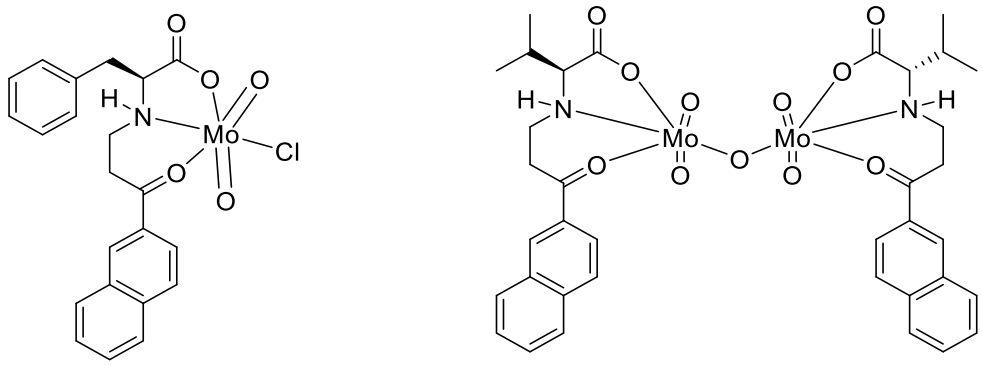

MoL18 **MoL19**

Figure IV-4: Structural formulae of the prepared Mo(VI) amino acid compounds **MoL18** and **MoL19**, based on their elemental analyses.

For the synthesis of **MoL18** and **MoL19** compounds **L18** and **L19** were used as ligand precursors, respectively. In an open vessel at room temperature the corresponding ligand precursor was suspended in ethanol and concentrated HCl was added dropwise until complete solubilization, followed by addition of $MoO_2(acac)_2$. After 10 minutes under stirring, water was added to the reaction and a white precipitate immediately formed, which was filtered and washed with distilled water and petroleum ether, yielding **MoL18** and **MoL19** as white solids in 73 and 77% yields, respectively (**Scheme IV-4**).

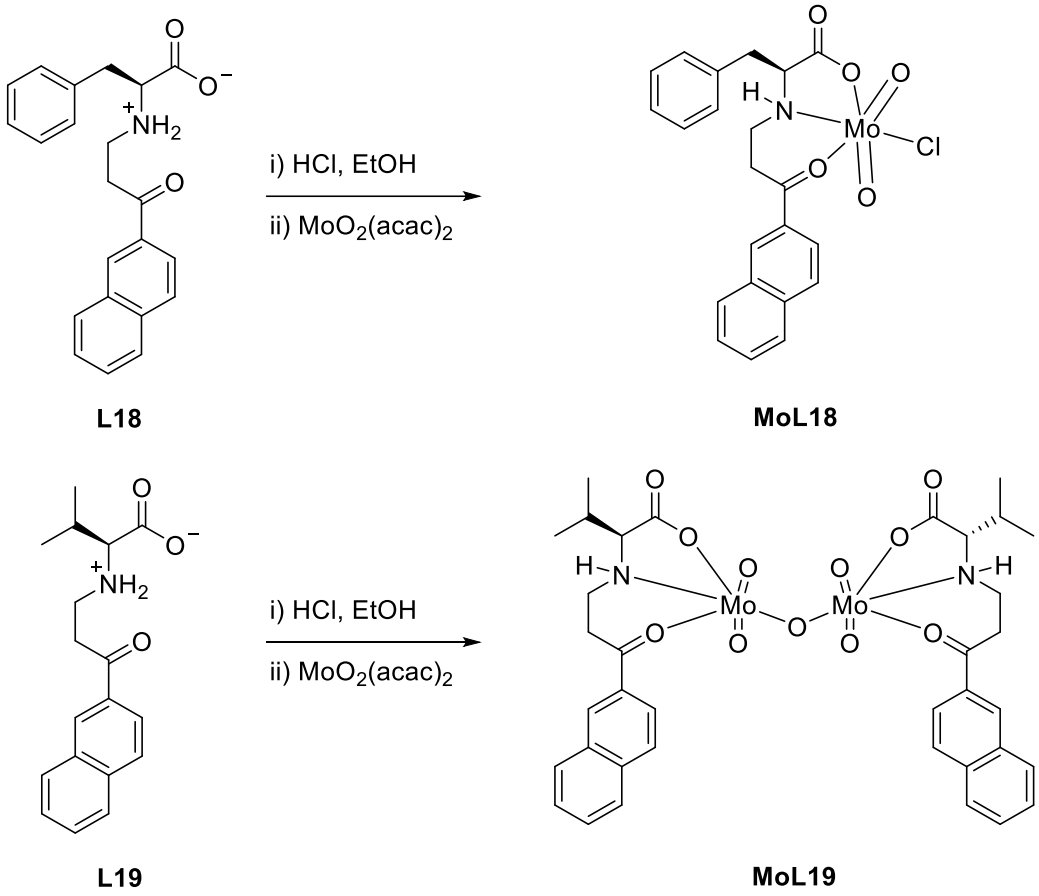

Scheme IV-4: Synthetic procedure for the preparation of Mo(VI) complexes **MoL18** and **MoL19**.

The preparation of Mo(VI) compounds derived from ligand precursors **L16** and **L17** was uncussessfully tried within the same reaction conditions. In all cases the results obtained from elemental analyses of all the isolated solids were not in agreement with the desired Mo(VI) compound structure and the syntheses of such compounds was abandoned.

IV.2.5 – Characterization by UV-Vis and CD spectroscopy

The obtained UV-Vis and CD spectra of the Mo(VI) compounds **MoL2**, **MoL5**, **MoL6**, **MoL9** and **MoL18**-**19** are presented in **Figure IV-5** and **Figure IV-6**, respectively, and the most relevant λ_{max}, ε and $\Delta\varepsilon$ values are listed in **Table IV-1**. These experiments were not conducted for **MoL1** because this compound was not soluble in the solvents used in the experiments.

All the analysed Mo(VI) complexes exhibit absorption bands in the UV region tailing into the visible region. This can account for the faint colouration of all compounds in both solution and in solid state, with exception of **MoL6** which presents an orange colour. The observed absorption bands may correspond to intraligand-based transitions or to LMCT transitions and compounds containing similar ligands show similar UV-Vis spectra profiles in general.

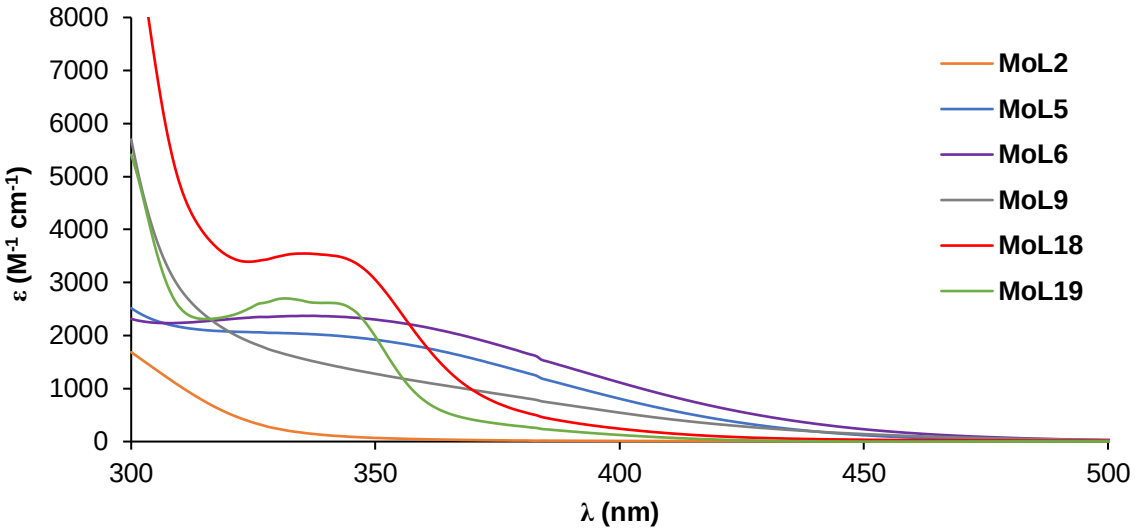

Figure IV-5: Electronic absorption (UV-Vis) spectra of compounds **MoL2** (DMSO, 0.198 mM), **MoL5** (DMSO, 0.207 mM), **MoL6** (EtOH, 0.220 mM), **MoL9** (DMSO, 0.208 mM), **MoL18** (DMSO, 0.199 mM) and **MoL19** (DMSO, 0.199 mM) at room temperature with 1 cm optical path quartz cells.

The CD spectra of Mo(VI) compounds confirm they are chiral and CD bands also appear in the UV region, assigned to ligand-based and CT transitions, considering that the chiral centers are no less than two bonds away from aromatic groups.

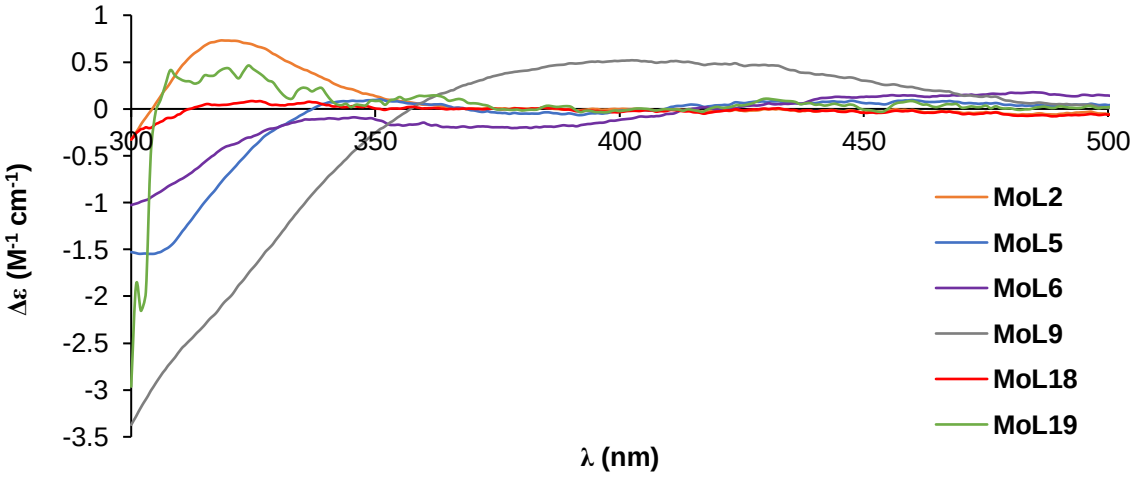

Figure IV-6: Circular Dichroism (CD) spectra of compounds **MoL2** (DMSO, 0.198 mM), **MoL5** (DMSO, 0.207 mM), **MoL6** (EtOH, 0.220 mM), **MoL9** (DMSO, 0.208 mM), **MoL18** (DMSO, 0.199 mM) and **MoL19** (DMSO, 0.199 mM) at room temperature with 1 cm optical path quartz cells.

Table IV-1: Experimental λ_{max}, ε and $\Delta\varepsilon$ values obtained in the UV-Vis and CD spectra of compounds **MoL1**, **MoL2**, **MoL5**, **MoL6**, **MoL9**, **MoL18** and **MoL19**.

	UV-Vis		CD	
Compound	**λ_{max} (nm)**	**ε (M^{-1} cm^{-1})**	**λ_{max} (nm)**	**$\Delta\varepsilon$ (M^{-1} cm^{-1})**
MoL2	300	1686.1	319	0.732
MoL5	331	2046.4	303	-1.547
MoL6	337	2371.7	378	-0.205
MoL9	300	5698.7	402	0.517
MoL18	344 335	3452.4 3546.4	-	-
MoL19	343 333	2592.6 2689.5	302	-2.155

IV.2.6 – Characterization by Mass spectrometry

The Mo(VI) compounds synthesized were analysed by ESI-MS negative and positive modes in DMSO or methanol (**MoL6**), and the mass peaks were assigned for the most probable species having no more than ±1 divergence in m/z from the observed peak. Compound **MoL1** was not analysed given its insolubility in the solvents used for the experiments.

Compound **MoL2** ESI-MS spectra were obtained in DMSO and are presented in **Figure IV-7**, showing a greater occurrence of mononuclear dioxido MoO_2**L2** species under the conditions used for the analyses. In the negative mode spectrum the more relevant mass peaks are assigned to a solvated dinuclear μ-methoxido $\{[(MoO_2\mathbf{L2})_2(OMe)]\bullet 2MeOH\}^-$ species (m/z= 766.2), a solvated mononuclear $\{[MoO_2\mathbf{L2}Cl]\bullet 3H_2O\}^-$ species (m/z= 423.2), a mononuclear $[MoO_2\mathbf{L2}(MeO)]^-$ species as the major peak (m/z= 367.4) and to a mononuclear $[MoO_2\mathbf{L2}]^-$ species (m/z= 335.2). Mass peaks with lower relative abundance appear at m/z values below 335 and are mainly assigned to products derived from the amino acid ligand decomposition. In the positive mode spectrum the peak with higher relative abundance is assigned to a diprotonated mononuclear $\{H_2[MoO_2\mathbf{L2}(OH)]\}^{2+}$ species, with an hydroxide ligand coordinated to the Mo centre (m/z= 178.7). Two other species are assigned to the protonated amino acid ligand: the $H\mathbf{L2}^+$ species (m/z= 209.1) and $\{H(\mathbf{L2})\bullet EtOH\}^+$ species (m/z= 256.4), indicating the occurrence of dissociation of **L2** from the metal centre under the conditions used for the analysis.

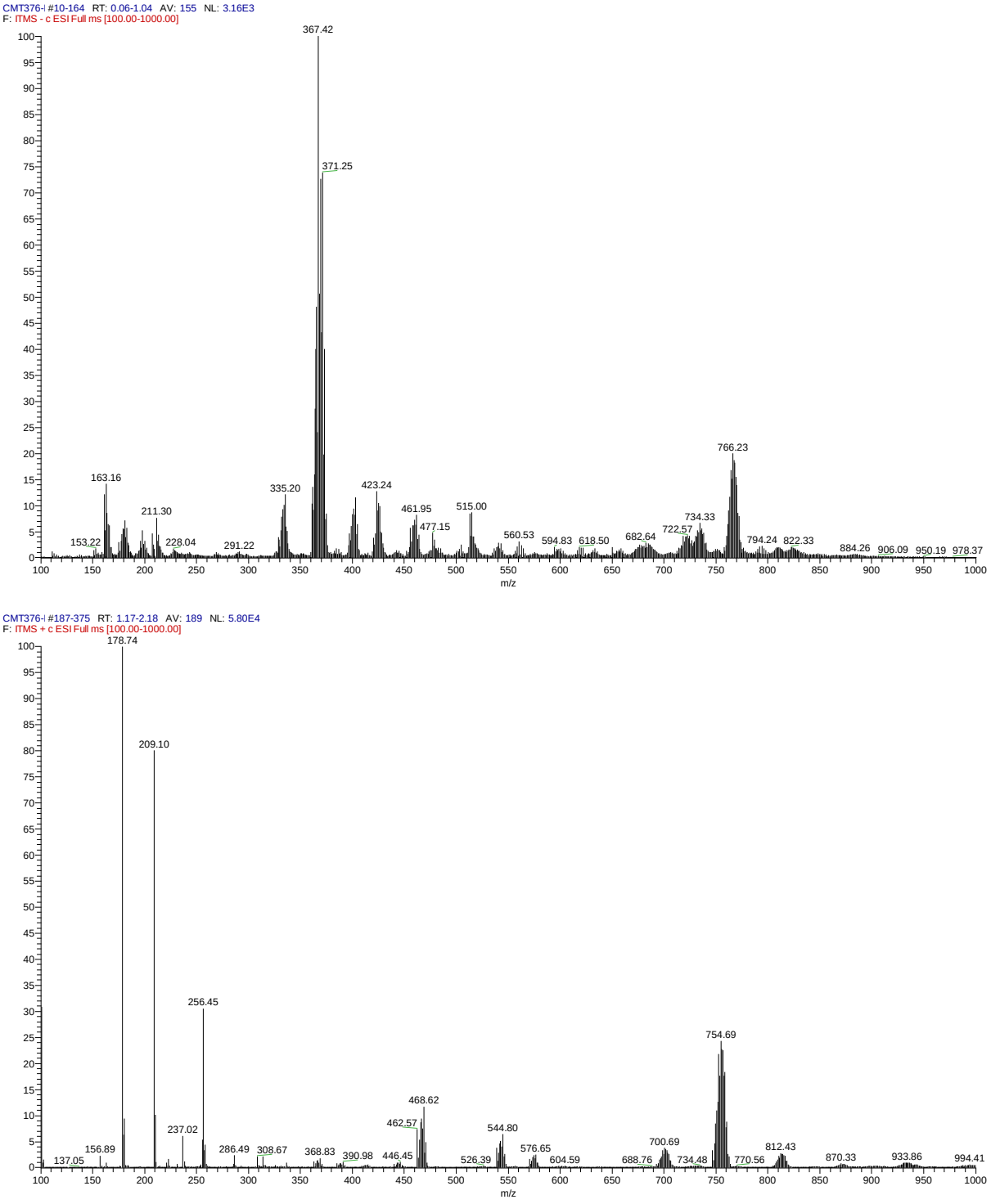

Figure IV-7: Negative (up) and positive (down) ESI-MS spectra of **MoL2** in DMSO.

The ESI-MS spectra of **MoL5** were obtained in DMSO and are presented in **Figure IV-8**. In the negative mode spectrum the relevant mass peaks are assigned to dinuclear and mononuclear MoO_2**L5** species: a dinuclear μ-methoxido $[(MoO_2\mathbf{L5})_2(OMe)]^-$ species (m/z= 880.8), a dinuclear $\{[MoO_2\mathbf{L5}]_2\}^-$ species (m/z= 848.8), a mononuclear $[(MoO_2\mathbf{L5})\mathbf{L5}]^-$ species containing an extra amino acid ligand (m/z= 724.9), a mononuclear solvated

{[MoO_2**L5**]•MeOH}$^-$ species (m/z= 456.2) and an unsolvated mononuclear [MoO_2**L5**]$^-$ species (m/z= 426.5). In the positive mode the peak with major relative abundance is assigned to the protonated amino acid ligand H**L5**$^+$ (m/z= 300.06) and the respective solvated sodium adduct {Na(**L5**)•3H_2O}$^+$ species is also detected (m/z= 377.5). The assignment of such species confirm the occurrence of dissociation of the amino acid ligand under the conditions used for the analysis. Two mass peaks are also assigned to mononuclear MoO_2**L5** species such as the solvated dicationic sodium adduct {Na_2[MoO_2**L5**]•MeOH•7H_2O}$^{2+}$ species (m/z= 314.0) and the protonated {H[MoO_2**L5**]}$^+$ species, this one with a very residual relative abundance (m/z= 726.4).

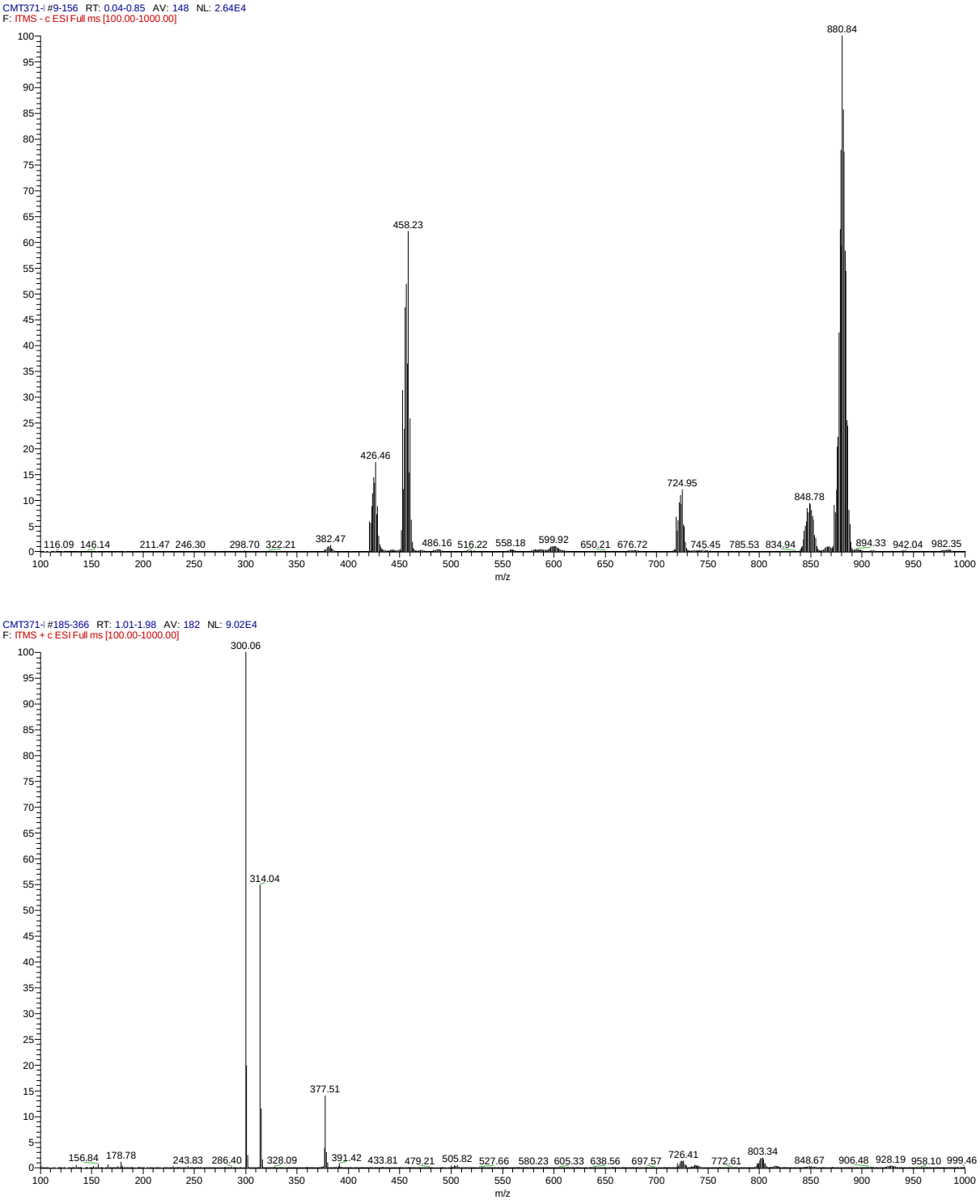

Figure IV-8: Negative (up) and positive (down) ESI-MS spectra of **MoL5** in DMSO. Negative mode spectrum shows the presence of dinuclear and mononuclear dioxido MoO_2**L5** species and dioxido MoO_2**L5**$_2$ aggregates; positive mode spectrum clearly indicate dissociation of the amino acid ligand.

Compound **MoL6** ESI-MS spectra were obtained in methanol and are presented in **Figure IV-9**, with the mass peak assignments indicating dissociation of **L6** and the presence of oligonuclear dioxido MoO_2**L6** aggregates under the conditions used for the analyses. In the negative mode the mass peaks are assigned to the dinuclear $[(MoO_2\mathbf{L6})_2\mathbf{L6}]^-$ species containing an extra amino acid ligand (m/z= 1400.1), the dinuclear $\{[MoO_2\mathbf{L6}]_2\}^-$ species (m/z= 1017.5), the mononeric $[(MoO_2\mathbf{L6})\mathbf{L6}]^-$ species containing an extra amino acid ligand (m/z= 892.9), the mononuclear $[MoO_2\mathbf{L6}]^-$ species (m/z= 510.2) and its respective dianionic $[MoO_2\mathbf{L6}]^{2-}$ species, which depicts the major relative abundance (m/z= 253.2). In the positive mode spectrum the more relevant mass peaks are assigned to a trinuclear monoanionic sodium adduct $\{Na[(MoO_2\mathbf{L6})_3]\}^+$ species with the major peak (m/z= 1550.7), the mononuclear protonated $\{H[(MoO_2\mathbf{L6})\mathbf{L6}]\}^+$ species with an extra amino acid ligand (m/z= 1421.7) and the protonated amino acid $H\mathbf{L6}^+$ (m/z= 384.2).

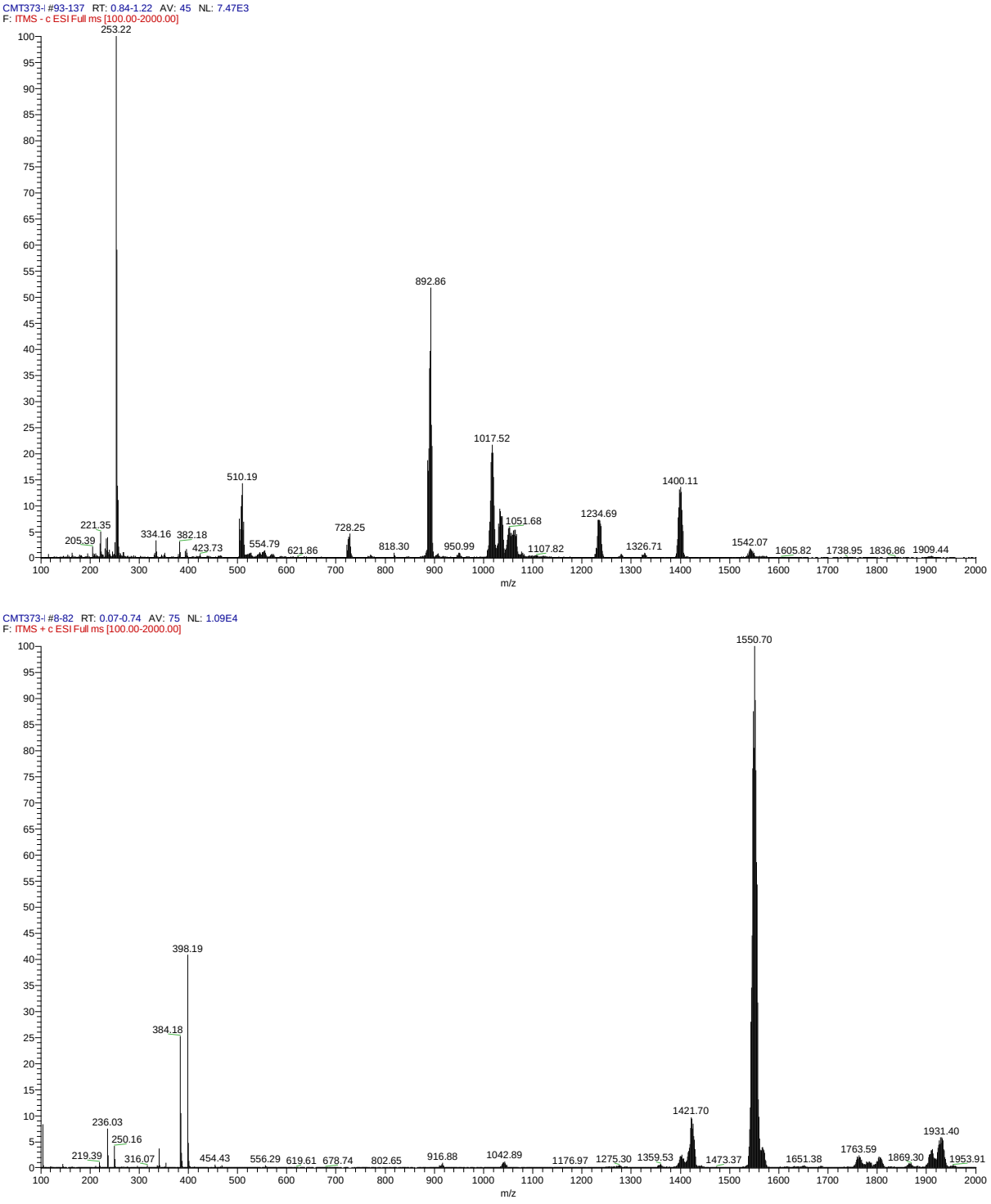

Figure IV-9: Negative (up) and positive (down) ESI-MS spectra of **MoL6** in MeOH. The mass peak assignments indicate dissociation of **L6** and the presence of oligonuclear dioxido MoO_2**L6** aggregates under the conditions used for the analyses.

The ESI-MS spectra of **MoL9** were obtained in DMSO and are presented in **Figure IV-10**, indicating the occurrence of demetallation of **L9** during the experiments. In the negative mode spectrum the mass peaks are attributed to a mononuclear $[(MoO_2$**L9**$)$**L9**$]^-$ species containing an extra amino acid ligand (m/z= 826.8) and to a solvated mononuclear $\{[MoO_2$**L9**$]$•MeOH$\}^-$

species as the major peak (m/z= 509.1). In the positive mode spectrum the major peak is assigned to the protonated amino acid ligand adduct (H**L9**$^{+}$, m/z= 351.1).

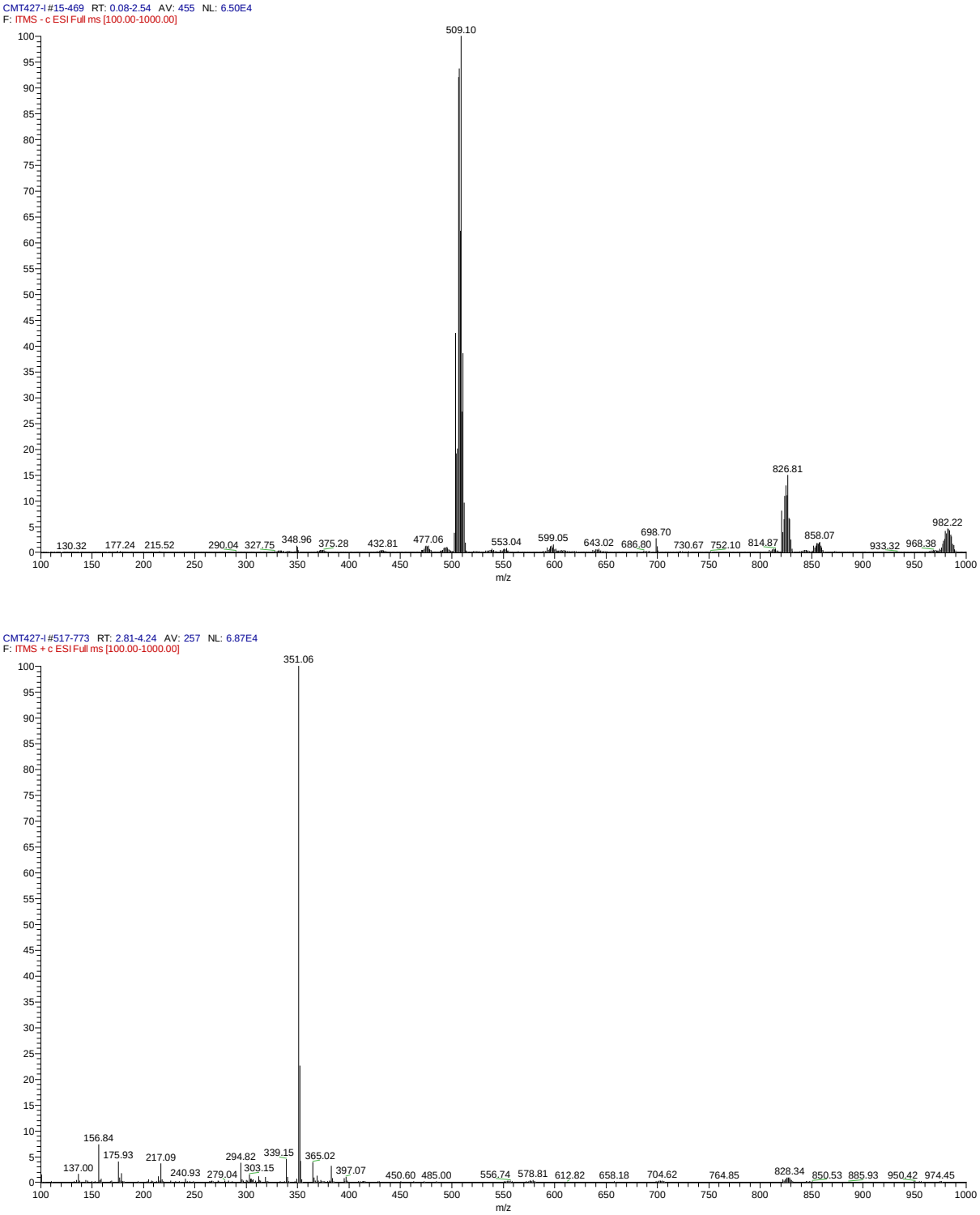

Figure IV-10: Negative (up) and positive (down) ESI-MS spectra of **MoL9** in DMSO. Negative mode spectrum shows the presence of mononuclear dioxido MoO_2**L9** species and dioxido MoO_2**L9**$_2$ aggregates; positive mode spectrum indicate dissociation of the amino acid ligand.

Compound **MoL18** ESI-MS spectra were obtained in DMSO and are presented in **Figure IV-11**, with the mass peak assignments indicating dissociation of **L18** and the presence of oligonuclear dioxido MoO_2**L18** aggregates under the conditions used for the analyses. The negative mode spectrum show several mass peaks with moderate relative abundances, attributed to a mononuclear $[(MoO_2\mathbf{L18})\mathbf{L18}]^-$ species containing an extra amino acid ligand (m/z= 820.9), a solvated oligonuclear trianionic $\{[MoO_2\mathbf{L18}(OH)]_4 \bullet 3MeOH \bullet 2H_2O\}^{3-}$ species (m/z= 704.8), a dianionic $[MoO_2\mathbf{L18}(OH)]^{2-}$ species (m/z= 492.0), a solvated mononuclear $\{[(MoO_2\mathbf{L18})\mathbf{L18}] \bullet 3MeOH]\}^{2-}$ species (m/z= 458.1) and the amino acid ligand $\mathbf{L18}^-$ (m/z= 345.9). The major peak is assigned to a solvated oligonuclear trianionic $\{[MoO_2\mathbf{L18}(OH)]_4 \bullet 2MeOH \bullet 2H_2O\}^{3-}$ species (m/z= 692.9). In the positive mode spectrum the mass peaks are assigned to the mononuclear deprotonated sodium adduct $\{H_2Na[MoO_2\mathbf{L18}(OH)]\}^{3+}$ species, respective to the major mass peak (m/z= 178.8), the solvated mononuclear sodium adduct $\{Na_2[MoO_2\mathbf{L18}] \bullet MeOH \bullet 2H_2O\}^{2+}$ species (m/z= 310.5) and the protonated amino acid ligand $H\mathbf{L18}^+$ (m/z= 348.1).

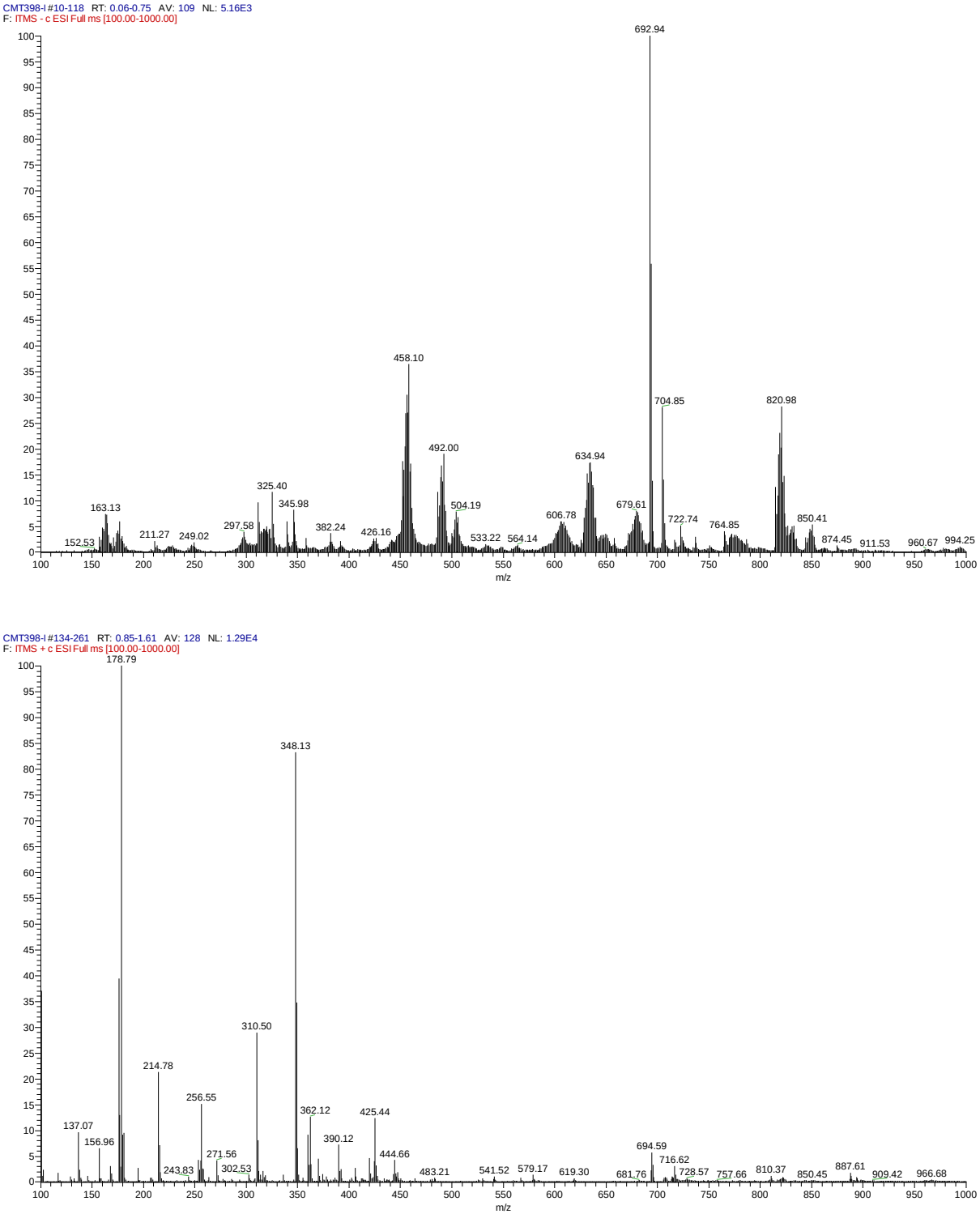

Figure IV-11: Negative (up) and positive (down) ESI-MS spectra of **MoL18** in DMSO, with the mass peaks being attributed to oligonuclear and mononuclear dioxido MoO_2**L18** species, dioxido MoO_2**L18**$_2$ aggregates and amino acid ligand **L18**.

The ESI-MS spectra of compound **MoL19** were obtained in DMSO and are depicted in **Figure IV-12**, indicating dissociation of the amino acid ligand and the existence of mononuclear dioxido MoO_2**L19** species under the conditions applied for the analyses. The mass peaks in

the negative mode spectrum are assigned to a mononuclear [(MoO_2**L19**)**L19**]$^-$ species containing an extra amino acid ligand (m/z= 725.0), two solvated mononuclear species, {[(MoO_2**L19**)(OH)]•EtOH•6H_2O}$^-$ and {[(MoO_2**L19**)(OH)]•3EtOH•3H_2O}$^-$ with the first being the major peak (m/z= 597.1 and 319.1, respectively) and the corresponding [(MoO_2**L19**)(OH)]$^-$ species without a solvation pattern (m/z= 444.2) and to the amino acid ligand **L19**$^-$ (m/z= 298.1). The positive mode sees the mass peaks assigned to a mononuclear protonated [H(MoO_2**L19**)**L19**]$^+$ species containing an extra amino acid ligand (m/z= 726.9), a protonated mononuclear {H[(MoO_2**L19**)(OH)]•2H_2O}$^+$ species with a coordinated hydroxide ligand (m/z= 598.5), a solvated dinuclear μ-oxido {HNa[(MoO_2**L19**)$_2$(O)]•4H_2O}$^{2+}$ sodium adduct (m/z= 483.7), the sodium adduct {Na(**L19**)•3H_2O}$^+$ species of the amino acid ligand as the major peak (m/z= 377.4) and the monopositive amino acid ligand **L19**$^+$ (m/z= 300.1).

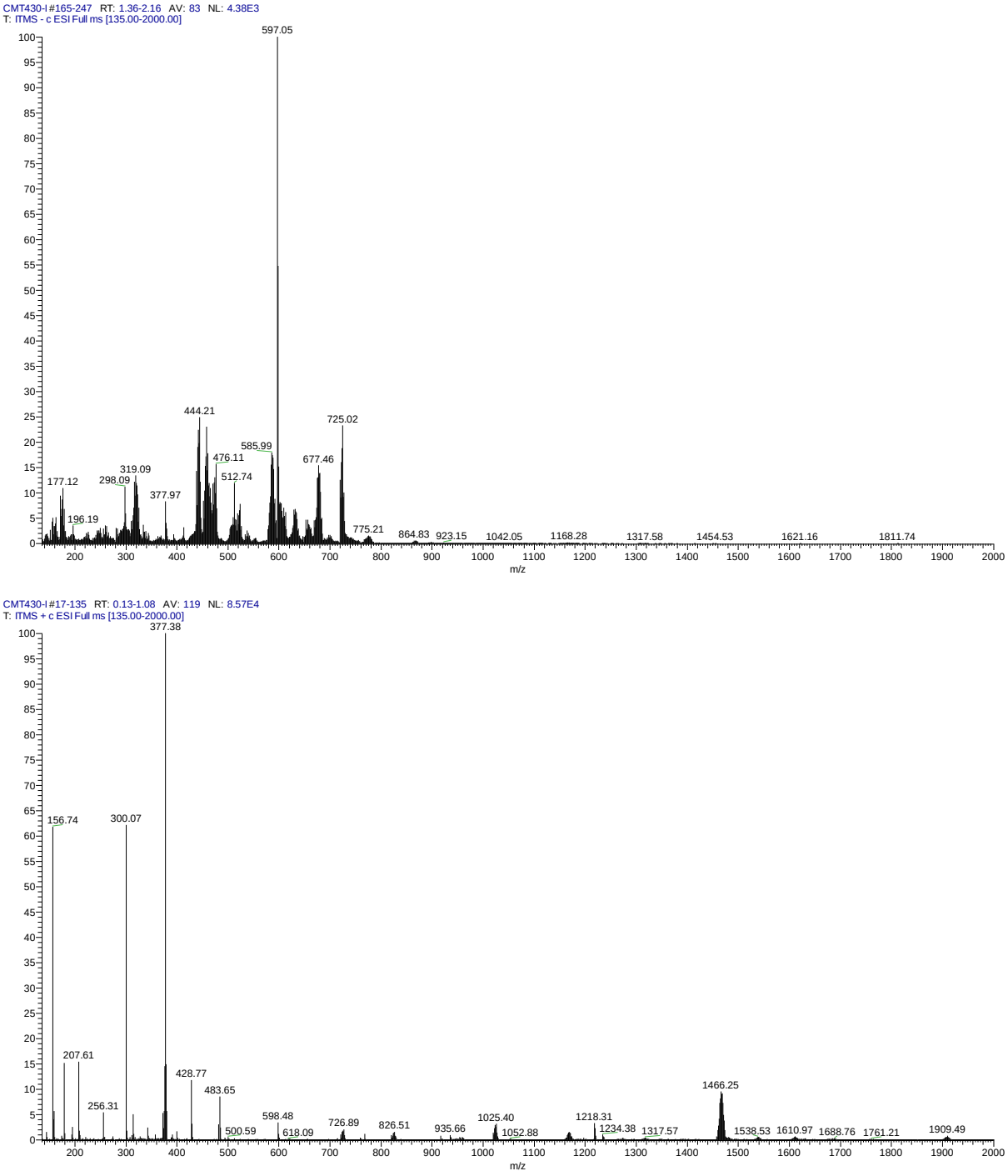

Figure IV-12: Negative (up) and positive (down) ESI-MS spectra of **MoL19** in DMSO. Both spectra indicate the presence of dinuclear and mononuclear dioxido MoO_2**L19** species, dioxido MoO_2**L19**$_2$ aggregates and the occurrence of dissociation of the amino acid ligand.

IV.2.7 – Characterization by Infrared spectroscopy

The FT-IR spectra of solid samples of the prepared Mo(VI) compounds were analysed and the most relevant vibrational frequencies are listed in **Table IV-2**. All compounds exhibited ν(N-H) and a ν(C=O) stretching vibration bands at *ca*. 3000-3200 and 1600 cm^{-1} correspondent to the

amino and carboxyl groups of the amino acid ligand, respectively, and two strong ν(Mo=O) stretching bands at *ca*. 900 cm^{-1}, which is the most relevant information given by FT-IR for dioxido-Mo(VI) compounds.[173,174] Compounds **MoL1** and **MoL19** show two bands each at *ca*. 740 and 475 cm^{-1} respective to antisymmetric and symmetric ν(Mo-O-Mo) bridge-stretching modes, respectively.[173] Compounds **MoL5**, **MoL6** and **MoL9** show a ν(C-O) bending vibration band at ca. 1220 cm^{-1}, coresponding to the phenolate moiety.

Table IV-2: IR stretching frequencies for the prepared Fe(III) compounds **FeL5**, **FeL6** and **Fe8**-**11**.

Stretching mode	**MoL1**	**MoL2**	**MoL5**	**MoL6**	**MoL9**	**MoL18**	**MoL19**
	Wavenumber (cm^{-1})						
ν(N-H)	3232	3047	3127	3242	3056	3054	3055
ν(C=O)	1656	1622	1624	1660	1616	1676	1679
ν(C-O_{Phenol})	-	-	1233	1235	1218	-	-
ν(Mo=O)	939; 897	937; 904	947; 923	919; 909	911; 896	946; 909	942; 906
ν(Mo-O-Mo)	743; 478	-	-	-	-	-	742; 476

IV.2.8 – Elemental analysis

Compounds **MoL2**, **MoL5**, **MoL6**, **MoL9**, and **MoL18** gave elemental analysis results consistent with mononuclear species having either water or alcohols as contaminants. The elemental analysis from compounds **MoL1** and **MoL19** afforded elemental analysis results consistent with dinuclear species containing either water or alcohols as vestigial contaminants.

IV.2.9 – Cyclic Voltammetry

The redox properties of the Mo(VI) compounds **MoL2**, **MoL5**-**6**, **MoL9** and **MoL18**-**19** were studied by CV and the results are presented below. Data collected in these experiments is listed in **Table IV-3**. The redox properties were not performed to compound **MoL1** due to its insolubility in several organic solvents tested (*e.g.* DMF, DMSO, MeCN).

Table IV-3: Cyclic voltammetry data for Mo(VI) complexes in Bu_4NBF_4 / DMSO, corresponding Mo(VI)→Mo(V) reduction processes.

Compound	E_p^{red} (V)
MoL2	-0.88[a]
MoL5	-1.29
MoL6	-1.33
MoL9	-1.29
MoL18	-0.95
MoL19	-0.92

[a]Reversible wave $E_{1/2}^{Red}$= -0.83 V. Values (±10 mV) measured vs. SCE at 200 mV s^{-1} using ferrocene as an internal reference ($[Fe(\eta^5\text{-}C_5H_5)_2]^{0/+}$, $E_{1/2}^{ox}$=0.440 in DMSO)

Mo(VI) complex **MoL2** shows two overlapped cathodic waves at E_p^{red}= -0.79 V and -0.88 V, with an oxidation counterpart at E_p^{ox}= -0.74 V (**I**, **II** and **III**, respectively, in **Figure IV-13**).

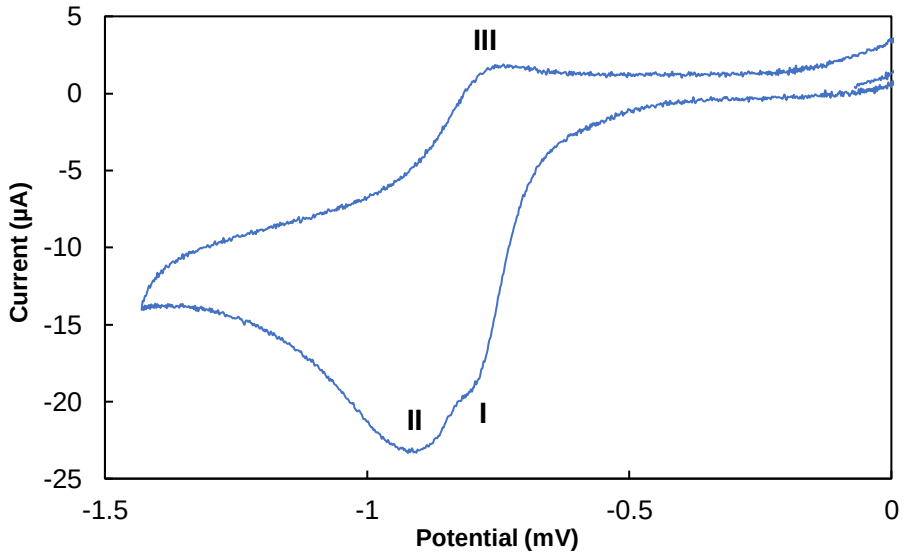

Figure IV-13: Cyclic voltammogram (cathodic scan) of **MoL2** in Bu_4NBF_4 / DMSO.

These redox processes are characteristic of **MoL2** since no similar redox waves are visible in the potential range of -0.70 to -0.90 V in the isolated ligand (see **Figure III-37**, orange line). The reduction wave **II** can be attributed to Mo(VI)→Mo(V) reduction, based on previous reports in the literature.[175,176] Wave **I** may correspond to the formation of a reduced anionic $[Mo(V)]^-$ species, which after dissociation of a Cl^- anion also generates a neutral [Mo(V)] species (**Scheme IV-5**).

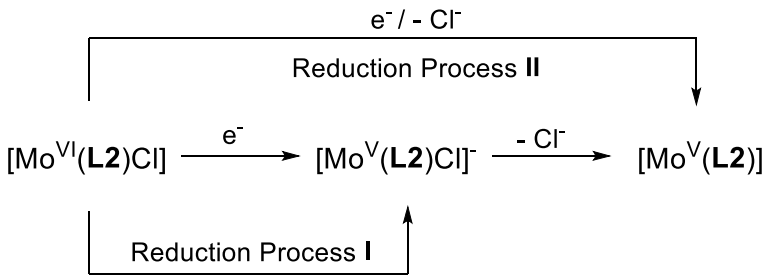

Scheme IV-5: Reduction processes **I** and **II** corresponding to waves **I** and **II** of **Figure IV-13**, respectively.

The oxidation process **III** is the counterpart of the referred reduction process **II**, and its intensity increase with the increase on the current density (**Figure IV-14**); a linear relationship between the current intensity vs the square-root of the scan rate is observed, in agreement with the Randles-Sevcik equation (**Eq.III-1**).

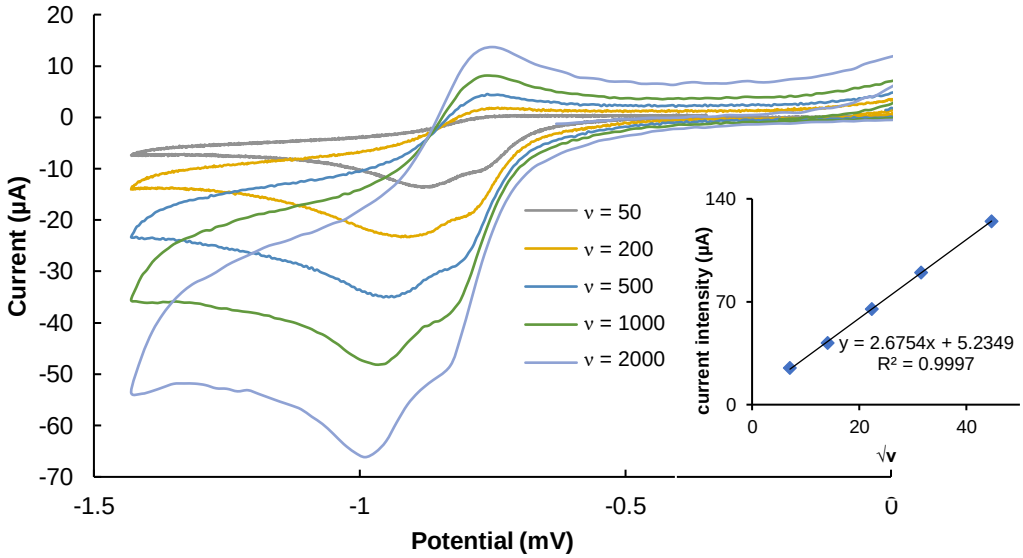

Figure IV-14: Cyclic voltammogram (cathodic scan) of **MoL2** in Bu_4NBF_4 / DMSO for different scan rates.

Mo(VI) compounds **MoL5**, **MoL6** and **MoL9** show comparable redox behaviour and a cathodic scan voltammogram of compound **MoL5** is presented in **Figure IV-15**. An irreversible cathodic reduction wave appears at E_p^{red}= -1.29 V, corresponding to a Mo(VI)→Mo(V) reduction process, as described in the literature for phenolate-containing Mo(VI) compounds[176] (**I**, **Figure IV-15**), and an independent oxidation wave at E_p^{ox}~0 V (**II**, **Figure IV-15**).

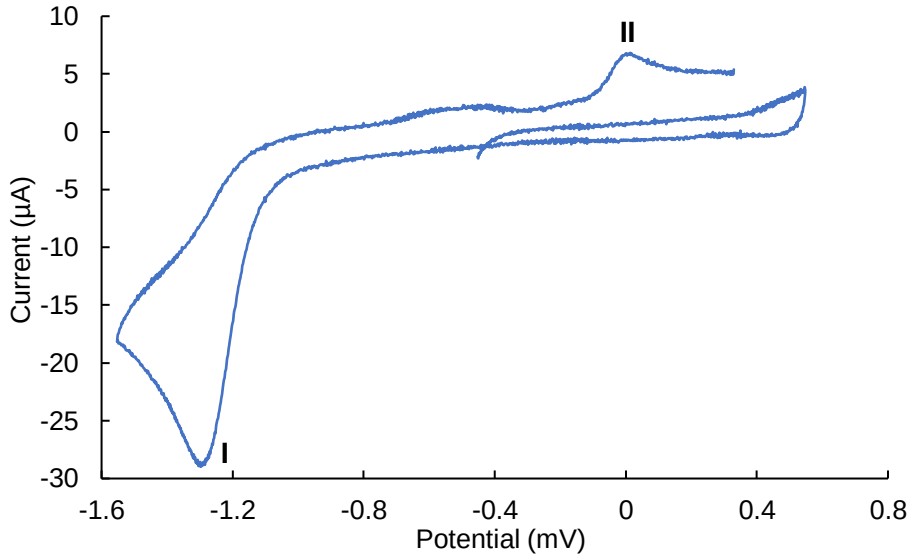

Figure IV-15: Anodic cyclic voltammogram of **MoL5** in Bu_4NBF_4 / DMSO.

The oxidation process **II** is not original of these compounds and corresponds to an electrochemical species formed after a cathodic scan till potentials below *ca.* -1.2 V. No similar oxidation waves appear if an anodic scan is firstly performed (**Figure IV-15**, from -0.5 V to 0.5 V).

Mo(VI) compounds **MoL18** and **MoL19** show an irreversible cathodic reduction wave at E_p^{red}= -0.95 V and E_p^{red}= -0.93 V, respectively, attributed to a Mo(VI)→Mo(V) reduction process based on values reported in the literature for Mo(VI) compounds.[175,176]

IV.3 – Catalytic applications

The catalytic performance of the prepared Mo(VI) complexes was evaluated under the same catalytic conditions applied with the Fe(III) complexes in Section **III.5.2.1**. A schematic representation of the tested reactions in the epoxidation of **HC** and **MeOC** is presented below in **Scheme IV-6**.

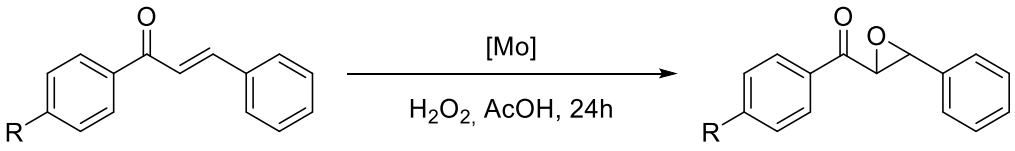

HC: R= H;
MeOC: R= OMe

Scheme IV-6: Epoxidation of benzalacetophenones **HC** and **MeOC** with H_2O_2 and AcOH.

These studies were initially performed for **HC** epoxidation (i) without any additive and (ii) with addition of 2 mole equivalents of H_2O_2 with and without 10 mol% of AcOH in MeCN. Results are shown in **Table IV-4**, and no epoxide products or even substrate conversion was observed at room temperature upon 24 h reactions. The same outcomes were obtained in acetone or acetone:H_2O (3:1) for both substrates. The use of stronger oxidants such as cumene hydroperoxide (CHP) or TBHP, without any addition of AcOH, was also tested but afforded the same outcomes. Therefore, catalytic epoxidation with these conditions were abandoned.

The Mukaiyama epoxidation procedure developed in Section **III.5.2.2** was also tested with the prepared Mo(VI) complexes within the optimized conditions: 1 mmol substrate, 4 mol % [Mo], 4 mL solvent, 2 mole equivalents of isobutyraldehyde and addition of 2 more equivalents after the first 12 h in a 24 h reaction. Unfortunately, no substrate conversion or epoxide yields were obtained in these conditions for both substrates, and these studies were also excluded.

Table IV-4: Results obtained in the non-heme epoxidation of **HC** with H_2O_2 and AcOH.

Entry	[Mo]	Substrate	Oxidant	Additive	Solvent	Conv. (%)	Oxirane (%)
1	**MoL1**	**HC**	-	-	MeCN	-	-
2	**MoL2**	**HC**	-	-	MeCN	-	-
3	**MoL5**	**HC**	-	-	MeCN	-	-
4	**MoL6**	**HC**	-	-	MeCN	-	-
5	**MoL9**	**HC**	-	-	MeCN	-	-
6	**MoL18**	**HC**	-	-	MeCN	-	-
7	**MoL19**	**HC**	-	-	MeCN	-	-
8	**MoL1**	**HC**	2 H_2O_2	-	MeCN	-	-
9	**MoL2**	**HC**	2 H_2O_2	-	MeCN	-	-
10	**MoL5**	**HC**	2 H_2O_2	-	MeCN	-	-
11	**MoL6**	**HC**	2 H_2O_2	-	MeCN	-	-
12	**MoL9**	**HC**	2 H_2O_2	-	MeCN	-	-
13	**MoL18**	**HC**	2 H_2O_2	-	MeCN	-	-
14	**MoL19**	**HC**	2 H_2O_2	-	MeCN	-	-
15	**MoL1**	**HC**	2 H_2O_2	10% AcOH	MeCN	-	-
16	**MoL2**	**HC**	2 H_2O_2	10% AcOH	MeCN	-	-
17	**MoL5**	**HC**	2 H_2O_2	10% AcOH	MeCN	-	-
18	**MoL6**	**HC**	2 H_2O_2	10% AcOH	MeCN	-	-
19	**MoL9**	**HC**	2 H_2O_2	10% AcOH	MeCN	-	-
20	**MoL18**	**HC**	2 H_2O_2	10% AcOH	MeCN	-	-
21	**MoL19**	**HC**	2 H_2O_2	10% AcOH	MeCN	-	-

Reaction conditions: In a closed 10 mL vessel, 1 mmol chalcone, 1 mol% [Mo], 4 mL solvent, r.t., 24 h. Conversion of chalcone and epoxide yields were determined by HPLC.

The amino acid-derived ligands can stabilize to a wide extent the obtained Mo(VI) complexes, greatly influencing their poor catalytic behaviour within these conditions in the epoxidation of chalcones. Wang and co-workers[99] applied *in situ*-formed amino alcohol and amino acid-derived Mo(VI) complexes in the catalytic epoxidation of styrene and styrene derivatives, and observed that with amino acid ligands residual epoxide yields, up to 9%, were detected at room temperature, even using a strong oxidant such as CHP. Also important seems to be the redox behaviour of the amino acid complexes prepared in this work, with $\boldsymbol{E_p^{red}}$ values ranging between -0.88 and -1.29 V with an irreversible behaviour in general; such observation indicate that these complexes are not easily reduced and therefore, if the catalytic cycle requires reduction of the Mo(VI) complex, such reduction is difficult. The same can be pointed in the Mukaiyama epoxidations; in metal-assisted Mukaiyama epoxidations, the role of the metal complex is in the initiation step of the radical chain process and in the stabilization of the acylperoxy radical (see **Scheme I-22**).[84,85] With such negative potentials, the prepared Mo(VI) compounds may not be so prone in accepting electrons and promote these steps.

The pointed reasons may justify the poor catalytic behaviour of the prepared Mo(VI) complexes.

IV.4 – Conclusions

A series of Mo(VI) complexes containing amino acid-pyridyl, amino acid-phenol and β-ketoamino acid ligands were prepared applying simple and mild one-pot conditions. All compounds were isolated as white solids, except **MoL6** wich presented an orange colour. All compounds were characterized by UV-Vis and CD spectroscopy, ESI-MS, FTIR, Cyclic Voltammetry and elemental analysis. All the compounds CD spectra showed chirality in solution. The ESI-MS spectra analysis confirms the presence of mononuclear and dinuclear Mo(VI) species, showing the occurrence of dissociacion of the amino acid ligand from the metal centre, under the conditions applied in the experiments. The Infrared spectroscopy confirmed the presence of the functional groups of the amino acid ligands in the Mo(VI) complexes, as well as the presence of two strong ν(Mo=O) stretching bands at *ca*. 900 cm^{-1} to all compounds. Cyclic Voltammetry data showed that all Mo(VI) complexes display one cathodic irreversible reduction wave at potentials in the range -1.29 to -0.92V, except **MoL2** which shows a quasi-reverible cathodic wave at -0.83 V.

All the synthesized Mo(VI) complexes were applied as pre-catalysts in the epoxidation of benzalacetophenones. Under the applied catalytic conditions, these Mo(VI) compounds prove to be inactive pre-catalysts for these reactions. The stabilization of Mo(VI) by the amino acid

ligands, allied with the low reduction potencials presented by these complexes, can justify the poor results presented.

IV.5 – Experimental Section

IV.5.1 – General considerations

All Mo(VI) compounds synthesis, isolation and purification were done without air exclusion. All solvents and reagents were purchased from commercial suppliers and used as received.

IV.5.2 – Characterization Techniques

IV.5.2.1 – UV-Vis and CD Spectroscopy

UV-Vis spectra were recorded using a Shimadzu U-2000 spectrophotometer. CD spectra were recorded using a Jasco J-720 Spectropolarimeter.

IV.5.2.2 – Electrospray Ionization Mass Spectrometry (ESI-MS)

The ESI mass experiments were made by Prof. Maria da Conceição Oliveira and Msc. Ana Dias at Centro de Química Estrutural of Instituto Superior Técnico. The ESI mass spectra were obtained on a LCQ Fleet ion trap mass spectrometer equipped with an electrospray ion source, operated in the positive and negative mode. The operated parameters were optimized for maximum abundance of the ions of interest, as follows: ion spray voltage, +5 kV; capillary voltage, 5/-20 V; tube lens offset, -125/63 V, sheath gas (N_2), 20 arbitrary units; capillary temperature, 275ºC. Spectra obtained are the average results from 20 to 35 scans, and were saved within the range 100-2000 Da.

IV.5.2.3 – Infrared Spectroscopy (FT-IR)

FT-IR spectra were recorded in KBr disks using a JASCO FT/IR-430 spectrometer. The frequency correspondent to the maximum absorption is presented in cm^{-1}, followed by the molecular group attributed and band intensities: s (strong), m (medium), w (weak), b (broad).

IV.5.2.4 – Elemental Analysis

Elemental analyses were carried out at Laboratório de Análises of Instituto Superior Técnico, using a Perkin Elmer EA110 CE automatic analyzer Instrument. The results presented are the average values obtained from two independent determinations.

IV.5.2.5 – Cyclic Voltammetry

The redox properties were studied by Cyclic Voltammetry (under nitrogen) using a three-compartment cell, equipped with Pt electrodes using a Radiometer Analytical Voltammetry PST050 VoltaLab equipment, interfaced with a computer. The cyclic voltammograms were obtained in a $[Bu_4N][BF_4]$/DMSO solution (0.10 M), depending on the analysed Mo(VI) compound. DMSO was distilled and dried with molecular sieves before use. The potentials (±10 mV) are quoted *versus* the saturated calomel electrode (SCE) and measured at 200 mV s^{-1} using ferrocene ($[Fe(\eta^5\text{-}C_5H_5)_2]^{0/+}$, $E_{1/2}^{ox}$=0.440 V in DMSO) as an internal reference.

IV.5.3 – Catalytic studies

IV.5.3.1 – Techniques applied in the control of catalytic reactions

IV.5.3.1.1 – High Performance Liquid Chromatography (HPLC)

The analyses of the products obtained in epoxidation reactions were done by HPLC using a Jasco system equipped with a Daicel Chiralpak IA column, a 870-UV Intelligent UV-Vis detector, two 880-PU Intelligent HPLC Pumps, a 2-line degasser 880-51 and a Rheodyne 725i injector (5 µL). The system uses Borwin software for data acquisition and analysis. The calibration of each reagent and product was performed by single point calibration, using toluene as internal standard. The detection wavelength used was 220 nm. The eluent used was *n*-heptane:propan-1-ol (98:2) and *n*-heptane:propan-2-ol (9:1), respectively, for the catalytic reactions with **HC** and **MeOC**, with a flow rate of 1.0 mL min^{-1}. Before analysis by HPLC, 1 mmol of toluene (internal standard) was added to the reaction mixture.

General procedures for the epoxidation of benzalacetophenones under non-heme hydrogen peroxyde-acetic acid conditions

The catalytic experiments were carried out at constant temperature in a closed 10 mL glass batch reactor, equipped with a magnetic stirrer. In a typical run, substrate **HC** (1.0 mmol), Fe(III) complex (1.0 mol %), H_2O_2 (2.0 mmol) and AcOH (0.1 mol%) were mixed in 4 mL of MeCN. The reaction mixture was magnetically stirred for 24 hours at 25ºC. Control experiments were carried out by HPLC in the absence of the pre-catalyst.

General procedures for the epoxidation of benzalacetophenones under Mukaiyama conditions

The catalytic experiments were carried out at atmospheric pressure and at constant temperature in an opened 10 mL glass batch reactor, equipped with magnetic stirrer. In a typical run, substrate **HC** or **MeOC** (1.0 mmol), Fe(III) complex (4.0 mol%) and isobutyraldehyde (2.0 mmol) were mixed in the respective solvent (4 mL). The reaction mixture was magnetically stirred for 24 h at 25ºC. Control experiments were carried out in the absence of pre-catalyst.

IV.5.4 – Mo(VI) Compounds Preparation Methods

IV.5.4.1 – Mo(VI) complexes bearing amino acid-pyridyl and amino acid-imidazolyl ligands

General synthetic procedure: Ligand precursor **L1** or **L2**, depending on the desired Mo(VI) compound, was suspended in EtOH (5.0 mL/mmol ligand precursor) in a round bottom flask at room temperature and concentrated HCl (1.0 eq/mmol ligand precursor) was added dropwise to the ethanolic suspension. After complete solubilization of the reaction mixture under magnetic stirring, $MoO_2(acac)_2$ (1.0 eq/mmol ligand precursor) was added to the mixture which was let to stir for additional 10 minutes, resulting in yellow-orange solution. Then, diethyl ether was added to the flask and different *work-up* procedures were performed for each compound preparation that will be specified in each case.

Synthesis of MoL1:

Reagents: **L1** (1 g, 3.91 mmol), concentrated HCl (0.33 mL, 3.91 mmol), $MoO_2(acac)_2$ (1.27 g, 3.91 mmol), EtOH (19.6 mL). After addition of diethyl ether, distilled water was added to the reaction mixture to aid in the formation of a precipitate which was filtered and washed with distilled water (2x20 mL) and petroleum ether (2x20 mL), affording **MoL1** as a white solid. Yield: 40% (0.61 g). ν_{max}/cm^{-1}: 3232 (N-H, w), 1656 (C=O, s), 939, 897 (Mo=O, s, s), 743, 478 (Mo-O-Mo, s, m). Elemental analysis for $C_{30}H_{30}Mo_2N_4O_9 \cdot 0.5H_2O$: calcd. C 45.53, H 3.95, N 7.08; found C 45.37, H 3.79, N 6.91.

Synthesis of MoL2:

Reagents: **L2** (1 g, 4.80 mmol), concentrated HCl (0.41 mL, 4.80 mmol), $MoO_2(acac)_2$ (1.57 g, 4.80 mmol), EtOH (24 mL). After addition of diethyl ether a precipitate formed, which was filtered and washed with distilled water (2x20 mL) and petroleum ether (2x 20 mL), affording **MoL2** as a white solid. Yield: 25% (0.47 g). ESI-MS [DMSO]: m/z= 766.23

($\{[(MoO_2$**L2**$)_2(OMe)]\bullet 2MeOH\}^-$, 20%), m/z= 423.24 ($\{[MoO_2$**L2**$Cl]\bullet 3H_2O\}^-$, 15%), m/z= 367.42 ($[MoO_2$**L2**$(MeO)]^-$, 100%), m/z= 335.20 ($[MoO_2$**L2**$]^-$, 15%), m/z= 178.74 ($\{H_2[MoO_2$**L2**$(OH)]\}^{2+}$, 100%). ν_{max}/cm^{-1}: 3047 (N-H, w), 1622 (C=O, s), 937, 904 (Mo=O, s, s). Elemental analysis for $C_{11}H_{15}MoN_2O_4\bullet H_2O$: calcd. C 33.99, H 4.41, N 7.21; found C 34.28, H 4.27, N 6.97.

IV.5.4.2 – Mo(VI) complexes bearing amino acid-phenol ligands

General synthetic procedure: Ligand precursor **L5**, **L6** or **L9**, depending on the desired Mo(VI) compound, was dissolved in MeOH (10.0 mL/mmol ligand precursor) in a round bottom flask at room temperature and $MoO_2(acac)_2$ (1.0 eq/mmol ligand precursor) was mixed into the ethanolic solution affording an yellow-orange solution. After 10 minutes under magnetic stirring, distilled water (30 mL/mmol ligand precursor) was added to the reaction, inducing the formation of a precipitate which was filtered under vacuum and washed with distilled water (3x20 mL) and petroleum ether (1x 30 mL).

Synthesis of MoL5:

Reagents: **L5** (0.5 g, 1.67 mmol), $MoO_2(acac)_2$ (0.55 g, 1.67 mmol), MeOH (8.3 mL). Obtained as a white solid. Yield: 67% (0.52 g). ESI-MS [DMSO]: m/z= 880.84 ($[(MoO_2$**L5**$)_2(OMe)]^-$, 100%), m/z= 848.78 ($\{[MoO_2$**L5**$]_2\}^-$, 13%), m/z= 726.41 ($\{H[MoO_2$**L5**$]\}^+$, 2%), m/z= 724.95 ($[(MoO_2$**L5**$)$**L5**$]^-$, 15%), m/z= 456.23 ($\{[MoO_2$**L5**$]\bullet MeOH\}^-$, 65%), m/z= 426.46 ($[MoO_2$**L5**$]^-$, 20%), m/z= 314.04 ($\{Na_2[MoO_2$**L5**$]\bullet MeOH\bullet 7H_2O\}^{2+}$, 55%). ν_{max}/cm^{-1}: 3127 (N-H, w), 1624 (C=O, s), 1233 (C-O_{Phenol}, m), 947, 923 (Mo=O, s, s). Elemental analysis for $C_{18}H_{19}MoNO_5\bullet 2.5H_2O$: calcd. C 45.97, H 5.14, N 2.98; found C 46.09, H 4.69, N 2.91.

Synthesis of MoL6:

Reagents: **L6** (0.65 g, 1.71 mmol), $MoO_2(acac)_2$ (0.56 g, 1.71 mmol), MeOH (8.6 mL). Obtained as an orange amorphous solid. Yield: 52% (0.46 g). ESI-MS [MeOH]: m/z= 1550.70 ($\{Na[(MoO_2$**L6**$)_3]\}^+$, 100%), m/z= 1421.70 ($\{H[(MoO_2$**L6**$)$**L6**$]\}^+$, 10%), m/z= 1400.11 ($[(MoO_2$**L6**$)_2$**L6**$]^-$, 15%), m/z= 1017.52 ($\{[MoO_2$**L6**$]_2\}^-$, 22%), m/z= 892.86 ($[(MoO_2$**L6**$)$**L6**$]^-$, 55%), m/z= 510.19 ($[MoO_2$**L6**$]^-$, 15%), m/z= 253.22 ($[MoO_2$**L6**$]^{2-}$, 100%). ν_{max}/cm^{-1}: 3242 (N-H, w), 1660 (C=O, s), 1235 (C-O_{Phenol}, m), 919, 909 (Mo=O, s, s). Elemental analysis for $C_{24}H_{31}MoNO_5\bullet 0.5MeOH$: calcd. C 56.00, H 6.33, N 2.67; found C 56.06, H 6.48, N 2.57.

Synthesis of MoL9:

Reagents: **L9** (0.5 g, 1.36 mmol), $MoO_2(acac)_2$ (0.5 g, 1.36 mmol), MeOH (6.8 mL). Obtained as a white solid. Yield: 71% (0.47 g). ESI-MS [DMSO]: m/z= 826.81 ($[(MoO_2$**L9**$)$**L9**$]^-$,15%), m/z= 509.10 ($\{[MoO_2$**L10**$]\bullet MeOH\}^-$, 100%). ν_{max}/cm^{-1}: 3056 (N-H, w), b, 1616 (C=O, s, b), 1218 (C-

O_{Phenol}, s), 911, 896 (Mo=O, s, s). Elemental analysis for $C_{21}H_{20}MoN_2O_5$•0.5MeOH: calcd. C 52.45, H 4.50, N 5.69; found C 52.18, H 4.83, N 5.59.

IV.5.4.3 – Mo(VI) complexes bearing *β*-ketoamino acid ligands

General synthetic procedure: Ligand precursor **L18** or **L19**, depending on the desired Mo(VI) compound, was suspended in EtOH (10.0 mL/mmol ligand precursor) in a round bottom flask at room temperature and concentrated HCl (1.0 eq/mmol ligand precursor) was added dropwise to the ethanolic suspension. After complete solubilization of the reaction mixture under stirring, $MoO_2(acac)_2$ (1.0 eq/mmol ligand precursor) was added to the mixture which was let to stir for additional 10 minutes resulting in an yellow-orange solution. Then, distilled water 30 mL/mmol ligand precursor), inducing the formation of a precipitate which was filtered under vacuum and washed with distilled water (3x20 mL) and petroleum ether (1x 30 mL).

Synthesis of MoL18:

Reagents: **L18** (0.5 g, 1.40 mmol), concentrated HCl (0.12 mL, 1.40 mmol), $MoO_2(acac)_2$ (0.46 g, 1.40 mmol), EtOH (14 mL). Obtained as a white solid. Yield: 73% (0.54 g). ESI-MS [DMSO]: m/z= 820.96 ([(MoO_2**L18**)**L18**]$^-$, 28%), m/z= 704.85 ({[MoO_2**L18**(OH)]$_4$•3MeOH•2H_2O}$^{3-}$, 28%), m/z= 692.94 ({[MoO_2**L18**(OH)]$_4$•2MeOH•2H_2O}$^{3-}$, 100%), m/z= 492.00 ([MoO_2**L18**(OH)]$^{2-}$, 20%), m/z= 458.10 ({[(MoO_2**L18**)**L18**]•3MeOH]}$^{2-}$, 40%), m/z= 310.50 ({H_2Na[MoO_2**L18**(OH)]}$^{3+}$, 30%), m/z= 178.79 ({Na_2[MoO_2**L18**]•MeOH•2H_2O}$^{2+}$, 100%). ν_{max}/cm^{-1}: 3054 (N-H, w), 1676 (C=O, s), 946, 909 (Mo=O, s, s). Elemental analysis for $C_{22}H_{20}ClMoNO_5$•0.5H_2O: calcd. C 50.93, H 4.08, N 2.70; found C 50.84, H 4.20, N 2.47.

Synthesis of MoL19:

Reagents: **L19** (0.5 g, 1.67 mmol), concentrated HCl (0.14 mL, 1.67 mmol), $MoO_2(acac)_2$ (0.60 g, 1.67 mmol), EtOH (17 mL). Obtained as a white solid. Yield: 77% (0.54 g). ESI-MS [DMSO]: m/z= 726.89 ([H(MoO_2**L19**)**L19**]$^+$, 3%), m/z= 725.02 ([(MoO_2**L19**)**L19**]$^-$, 25%), m/z= 598.48 ({H[(MoO_2**L19**)(OH)]•2H_2O}$^+$, 5%), m/z= 597.05 ({[(MoO_2**L19**)(OH)]•EtOH•6H_2O}$^-$, 100%), m/z= 483.65 ({HNa[(MoO_2**L19**)$_2$(O)]•4H_2O}$^{2+}$, 8%), m/z= 444.21 ([(MoO_2**L19**)(OH)]$^-$, 26%), m/z= 319.09 ({[(MoO_2**L19**)(OH)]•3EtOH•3H_2O}$^-$, 15%). ν_{max}/cm^{-1}: 3055 (N-H, w), 1679 (C=O, s), 942, 906 (Mo=O, s, s), 742, 476 (Mo-O-Mo, s, m). Elemental analysis for $C_{36}H_{40}Mo_2N_2O_{11}$•2EtOH: calcd. C 50.01, H 5.46, N 2.92; found C 50.24, H 5.07, N 2.88.

V – Future Prospects

In the present work, several Fe(III) and Mo(VI) complexes were successfully prepared and applied as catalysts or pre-catalysts in homogeneous oxidative catalysis. The Fe(III) compounds synthesized revealed an interesting potential as pre-catalysts in the asymmetric oxidative coupling of 2-naphthol and 3-bromo 2-naphthol, Mukaiyama epoxidation of benzalacetophenones and oxidation of 1-phenylethan-1-ol to acetophenone. The Mo(VI) complexes prepared, however, presented only low activity as revealed to be inefficient pre-catalysts in the epoxidation of benzalacetophenones.

The Fe(III) compounds prepared in this work may find application as pre-catalysts in the asymmetric oxidative homo- and cross-coupling of other 2-naphthol derivatives, especially those containing C3-substituents.

The conditions applied in the Mukaiyama epoxidation reaction of benzalacetophenones may be extended to bulkier chalcones, to study the effects the overall enantioselectivity of the pre-catalysts. The same conditions could be tested in the epoxidation of other substrates such as cholesterol derivatives or even stilbenes.

The alcohol oxidation with Fe(III) with the applied catalytic conditions can be extended to several other aromatic, alicyclic and aliphatic secondary alcohols, also testing distinct solvents. The same studies can be extended to the oxidation of primary alcohols for the preparation of the respective aldehydes or carboxylic acids-

The mentioned reactions are projected for future research works, hoping to contribute to the development of more sustainable catalytic reactions in oxdative catalysis with Fe(III) complexes as pre-catalysts.

VI – Bibliography

[1] Enthaler, S.; Junge, K.; Beller, M., *Angew. Chem., Int. Ed.* **2008**, 47, 3317.

[2] Burgess, J.; Twigg, M. V., *Encyclopedia of Inorganic Chemistry,* John Wiley & Sons, Ltd **2006**.

[3] McCleverty, J. A., *Encyclopedia of Inorganic Chemistry,* John Wiley & Sons, Ltd, **2006**.

[4] Ullmann, F.; Bielecki, J. F. Ullmann, *Chem. Ber.* **1901**, 34, 2174.

[5] Heck, R. F.; Nolley, J. P., *J. Org. Chem.* **1972**, 37, 2320.

[6] Miyaura, N.; Yamada, K.; Suzuki, A., *Tetrahedron Lett.* **1979**, 20, 3437.

[7] Sonogashira, K.; Tohda, Y.; Hagihara, N., *Tetrahedron Lett*. **1975**, 16, 4467.

[8] Shaughnessy, K. H., *Metal-Catalyzed Reactions in Water*, 1st Edition, Wiley-VCH Verlag GmbH & Co. KGaA. **2013**.

[9] Grzybowski, M.; Skonieczny, K.; Butenschön, H.; Gryko, D. T., *Angew. Chem., Int. Ed.* **2013**, 52, 9900.

[10] Kharasch, M. S.; Fields, E. K., *J. Am. Chem. Soc.* **1941**, 63, 2316.

[11] Bauer, E. B., *Curr. Org. Chem.* **2008**, 12, 1341.

[12] Bauer, I.; Knölker, H.-J., *Chem. Rev.* **2015**, 115, 3170.

[13] Tamura, M.; Kochi, J., *J. Am. Chem. Soc.* **1971**, 93, 1487.

[14] Neumann, S. M.; Kochi, J. K., *J. Org. Chem.* **1975**, 40, 599.

[15] Bolm, C.; Legros, J.; Le Paih, J.; Zani, L., *Chem. Rev.* **2004**, 104, 6217.

[16] Sarhan, A. A. O.; Bolm, C., *Chem. Soc. Rev.* **2009**, 38, 2730.

[17] Jegelka, M.; Plietker, B. *Top. Organomet. Chem.* **2011**, 33, 177.

[18] Ackermann, L.; Vicente, R.; Kapdi, A. R., *Angew. Chem., Int. Ed.* **2009**, 48, 9792.

[19] Hussain, I.; Singh, T., *Adv. Synth. Catal.* **2014**, 356, 1661.

[20] Yu, D. G.; Li, B. J.; Shi, Z. J., *Tetrahedron* **2012**, 68, 5130.

[21] Yeung, C. S.; Dong, V. M., *Chem. Rev.* **2011**, 111, 1215.

[22] Alberico, D.; Scott, M. E.; Lautens, M., *Chem. Rev.* **2007**, 107, 174.

[23] Kulkarni, A. A.; Daugulis, O., *Synthesis* **2009**, 24, 4087.

[24] Sun, C. L.; Li, B. J.; Shi, Z. J., *Chem. Rev.* **2011**, 111, 1293.

[25] Jia, F.; Li, Z., *Org. Chem. Front.* **2014**, 1, 194.

[26] Norinder, J.; Matsumoto, A.; Yoshikai, N.; Nakamura, E., *J. Am. Chem. Soc.* **2008**, 130, 5858.

[27] Wen, J.; Zhang, J.; Chen, S.-Y.; Li, J.; Yu, X.-Q., *Angew. Chem., Int. Ed.* **2008**, 47, 8897.

[28] Wen, J.; Qin, S.; Ma, L. F.; Dong, L.; Zhang, J.; Liu, S. S.; Duan, Y. S.; Chen, S. Y.; Hu, C. W.; Yu, X. Q., *Org. Lett.* **2010**, 12, 2694.

[29] Wang, J.; Wang, S.; Wang, G.; Zhang, J.; Yu, X.-Q., *Chem. Commun.* **2012**, 48, 11769.

[30] Komeyama, K.; Kashihara, T.; Takaki, K., *Tetrahedron Lett.* **2013**, 54, 1084.

[31] Uchiyama, N.; Shirakawa, E.; Nishikawa, R.; Hayashi, T., *Chem. Commun.* **2011**, 47, 11671.

[32] Ohta, M.; Quick, M. P.; Yamaguchi, J.; Wünsch, B.; Itami, K., *Chem. Asian J.* **2009**, 4, 1416.

[33] Yoshikai, N.; Matsumoto, A.; Norinder, J.; Nakamura, E., *Angew. Chem., Int. Ed.* **2009**, 48, 2925.

[34] Yoshikai, N.; Matsumoto, A.; Norinder, J.; Nakamura, E., *Synlett* **2010**, 2, 313.

[35] Zhang, G.; Lv, G.; Pan, C.; Cheng, J.; Chen, F., *Synlett* **2011**, 20, 2991.

[36] Brunel, J. M., *Chem. Rev.* **2005**, 105, 857.

[37] Kozlowski, M. C.; Morgan, B. J.; Linton, E. C., *Chem. Soc. Rev.* **2009**, 38, 3193.

[38] Langeslay, R. R.; Kaphan, D. M.; Marshall, C. L.; Stair, P. C.; Sattelberger, A. P.; Delferro, M., *Chem. Rev.* **2019**, 119, 2128.

[39] Shalit, H.; Dyadyuk, A.; Pappo, D., *J. Org. Chem.* **2019**, 84, 1677.

[40] Egami, H.; Katsuki, T., *J. Am. Chem. Soc.* **2009**, 131, 6082.

[41] Egami, H.; Matsumoto, K.; Oguma, T.; Kunisu, T.; Katsuki, T., *J. Am. Chem. Soc.* **2010**, 132, 13633.

[42] Narute, S.; Parnes, R.; Toste, F. D.; Pappo, D., *J. Am. Chem. Soc.* **2016**, 138, 16553.

[43] Smrčina, M.; Vyskočil, S.; Máca, B.; Polášek, M.; Claxton, T. A.; Abbot, A. P.; Kočovský, P., *J. Org. Chem.* **1994**, 59, 2156.

[44] Jasen, A. C. A.; Brussee, J., *Tetrahedron Lett.* **1983**, 24, 3261.

[45] Smith, M. B.; March, J.; *March's Advanced Organic Chemistry: Reactions, Mechanism and Structure*, 6th Edition, John Wiley and Sons, Inc., **2007**.

[46] Sharpless, K. B.; Katsuki, T., *J. Am. Chem. Soc.* **1980**, 102, 5974.

[47] Irie, R.; Noda, K.; Ito, Y.; Matsumoto, N.; Katsuki, T. *Tetrahedron Lett.* **1990**, 31, 7345.

[48] Zhang, W.; Loebach, J. L.; Wilson, S. R.; Jacobsen, E. N., *J. Am. Chem. Soc.* **1990**, 112, 2801.

[49] Guengerich, F. P.; Yoshimoto, F. K., *Chem. Rev.* **2018**, 118, 6573.

[50] Pereira, M. M.; Dias, L. D.; Calvete, M. J. F., *ACS Catal.* **2018**, 8, 10784.

[51] Mukaiyama, T.; Yamada, T., *Bull. Chem. Soc. Jpn*. **1995**, 68, 17.

[52] Peter, G. F., *J. Biochem. Mol. Toxicol.* **2007**, 21, 163.

[53] Gopalaiah, K., *Chem. Rev.* **2013**, 113, 3248.

[54] Talsi, E. P.; Bryliakov, K. P., *Coord. Chem. Rev.* **2012**, 256, 1418.

[55] Wai, T.; Chow, -Shan; Chen, G.-Q.; Liu, Y.; Zhou, C.-Y.; Che, C.-M., *Pure Appl. Chem* **2012**, 84, 1685.

[56] Fingerhut, A.; Serdyuk, O. V.; Tsogoeva, S. B., *Green Chem.* **2015**, 17, 2042.

[57] Murch, B. P.; Bradley, F. C.; Que, L., *J. Am. Chem. Soc.* **1986**, 108, 5027.

[58] Wie,, J. F.; Yu, X. D.; Jin, D. S., *Chin. Chem. Lett.* **1996**, 7, 962.

[59] Francis, M. B.; Jacobsen, E. N., *Angew. Chem., Int. Ed.* **1999**, 38, 937.

[60] White, M. C.; Doyle, A. G.; Jacobsen, E. N., *J. Am. Chem. Soc.* **2001**, 123, 7194.

[61] Fujita, M.; Que, L., *Adv. Synth. Catal.* **2004**, 346, 190.

[62] Mas-Ballesté, R.; Fujita, M.; Hemmila, C.; Que, L., *J. Mol. Catal. A: Chem.* **2006**, 251, 49.

[63] Chen, K.; Costas, M.; Kim, J.; Tipton, A. K.; Que, L., *J. Am. Chem. Soc.* **2002**, 124, 3026.

[64] Dubois, G.; Murphy, A.; Daniel, T.; Stack, P., *Org. Lett.* **2003**, 5, 2469.

[65] Mas-Balleste, R.; Que, L., *J. Am. Chem. Soc.* **2007**, 129, 15964.

[66] Gelalcha, F. G.; Bitterlich, B.; Anilkumar, G.; Tse, M. K.; Beller, M., *Angew. Chem., Int. Ed.* **2007**, 46, 7293.

[67] Yeung, H.-L.; Sham, K.-C.; Tsang, C.-S.; Lau, T.-C.; Kwong, H.-L., *Chem. Commun.* **2008**, 32, 3801.

[68] Nishikawa, Y.; Yamamoto, H., *J. Am. Chem. Soc.* **2011**, 133, 8432.

[69] Wu, M.; Miao, C.-X.; Wang, S.; Hu, X.; Xia, C.; Kühn, F. E.; Sun, W. *Adv. Synth. Catal.* **2011**, 353, 3014.

[70] Wang, B.; Wang, S.; Xia, C.; Sun, W., *Chem. Eur. J.* **2012**, 18, 7332.

[71] Cussó, O.; Garcia-Bosch, I.; Ribas, X.; Lloret-Fillol, J.; Costas, M., *J. Am. Chem. Soc.* **2013**, 135, 14871.

[72] Cussó, O.; Ribas, X.; Costas, M., *Chem. Commun.* **2015**, 51, 14285.

[73] Cussó, O.; Cianfanelli, M.; Ribas, X.; Klein Gebbink, R. J. M.; Costas, M., *J. Am. Chem. Soc.* **2016**, 138, 2732.

[74] Takai, T.; Yamada, T.; Rhode, O.; Mukaiyama, T., *Chem. Lett*. **1991**, 281.

[75] Yamada, T.; Takahashi, K.; Kato, K.; Takai, T.; Inoki, S.; Mukaiyama. T., *Chem. Lett*. **1991**, 641.

[76] Yamada, T.; Takai, T.; Rhode, O.; Mukaiyama, T., *Bull. Chem. Soc. Jpn.* **1991**, 64, 2109.

[77] Takai, T.; Hata, E.; Yamada, T.; Mukaiyama, T., *Bull. Chem. Soc. Jpn.* **1991**, 64, 2513.

[78] Yamada, T.; Takai, T.; Rhode, O.; Mukaiyama, T., *Chem. Lett*. **1991**, 1.

[79] Mukaiyama, T.; Yamada, T.; Nagata, T.; Imagawa, K., *Chem. Lett*. **1993**, 327.

[80] Hata, E.; Takai, T.; Yamada, T.; Mukaiyama, T., *Chem. Lett.* **1994**, 535.

[81] Nagata, T.; Imagawa, K.; Yamada, T.; Mukaiyama, T., *Bull. Chem. Soc. Jpn.* **1995**, 68, 3241.

[82] Kaneda, K.; Haruna, S.; Imanaka, T.; Hamamoto, M.; Nishiyama, Y.; Ishii, Y., *Tetrahedron Lett.* **1992**, 33, 6827.

[83] Lassila, K. R.; Waller, F. J.; Werkheiser, S. E.; Wressell, A. L., *Tetrahedron Lett.* **1994**, 35, 8077.

[84] Nam, W.; Kim, H. J.; Kim, S. H.; Ho, R. Y. N.; Valentine, J. S., *Inorg. Chem.* **1996**, 35, 1045.

[85] Nishida, Y.; Fujimoto, T.; Tanaka, N., *Chem. Lett.* **1992**, 1291.

[86] Wentzel, B. B.; Alsters, P. L.; Feiters, M. C.; Nolte, R. J. M., *J. Org. Chem.* **2004**, 69, 3453.

[87] Heinze, K., *Coord. Chem. Rev.* **2015**, 300, 121.

[88] Kühn, F. E.; Santos, A. M.; Abrantes, M., *Chem. Rev.* **2006**, 106, 2455.

[89] Trost, M. K.; Bergman, R. G., *Organometallics* **1991**, 10, 1172.

[90] Mimoun, H.; de Roch, S. I.; Sajus, L.; *Tetrahedron* **1970**, 26, 37.

[91] Chong, A. O.; Sharpless, K. B., *J. Org. Chem.* **1977**, 42, 1587.

[92] Xia, Q.-H.; Ge, H.-Q.; Ye, C.-P.; Liu, Z.-M.; Su, K.-X., *Chem. Rev.* **2005**, 105, 1603.

[93] Brito, J. A.; Royo, B.; Gómez, M., *Catal. Sci. Technol.* **2011**, 1, 1109.

[94] Abrantes, M.; Sakthivel, A.; Romão, C. C.; Kühn, F. E., *J. Organomet. Chem.* **2006**, 691, 3137.

[95] Kagan, H. B.; Mimoun, H.; Mark, C.; Schurig, V., *Angew. Chem., Int. Ed.* **1979**, 18, 485.

[96] Schurig, V.; Hintzer, K.; Leyrer, U.; Mark, C.; *J. Organomet. Chem.* **1989**, 370, 81.

[97] Wang, X. Y.; Shi, H. C.; Sun, C.; Zhang, Z. G., *Tetrahedron* **2004**, 60, 10993.

[98] Barlan, A. U.; Basak, A.; Yamamoto, H., *Angew. Chem., Int. Ed.* **2006**, 45, 5849.

[99] Wang, Y.; Wu, Z.; Li, Z.; Zhou, X. G., *Tetrahedron Lett.* **2009**, 50, 2509.

[100] Nakajima, K.; Kojima, M.; Toriumi, K.; Saito, K.; Fujita, J. J., *Bull. Chem. Soc. Jpn.* **1989**, 62, 760.

[101] Iseki, Y.; Kudo, M.; Mori, A.; Inoue, S., *J. Org. Chem.* **1992**, 57, 6329.

[102] Luo, Z.; Liu, Q.; Gong, L.; Cui, X.; Mi, A.; Jiang, Y., *Chem. Commun*. **2002**, 914.

[103] Somei, H.; Asano, Y.; Yoshida, T.; Takizawa, S.; Yamataka, H.; Sasai, H., *Tetrahedron Lett.* **2004**, 45, 1841.

[104] Takizawa, S.; Katayama, T.; Somei, H.; Asano, Y.; Yoshida, T.; Kameyama, C.; Rajesh, D.; Onitsuka, K.; Suzuki, T.; Mikami, M.; Yamataka, H.; Jayaptakash, D.; Sasai, H., *Tetrahedron* **2008**, 64, 3361.

[105] Ando, R.; Inden, H.; Sugino, M.; Ono, H.; Sakaeda, D.; Yagyu, T.; Maeda, M., *Inorg. Chim. Acta* **2004**, 357, 1337.

[106] Chen, C. T.; Kao, J. Q.; Salunke, S. B.; Lin, Y. H., *Org. Lett.* **2011**, 13, 26.

[107] Adão, P.; Barroso, S.; Carvalho, M. F. N. N.; Teixeira, C. M.; Kuznetsov, M. L.; Costa Pessoa, J., *Dalton Trans.* **2015**, 44, 1612.

[108] Miyake, H.; Watanabe, M.; Takemura, M.; Hasegawa, T.; Kojima, Y.; Inoue, M. B.; Inoue, M.; Fernando, Q., *J. Chem. Soc., Dalton Trans.* **2002**, 33, 1119.

[109] Adão, P.; Pessoa, J. C.; Henriques, R. T.; Kuznetsov, M. L.; Avecilla, F.; Maurya, M. R.; Kumar, U.; Correia, I., *Inorg. Chem.* **2009**, 48, 3542.

[110] Driessen, W. L.; Rehorst, D.; Reedijk, J.; Mutikainen, I.; Turpeinen, U., *Inorg. Chim. Acta* **2003**, 355, 64.

[111] Miyano, S.; Abe, N.; Abe, A.; Hamachi, K., *Chem. Pharm. Bull*. **1971**, 19, 1131.

[112] Fontolan, E.; Alegria, E. C. B. A.; Ribeiro, A. P. C.; Kopylovich, M. N.; Bertani, R.; Pombeiro, A. J. L., *Inorg. Chim. Acta* **2017**, 455, 653.

[113] Lanznaster, M.; Neves, A.; Bortoluzzi, A. J.; Assumpção, A. M. C.; Vencato, I.;

Machado, S. P.; Drechsel, S. M., *Inorg. Chem.* **2006**, 45, 1005.

[114] Roy, M.; Saha, S.; Patra, A. K.; Nethaji, M.; Chakravarty, A. R., *Inorg. Chem.* **2007**, 46, 4368.

[115] Casella, L.; Gullotti, M.; Pintar, A.; Messori, L.; Rockenbauer, A.; Gyor, M., *Inorg. Chem.* **1987**, 26, 1031.

[116] Velusamy, M.; Mayilmurugan, R.; Palaniandavar, M., *Inorg. Chem.* **2004**, 43, 6284.

[117] Snodin, M. D.; Ould-Moussa, L.; Wallmann, U.; Lecomte, S.; Bachler, V.; Bill, E.; Hummel, H.; Weyhermüller, T.; Hildebrandt, P.; Wieghardt, K., *Chem. Eur. J.* **1999**, 5, 2554.

[118] G. M. Sheldrick, SADABS, Program for Empirical Absorption Correction of Area Detector Data, University of Göttingen, Germany, **1996**.

[119] Stewart, C. D.; Arman, H.; Bawazir, H.; Musie, G. T., *Inorg. Chem.* **2014**, 53, 10974.

[120] Auerbach, U.; Eckert, U.; Wieghardt, K.; Nuber, B.; Weiss, J., *Inorg. Chem.* **1990**, 29, 938.

[121] Dhanalakshmi, T.; Bhuvaneshwari, M.; Palaniandavar, M., *J. Inorg. Biochem.* **2006**, 100, 1527.

[122] Velusamy, M.; Palaniandavar, M.; Gopalan, R. S.; Kulkarni, G. U., *Inorg. Chem.* **2003**, 42, 8283.

[123] Saha, S.; Majumdar, R.; Roy, M.; Dighe, R. R.; Chakravarty, A. R., *Inorg. Chem.* **2009**, 48, 2652.

[124] Váradi, T.; Pap, J. S.; Giorgi, M.; Párkányi, L.; Csay, T.; Speier, G.; Kaizer, J., *Inorg. Chem.* **2013**, 52, 1559.

[125] Piguet, C., *J. Chem. Educ.* **1997**, 7, 815.

[126] Bain, G. A.; Berry, J. F., *J. Chem. Educ.* **2008**, 85, 532.

[127] Weyhermüller, T.; Wagner, R.; Chaudhuri, P., *Eur. J. Inorg. Chem.* **2011**, 2547.

[128] Whiteoak, C. J.; Gjoka, B.; Martin, E.; Belmonte, M. M.; Escudero-Adán, E. C.; Zonta, C.; Licini, G.; Kleij, A. W., *Inorg. Chem.* **2012**, 51, 10639.

[129] Linnell, R. H., *J. Org. Chem.* **1960**, 25, 290.

[130] Hosmane, R. S.; Liebman, J. F., *Struct. Chem.* **2009**, 20, 693.

[131] Durand, J.; Zangrando, E.; Stener, M.; Fronzoni, G.; Carfagna, C.; Binotti, B.; Kamer, P. C. J.; Müller, C.; Caporali, M.; Van Leeuwen, P. W. N. M.; Vogt, D.; Milani, B., *Chem. Eur. J.* **2006**, 12, 7639.

[132] Piedra-Arroni, E.; Brignou, P.; Amgoune, A.; Guillaume, S. M.; Carpentier, J. F.; Bourissou, D., *Chem. Commun.* **2011**, 47, 9828.

[133] Kobayashi, S.; Higashimura, H., *Prog. Polym. Sci.* **2003**, 28 1015.

[134] Guo, Q. X.; Wu, Z. J.; Luo, Z. Bin; Liu, Q. Z.; Ye, J. L.; Luo, S. W.; Cun, L. F.; Gong, L. Z., *J. Am. Chem. Soc.* **2007**, 129, 13927.

[135] Hovorka, M.; Günterová, J.; Závada, J, *Tetrahedron Lett.* **1990**, 31, 413.

[136] Libman, A.; Shalit, H.; Vainer, Y.; Narute, S.; Kozuch, S.; Pappo, D., *J. Am. Chem. Soc.* **2015**, 137, 11453.

[137] Yudin, A. K.; Martyn, L. J. P.; Pandiaraju, S.; Zheng, J.; Lough, A., *Org. Lett.* **2000**, 2, 41.

[138] Asiri, A. M.; Khan, S. A., *Molecules* **2011**, 16, 523.

[139] Jaiswal, P.; Pathak, D. P.; Bansal, H.; Agarwal, U., *J. Chem. Pharm. Res.* **2018**, 10, 160.

[140] Ho, T. L.; Liu, S. H., *Synth. Commun.* **1983**, 13, 685.

[141] Huo, C.; Xu, X.; Jia, X.; Wang, X.; An, J.; Sun, C., *Tetrahedron* **2012**, 68, 190.

[142] Zhu, Y.; Wang, Q.; Cornwall, R. G.; Shi, Y., *Chem. Rev.* **2014**, 114, 8199.

[143] Zhuang, C.; Zhang, W.; Sheng, C.; Zhang, W.; Xing, C.; Miao, Z., *Chem. Rev.* **2017**, 117, 7762.

[144] Helder, R.; Hummelen, J. C.; Laane, R. W. P. M.; Wiering, J. S.; Wynberg, H., *Tetrahedron Lett.* **1976**, 21, 1851.

[145] Juliá, S.; Masana, J.; Vega, J. C., *Angew. Chem., Int. Ed. Engl.* **1980**, 19, 929.

[146] Elston, C. L.; Jackson, R. F. W.; MacDonald, S. J. F.; Murray, P. J., *Angew. Chem., Int. Ed. Engl.* **1997**, 36, 410.

[147] Nemoto, T.; Ohshima, T.; Yamaguchi, K.; Shibasaki, M., *J. Am. Chem. Soc.* **2001**, 123, 2725.

[148] Lane, B. S.; Burgess, K., *Chem. Rev.* **2003**, 103, 2457.

[149] Baglia, R. A.; Zaragoza, J. P. T.; Goldberg, D. P., *Chem. Rev.* **2017**, 117, 13320.

[150] Dai, W.; Li, G.; Chen, B.; Wang, L.; Gao, S., *Org. Lett.* **2015**, 17, 904.

[151] Hölzl, S. M.; Altmann, P. J.; Kück, J. W.; Kühn, F. E., *Coord. Chem. Rev.* **2017**, 352, 517.

[152] Wada, A.; Ogo, S.; Nagatomo, S.; Kitagawa, T.; Watanabe, Y.; Jitsukawa, K.; Masuda, H., *Inorg. Chem.* **2002**, 41, 616.

[153] Kitagawa, T.; Dey, A.; Lugo-Mas, P.; Benedict, J. B.; Kaminsky, W.; Solomon, E.; Kovacs, J. A., *J. Am. Chem. Soc.* **2006**, 128, 14448.

[154] Martinho, M.; Banse, F.; Sainton, J.; Philouze, C.; Guillot, R.; Blain, G.; Dorlet, P.; Lecomte, S.; Girerd, J.-J., *Inorg. Chem.* **2007**, 46, 1709.

[155] Girerd, J.-J.; Banse, F.; Simaan, A. J., *Struct. Bonding* **2000**, 97, 143.

[156] Billany, M. R.; Khatib, K.; Gordon, M.; Sugden, J. K., *Int. J. Pharm.* **1996**, 137, 143.

[157] Ngo, D.; Kalala, M.; Hogan, V.; Manchanayakage, R., *Tetrahedron Lett.* **2014**, 55, 4496.

[158] Wang, D.; Weinstein, A. B.; White, P. B.; Stahl, S. S., *Chem. Rev.* **2018**, 118, 2636.

[159] Allen, S. E.; Walvoord, R. R.; Padilla-Salinas, R.; Kozlowski, M. C., *Chem. Rev.* **2013**, 114, 899.

[160] Sorokin, A. B., *Chem. Rev.* **2013**, 113, 8152.

[161] D'Alessandro, N.; Liberatore, L.; Tonucci, L.; Morvillo, A.; Bressan, M., *J. Mol. Catal. A: Chem.* **2001**, 175, 83.

[162] Nam, W.; Lee, Y. M.; Fukuzumi, S., *Acc. Chem. Res.* **2014**, 47, 1146.

[163] Sinha, S.; Das, S.; Sikari, R.; Parua, S.; Brandão, P.; Demeshko, S.; Meyer, F.; Paul,

N. D., *Inorg. Chem.* **2017**, 56, 14084.

[164] Ghosh, M.; Nikhil, Y. L. K.; Dhar, B. B.; Sen Gupta, S., *Inorg. Chem.* **2015**, 54, 11792.

[165] Pinto, M. F.; Cardoso, B. de P.; Barroso, S.; Martins, A. M.; Royo, B., *Dalton Trans.* **2016**, 45, 13541.

[166] *Org. Synth.* **1922**, 2 (DOI: 10.15227/orgsyn.002.0001)

[167] Sheldrick, G. M., *Acta Crystallogr. Sect. C Struct. Chem.* **2015**, 71, 3.

[168] Sheldrick, G. M., *Acta Crystallogr. Sect. A Found. Crystallogr.* **2015**, 71, 3.

[169] Burla, M. C.; Caliandro, R.; Carrozzini, B.; Cascarano, G. L.; Cuocci, C.; Giacovazzo, C.; Mallamo, M.; Mazzone, A.; Polidori, G., *J. Appl. Crystallogr.* **2015**, 48, 306.

[170] Farrugia, L. J., *J. Appl. Crystallogr.* **2012**, 45, 849.

[171] Allen, F. H., *Acta Crystallogr. Sect. B Struct. Sci.* **2002**, 58, 380.

[172] Macrae, C. F.; Bruno, I. J.; Chisholm, J. A.; Edgington, P. R.; McCabe, P.; Pidcock, E.; Rodriguez-Monge, L.; Taylor, R.; Van De Streek, J.; Wood, P. A., *J. Appl. Crystallogr.* **2008**, 41, 466.

[173] Melby, L. R., *Inorg. Chem.* **1969**, 8, 349.

[174] C.J. Hinshaw, G. Peng, R. Singh, J.T. Spence, J.H. Enemark, M. Bruck, J. Kristofzski, S. L. Merbs, R.B. Ortega, P. A. W., *Inorg. Chem.* **1989**, 28, 4483.

[175] Majumder, S.; Pasayat, S.; Panda, A. K.; Dash, S. P.; Roy, S.; Biswas, A.; Varma, M. E.; Joshi, B. N.; Garribba, E.; Kausar, C.; Patra, S. K.; Kaminsky, W.; Crochet, A.; Dinda, R., *Inorg. Chem.* **2017**, 56, 11190.

[176] Hammes, B. S.; Chohan, B. S.; Hoffman, J. T.; Einwächter, S.; Carrano, C. J., *Inorg. Chem.* **2004**, 43, 7800.